

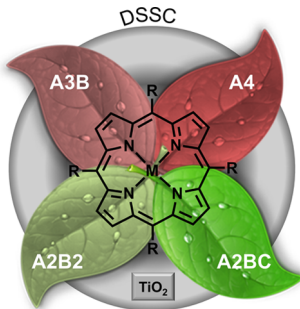
Meso-Substituted Porphyrins for Dye-Sensitized Solar Cells

Maxence Urbani,^{†,‡} Michael Grätzel,[§] Mohammad Khaja Nazeeruddin,^{*,§} and Tomás Torres^{*,†,‡}

[†]Departamento de Química Orgánica, Universidad Autónoma de Madrid, Cantoblanco, 28049 Madrid, Spain

[‡]Instituto Madrileño de Estudios Avanzados (IMDEA)—Nanociencia, c/Faraday, 9, Cantoblanco, 28049 Madrid, Spain

^{*}Laboratory of Photonics and Interfaces, Institute of Chemical Science and Engineering, Swiss Federal Institute of Technology, Station 6, CH 1015 Lausanne, Switzerland



CONTENTS

1. Introduction	12330
1.1. Operational Principles of Dye-Sensitized Solar Cells (DSSCs)	12331
1.2. Porphyrins for DSSCs	12337
1.3. Meso-Substituted Porphyrins for DSSCs	12337
2. A4-Type Design for Meso-Substituted Porphyrin Dyes	12340
3. A3B- and A2B-Type Designs for Meso-Substituted Porphyrin Dyes	12344
3.1. Phenyl Tetra-Substituted A3B-Type Porphyrins	12344
3.2. A3B- and A2B-Type Porphyrin Dyes Anchored through Coupled π -Conjugated Spacers	12349
3.3. A3B-Type Porphyrin Dyes Substituted with Heteroaromatic Groups	12355
3.3.1. A3B-Type Porphyrin Dyes Anchored through Pyridyl Groups	12355
3.3.2. A3B-Type Porphyrin Dyes Anchored through Five-Membered Ring Heteroaromatic Groups and Thienyl Appended Porphyrins	12355
4. <i>trans</i> - and <i>cis</i> -A2B2-Type Designs for Meso-Substituted Porphyrin Dyes	12357
5. <i>trans</i> -A2BC-Type Design for Meso-Substituted Porphyrin Dyes: Donor-Bridge Chromophore-Acceptor (D-B-A), Donor- π -Bridged Chromophore-Acceptor (D- π -A or "Push-Pull"), and Hybrid Systems	12361
5.1. "D-B-A" Systems: Phenyl Tetra-Substituted <i>trans</i> -A2BC-Type Porphyrins	12361
5.2. Push-Bridge-Acceptor' Systems: Amino-linked Donor, Phenyl Tris-Substituted <i>trans</i> -A2BC-Type Porphyrins	12363
5.3. "Donor-Bridge-Pull" Systems: Phenyl Tris-Substituted <i>trans</i> -A2BC-Type Porphyrins Anchored through an Ethynylcarboxyphenyl Group	12364
5.4. D- π -A Systems: "Push-Pull" Porphyrins	12365
5.4.1. Ethyne-Linked Donor "Push-Pull" Porphyrins Anchored through an Ethynylcarboxyphenyl Group	12365
5.4.2. Amino-Linked Donor "Push-Pull" Porphyrins Anchored through an Ethynylcarboxyphenyl Group	12367
5.4.3. Polycyclic Aromatic Hydrocarbons-Modified Analogues of LD1 and YD11	12369
5.4.4. "Alkoxy Wrapped Push-Pull" Porphyrins	12369
5.4.5. Panchromatic Response Toward the Near-IR Region through π -Extended Donor Systems in "Push-Pull" Porphyrins	12372
5.4.6. Panchromatic Response Toward the Near-IR Region and Improvement of Charge-Transfer Ability through Modification of the Acceptor Moiety in "Push-Pull" Porphyrins	12376
6. Asymmetrical, Multi-Donors, and Highly Conjugated, Meso-Substituted "Push-Pull" Porphyrin Dyes	12383
7. Conclusion	12389
Author Information	12389
Corresponding Authors	12389
Notes	12389
Biographies	12389
Acknowledgments	12390
References	12390
Note Added in Proof	12396

1. INTRODUCTION

Among the several approaches for harnessing solar energy and converting it into electricity, dye-sensitized solar cells (DSSCs) represent one of the most promising methods for future large-scale power production from renewable energy sources. In these cells, the sensitizer is one of the key components harvesting solar radiation and converting it into electric current. The electrochemical, photophysical, and ground and excited state properties of the sensitizer play an important role for charge transfer dynamics at the semiconductor interface. Over the last 20 years, ruthenium complexes and donor-bridge-acceptor organic sensitizers endowed with anchoring groups have maintained a clear lead in generating power conversion efficiencies over 11%. The validated DSSC efficiency record under standard air mass 1.5G reporting conditions

Received: April 7, 2014

Published: December 12, 2014

using porphyrin sensitizers stands presently at $12.4 \pm 0.3\%$. In this review, we discuss porphyrin sensitizers and their design strategies for obtaining directionality in the excited state, and panchromatic response to harvest the visible and near IR spectra.

1.1. Operational Principles of Dye-Sensitized Solar Cells (DSSCs)

A schematic representation and processes occurring in a conventional n-type, TiO_2 dye-sensitized solar cell (DSSC)^{1–19} are depicted in Figures 1, 2, and 3. There are four main processes that occur in a DSSC: (I) absorption of the light by a

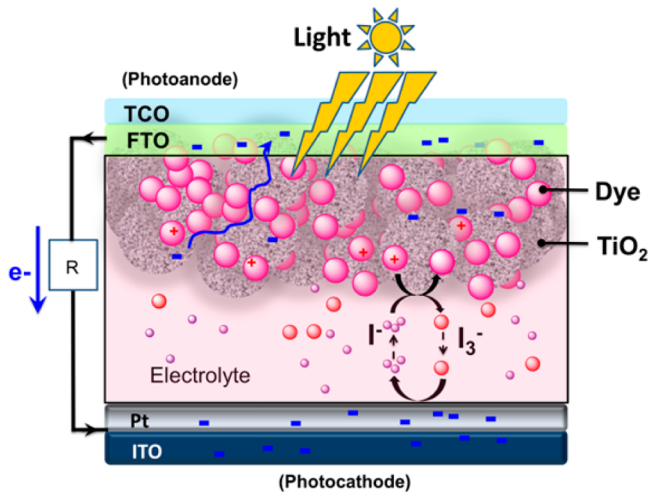


Figure 1. Schematic representation of an operative TiO_2 -DSSC using the I_3^-/I^- redox couple in the electrolyte (ITO = indium tin oxide, Pt = platinum, FTO = fluorine-doped tin oxide, TCO = transparent conductive oxide).

sensitizer, leading to the electronic excitation of the sensitizer to an excited state (Dye^*) (i.e., HOMO \rightarrow LUMO transition), (II) the generated exiton²⁰ dissociates (charge separation process)²¹ to inject an electron into the metal oxide (typically TiO_2 nanoparticles^{22–26} conduction band (CB)^{27,28} from the excited state of the dye (charge transfer process),^{29,30} (III) the resulting oxidized dye (Dye^+) is restored to the fundamental state (Dye) by a reducing agent present in the electrolyte (typically I^- ions), (IV) the photogenerated electrons at the anode flow through an external circuit to reach the Pt counter electrode (cathode), where the oxidized redox mediator is regenerated (e.g., $\text{I}_3^- + 2\text{e}^- \rightarrow 3\text{I}^-$). For a typical iodine-based liquid electrolyte,^{31–35} I_3^- and I^- ions are commonly admitted as the active redox species involved in a DSSC, even though it is now demonstrated that redox reactions involving $\text{I}_2/2\text{I}^-$, $\text{I}_2^\bullet/2\text{I}^-$, and $\text{I}_2/\text{I}_2^\bullet$ species predominate.^{31,36–39} To date, the complexity of these innersphere and multielectron reactions is still problematic, and a clear understanding of all mechanism aspects and fundamental processes of iodine-based electrolytes in DSSCs remain under debate. Moreover, for long-term stability and practical applications, electrolytes based on the iodine/triiodine couple also suffer from two other disadvantages: the corrosive effect toward the metal electrodes, and the partial absorption of the visible light by triiodine anions. These issues hence constitute one of the reasons that have encouraged the development of alternative iodine-free redox couples in liquid electrolytes for DSSCs.^{40–44} The possible occurrence of a “hole-hopping” process in DSSCs using liquid electrolytes, resulting from charge transfer between neighboring dye molecules to transport the charge at the interface between the semiconductor and the hole-redox shuttle, was suggested by some recent works⁴⁵ and will be only mentioned but not detailed in this review. The solar-to-electric power conversion

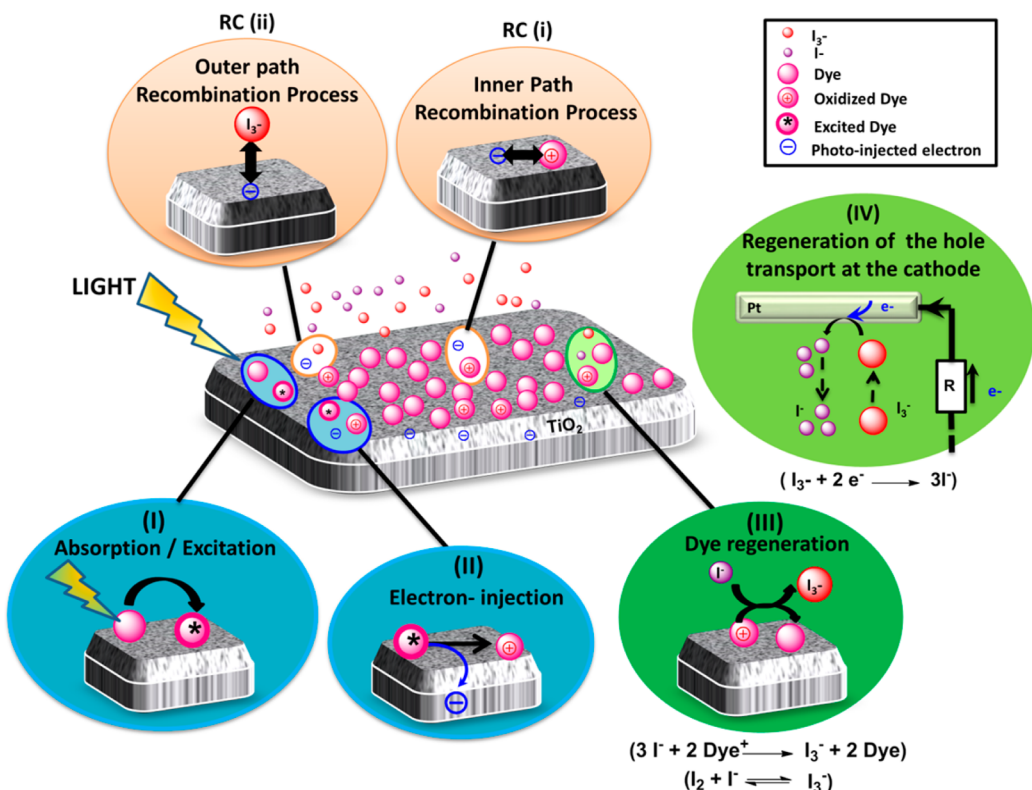


Figure 2. Schematic operational principles occurring in a typical TiO_2 -DSSC.

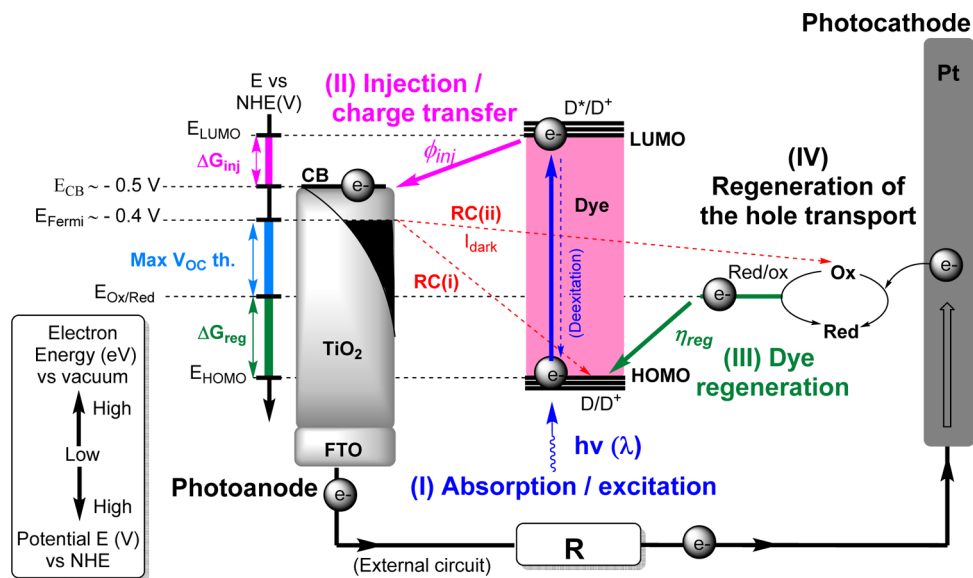


Figure 3. Schematic energetic diagram of an operative and conventional (n-type) TiO_2 -DSSC using a redox couple in the electrolyte ($D = \text{dye}$, $D^* = \text{excited dye}$, $D^+ = \text{oxidized dye}$, $\text{CB} = \text{conduction band of } \text{TiO}_2$, $V_{\text{OC}} = \text{open circuit voltage}$, $\text{Red} = \text{reduced shuttle}$, $\text{Ox} = \text{oxidized shuttle}$, $\text{RC} = \text{recombination process}$, $I_{\text{dark}} = \text{dark current}$, $\text{HOMO/LUMO} = \text{highest occupied/lowest unoccupied molecular orbital}$, $\phi_{\text{inj}} = \text{quantum yield/efficiency for electron injection}$, $\eta_{\text{reg}} = \text{efficiency for dye regeneration}$, $\Delta G_{\text{inj}} = \text{driving-force for electron injection}$, $\Delta G_{\text{reg}} = \text{driving-force for dye regeneration}$).

efficiency (PCE, η) of a solar cell is determined by the product of the short-circuit current (J_{SC}), open-circuit voltage (V_{OC}), and the fill factor (F.F.) divided by the solar photon flux (100 $\text{mW}\cdot\text{cm}^{-2}$ under one sun, AM 1.5G standard conditions (eq 1, Figure 4)). Hence, higher PCE of a DSSC can be reached by increasing the J_{SC} , V_{OC} , and improving the fill factor (the latter parameter reflecting the “losses” in performance of the cell, related with recombination and resistance processes).

The density of photogenerated electrons will depend on the amount of photons absorbed by the sensitizer, the efficiency of processes (I)–(IV), recombination processes RC (i) and (ii). First of all, a sensitizer inside an operative solar cell must obviously be able to absorb photons from sunlight (the largest amount as possible) to make any further photoinduced process possible. The light harvesting efficiency (LHE) will quantify this capability of a device to absorb photons, as a function of the extinction coefficient of the dye (intrinsic property) and concentration/amount of dye-molecules adsorbed onto the TiO_2 surface (LHE(λ) for monochromatic light or integrated LHE value for a spectral region). After photoexcitation of the dye, the generated exciton²⁰ must then dissociate efficiently (charge separation process²¹) to inject an electron into the TiO_2 CB. For such a process, the charge separation energy is tightly related and proportional to the exciton binding energy (EBE), which depends strongly on both the electronic structure and the geometry of the dye. The binding energy and intrinsic relaxation dynamics of the exciton, hence constitute a first crucial factor that governs the electron-injection efficiency, and hence the J_{SC} of the cell.^{46,47} The second key parameter is the driving force for electron injection (ΔG_{inj}), defined as the difference between the LUMO level of the dye and the conduction band of the semiconductor (typically the TiO_2 CB lies at around -0.5 V versus NHE). To make the electron-injection process thermodynamically possible (i.e., $\Delta G_{\text{inj}} < 0$), the LUMO level of the dye must lie above the TiO_2 CB (in a conventional n-type DSSC), and the resulting overpotential satisfies a minimum value to make it efficient. The best

performing dyes are usually able to reach a quantum yield of electron injection efficiency (ϕ_{inj}) close to unity.

The potential-energy difference between the HOMO level of the oxidized dye (e.g., porphyrin dye cation) and the potential of the redox mediators (e.g., $E(\text{I}_3^-/\text{I}^-)$) will govern the driving force for dye regeneration (ΔG_{reg}). The effect of ΔG_{reg} on the dye-regeneration kinetics⁴⁸ (k_{reg}) had been largely unknown for a long time in DSSCs and subjected to controversies. Until recently, a minimum potential difference of ~ 500 mV was believed to be necessary for efficient dye regeneration when using a standard iodine-based liquid electrolyte.⁴ Nevertheless, new electrolytes using one-electronoutersphere redox couples have recently proved to be able to break this barrier, requiring smaller overpotential than the conventional I_3^-/I^- redox couple.^{40–42,48} For instance, Daeneke et al. reported recently a detailed study using ferrocene-based redox shuttles with varying potentials⁴⁹ and proposed that a ΔG_{reg} of only 20–25 kJ/mol should be sufficient to ensure a quantitative dye regeneration under typical operative DSSC conditions (theoretical regeneration yield 99.9%), equivalent to a potential difference of ~ 200 –250 mV between a dye and the redox couple of the electrolyte. In agreement with their experimental results, they evidenced that the dye-regeneration rate follows a Marcus normal-region behavior below 29 kJ/mol, and further increase of the ΔG_{reg} results in a diffusion-controlled reaction. Other one-electronoutersphere redox shuttles were also reported to require much lower driving force for efficient dye-regeneration than the iodine-triiodine couple (Figure 5), such as the cobalt-complexes cobalt bis(trithiacyclononane)⁵⁰ $[\text{Co}(\text{ttcn})_2]^{3+/2+}$, (minimum $\Delta G_{\text{reg}} \sim 200$ mV), cobalt tris(2,2'-bipyrrine) $[\text{Co}(\text{bipy})_3]^{3+/2+}$, or cobalt tris(5-chloro-1,10-phenanthroline)⁵¹ $[\text{Co}(5\text{-chlorophen})]^{3+/2+}$ ($\eta_{\text{reg}} = 80\%$ for $\Delta G_{\text{reg}} \approx 390$ mV).

For an ideal DSSC without recombination processes (i.e., F.F. = 1) and quantum yield efficiencies of unity for all processes, the current density would be limited only by the light-harvesting efficiency (LHE) of the dye (eqs 2–7, Figure 4). As illustrated in Figure 6, the distribution of the photon-flux

$$\eta = \frac{J_{SC} \times V_{OC} \times FF}{I_0} \quad (\text{Eq. 1})$$

$$J_{SC} = e \int I_0(\lambda) \times IPCE(\lambda) d\lambda \quad (\text{Eq. 2})^{15}$$

$$IPCE(\lambda) = LHE(\lambda) \times \varphi_{inj}(\lambda) \times \eta_c \quad (\text{Eq. 3})^{119}$$

$$IPCE(\lambda) = LHE(\lambda) \times \varphi_{inj}(\lambda) \times \eta_{reg} \times \eta_{coll} \quad (\text{Eq. 4})^{65}$$

$$APCE(\lambda) = \varphi_{inj}(\lambda) \times \eta_c \quad (\text{Eq. 5})^{274}$$

$$IPCE(\lambda) = APCE(\lambda) \times LHE(\lambda) \quad (\text{Eq. 6})^{274}$$

$$FF = \frac{P_{max}}{J_{SC} \times V_{OC}} \quad (\text{Eq. 7})$$

$$\varphi_{reg} \text{ (or } \eta_{reg}) = \frac{k_{reg}}{k_{reg} + k_{rec}} \quad (\text{Eq. 8})^{4, 49}$$

η :	Solar-to-electric power conversion efficiency (PCE)
J_{SC} :	Short-circuit current
V_{OC} :	Open-circuit voltage
FF :	Fill Factor
I_0 :	Photon flux ($100 \text{ mW} \cdot \text{cm}^{-2}$ under 1 sun standard AM 1.5G conditions)
(λ) :	Wavelength-dependent parameters
e :	elementary charge
$I_0(\lambda)$:	Solar irradiance spectrum at a wavelength λ under AM 1.5G conditions
$IPCE$:	Conversion efficiency of incident photons to photocurrent
LHE :	Light-harvesting efficiency
$APCE$:	Adsorbed photon-to-current efficiency
φ_{inj} :	Quantum yield of electron injection
η_c :	Efficiency of charge collection at the counter electrode
η_{reg} or φ_{reg} :	Efficiency for dye regeneration
η_{coll} :	Collection efficiency of the photo-generated charge carriers
P_{max} :	Maximum power point
k_{reg} :	Rate constant for dye-regeneration
k_{rec} :	(pseudo-) First-order rate constant for electron-oxidized dye recombination

Figure 4. Equations 1–8

irradiance is not constant over the whole solar spectrum, the 500–800 nm region being the most photon-rich part of sunlight. Based on AM1.5G solar simulations, the expected current density between 400 and 900 nm is $\sim 7 \text{ mA} \cdot \text{cm}^{-2}$ for every 100 nm, which constitute a maximum cumulated J_{SC} value of $\sim 35 \text{ mA} \cdot \text{cm}^{-2}$ for an ideal dye that would harvest whole sunlight in this region. However, as all organic dyes have a limited absorption bandwidth, an efficient dye should be able to absorb the maximum of sunlight in the widest range possible (especially between 400–920 nm) to produce the maximum photocurrent. Next, the theoretical maximum attainable V_{OC} of a DSSC is only limited by the difference between the quasi Fermi

level of electrons (nE_F)^{19,27,28,52–59} in the oxide semiconductor and the potential of the redox shuttle in the electrolyte, as illustrated by eqs 9–11 (Figure 8) and Figure 3. Thus, higher V_{OC} can be in principle achieved by two complementary strategies: by upshifting the TiO_2 –CB (exactly the quasi Fermi level) and/or using a redox shuttle with higher potential than the typical I_3^-/I^- couple. These strategies are however limited. For the former, raising the TiO_2 –CB concurrently decreases the driving-force for electron injection (ΔG_{inj}), which can degrade drastically the J_{SC} . Regarding the latter, a minimum overpotential for dye-regeneration must be satisfied in order to prevent charge recombination between oxidized dyes and photojected

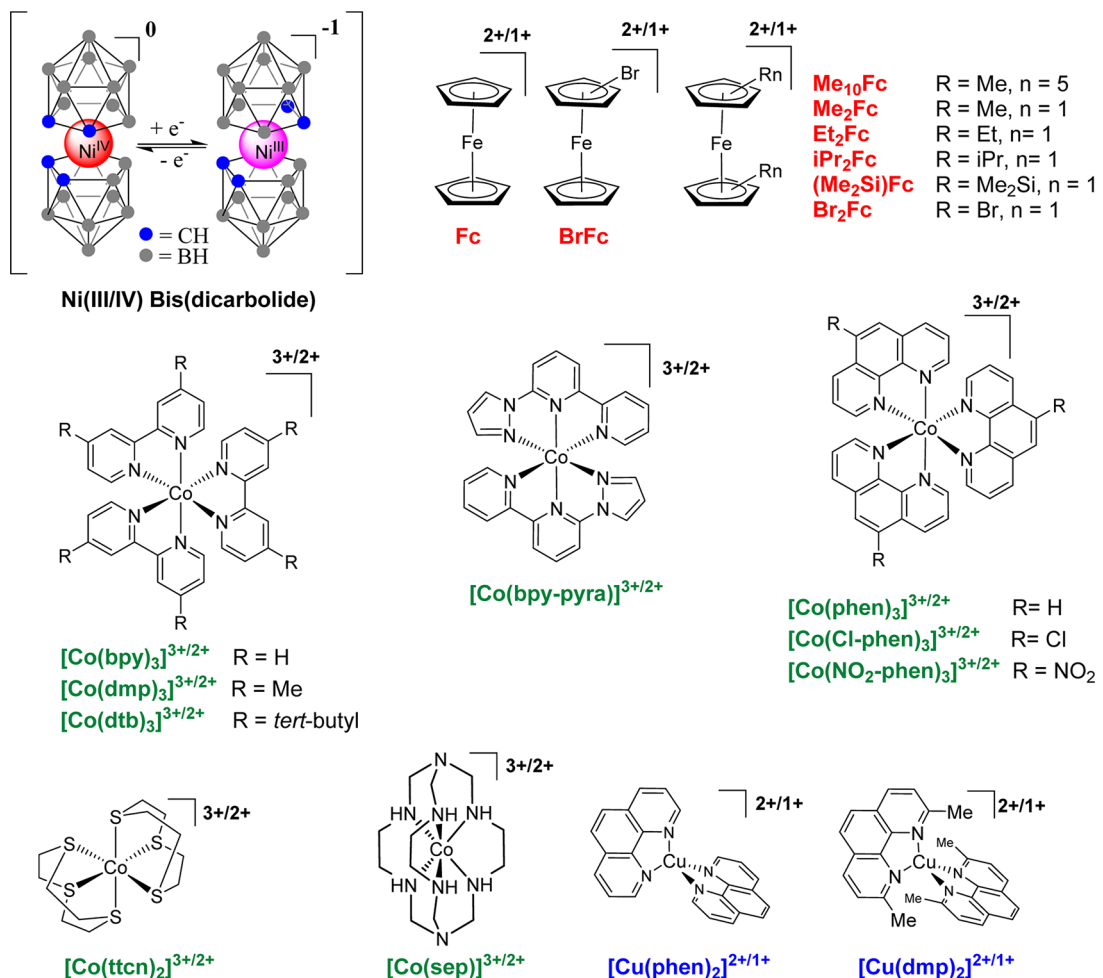


Figure 5. Molecular structures of one-electronouterspheres alternatives shuttles to the conventional iodine-triiodine redox couple in DSSCs: ferrocene derivatives,⁶¹ copper,⁶³ nickel,⁶⁴ and cobalt^{50,51,65–73} complexes.

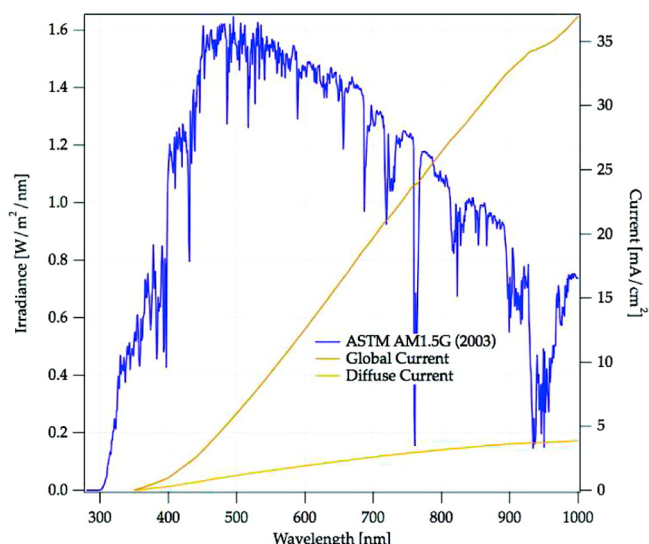


Figure 6. Spectral distribution of the intensity for AM 1.5G solar radiation (blue curves) and J_{SC} values for a device converting all incidents photons bellow the absorption onset wavelength into electric current (yellow and brown curves). Reproduced with permission from ref 2. Copyright 2009 American Chemical Society.

electrons $TiO_2(e^-)$ (vide infra) and hence avoid a drop in the J_{SC} . On the other hand, an excessive regeneration driving force leads

to lower V_{OC} , thus limiting the overall power conversion efficiency of a DSSC cell. The large driving force (~ 500 mV) most often required to attain efficient dye-regeneration when using a standard iodine-based electrolyte represents the largest single free-energy loss in a DSSC device. Moreover, the redox potential of the I_3^-/I^- redox couple ($E \approx +0.4$ V versus NHE) hampered until now, further improvement of the V_{OC} (theoretical maximum V_{OC} value ~ 0.8 V). On this scope, recent efforts have been devoted to develop other new shuttles with higher redox potential and/or lower overpotential needed for efficient dye-regeneration^{39–42,48} in order to reach greater V_{OC} in DSSCs, such as one-electron outerphere redox couples including ferrocene derivatives^{49,60–62} copper,⁶³ nickel,⁶⁴ or cobalt^{50,51,65–73} complexes (Figure 5).

Besides a wide absorption of sunlight by the sensitizer, engineering a performing DSSC will hence require an optimal matching between four-components that are (1) HOMO and (2) LUMO levels of the dye, (3) redox potential of the redox couple in the electrolyte, and (4) semiconductor conduction band. Design, synthesis, and subtle changes in the molecular structure of the dye will help to fine-tune the MOs at adequate levels with respect to those of the semiconductor and electrolyte, as well as the orientation and geometry adopted by the dye onto the surface. Accordingly, the redox shuttle must fulfill the compromise between high redox potential to attain high V_{OC} in the DSSC and satisfy a minimum

overpotential needed for an efficient dye-regeneration to avoid a drop in the J_{SC} .

In practice, mainly two types of unwelcome recombination processes degrade drastically the performance of an operative DSSC⁷⁴ and must be avoided or at least minimized in order to reach high PCE. The first one occurs between the oxidized dye and the semiconductor conduction band electrons (inner-path recombination, CR(i)). In this pathway, the oxidized-dye cations and photo-generated electrons in the semiconductor recombine before dye-regeneration by the redox shuttle (e.g., I^-) can take place, which deteriorate the J_{SC} . The rate of inner-recombination process will be strongly dependent on the molecular structure and geometry adopted by the dye attached to the surface. On this line, dye-regeneration efficiency (η_{reg} or ϕ_{reg}) is a crucial factor in an operating DSSC (Figures 2, 3, and 4 (eq 8)).^{42,49–61} Low dye regeneration efficiency results in a drastic decrease of both V_{OC} and J_{SC} , because of faster charge recombination between photoinjected electrons and oxidized dyes (RC(i)). The other recombination process in DSSCs occurs between the oxidized redox mediator (e.g., I_3^-) in the electrolyte and the electrons from the semiconducting oxide electrode⁷⁵ (outer-path recombination, RC(ii), Figures 2 and 3). Actually, O'Regan and co-workers proposed that electron recombination to the electrolyte occurs predominantly by iodine reduction rather than reduction of triiodide.³⁶ The loss of injected electrons through this recombination process generates a dark-current (I_{dark}) that decreases the performances of a cell⁷⁶ (especially the V_{OC}). In fact, most of the dark current is generated at the TiO_2 /electrolyte interface where no dyes are adsorbed. To block this main recombination pathway and improve the performances of a DSSC, many strategies have been applied successfully. A first one consists in the incorporation of an adequate additive in the electrolyte such as 4-*tert*-butylpyridine^{77–81} (TBP) or related pyridine-based derivatives,⁸² guanidinium acids or salts^{81,83,84} (Figure 7). By modifying the

different way for each DSSC, and the compensation gain/loss between V_{OC} , J_{SC} , and F.F. will determine the net effect on the photovoltaic performances of the device. Some additives can cause an upward shift of the TiO_2 –CB (i.e., shifted at lower potential/higher energy), which may increase remarkably the V_{OC} because of the larger resulting potential-energy difference between the Fermi level of TiO_2 (nE_F) and the redox shuttle. A serious limitation of this strategy is, however, that, despite a possible increase in the V_{OC} , these kinds of additives concurrently may reduce the electron-injection efficiency of the dye (because of lifting up the TiO_2 –CB, ΔG_{ing} gets smaller). In addition, the eventual increase in recombination rate can also contribute to alter drastically the J_{SC} . By contrast, others additives can displace the TiO_2 band-edge in the opposite direction⁸⁵ (shifted at higher potential, i.e., stabilized at lower energy), which may result in an improvement of the J_{SC} (because of a larger ΔG_{ing}) but as a counterpart decrease the V_{OC} (because of the resulting overpotential between nE_F (TiO_2) and redox shuttle is smaller).

A similar strategy consists of the addition of a coadsorbent in the dye solution during the fabrication of the device, such as cholic acids or salts,^{80,86,87} which in some cases can improve simultaneously V_{OC} , J_{SC} , and F.F. The use of a coadsorbent (such as chenodeoxycholic acid, abbreviated as "CDCA" or "CHENO"), or incorporation of bulky hydrophobic groups in the molecular structure of the dye itself, can reduce the penetration of oxidized species of the electrolyte (e.g., I_3^- ions) to the metal oxide surface, which are others common strategies to reduce the dark current and improve the V_{OC} and F.F. Additionally, they also help to reduce dye aggregation (vide infra, discussed later in this section), which can contribute to improving significantly the J_{SC} by reducing Dye–Dye* deactivation pathways. In the same manner than the additives, a coadsorbent will also influence the movements of the TiO_2 edge-band and hence the V_{OC} and J_{SC} . Kim and co-workers developed recently multifunctional Y-shaped, low-molecular weighted, and hole-conducting (HC) acidic coadsorbents that can improve significantly the performances of a DSSC.⁸⁸ They display a 3-fold advantage: (1) they prevent aggregation of dyes, (2) they absorb light to short wavelength, which may help to improve the LHE of the DSSC device, and (3) owing to their low-lying HOMO level, they fasten dye-regeneration through a cascade-type hole-transfer processes.

One drawback of these strategies is that, either the sterically hindered dye-structure or incorporation of coadsorbents may reduce drastically the amount of adsorbed dyes on the TiO_2 surface, which would decrease the absolute amount of injected electrons from the dyes to the electrode and result in poorer photocurrent generation. Along this line, various other approaches involving the postpassivation of a dye-coated TiO_2 surface have been attempted with more or less success. For instance, Zhou and co-workers reported that the passivation by silanization of a dye loaded on TiO_2 -nanowire array electrodes is much more efficient than in the case of the commonly used TiO_2 nanoparticles films.⁸⁹ Because these 1D-nanowires have a more spatially accessible and organized structure, they facilitate the formation of uniform polysiloxane films to block more efficiently the interfacial recombination process at the interface, resulting in higher V_{OC} and PCE. The use of 1D- and well-ordered TiO_2 -nanomaterials^{22–25,58,59} as photoanodes, such as nanowires,^{89,90} nanorods,⁹¹ nanotubes,^{92,93} or nanobelt,⁹⁴ has received great attention and appears as a promising alternative to suppress more efficiently

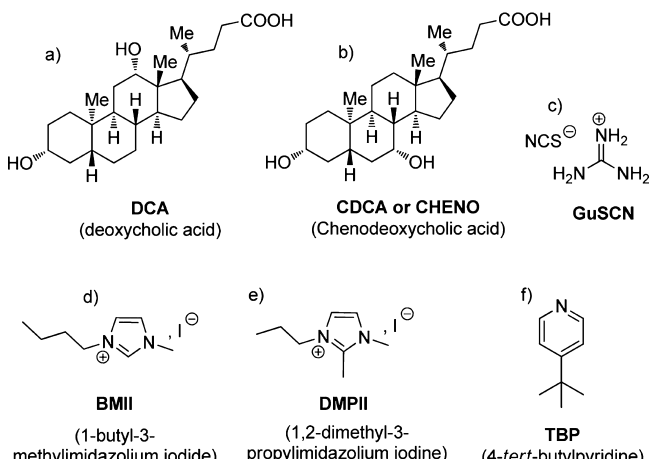


Figure 7. Molecular structures of coadsorbents (a and b) and additives (c–f) commonly used in DSSCs.

TiO_2 surface, these additives can affect strongly the rate of recombination at the TiO_2 /electrolyte interface (hence FF, V_{OC} , and J_{SC}), and at the same time can shift the band-edge of TiO_2 , which, on the other hand, will affect both V_{OC} and injection kinetics (hence J_{SC}). Accordingly, they will usually balance photovoltage against photocurrent to promote the V_{OC} with sacrifice in J_{SC} , or vice versa J_{SC} over V_{OC} . The concentration and kind of additives will influence these parameters in a

General ‘Diode equation’:

$$V_{OC} = \left(\frac{kT}{e} \right) \ln \left(\frac{I_{inj}}{n \sum_i k_i [A]_i} \right) \text{ (Eq 9)}^{250}$$

 k_i = electron rate constants to acceptors $[A]_i$ = concentration of the acceptors n = concentration of electrons in TiO_2 I_{inj} = electron flux to the semi-conductor. V_{OC} = open-circuit voltage k = Boltzman constant e = electron charge T = absolute temperature(n.b.: $\sum_i k_i [A]_i$ represent the summation of all recombination rate constants for injected electron to acceptors)Diode equation applied to the I_3^-/I^- redox couple mediator in a liquid electrolyte

$$V_{OC} = \left(\frac{kT}{q} \right) \ln \left(\frac{\eta \phi_0}{n_0 k_{et} [\text{I}_3^-]} \right) \text{ (Eq 10)}^{120}$$

 V_{OC} = Open circuit voltage k = Boltzman constant q = magnitude of the electron charge η = quantum yield for photo-generated electron ϕ_0 = incident photon flux n_0 = electron density of the conduction band of TiO_2 in the dark k_{et} = rate constant for recombination $[\text{I}_3^-]$ = concentration of I_3^- in the electrolyte

Diode equation applied to any redox couple mediator in a liquid electrolyte

$$V_{OC} = \frac{E_{CB}}{e} + \frac{kT}{e} \ln \left(\frac{n}{N_{CB}} \right) - E_{redox} \text{ (Eq 11)}^{15}$$

 E_{CB} = energy level of the semi-oxide conduction band (exactly the Fermi level (E_f)) e = elementary charge E_{Redox} = redox potential of the redox couple T = absolute temperature n = number of electrons in TiO_2 N_{CB} = effective density of states

Figure 8. Equations 9–11.

these recombination processes at the TiO_2 /electrolyte interface. Following a different strategy, Chang et al. reported the postadsorption of small molecules (a phenothiazine-based dye) on a porphyrin-sensitized TiO_2 anode surface, which is another approach to improve significantly the overall performance of a DSSC.⁹⁵ The small molecules adsorbed in the interstitial sites of porphyrin dyes play dual roles: they formed densely packed molecules on the surface that impede the approach of I_3^- to the TiO_2 surface, which greatly retard the back electron reaction and on the other hand enhance the spectral response of the cell.

The magnitude and direction of the interfacial dipole moment of a dye (which originates from donor–acceptor within the dye molecule in the excited state) also influence the shift of the electron conduction band (ECB) of TiO_2 , which is another way to enhance the V_{OC} .^{6,96,97} Thus, a proper arrangement of a dye on the oxide surface also affects positively the performance of a DSSC. Reductive^{98–101} or oxidative

quenching¹⁰² of the excited dye by the redox shuttle are two other possible pathways but were evidenced only in few cases for conventional n-type DSSCs. The type of sensitizer and concentration of redox couple in the electrolyte will determine the extent of these quenching processes, which in most cases remain rather limited (at least for porphyrin dyes). The reductive quenching may still allow an alternative pathway for dye-sensitization if the reduced dye (Dye^-) is capable of injecting an electron into the metal oxide semiconductor. This competitive electron-injection pathway can be significant if the electron-injection rate of the excited dye is rather low, and usually requires, however, an extremely high concentration of iodine, which in turn strongly increases recombination rate between I_3^- and injected TiO_2 electrons. For instance, a significant increase in reductive quenching was observed for the ruthenium dye Z-907Na upon high iodine concentration (reductive quenching of Dye^* up to ~25%), while Ru(II)

N719 seems insensitive to this process. Last but not least, dye aggregation phenomena,^{103,104} ubiquitous in DSSC, will most often open the way to additional deactivation channels through Dye–Dye* interactions (intermolecular energy transfers) enhancing nonradiative decay pathways, and/or dipole–dipole interactions (exciton delocalization).¹⁰⁵ The well-known behavior of porphyrins to undergo aggregation by π – π stacking¹⁰⁶ (ordered *J*, *H*, or disordered aggregates),^{107–111} and the impact on the performance of a DSSC,¹¹² will be commented on in the different sections. *J* or *H* aggregates are two ideal cases of highly ordered molecules, and as for porphyrins, very few examples are known to form exclusively one pure type or the other. In *J* aggregates, porphyrins are organized in one dimension within their transition dipole moment aligned parallel with the line that joins the molecular centers, in a “head-to-tail” fashion. *H* aggregates, as well, are also organized in one dimension but within the transition dipole moments of the monomeric species aligned perpendicularly to the line of the centers, in a “face-to-face” fashion. As predicted by theory and supported experimentally, a red-shift in the UV–vis absorption spectra in comparison with that of the monomeric species is commonly admitted as a proof for formation of *J* aggregates, whereas a blue-shift is assigned to *H* aggregates (additionally accompanied by broadening of the absorption bands, especially for *H* aggregates). In the overwhelming majority, dye aggregation is detrimental for the performance of a DSSC and is thoroughly sought to be avoided. However, some works evidenced that this is not necessarily true. For instance, if disordered and *H*-type porphyrin aggregates do follow this trend, the *J*-type, on the contrary, can benefit strongly to the performance of a cell.^{47,113–115} It has been proposed that well-ordered porphyrin *J* aggregates display better spectral coverage and exciton dynamics than discrete species or other aggregates, resulting in better exciton-coupled charge-transfer process that improves the photoinduced charge separation at the porphyrin/TiO₂ interface. To achieve high power conversion efficiency in a DSSC,¹¹⁶ an ideal sensitizer should bind strongly the semimetal oxide surface,¹¹⁷ reach high electron injection (ϕ_{inj}), electron collection (η_{coll}),¹¹⁸ dye regeneration (η_{reg}), and light harvesting efficiencies (LHE), avoid recombination processes, absorb over the wider range of the solar spectrum, and be stable enough over a long period of time.^{119,120}

1.2. Porphyrins for DSSCs

To be useful for a DSSC device, a porphyrin sensitizer must possess at least one anchoring group (or bridged-binding group) in its molecular structure to allow the attachment of the dye to the TiO₂ metal oxide.¹²¹ Inevitably, the anchoring moiety is also an inherent acceptor, and simultaneously acts as an electron-withdrawing group (EWG). A porphyrin features eight β and four meso positions that are potentially available for functionalization with one or more anchoring groups and other substituents. This extensive number of functionalizable positions of the macrocycle (12) offers a large panel of possible molecular designs for porphyrin dyes. Historically, the first use of porphyrinoid sensitizers in TiO₂-DSSCs was reported in 1993 for β -substituted chlorophyll derivatives and related natural porphyrins, reaching a maximum PCE of 2.6%.¹²² Since then, the performance of DSSCs based on β -substituted porphyrins had not progressed for more than 11 years, until Grätzel and co-workers reported between 2004–2005 β -porphyrins dyes reaching PCE between 4.8–5.6%^{123,124} and 7.1% in 2007.¹²⁵ In 2011, Ishida et al. reported one of the best

performing β -linked porphyrin dyes to date (tda-2b-bd-Zn) with a PCE of 7.5% (Figure 9).^{126,127} More recently, covalently linked porphyrin dimers^{128–133} trimer/tryad,^{134–136} π -elongated porphyrins¹³⁷ fused with naphthalene,¹³⁸ antracene,^{139–142} perylene,¹⁴³ quinoxaline,^{144–146} or porphyrin itself^{128,147} (fused-porphyrin dimers) were reported as promising dyes featuring extended absorption in the visible (red) and NIR regions. Since 2009 and until now, *meso*-porphyrins have been the most efficient class of porphyrin sensitizers reported in DSSCs.^{148–158} In 2011, Grätzel and collaborators reported the *meso*-porphyrin dye YD2-o-C8 achieving a PCE of 11.9% in conjunction with the cobalt(III/II) tris(2,2'-bipyridine)-based redox electrolyte and up to 12.3% when cosensitized with another organic dye which, until recently, had been the record of efficiency in DSSC over the past three years.⁶⁵ This record was recently broken (February 2014) with the dye SM315 reported by Nazzeruddin and co-workers, achieving an unprecedented PCE of ~13%.¹⁵⁹ Although β -linked^{160–164} and fused^{128,137–147} porphyrins remain extensively studied, and appear as promising alternative sensitizers,^{165–167} this review aims to survey the recent progress of *meso*-substituted porphyrins in DSSCs. Additionally, noncovalent self-assembled systems of metallo-porphyrin through axial coordination remain marginal in DSSCs and will be only mentioned but not reviewed herein.^{168–170}

1.3. Meso-Substituted Porphyrins for DSSCs

The relative ease of synthesis and high-versatility of their molecular structure¹⁷¹ offer many possible designs for *meso*-porphyrin dyes (Figure 10). Free base porphyrin (H2-Por) and zinc porphyrin (Zn(II)-Por) remain by far the most studied in DSSCs. Zinc porphyrin dyes are usually preferred to other metallo-porphyrins, such as Cu, Pt, Mg, Mn, Sn, and other metals for many reasons. First, metallo-porphyrin dyes (and in particular Zn(II)-Pors) usually exhibit higher short circuit current (J_{SC}) in TiO₂-sensitized cells than their free-base porphyrin analogue, which most often results in higher PCE. The higher J_{SC} in cells sensitized with Zn(II)-Por dyes compared to H2-Pors is explained first by the difference of their excited state levels.¹⁷² Zn(II)-Pors exhibit a longer-lived singlet excited state (>1 ns) without singlet/triplet mixing and display adequate HOMO–LUMO levels, with their LUMO lying beyond the conduction band of TiO₂, whereas their HOMOs remain lower than the redox couple of the electrolyte, two primordial factors to reach efficient electron injection and dye regeneration, respectively (Figure 11).

Next, zinc porphyrin shares similar photophysical properties in absorption/emission than its free-base analogues, but have much lower oxidation potentials (typically, $\Delta V \approx 200$ –400 mV). As a first consequence the HOMO level of Zn(II)-Pors, determined by their first oxidation potential, lies typically about 200–400 mV higher than their free-base analogue. Thus, in principle, the resulting lower driving force for dye regeneration (ΔG_{reg}) of Zn(II)-Por with respect to H2-Por should lead to less efficient dye regeneration (η_{reg}). However, based on the recent studies of Daeneke et al.^{49,60,61} (vide supra), a larger driving force would have only minor effects on dye regeneration efficiency if the potential difference between the dye and electrolyte satisfies the minimum required value. As the first oxidation potential of most zinc porphyrin dyes usually lies at around ~+0.8–1.2 V (versus NHE), the resulting potential difference ($\Delta E \approx 400$ –800 mV) with a standard I₃[–]/I[–] redox couple ($E \approx +0.4$ V vs NHE) most often remains by far sufficient to ensure an efficient

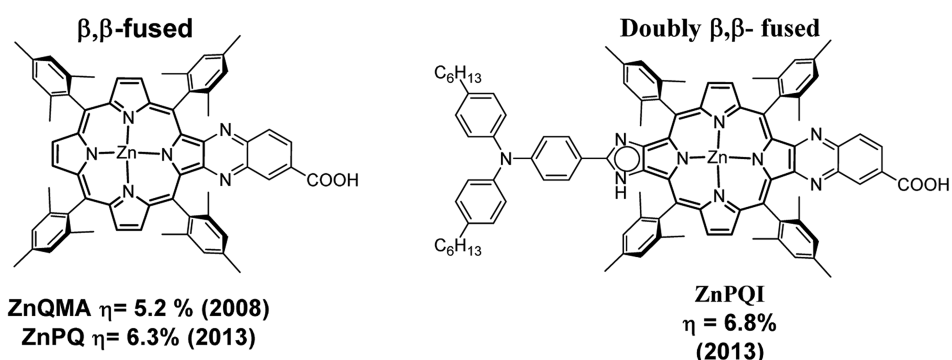
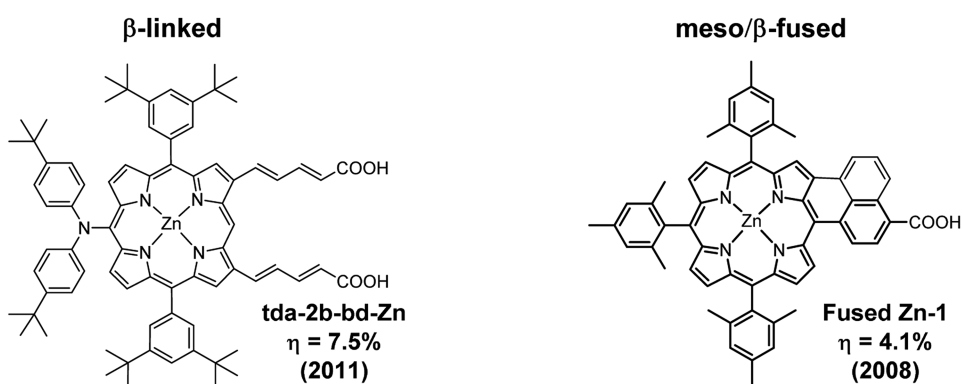
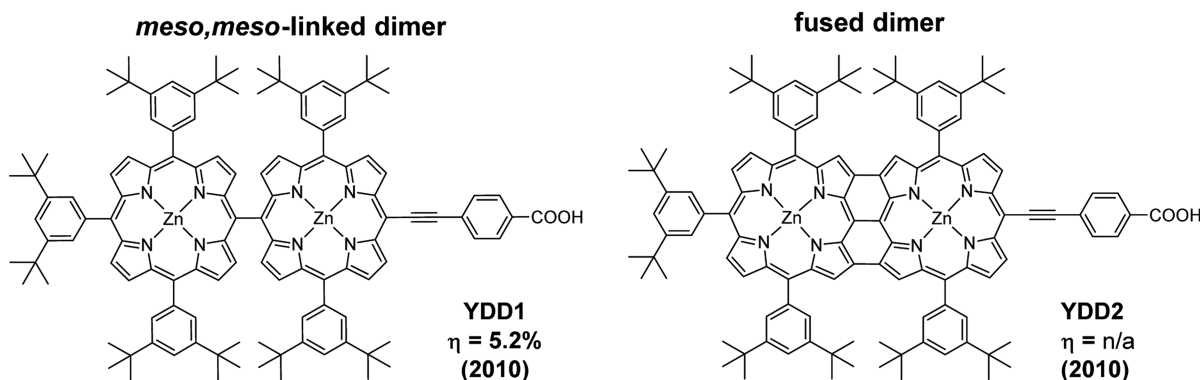
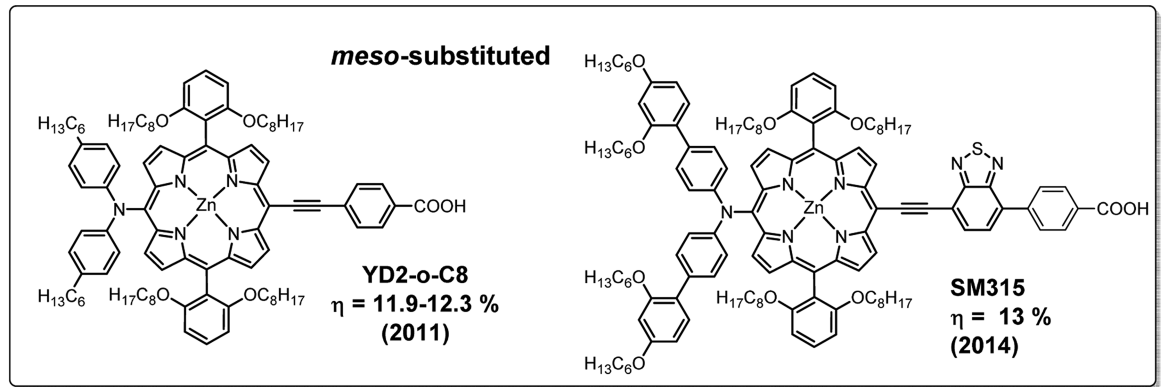


Figure 9. Some representative examples of performing porphyrin dyes in DSSCs by class: YD2-o-C8,⁶⁵ SM315,¹⁵⁹ YDD1,¹²⁸ YDD2,¹²⁸ Tda-2B-db-Zn,¹²⁶ Fused Zn-1,¹³⁸ ZnQMA/ZnPQ,^{144–146} and ZnPQI.¹⁴⁶

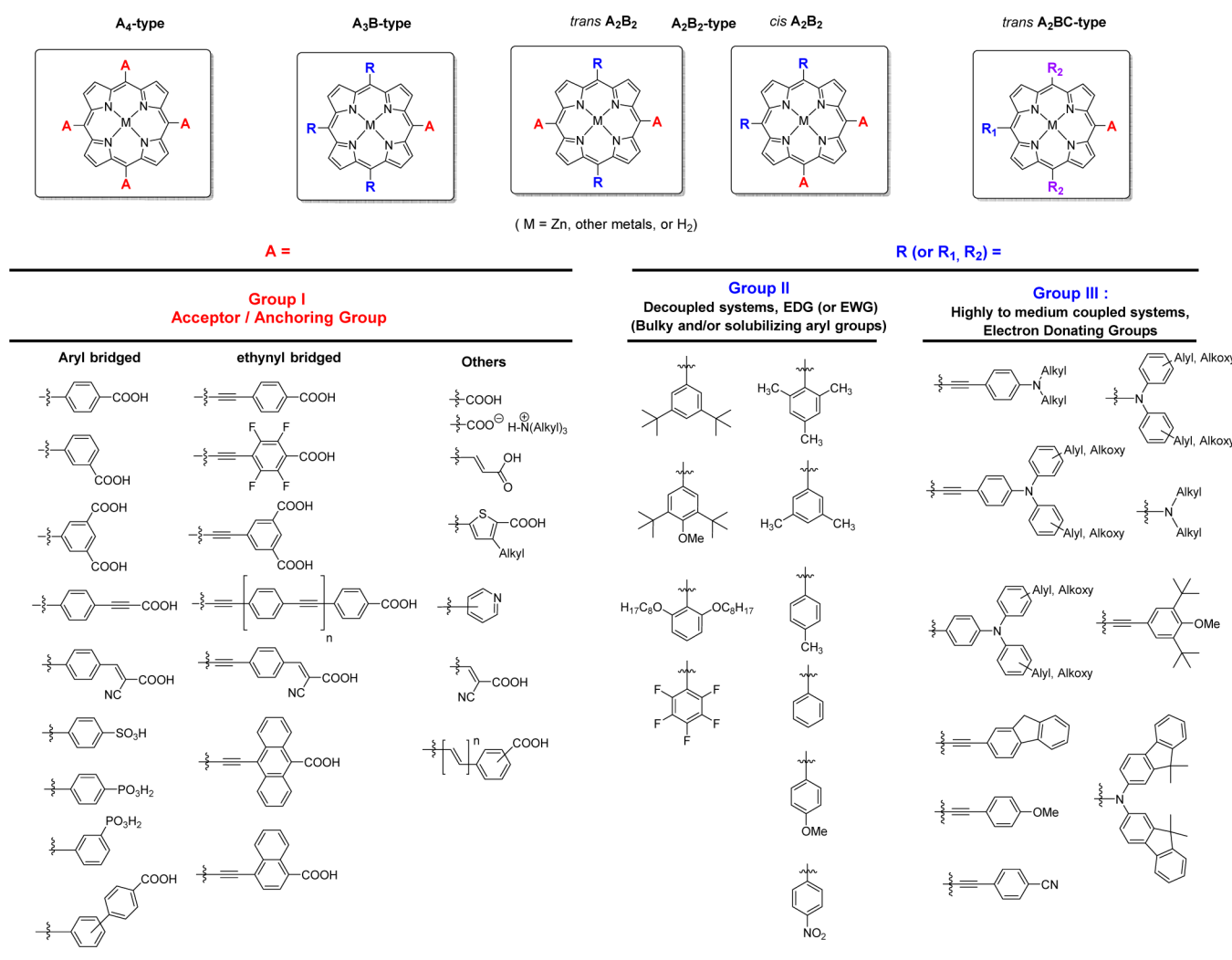


Figure 10. General structures of A4-, A3B-, A2B2-, and A2BC-type meso-substituted porphyrin dyes and general overview of some appended meso substituents: acceptor/anchoring, donor, and solubilizing/bulky groups (nonexhaustive list).

dye-regeneration in an operative DSSC. Thus, the destabilized HOMO level of a Zn(II)-Por relative to H2-Por analogue does not appear to be a limiting factor for dye regeneration, and hence for the performances of the cell. On the other hand, however, since the zero-zero excitation energies (E_{0-0}) of H2- and Zn(II)-Pors, obtained from the onset in absorption/emission, are likewise similar (i.e., similar HOMO–LUMO gap), the oxidation potential energy of their excited state (i.e., LUMO level, with $E_{0-0^*} = E_{\text{ox}} - E_{0-0}$) is equally negatively shifted from their HOMO level. Since the conduction band of TiO₂ lies at around −0.5 V, the upper-lying LUMO level of Zn(II)-Pors usually results in a better overlap with the TiO₂ CB and increases the driving force for electron injection of the exited zinc-porphyrin in the semiconductor. This confers to ZnPors faster and hence potentially more efficient electron injection than their free base analogues. Recently, some theoretical computational studies have been devoted to rationalizing the working principles of zinc porphyrins in DSSCs¹⁷³ and attempted to predict new and potentially more efficient Zn-porphyrin sensitizers.^{174–178}

Nevertheless, in practice, some free base-porphyrin dyes have been reported in DSSCs with better performances than their corresponding ZnPors under the same conditions. Many works also evidenced that the charge recombination rates

might increase considerably for Zn(II)-porphyrins dyes if their positively charged zinc center metal ion is directly exposed to the electrolyte, which tends to trap more easily the I₃[−] ions, and therefore can lead to lower efficiencies. This issue can be minimized whether incorporating long and bulky hydrophobic chains in the molecular structure of the porphyrin, and/or adding a hydrophobic coadsorbent in the dye solution, such as cholic acids, acting as a barrier to protect the zinc porphyrin core from the I₃[−] electrolyte interface. Another main advantage of these strategies is, of course, to prevent π–π stacking aggregation between porphyrins, a factor of high-importance toward the performance of the dyes in the solar cell.

Other advantages of zinc-based porphyrins are their relative high thermal stability, robustness under light exposure, and avoidance the use of environmentally toxic (Sn, Hg) or expensive, rare metals (such as Pt, Au, and Ru), conditions that will be required to manufacture commercial modules. Finally, from the synthetic and characterization point of views, zinc porphyrins are easy to access from the metalation of their corresponding free base analogues (usually quantitative yield), their zinc center metal ion is relatively strongly coordinated to the macrocycle (not labile such as Mg^{II}) and are not paramagnetic (not as Cu^{II} Porphyrins), the latter allowing

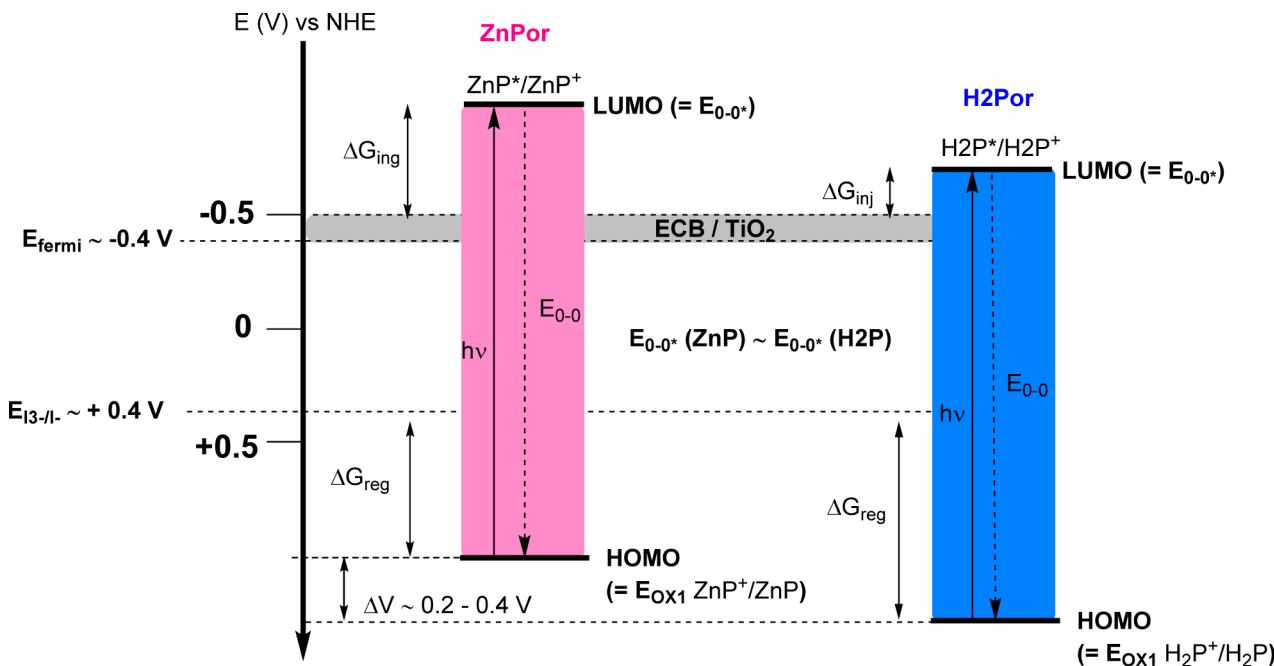
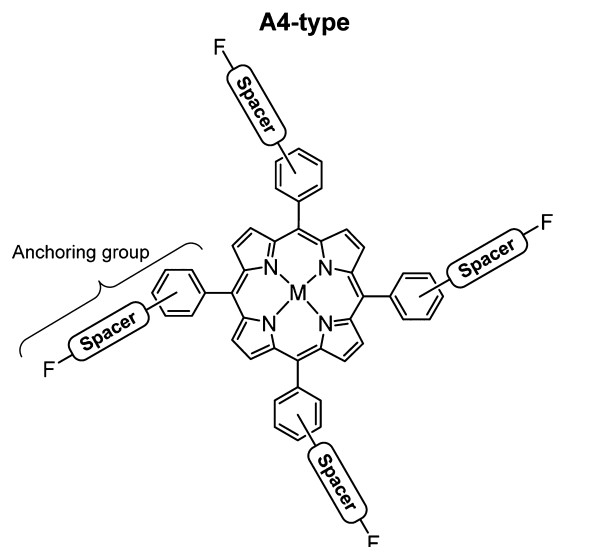


Figure 11. Comparison of the MO levels of free-base and zinc porphyrin sensitizers in a conventional DSSC using a standard iodine-based electrolyte (ZnPor or $\text{ZnP} = \text{Zn(II)}$ porphyrin, H2Por or H2P = free-base porphyrin).

^1H and ^{13}C NMR characterizations, to cite a few advantages. Various anchoring groups incorporating in their structure different kinds of bridges/spacers (see Figure 10) have been used to anchor porphyrin dyes to the TiO_2 surface,^{121,160} the most known and used being carboxyphenyl, ethynylcarboxyphenyl, cinnamic, (cyano)phenylacrylic, acrylic, or cyanoacrylic acid groups. Others anchoring groups appear as plausible alternatives for organic dyes in DSSCs, such as catechol,^{179,180} or more recently rhodanine,¹⁸¹ azo-bridged salicylic acid,¹⁸² gem-silanediols,¹⁸³ tetrazole,¹⁸⁴ pyridyl,^{185,194} and other related nitrogen containing heterocycles¹⁹⁵ (carboxypyridyl,¹⁹⁶ cyano-pyridyl,¹⁹⁷ pyridyl N-oxide,¹⁹⁸ pyridyl N-oxide carboxylic acid,¹⁹⁹ hydroxyquinoline,^{200,201} benzothienopyridyl,²⁰² bipyridyl,²⁰³ and pyrimidine²⁰⁴). The most studied and widely used remain, however, those based on carboxylic acid, which turned out to give the best performances to date.

2. A4-TYPE DESIGN FOR MESO-SUBSTITUTED PORPHYRIN DYES

The simplest design to build a porphyrin dye, and the easiest from the synthetic point of view, is the highly symmetrical A4-type, for which the four meso positions are grafted with the same substituents (Figure 12). To date, almost all A4-type porphyrin dyes reported and studied in DSSC are tetrakis-(phenyl)-substituted, easily obtained by condensation of the corresponding aryl aldehyde "A-CHO" and pyrrole under acidic conditions (Lindsey or Adler-Longo methods).¹⁷¹ Anchors with various types of functional binding groups have been used and tested for porphyrin dyes,^{121,160} such as carboxylic, phosphonic, or sulfonic acid; the most commonly and widely used remains however carboxyl-based. As a typical example, the tetrakis(4'-carboxyphenyl)porphyrins, free base ($\text{H2-}p\text{TCPP}$) and zinc ($\text{Zn-}p\text{TCPP}$), have been the former and by far the most studied over more than 20 years, and represent nowadays benchmarks in porphyrin-DSSCs. Ma et al.²⁰⁵ studied and compared the effect of different functional groups on the photochemical and photosensitization of a sulfonic acid



Spacer = None, or aryl, ethyne, etc...

F = Functional binding group (-COOH, -SO₃H, -PO₃H, etc...)

M = H₂, Zn, other metals

Figure 12. Common design for A4-type tetrakis(phenyl)-substituted meso-substituted porphyrin dyes.

anchored tetrakis(phenyl)-substituted porphyrin ($\text{H2-}p\text{TSPP}$), in comparison with the carboxylic acid analogue $\text{H2-}p\text{TCPP}$, together with a reference porphyrin without anchoring group, namely H2-tetrakis(phenyl) porphyrin ($\text{H2-}p\text{TPP}$) (Figure 13 and Table 1, entry 1). The PCE of the cells followed the order $\text{H2-}p\text{TCPP}$ (0.36%) \gg $\text{H2-}p\text{TSPP}$ (0.04%) \gg $\text{H2-}p\text{TPP}$ (0.006%). These results emphasize the high importance of the nature of the functional binding group toward the efficiency of the cells. They evidenced that the binding strength to the TiO_2 surface decreased drastically in the order $\text{H2-}p\text{TCPP} > \text{H2-}p\text{TSPP} > \text{H2-}p\text{TPP}$. Consequently, the amount of adsorbed

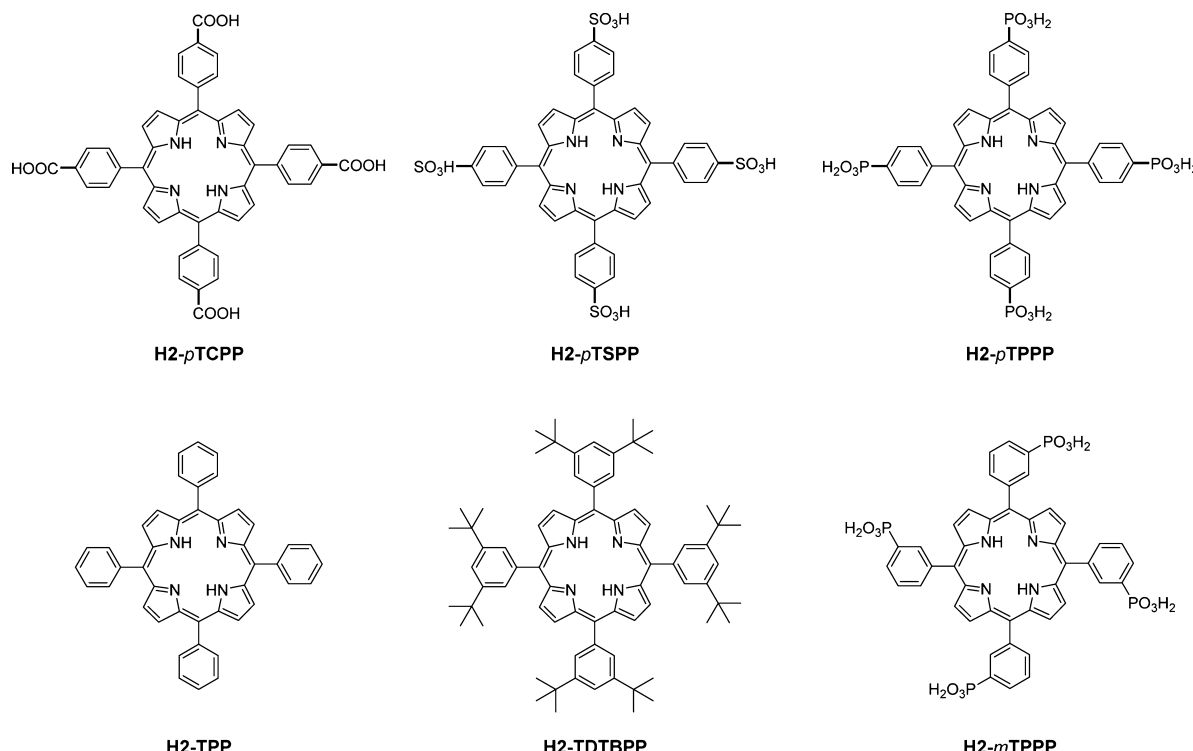


Figure 13. Tetrakis(phenyl)-substituted free base porphyrin dyes without and with anchoring groups of different nature (TCPP = tetrakis(carboxyphenyl) porphyrin, TSPP = Tetrakis(sulfonatophenyl) porphyrin, TPPP = tetrakis(phosphonatophenyl) porphyrin, TPP = tetrakis(phenyl) porphyrin, TDTBPP = tetrakis(3,5-di-*tert*-butylphenyl) porphyrin; refs 205, 207, 208, and 211).

Table 1. Photovoltaic Data for TiO₂-DSSCs Sensitized with TCCP, TSPP, TPPP, and TDTBPP

entry	dye	max IPCE (%)	V _{OC} (mV)	J _{SC} (mA·cm ⁻²)	F.F. (%)	η (%)	ref
1 ^a	H2-pTCPP	40	360	2.70	37	0.36	205
	H2-pTSPP	10	290	0.630	44	0.04	
	H2-TPP	2	340	0.320	5.1	0.006	
2 ^b	H2-pTCPP+DCA	60	344	0.928	61	0.69 ^c (0.51) ^d	207
	H2-pTCPP	60	287	0.471	55	0.26 ^c (0.20) ^d	
	H2-TDTBPP	1	306	0.072	49	0.04 ^c (0.03) ^d	
3 ^e	H2-pTCPP+DCA	55	460	0.17	62	3.5	208
4 ^f	H2-pTCPP	10	n/a	n/a	n/a	n/a	211
	H2-pTPPP	8	n/a	n/a	n/a	n/a	
	H2-mTPPP	8	n/a	n/a	n/a	n/a	

^aData reported under white light illumination (100 mW·cm⁻²). ^bData reported under low light-intensity illumination (37.85 mW·cm⁻²). ^cReported η values were corrected for 24% power loss due to attenuation caused by the FTO glass. ^dCalculated η values without corrections based on the data given in the article (J_{SC}, V_{OC}, F.F., and P_{in}). ^eData reported under low light-intensity illumination (1.4 mW·cm⁻²). ^fPower of irradiance and illumination conditions not specified.

dye on the surface for H2-pTCPP (4.3×10^{-8} mol·cm⁻²) was estimated to be seven times higher than H2-pTSPP (6.2×10^{-9} mol·cm⁻²) and 84 times higher than H2-TPP (5.1×10^{-10} mol·cm⁻²). H2-pTCPP and H2-pTSSP, bearing respectively carboxylic and sulfonic acid groups, are anchored to the TiO₂ surface mainly by chemical adsorption, while H2-TPP without anchoring group is anchored only by physical adsorption. These results, as many others, evidence that carboxyl is an efficient functional binding group to ensure a large and optimal adsorption of a porphyrin dye onto the TiO₂ surface. It was evidenced that carboxyl groups react spontaneously with the hydroxyl groups of the TiO₂ surface to form chemical or hydrogen bonding with relative good stability.²⁰⁶ Although the short circuit-current is directly dependent on the amount of adsorbed dye, and hence to the overall performances of the

DSSC, various independent works also evidenced that the superior efficiency of carboxyl-based anchors are coming from their ability to promote additional strong electronic interactions with TiO₂. The bonding of a carboxyl group to the surface can take place by different binding modes, from chemical bonding through carboxy(ester) linkage (unidentate, chelating or bridging bidentate) to H-bonding, allowing strong electronic coupling between the dye and TiO₂, thus favoring fast and efficient electron injection process. Jasieniak et al. also studied in detail H2-pTCPP in TiO₂-DSSC, together with H2-TDTBPP as benchmark (H2-tetrakis(3,5-di-*tert*-butylphenyl) porphyrin (Table 1, entry 2)).²⁰⁷ It is worth noticing that the use of chenolic acid (CHENO) as coadsorbent could help to reduce dye aggregation of H2-pTCPP, resulting in a significant increase of performances and PCE of the cell, from 0.26% to 0.69%

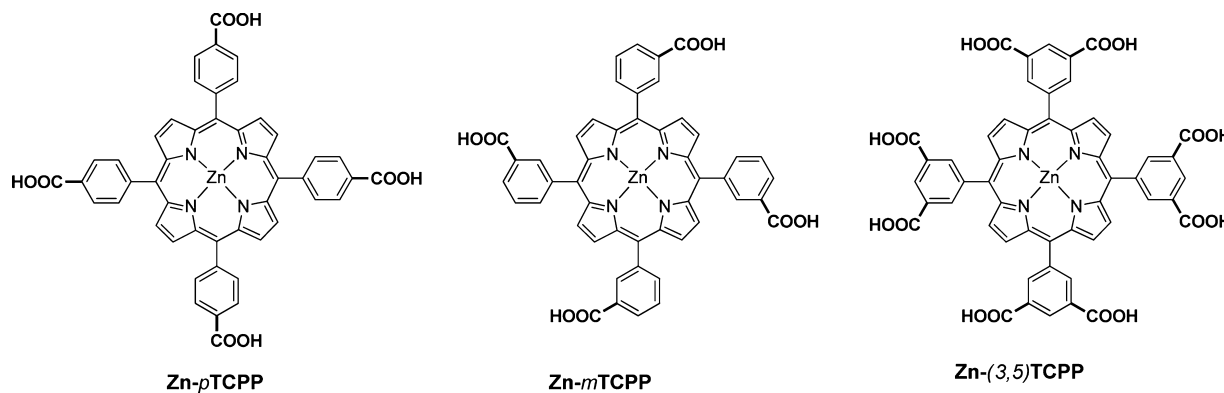


Figure 14. Molecular structures of *meta*- and *para*-tetrakis(carboxyphenyl) ZnTCPP and tetrakis(isophthalic acid) Zn-(3,5)TCPP zinc porphyrins: effect of the substitution position of the anchoring group on the photovoltaic performances (refs 152, 153, 212, and 213).

without and with CHENO, respectively. The best efficiency obtained for the sensitizer H2-*p*TCPP in TiO₂-DSSC was reported by Cherian and Wamser in 2000, reaching a PCE of 3.5% under low-light intensity (1.4 mW·cm⁻²) using CHENO as coadsorbent (Table 1, entry 3).²⁰⁸

The use of phosphonic/phosphinic acid anchor groups and their type of bonding to the TiO₂ surface are less known in porphyrin-based DSSCs. For Ruthenium-polypyridyl complexes, it was evidenced that dyes anchored through phosphonic acid groups bind much stronger to the TiO₂ surface than through carboxylic acid (about 80 times stronger) but give similar cell efficiencies.²⁰⁹ However, unlike carboxyl-anchored dyes, phosphonic analogues are not displaced by water and show excellent performance over a wide range of pH up to 9. Recently, Duarte et al. reported a series of phthalocyanine dyes anchored through either carboxylic or phosphinic acid groups. Their results showed that the carboxylic acid anchor leads to a higher amount of adsorbed dye than does the phosphinic acid analogue, thus giving slightly higher solar conversion efficiency of the sensitizer in DSSC. However, the phosphinic acid anchor was shown to have stronger binding properties than the carboxylic one, which is a major advantage to improve the durability of a DSSC.²¹⁰ Odobel et al. reported a series of phosphonato- and carboxyphenyl functionalized porphyrin dyes (H2-*p*TCPP, *p*-TPPP, and *m*-TPPP, see Figure 13 and Table 1, entry 4) and claimed that the nature of the functional group ($-\text{PO}_3\text{H}$ or $-\text{COOH}$) has a little influence toward the performance of the cells in comparison with the substitution position of the anchoring group.²¹¹ It is indeed known and well-established that apart from the intrinsic nature of the binding group the substitution position have a drastic influence toward the performances of the cell, caused by changes in both the binding geometry of the dye onto the TiO₂ surface and electronic interactions between dye and TiO₂ (mediated through the spacer linking binding group and porphyrin). As a straightforward example, the regiosomers Zn-*p*TCPP and Zn-*m*TCPP, differing only by the para or meta position of the carboxyl group attached to the meso-phenyl substituents, display very different behaviors and performances in TiO₂-DSSCs (Figure 14 and Table 2, entries 1–3).^{153,153,128,213} In comparison with Zn-*p*TCPP sensitized TiO₂-DSSCs, Zn-*m*TCPP most usually display much larger J_{SC} ascribed to a better electron injection efficiency and significant greater V_{OC} . Surprisingly, dye Zn-(3,5)TCPP bearing four isophthalic acid groups (i.e., both meta positions of the phenyls are occupied by a carboxyl group) reported by Campbell et al. displayed superior performances than Zn-*p*TCPP in TiO₂-DSSC

Table 2. Representative Examples of Photovoltaic Data Reported in the Literature for TiO₂-DSSCs sensitized with Zn-*p*TCPP, Zn-*m*TCPP, and Zn-(3,5)TCPP

entry	dye	V_{OC} (mV)	J_{SC} (mA·cm ⁻²)	refs
1 ^a	Zn- <i>p</i> TCPP	360	0.85	153 and 212
2 ^b	Zn- <i>p</i> TCPP-[S] ^c	440	0.39	153 and 213
	Zn- <i>m</i> TCPP-[S] ^c	510	3.33	
3 ^d	Zn- <i>p</i> TCPP	204	0.079	152
	Zn- <i>m</i> TCPP	363	0.41	
	Zn-(3,5)TCPP	285	0.15	

^aData reported under white light illumination of low intensity (160 W·m⁻²). ^bData reported under full sun conditions (1000 W·m⁻²).

^cThese dyes were used under their carboxylate triethylammonium salts (vide infra). ^dPower of irradiance and illumination conditions not specified.

but much lower than the Zn-*m*TCPP analogue under the same experimental conditions.¹⁵² The lower dye surface coverage of Zn-(3,5)TCPP is believed to be the main factor responsible for its lower performances in DSSC.

In 2000, Cherian and Wamser investigated in details the nature of binding mode of H2-*p*TCPP on the TiO₂ surface, using X-ray photoelectron spectroscopy (XPS) and resonance Raman spectroscopy (RRS).²⁰⁸ They concluded that H2-*p*TCPP dyes bind to the surface in a variety of different adsorption modes and suggested the predominance of porphyrin–porphyrin lateral interactions. In 2007, Galoppini and co-workers further investigated deeper Zn-*p*TCPP, Zn-*m*TCPP, and other meso-substituted tetra(carboxyphenyl) Zn(II)-porphyrin dyes with rigid linkers of various lengths (P: phenyl, PP: biphenyl, and PEP: diphenylethylnyl) bounded to various metal oxide surfaces ZnO, ZrO₂, and TiO₂ (Figure 15 and Table 3).²¹³ They rationalized the effect of both the position (meta or para) of the anchoring group and the length of the spacer toward the photoelectrochemical properties and efficiencies of these dyes in DSSCs, using various spectroscopic techniques (UV and IR). Noteworthy, they obtained similar performances of the cells whether using the dyes under carboxylic acid forms (COOH) or their corresponding ammonium carboxylate salts (COONET₃). Although the reason is not clear, the free carboxylic acid forms of porphyrin dyes are usually preferred to their corresponding salts (sodium or tetrabutylammonium) because they tend to give superior cell performances.

While Zn-*p*TCPP binds the surface in a vertical/perpendicular binding mode geometry (“edge-to-face” fashion: modes I and II; Figure 16, left), the meta-substitution pattern

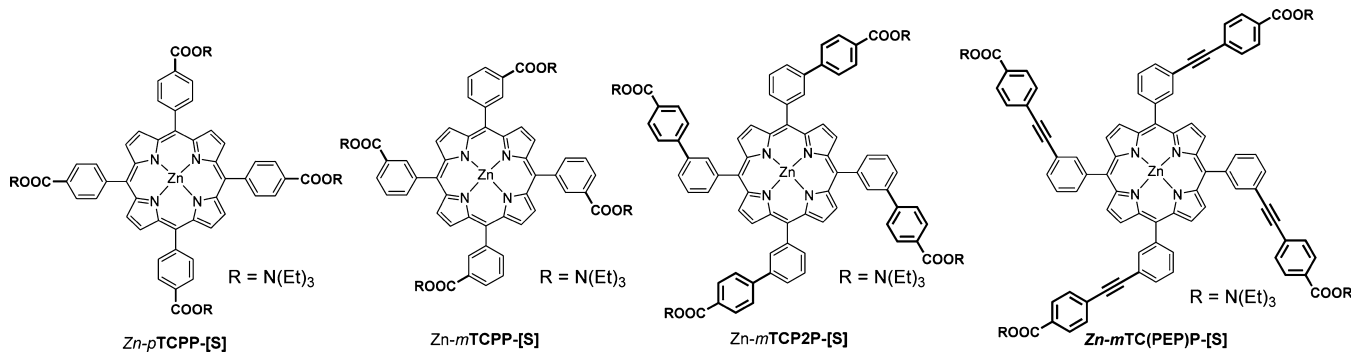


Figure 15. Molecular structures of tetrakis(phenyl carboxylate) triethylammonium salts zinc porphyrins reported by Galoppini and co-workers (ref 213).

Table 3. Dye-Loading and Photovoltaic Parameters of the TiO₂-DSSCs Sensitized with Zn(II)-Porphyrins *p*/m-TCPP-[S], mTCP2P-[S], and *m*TC(PEP)P-[S] under Full Sun Conditions (Power 100 mW·cm⁻²)^a

dye	dye loading ^b ($\mu\text{mol}\cdot\text{g}^{-1}$)	IPCE Soret (%)	V_{OC} (mV)	J_{SC} ($\text{mA}\cdot\text{cm}^{-2}$)	F.F. (%)	η^c (%)
Zn- <i>p</i> TCPP-[S]	26	18.5	440	0.39	54	0.09 ^c
Zn- <i>m</i> TCPP-[S]	20	58.6	510	3.33	41	0.70 ^c
Zn- <i>m</i> TCP2P-[S]	19	56.9	500	3.72	42	0.78 ^c
Zn- <i>m</i> TC(PEP)P-[S]	12	25.3	430	1.36	45	0.26 ^c

^aData derived from ref 213. ^bCalculated amount of adsorbed dyes on the TiO₂ films (values expressed in μmol of dyes per gram of TiO₂ particles).

^cPCE values (η) were not reported, and calculated from eq 1 and the information given in the article for ref 213.

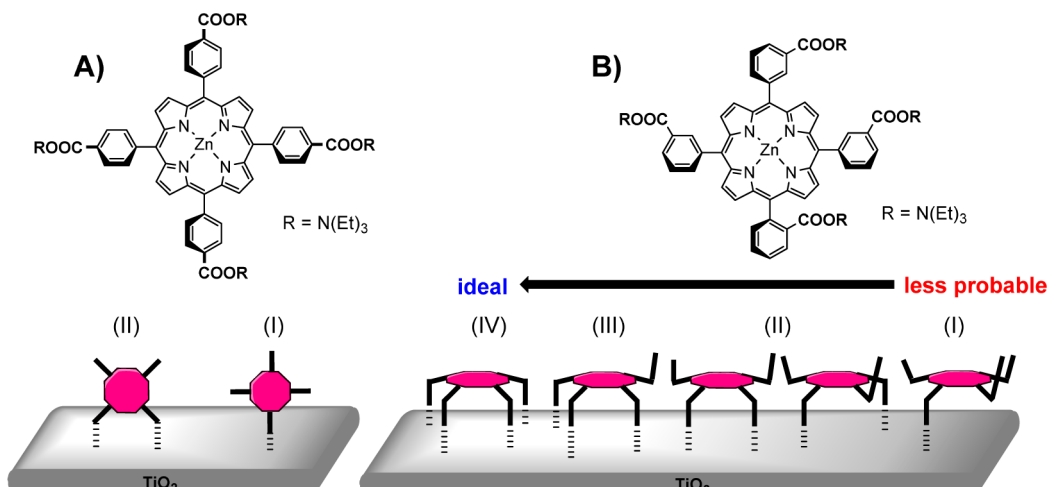


Figure 16. Schematic possible binding geometries of the dyes onto the TiO₂ surface: (A) edge-to-face fashion binding of Zn-*p*TCPP-[S] and (B) face-to-face fashion binding of meta derivatives Zn-*m*TCPP-[S], Zn-*m*TCP2P-[S], and Zn-*m*TC(PEP)P-[S]: ideal case of a 4-fold binding mode (IV), and three (III), two (II), and one- (I) other possible binding modes. Adapted with permission from ref 213. Copyright 2007 American Chemical Society.

of Zn-*p*TCPP-[S], Zn-*p*TCP2P-[S], and Zn-*p*TC(PEP)P-[S] allows a coplanar attachment of the dye, (“face-to-face” fashion: modes I–IV; Figure 16, right). The flat binding modalities of these meta derivatives are expected to allow multibinding attachment of the four available carboxyl groups. As commented by the authors, the 4-fold binding mode is of course an ideal behavior, but from statistical considerations on the relative position of the carboxyphenyl groups (considering that rotation of a *meso*-phenyl is sterically restricted around a porphyrin macrocycle), one can expect that at least three anchoring groups should be involved in the coplanar attachment of the dye to the surface. However, despite the presence of numerous anchoring groups orientated in a favorable manner, the surface coverage of these dyes was found considerably lower ($12\text{--}20 \mu\text{mol}\cdot\text{g}^{-1}$)²¹³ than Zn-*p*TCPP-[S] ($26 \mu\text{mol}\cdot\text{g}^{-1}$)²¹³ or H2-*p*TCPP

($47\text{--}77 \mu\text{mol}\cdot\text{g}^{-1}$).²⁰⁸ That lies in the fact that the dyes binding parallel the surface need more space to accommodate than in a perpendicular/vertical fashion, the latter allowing a more densely packing of the porphyrins. The superior performances obtained for Zn-*m*TCPP-[S], Zn-*m*TCP2P-[S], and Zn-*m*TC(PEP)P-[S] were therefore ascribed to a better electron injection efficiency of the porphyrin rings that lie flat on the surface. The distance between the porphyrin macrocycle and the surface was also found to be strongly influent toward the cell performance. Whereas the shorter bridges in Zn-*m*TCPP-[S] and Zn-*m*TCP2P-[S] dyes both result in much higher performances of the cell than Zn-*p*TCPP (in particular a $\sim 8\text{--}9$ fold enhancement of the J_{SC}), the longer bridge in Zn-*m*TC(PEP)P-[S] results in a drastic drop of its photovoltaic performances (only a ~ 3 fold enhancement of the J_{SC}).

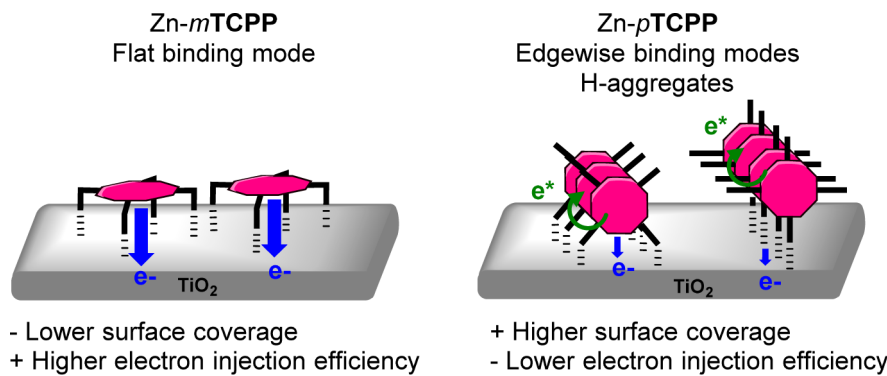


Figure 17. Left: main deexcitation channel for a photoexcited Zn-*m*TCPP (blue arrows): electron injection into the substrate conduction band. Right: additional deexcitation channel (green arrows) enabled by the stacked geometry of the Zn-*p*TCPP molecules: exciton delocalization through dipole–dipole interaction. Adapted with permission from ref 214. Copyright 2012 American Chemical Society.

This drop in performance may be first explained by an important decrease of the amount of adsorbed dyes on the surface for Zn-*m*TCP(PEP)P-[S] ($12 \mu\text{mol}\cdot\text{g}^{-1}$) compared to Zn-*m*TCPP ($20 \mu\text{mol}\cdot\text{g}^{-1}$) or Zn-*m*TCP2P[S] ($19 \mu\text{mol}\cdot\text{g}^{-1}$). Next, the better performances obtained for Zn-*m*TCP2P[S] tethered with a longer biphenyl spacer than for Zn-*p*TCPP[S] with a shorter phenyl, seem to suggest that there must exist an optimal distance between the porphyrin macrocycle and the surface to reach an optimum electron injection rate in these kind of systems, in which the porphyrin lies flat on the surface. Between 2009–2012, the same author and co-workers used various advanced spectroscopic techniques, together with computational studies, to investigate in detail the relationship between energy alignment, adsorption geometry, and electron transfer between a chromophore and an oxide surface for a series of Zn(II)tetr phenylporphyrin derivatives adsorbed on TiO₂ or ZnO surfaces.^{214,215} Spectroscopic studies evidenced H-aggregates in the case of dyes Zn-*p*TCPP, which must imply edgewise binding mode geometries that allow $\pi-\pi$ stacking interactions between porphyrin macrocycles (Figure 17). NEXAFS, STM, and UV-visible spectroscopy, further point out a close and organized regular packing for Zn-*p*TCPP with a relatively large angle plane from the surface (with a possibly tilt angle of 50°). On the contrary, it was evidenced a face-to-face alignment of Zn-*m*TCPP that binds flat on the surface. They proposed that the main deexcitation channel for a photoexcited electron of Zn-*m*TCPP must occur through injection into the TiO₂ semiconductor (Figure 17, left; blue arrows), while the $\pi-\pi$ stacked arrangement of porphyrin macrocycles in Zn-*p*TCPP might open a new deexcitation channel through dipole–dipole interaction, responsible for lower J_{SC} and therefore lower overall performances (Figure 17, right; green arrows).

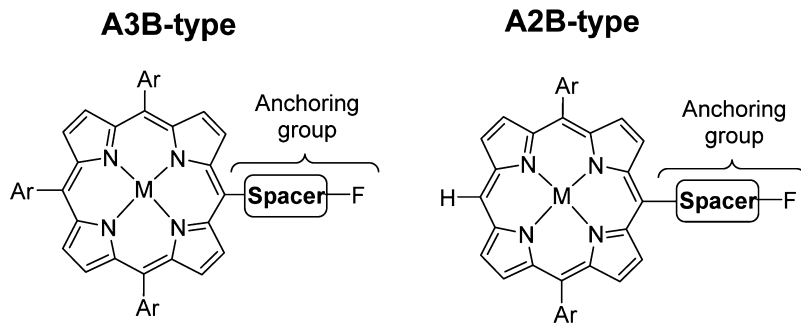
3. A3B- AND A2B-TYPE DESIGNS FOR MESO-SUBSTITUTED PORPHYRIN DYES

The synthetic versatility of meso-substituted porphyrins allows access quite easily to the lower-symmetrical A3B-type porphyrins. This loss of symmetry disturbs the π -delocalized electrons system of the macrocycle creating a dipole moment that affects notably the photophysical and electrochemical properties of the porphyrin. In DSSC, this permanent and intrinsic dipole moment would be assumed to favor the electron injection of the excited dye into the TiO₂ conduction band. This design offers various advantages counterbalanced by some disadvantages compared to the A4's. The first obvious

disadvantage from the synthetic point of view lies on the fact that the access to A3B type porphyrins is less straightforward than A4s. Indeed, the most commonly used and simple strategy to synthesize A3B-type porphyrins (and especially tetraaryl-substituted A3B porphyrins) remains the statistical condensation of aldehydes A-CHO (3eq), B-CHO (1 equiv) and pyrrole (4eq) under the conditions optimized by Lindsey, leading to a mixture of six different porphyrins (A4, A3B, *trans*- and *cis*-A2B2, B3A, and B4). Consequently, various (and often tedious) chromatographic separations are required to isolate the desired A3B-type porphyrin in much lower yields (typically 10–20% yield) than for A4 type (40–50%). Although in principle an A2B-type porphyrin should be considered from the structural point of view as A2BC-type (with B or C = H, and A ≠ B ≠ C), this kind of porphyrin is closer to A3B-type in terms of electronic, optical properties and efficiency in DSSC, and will be dealt together in this section. The most common A3B-type porphyrin dyes (Figure 18) incorporate three aryl moieties, acting as solubilizing and/or bulky groups ("A") and one anchoring group ("B") (note that the latter may or may not be linked through a phenyl-type linker and will be discussed in detail in the next sections). The next disadvantage would be the reduced number of available anchoring groups, which might decrease the amount of adsorbed dyes on TiO₂. However, the presence of only one carboxyl binding group is usually sufficient to ensure an efficient adsorption of many porphyrin dyes. Although in principle an A3B-type porphyrin dye can be also designed in an upside-down "B3A" fashion, that is, three anchoring groups and another substituent, only very few examples of this kind of dye have been reported so far in DSSC.

3.1. Phenyl Tetra-Substituted A3B-Type Porphyrins

The main advantage of the A3B design is the possibility to incorporate easily a wide range of solubilizing and/or bulky groups at the periphery of the porphyrin, which is of high importance to reduce dye aggregation and recombination processes in the cell. It also offers the possibility to modulate the electronic and optical properties of the macrocycle, by introducing electron-rich or deficient substituents at three meso positions of the porphyrin. However, most of them are phenyl-based substituents, which limit somehow their electron-withdrawing (EW) or -donating (ED) capability. Indeed, due to steric hindrance with the β -pyrrolic protons, phenyl planes are considered almost orthogonal to the porphyrin ring, which impede the overlap of their π -orbitals with those of the macrocycle.



Spacer = phenyl, aryl, alkynylphenyl, cyanoacrylic, vinyl, etc...

Ar = phenyl or aryl groups

F = functionnal binding group (carboxyl, pyridyl, catechol, etc...)

M = 2H, Zn, other metals

Figure 18. Common molecular designs for A3B- and A2B- type *meso*-porphyrin dyes.

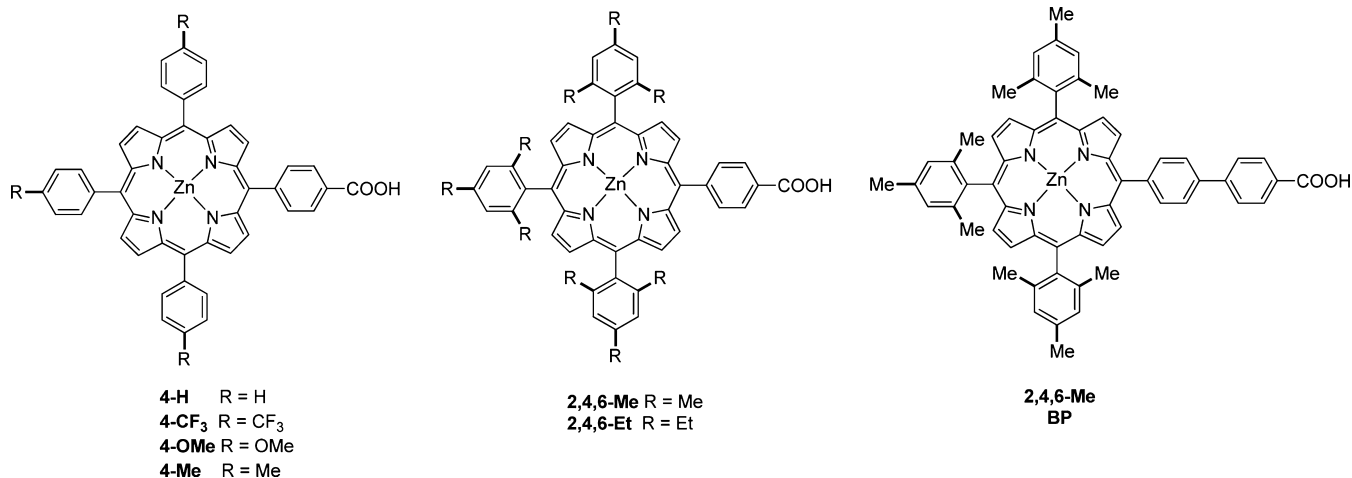


Figure 19. Molecular structures of A3B-type zinc porphyrin dyes reported by Imahori et al. (ref 216).

Imahori et al. reported a systematic study of the effect of porphyrin meso-substituents and adsorption conditions on photovoltaic properties in a series of phenyl tetra-substituted zinc porphyrins sensitized in TiO₂-DSSCs (Figures 19 and 20).²¹⁶ First, the driving force effects (ΔG_{inj}) from the porphyrin excited singlet state to the TiO₂ CB on the photovoltaic properties of 4-CF₃, 4-OMe, 4-H, and 4-Me-sensitized TiO₂ cells were evaluated. Except for 4-H, the increase of the driving force upon introducing electron-donating substituents (-0.52 (4-CF₃) < -0.56 (4-OMe) < -0.57 (4-H) < -0.61 eV (4-Me)) matches well with the increase of photovoltaic performances in the same order 4-CF₃ ($\eta_{\max} = 3.0\%$) $<$ 4-OMe ($\eta_{\max} = 3.5\%$) $<$ 4-Me ($\eta_{\max} = 3.8\%$). The drastic drop of performances for 4-H cells ($\eta_{\max} = 1.2\%$) is ascribed to both an inherent strong tendency of 4-H to aggregate due to small steric hindrance of the unsubstituted phenyl groups, and by lower dye surface coverage.

Next, the steric effect on the photovoltaic properties was examined in the series 4-Me, 2,4,6-Me, and 2,4,6-Et, which have comparable driving forces ($\Delta G_{\text{inj}} = -0.61$, -0.60 , and -0.59 eV, respectively) but different sizes of their substituents. The incorporation of methyl or ethyl groups at the ortho positions of the *meso*-phenyls in 2,4,6-Me and 2,4,6-Et is expected to enhance the geometrical constraint between the phenyl rings against the porphyrin plane, forcing better their orthogonal orientation. These bulkier substituents causing a

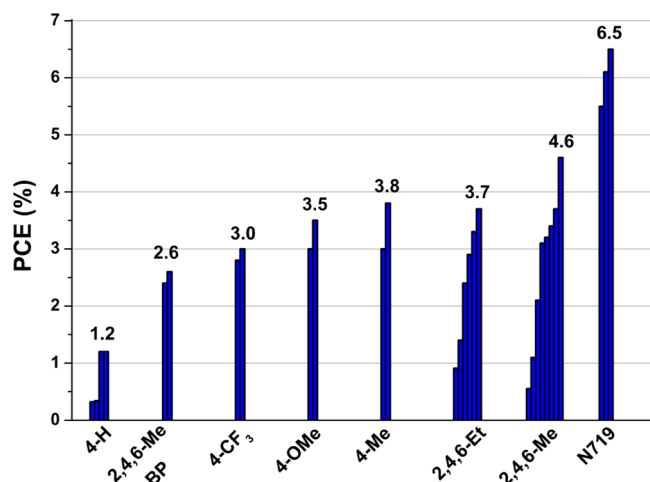


Figure 20. PCE values of TiO₂-sensitized porphyrin dyes solar cells under simulated AM1.5G full sun illumination (power 100 mW·cm⁻²), reported by Imahori et al. Each bar represents a value obtained under different experimental conditions, and the maxima obtained under optimized conditions are noted; devices made with the Ru(II) dye N719 were used as benchmarks in this study. Data derived from ref 216.

larger steric repulsion between porphyrin rings than the tolyl groups in 4-Me (i.e., without ortho substituents), they strongly

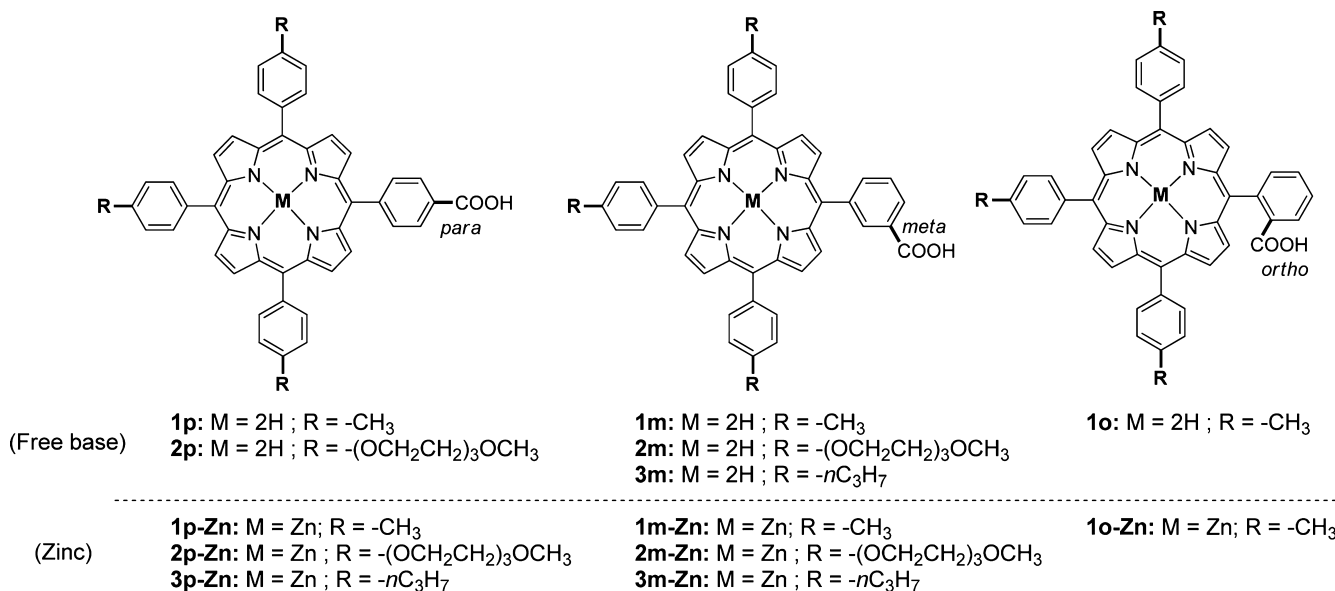


Figure 21. Molecular structures of A3B-type, phenyl tetra-substituted porphyrins dyes reported by D’Souza and co-workers: effect of the metalation, meso substituents, and orientation of the carboxyl anchoring group on the DSSC performance (ref 223).

impede π - π stacking between porphyrin cores and thereby hamper deexcitation channels through dipole–dipole interactions. As a result, significant increase in the PCEs were observed for 2,4,6-Me/DSSCs when compared to 4-Me/DSSCs under the same experimental conditions ($\eta_{\max} = 4.6\%$ and 3.8% , respectively). The lower performances of 2,4,6-Et cells ($\eta_{\max} = 3.7\%$) compared to 2,4,6-Me ($\eta_{\max} = 4.6\%$) were explained by lower surface coverage of the dyes on the TiO₂ electrode of the former ($\Gamma = 0.69\text{--}0.86 \times 10^{-11}$ mol·cm⁻² and $0.85\text{--}1.2 \times 10^{-11}$ mol·cm⁻², respectively), as a result of a bigger size of ethyl than methyl groups. Finally, the photovoltaic performances of 2,4,6-Me^{217–222} and 2,4,6-Me BP in DSSCs were compared to evaluate the electronic coupling effect. Taking into account that these two dyes have the same molecular structure except for their spacer moiety (phenyl versus biphenyl), they display very similar surface coverage under all experimental conditions and have comparable driving forces ($\Delta G_{\text{inj}} = -0.60$ eV for 2,4,6-Me and -0.58 eV for 2,4,6-Me BP). However, a strong decrease in the performances were observed for the 2,4,6-Me BP cells ($\eta_{\max} = 2.6\%$) when compared to 2,4,6-Me ($\eta_{\max} = 4.6\%$). These results evidence that the partially decoupled phenyl spacer versus the highly decoupled biphenyl spacer has a large impact on the cell performances and emphasize the importance of electronic coupling strength between porphyrin and TiO₂ (mediated through the spacer and anchoring group).

D’Souza and co-workers reported recently an exhaustive series of free-base and Zn(II)-A3B porphyrin dyes anchored through carboxyphenyl and studied the effect of metalation, orientation of the carboxyl group and incorporation of alkyl chains, toward the performances of the cells (Figures 21 and 22 and Table 4).²²³ Similarly to the A4-type TCPP dyes discussed previously in section 2, the ortho, meta, or para locations of the carboxyl group at the *meso*-phenyls induce changes in the geometry adopted by the dye onto the surface. While the para pattern substitution result most likely in a perpendicular edge-to-face attachment of the porphyrin dyes with respect to the TiO₂ surface, meta and ortho analogues are tilted (meta) or almost parallel (ortho) with much shorter distances TiO₂-porphyrin cores (the edge-to-edge distance in the series

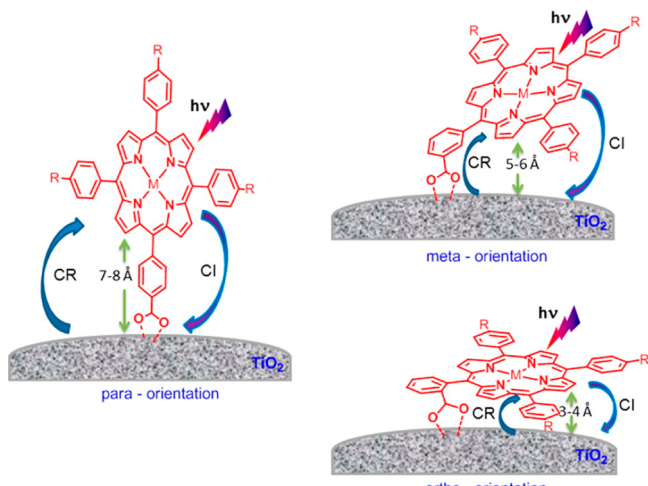


Figure 22. Relative orientation of *para*-, *meta*-, and *ortho*-carboxyphenyl functionalized porphyrin dyes adsorbed on TiO₂ surface (CI: charge injection; CR: charge recombination). Reproduced with permission from ref 223. Copyright 2013 American Chemical Society.

decreases in the order para ($7\text{--}8 \text{ \AA}$) > meta ($5\text{--}6 \text{ \AA}$) > ortho ($3\text{--}4 \text{ \AA}$)). As well, the substitution pattern and the resulting binding geometry affect both the electronic properties and amount of dyes adsorbed on the surface.

However, in contrast with the A4-type porphyrin mTCPP (vide supra), the meta A3B-type analogues do not lie flat on the surface but are tilted, which result in comparable amount of adsorbed dyes than the para A3B-type (219 and 176 nmol·cm⁻² for **1m-Zn** and **1p-Zn**, respectively). For the ortho A3B-type, the porphyrin core must lie almost flat on the surface (similarly to the A4-type mTCPP) and hence need more space to accommodate. Consequently the amount of adsorbed dye for the ortho series was less (132 nmol·cm⁻² for **1o-Zn**) than for the two others. Although dye loading was quite different in each series, this factor cannot explain solely the large difference observed in photovoltaic performances of the DSSCs, which

Table 4. Surface Coverage (Γ) and Photovoltaic Parameters^b of the TiO_2 -DSSCs Sensitized with A3B-Type Porphyrins Reported by D’Souza and Co-workers, under Simulated AM1.5G Full Sun Illumination^a

series	dye	$\Gamma/10^{-7}$ (mol·cm ⁻²)	V_{OC} (mV)	J_{SC} (mA·cm ⁻²)	F.F. (%)	η (%)
(Benchmark)	N719		620	18.13	66	7.39
para	1p		450	1.26	75	0.42
	2p		520	1.17	82	0.65
	1p-Zn	1.76	590	6.67	79	3.13
	2p-Zn		600	4.82	77	2.42
	3p-Zn		570	4.88	76	2.09
	1m		480	2.06	72	0.71
meta	2m		550	1.61	74	0.65
	3m		520	0.78	74	0.30
	1m-Zn	2.19	650	8.42	82	4.17
	2m-Zn		610	5.19	78	2.45
	3m-Zn		560	3.01	73	1.99
	ortho		450	0.31	83	0.11
	1o		510	1.01	71	0.37
	1o-Zn	1.32				

^aUnderlined values correspond to the best PCE obtained in each series. Data derived from ref 223. ^bAverage values of three DSSCs.

followed the same trend. Except for **1m-Zn** that outperformed significantly **1p-Zn**, meta and para dyes displayed comparable performances and systematically much higher than their corresponding ortho analogues. Moreover, cells made with Zn(II)-Por dyes always outperformed clearly their free-base analogues (V_{OC} , J_{SC} , F.F., and η) in each series. To get insights into the understanding of such difference of behavior, electrochemical impedance spectroscopy^{224–228} (EIS) and femtosecond transient absorption spectral studies were performed. First, the effect of the type of substitution (ortho, meta, or para) on the photovoltaic performances was investigated. The time profiles of the absorption changes at 660 nm (fingerprint of the radical porphyrin cation, $\text{ZnP}^{+}\bullet$) were recorded by femtosecond transient spectroscopy for **1p-Zn**/**1m-Zn**/**1o-Zn**/FTO/TiO₂ DSSCs after excitation at 440 nm (Soret band). The growing component was in a same range for the three dyes (0.37–0.42 ps), suggesting an ultrafast electron injection from the singlet excited state of the porphyrin in all cases. On the other hand, the decaying profiles were more complex to analyze, showing three distinct components. However, the slower decaying component was significantly shorter for **1o-Zn** than for the other two analogues, which suggests a faster recombination process for the former. Thus, assuming electron injection likewise similar for each isomer, the larger recombination rates in the ortho series DSSCs was ascribed as the main factor responsible of their lower photovoltaic performances, as supported by EIS studies. In view of these results, and in agreement with the recent work reported by Ye et al. for tilted porphyrin dyes,²²⁹ the authors suggested the occurrence of additional through-space, in addition to through-bond, deexcitation channels. The contribution of the through-space pathway in the ortho series can be assumed significantly larger than for meta and para analogues, because of the proximal location of the porphyrin macrocycle to the TiO₂ surface, which explains well why ortho-type DSSCs systematically displayed enhanced charge recombination. Regarding the effect of metalation, EIS studies systematically supported faster CR rates for a given free-base porphyrin than for a Zn(II) analogue, which constitute the main reason for their inferior performances in DSSC. Finally, the replacement of the *p*-CH₃ methyl groups at the *meso*-phenyls in series **1** by either long alkyl chains in **2** or ethylene oxide chains in **3** systematically resulted in a drop of performances of the DSSCs.

Although dye-loadings were not measured for the series **2** and **3**, it can be assumed that the presence of these long chains decreased significantly the amount of adsorbed dyes, which might explain the drop of photovoltaic performances for the latter, in agreement with others recently reported examples.²³⁰

Even though porphyrin dyes anchored through carboxyphenyl groups have been reported and studied a great deal, other anchors have been successfully used in porphyrin-DSSCs. For instance Mori and co-workers reported the dye **P199** anchored through a phenyl-cyanoacrylic acid group, reaching a PCE of 2.59% (Figure 23 and Table 5).¹⁶⁰ If we compare this value to the benchmark **N719** under similar experimental conditions (54% relative to the PCE of **N719**), this is of the same order as the analogue dye anchored through carboxyphenyl previously reported earlier by Imahori et al. (**4-Me**)²¹⁶ or later by D’Souza and co-workers (**1p-Zn**)²²³ (58% and 42% relative PCE of **N719**, respectively). These experimental results agree with recent theoretical computational studies, which predict that a porphyrin dye anchored through a (*meso*)phenyl-cyanoacrylic acid group should display improved intramolecular charge transfer properties and better electron injection from the anchoring group in comparison with a (*meso*)carboxyphenyl, because of the strong electron-withdrawing effect of the cyano moiety.²³¹ In principle then, this kind of dye should display superior performances in DSSCs.

Tan and co-workers successfully used thiophene-based linkers to bridge cyanoacrylic acid anchor and porphyrin, reaching remarkable efficiencies in DSSCs (up to 64% relative to the PCE of **N719** under similar conditions, Figure 24 and Table 6).^{232,233}

The incorporation of thiophene or polythiophene units in their molecular structure results in a significant broadening of the absorption spectra of these dyes, and they act as efficient π -conjugated linkers, both factors that contribute to the great performances obtained for these sensitizers in DSSCs. Considering the same molecular structure of **PZn-T** and **PZn-hT**, the latter differing only by an additional hexyl chain appended at one of the β -position of the thiophene linker, both dyes share similar absorption features (i.e., same light-harvesting capabilities) and driving forces but display significantly different photovoltaic performances in DSSCs ($\eta = 4.25$ and 5.14%, respectively). According to the authors, the long appended hexyl chain in **PZn-hT** is believed to impede

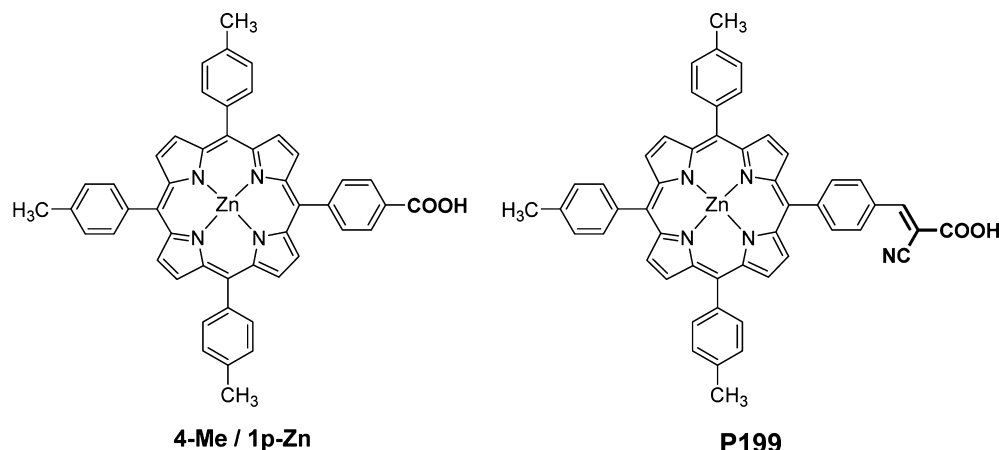


Figure 23. Molecular structures of phenyl tetra-substituted zinc porphyrins anchored through carboxylic (**4-Me**²¹⁶/**1p-Zn**²²³) or cyanoacrylic acid (**P199**¹⁶⁰).

Table 5. Comparative Photovoltaic Performances of 4-Me, 1p-Zn, and P199 vs Benchmark N719 in TiO₂-DSSCs

dye	V_{OC} (mV)	J_{SC} (mA·cm ⁻²)	F.F.	η (%)	rel. PCE of N719 (%)	ref
4-Me	680	8.3	68	3.8	58	216
N719	740	14.0	63	6.5	(100)	
1p-Zn	590	6.67	79	3.13	42	223
N719	620	18.13	66	7.39	(100)	
P199	585	6.55	67	2.59	54	160
N719	724	9.71	68	4.78	(100)	

more efficiently dye aggregation and reduce charge recombination by preventing the approach of I_3^- ions. Both factors should confer to **PZn-hT** a better electron collection efficiency (η_{coll}) value than **PZn-T**, which would explain the higher J_{sc} values (12.95 vs 9.94 mA·cm⁻² respectively) and hence higher η values, obtained for their respective cell. The superior efficiency of the **PZn-oT** cell ($\eta = 4.55\%$) compared to **PZn-T** ($\eta = 4.25\%$) was mainly ascribed to a much broader absorption of the former in the 460–540 nm range, while the lower efficiency compared to **PZn-hT** is explained by a less efficient electron transport along the ten thiophene moieties. Interestingly, the photovoltaic performances of **PZn-hT** evolved on the durative illuminating time (Figure 25). An important decrease of both the fill factor and V_{OC} was observed after 10–15 min of illumination, and then only slightly decrease to stabilize after 80 min.

Table 6. Photovoltaic Parameters of the TiO₂-DSSCs Sensitized with PZn-hT, PZn-oT, and PZn-T, under Simulated AM1.5G Full Sun Illumination (Power 100 mW·cm⁻²)^a

dye	IPCE max (%)	V_{OC} (mV)	J_{SC} (mA·cm ⁻²)	F.F.	η (%)	rel. PCE of N719 (%)
PZn-hT	72	600	12.95	66	5.14	64
PZn-oT	(~41) ^b	610	10.96	68	4.55	57
PZn-T	(~63) ^b	610	9.94	70	4.25	53
N719	n/a	n/a	n/a	n/a	7.99	(100)

^aThe device made with Ru(II) dye **N719** was used as benchmark and PV data are reported under the same conditions. Data derived from reference ref 232. ^bIPCE values roughly estimated from the graphs given in the article.

In turn, the J_{sc} and η values increased drastically during the first 10 min, then slightly, to stabilize finally at a maximum after 100 min. Some recent works elucidated the performance enhancement of porphyrin DSSC under visible light illumination soaking, as a result of photoinduced exchange cations in the electrolyte (e.g., Li⁺) at the TiO₂ interface.^{234–236}

For almost all A4- and A3B-type porphyrin dyes used in DSSCs, four, or at least three, of their meso positions are occupied by aryl groups due to the ease synthesis of tetra- or triaryl porphyrins. Moreover, apart from few exceptions, these aryl substituents are in the great majority phenyl groups.

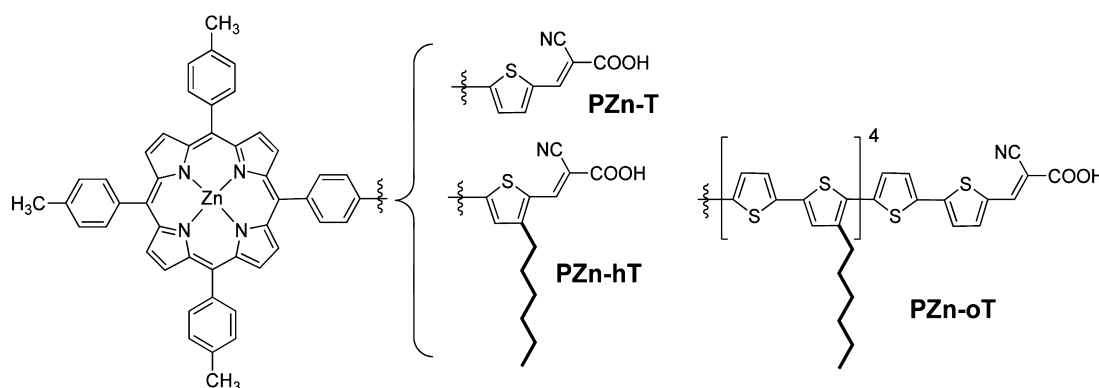


Figure 24. Phenyl tetra-substituted, thiophene-bridged, zinc porphyrins anchored through a cyanoacrylic acid group, reported by Tan and co-workers (ref 232).

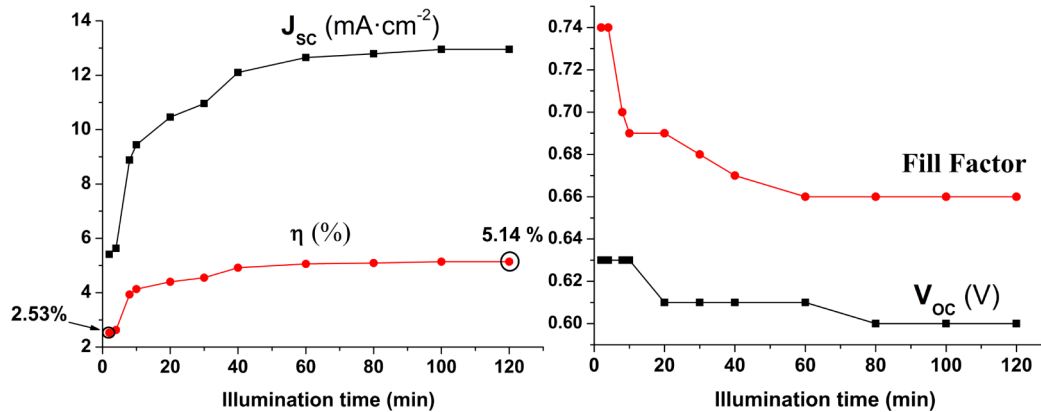


Figure 25. Evolution of the photovoltaic parameters of PZn-hT/TiO₂-DSSC on the durative illuminating time (data derived from the Supporting Information for ref 232).

In (*meso*)-phenyl tetra-substituted porphyrins, phenyl groups are typically considered orthogonal to the porphyrin plane due to the steric hindrance between the β -pyrrolic and phenylene protons and therefore are not, or poorly, conjugated with the 18 delocalized π -electrons system of the porphyrin macrocycle. Thus, the electronic influence of the surrounding substituents, electronically decoupled from the porphyrin ring, is largely limited, mostly through inductive effects.

3.2. A3B- and A2B-Type Porphyrin Dyes Anchored through Coupled π -Conjugated Spacers

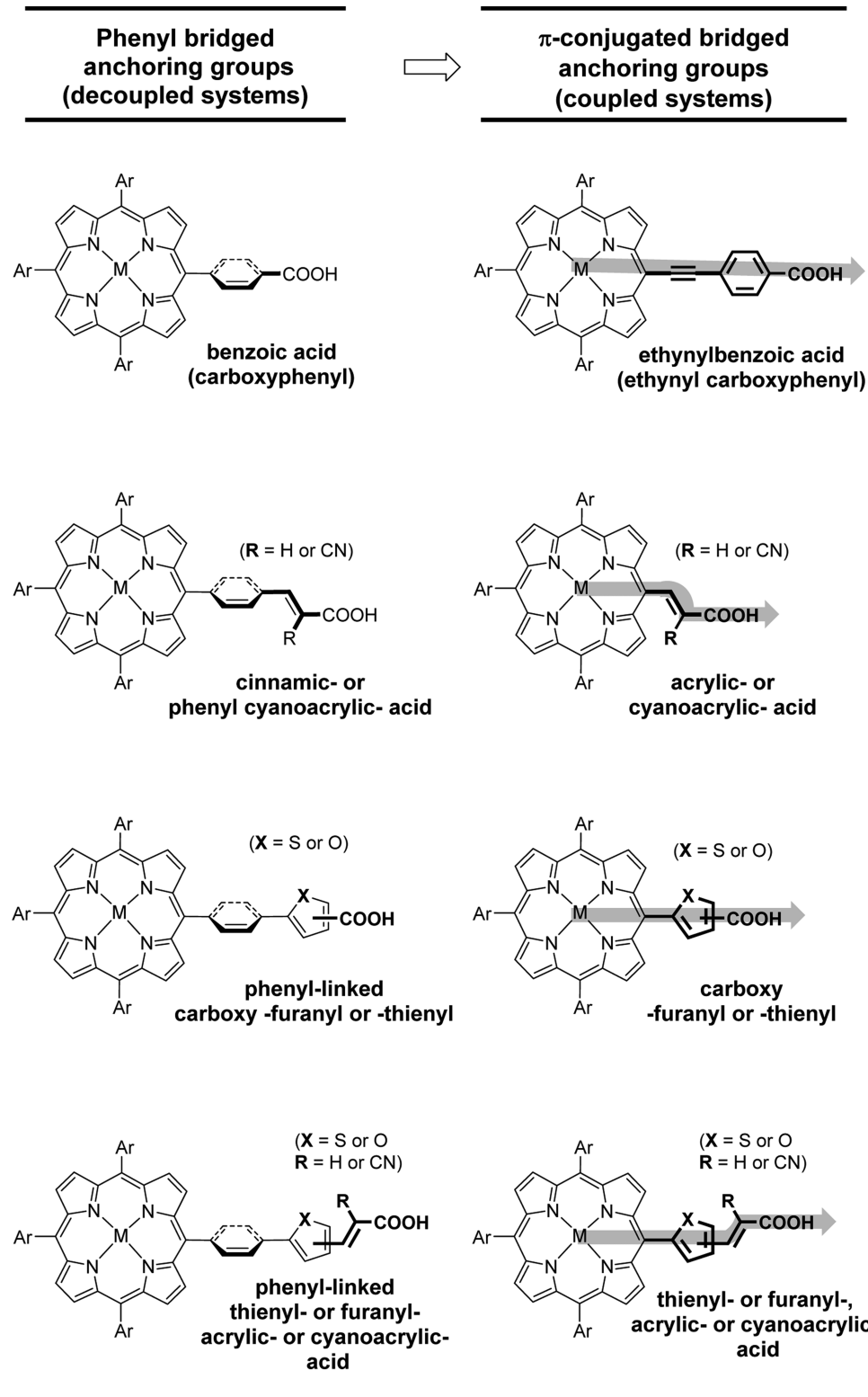
Since the first use of porphyrin derivatives in DSSC in 1993 reaching a PCE up to 2.5%,¹²² A4- and A3B-type *meso*-phenyl substituted porphyrins anchored through carboxyphenyl(s) have been studied in great deal. However, the best PCE achieved for these types of *meso*-substituted porphyrins did not change so much in more than 15 years: tetrakis(4'-carboxyphenyl) porphyrin $\eta = 3\text{--}3.5\%$ in 2000 (H₂-*p*TCPP),²⁰⁸ 5-(4-carboxyphenyl)-10,15,20-tris(2,4,6-trimethylphenyl) porphyrinatozinc(II): $\eta = 3.5\%$ in 2006 (ZnP²¹⁸), 4.6% in 2008–2009 (Zn-3,¹³⁸ 2,4,6-Me²¹⁶). From the following statement, the remaining concerns about the decoupling of phenyl rings from the conjugated system of the macrocycle, have prompted other structural design for porphyrin dyes. In particular, the use of a π -conjugated spacer bridging porphyrin and anchoring group has been revealed to enhance the electronic communication between the excited porphyrin and the semiconductor, which promotes the electron-injection process Dye* → TiO₂. On the other hand, all (*meso*)-phenyl tetra-substituted porphyrins display very similar absorption spectra, a sharp and strong Soret band centered at around 400–450 nm and medium Q-bands between 550–650 nm. Their relatively small bandwidth and lack of absorption in the 450–550 nm and 650–900 nm visible ranges, two photon-rich regions of sunlight, represent one of the limiting factors of these dyes in DSSCs. On this scope, the extension of the effective conjugation through a π -conjugated linker is expected to produce favorable changes of the porphyrin properties, including light harvesting capabilities (broadening and/or redshifts of both Soret and Q bands), oxidation potentials, and excited state redox levels. For instance, Therien and co-workers introduced in 1994 the concept, design, and synthesis of ethynyl substituted and acetylenyl bridged porphyrins as a new class of highly conjugated chromophores.²³⁷ On this line, the second main advantage of A3B design is the relative ease and synthetic feasibility to graft a new type of

π -conjugated spacers between the macrocycle and the anchoring group at one *meso* position of the porphyrin (Figure 26).

The use of these types of π -conjugated linkers is relatively recent for porphyrin dyes, and research of new efficient π -bridged anchoring groups remains under extensive investigation.^{174–178} For instance, Ragoussi et al., recently reported the synthesis and optical and electrochemical behavior of two series of A3B-type porphyrin bearing either bulky 2,4,6-triisopropylphenyl or triphenylamino donors substituents at three of the four *meso* positions, and anchored through different ethynylcarboxyphenyl or phenylpropiolic groups²³⁸ (Figure 27). Their potential as dyes and performances in TiO₂-DSSC are currently under investigation.

Stromberg et al. reported in 2007 a series of (4-methyl)-phenyl tris-substituted porphyrins anchored through ethynylisophthalic (ZnP-EI) or cyanoacrylic acid (ZnP-A), together with a phenyl tetra-substituted porphyrin (ZnP-I) bearing an isophthalic acid as the anchoring group²³⁹ (Figure 28, right). The photovoltaic performances of the DSSCs decreased in the order ZnP-A > ZnP-I ≫ ZnP-EI (Table 7, entry 1). In comparison with the phenyl tetra-substituted porphyrin ZnP-I, the incorporation of the directly tethered cyanoacrylic or ethynylaryl linkers caused important electronic perturbations of the macrocycle, resulting in slight redshifts and broadening of both Soret and Q bands (accompanied by significantly larger extinction molar absorption coefficients in the case of ZnP-A). Among these three dyes, ZnP-A was the best performing one, which was explained by both optical and redox favorable effects of the cyanoacrylic acid group.

First, ZnP-A displays significantly much broader absorption bands than the two other dyes (roughly a 2-fold greater spectral bandwidths), which should confer to this dye a better LHE. Next, ZnP-A is slightly more easily oxidized but much harder to reduce than ZnP-I, suggesting a more efficient electron collection efficiency. Computational studies explained these differences in terms of stabilizing effect of the HUMO levels, and a much larger stabilizing effect of LUMOs of the cyanoacrylic group. Additionally, the authors suggested that the electron density shifted to the cyano group of the tether should enhance the electronic coupling with the TiO₂-CB, resulting in better electron-injection efficiency. The combination of these favorable factors confers to ZnP-A the largest combined electron-injection/collection efficiency value, (estimated roughly twice more than ZnP-I) consistent with the larger photocurrent observed in the ZnP-A cell. Surprisingly, electron injection/collection



Ar = phenyl, aryl group
M = H₂, Zn, other metals

Figure 26. Some examples of phenyl- (decoupled systems) or π -conjugated (coupled systems) bridged anchoring groups used for A3B-type porphyrin dyes (nonexhaustive list: some other systems have been developed for push–pull porphyrins, see section 5.4.6; note that most but not all of these designs have been reported so far in DSSCs).

efficiency of **ZnP-EI** was found to be extremely low by comparison, and this result was directly attributable to the very low-amplitude IPCE spectrum of this dye. Galoppini and collaborators

studied in detail similar anchored-dyes, Zn(II)-5-(3,5-dicarboxyphenyl)-10,15,20-tri(phenyl)-porphyrin (**ZnTPP-Ipa**) and Zn(II)-5-(3,5-dicarboxyphenyl)-10,15,20-tri(mesityl)-porphyrin

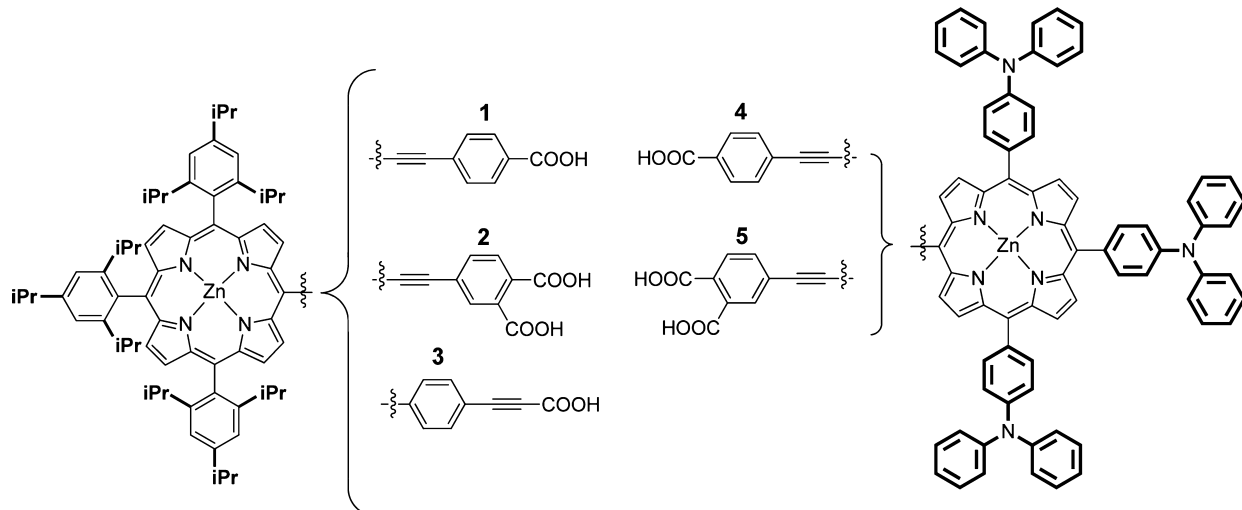


Figure 27. 2,4,6-Trisopropylphenyl- and triphenylamine-substituted A3B-type porphyrin anchored through various carboxyethynylphenyl groups, reported by Ragoussi et al. (ref 238).

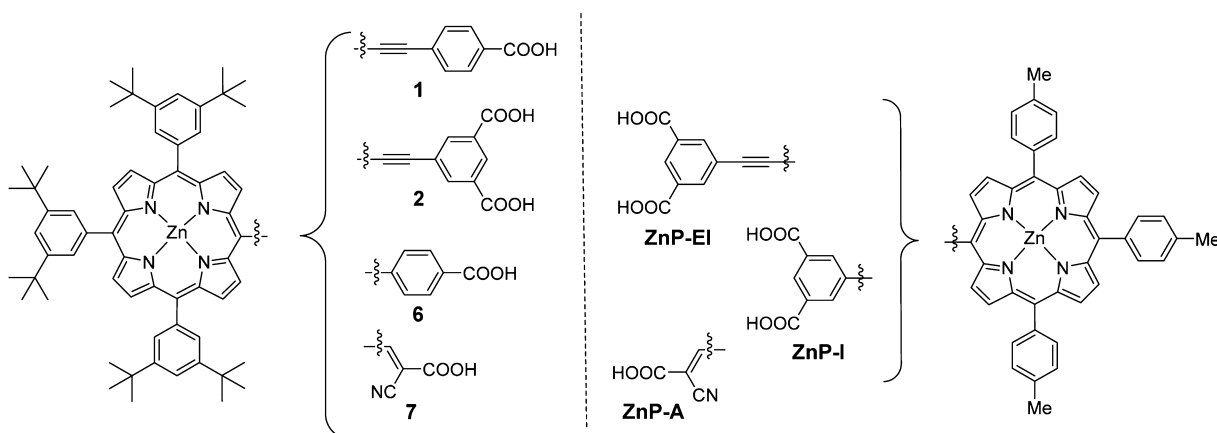


Figure 28. A3B-type porphyrins dyes anchored through benzoic, isophthalic, ethynylbenzoic, ethynylisophthalic, or cyanoacrylic acid groups (refs 239 and 241).

Table 7. Photovoltaic Parameters of the TiO₂-DSSCs Sensitized with ZnP-A, ZnP-I, and ZnP-EI Reported by Stromberg et al. and Dyes 1, 2, 6, and 7 Reported by Diau and Co-workers, under Simulated AM1.5G Full Sun Illumination

entry	dye	V _{OC} (mV)	J _{SC} (mA·cm ⁻²)	F.F. (%)	η (%)	ref
1	ZnP-A	n/a	7.6	n/a	n/a	239
	ZnP-I	n/a	2.8	n/a	n/a	
	ZnP-EI	n/a	0.035	n/a	n/a	
2 ^{a,b}	1 (= YD0)	617	5.79	66.7	2.4	241
	2	613	2.63	71.9	1.2	
	6	624	5.24	68.5	2.2	
	7	543	2.94	58.2	0.93	

^aCHENO was used as coadsorbent in the dye-uptake solutions: ratio CHENO/Dye of 1:1 ([0.2 mM]/[0.2 mM]). ^bActive area of the films 0.16 cm².

(ZnTMP-Ipa), and further provided evidence of the poor electronic conjugation and weak strength bonding between porphyrin and TiO₂ through this type of anchor.^{214,215,240}

The results of Stromberg et al. contrast partially with those reported later by Diau and co-workers²⁴¹ in 2009 for similar

structured dyes, a series of 3,5-di-*tert*-butylphenyl trisubstituted porphyrins anchored through ethynylcarboxyphenyl (1), ethynylisophthalic (2), or cyanoacrylic acid (7) together with a phenyl tetra-substituted porphyrin anchored through a carboxyphenyl group (6) (Figure 28 left, and Table 7 entry 2). It is important to notice, however, that the performances of the cells in this later study were obtained using CHENO as co-adsorbent, and additionally, the bulkier 3,5-di-*tert*-butylphenyl substituents (versus tolyl) play an important role to impede more efficiently dye aggregation. In agreement with the former results, comparison between the directly tethered ethynylaryl dye 1 and the carboxyphenyl analogue 6, showed that the introduction of the triple bond spacer in the molecular structure of 1 improved slightly the performance of the cell ($\eta = 2.4\%$ versus 2.2% , respectively) due to an increase of the effective π -conjugation with the porphyrin macrocycle and better electronic coupling with the TiO₂ CB. In comparison with the phenyl tetra-substituted porphyrin 6, similar trends were also observed in the absorption spectra of dyes 1, 2, and 7, that are, broadening and redshifts of absorption bands (sometimes accompanied by an intensification of the second Q-band). Interestingly, dye 1 bearing only one COOH anchoring group at the para position of the ethynylphenyl

performed much better than dye **2** with two groups in meta positions ($\eta = 2.4\%$ for **1** versus 1.2% for **2**). In contrast, however, the cyanoacrylic tethered dye **7** poorly performed in TiO_2 -DSSC reaching a maximum PCE of 0.93% , which is lower than ethynylisophthalic tethered dye **2** ($\eta = 1.2\%$), and even much lower than dyes **6** ($\eta = 2.2\%$) or **1** ($\eta = 2.4\%$). The authors suggested that the poor performances of **7** might lie in the fact that, even though the cyano groups have a superior electron-pulling capability, it might first pull the electrons but then transfer them back into the porphyrin core through space because of the short intramolecular distance.

In 2012, He et al. reported a simple A2B zinc porphyrin tethered with a cyanoacrylic acid group achieving, however, a much higher PCE of 5.1% under optimized conditions and without coadsorbent²⁴² (Figure 29 and Table 8). They also

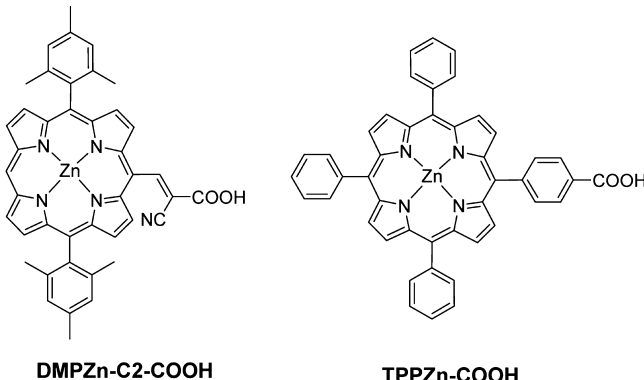


Figure 29. Molecular structures of dyes DMPZn-C2-COOH (left), an A2B-type porphyrin anchored through a cyanoacrylic acid group, and benchmark TPPZn-COOH (right), reported by He et al. (ref 242).

ascribed the broader light absorption and stronger electronic coupling between the dye and the TiO_2 nanoparticles responsible of the remarkably high performances obtained for the cyanoacrylate-anchored dye. Based on their geometry-optimized calculations, they proposed that the short distance TiO_2 -dye might widen the distance between neighboring porphyrins by steric repulsion of the mesityl groups, as attested by the significantly smaller amount of adsorbed dyes (twice less) for DMPZn-C2-COOH than the benchmark TPPZn-COOH. Thus, the mesityl groups must hamper porphyrin-porphyrin deexcitation channel by reducing aggregation and might also contribute to protect the porphyrin core from electron recombination with the electrolyte.

Gou et al. recently reported four A2B-type porphyrin dyes anchored either through ethynylsalicylic or ethynylbenzoic acid, with different locations of the carboxyl and/or hydroxyl groups (meta or ortho).²⁴³ In contrast with the performances obtained for the carboxyphenyl anchored dyes reported by D'Souza (vide supra, see Figure 22 and Table 4) for which the PCE of

meta series were similar or slightly superior than para's (both much higher than ortho's), these ethynylcarboxyphenyl analogues followed the reverse trend, with the para PE1 dye that performed way much better than the meta analogue PE1m. The PCE of PE1 (*p*-COOH, $\eta = 2.26\%$) and PEm (*m*-COOH, $\eta = 0.64\%$) are of the same order than similarly structured dyes anchored through ethynylcarboxyphenyl (Dye 1: *p*-COOH; $\eta = 2.4\%$) or ethynylisophthalic acid (Dye 2: *m,m'*-COOH, $\eta = 1.2\%$), respectively, reported by Diau and co-workers (vide supra, see Figure 28 and Table 7). The same trend was also observed in the ethynylsalicylic acid series, for which the para analogue PESp performed better than the meta one PESm. In contrast, however, these dyes achieved strikingly higher performances than their respective ethynylcarboxyphenyl analogues PE1 and PE1m (Figure 30). According to the

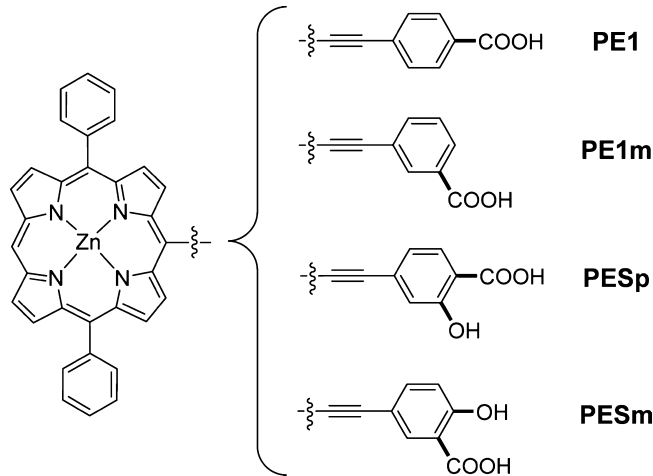


Figure 30. Molecular structures of A2B-type porphyrin dyes anchored through ethynylsalicylic acid (PESp and PESm) and their corresponding ethynylcarboxyphenyl analogues (PE1 and PE1m), reported by Gou et al. (ref 243).

authors, a possible tridentate binding mode of the PES dyes should be responsible of a stronger attachment of the dyes to the TiO_2 surface, better electronic communication between excited dye and TiO_2 -CB, and better electron injection of the excited dye in TiO_2 with respect to their ethynylcarboxyphenyl analogues (Table 9).

In 2009, Lin and co-workers studied a series of oligo-(phenylethynyl) porphyrins (PE1-4, Figure 31)^{244,245} in TiO_2 -DSSCs and demonstrated that the PCE of the cell systematically decreased by increasing the length of a rigid and linear PE π -conjugated spacer linking the porphyrin and the anchoring group ($\eta_{\text{PE1}}: 2.5\% > \eta_{\text{PE2}}: 2.0\% > \eta_{\text{PE3}}: 0.78\% > \eta_{\text{PE4}}: 0.2\%$, Table 10), in agreement with recent theoretical computational studies.²⁴⁶

Table 8. Surface Coverage (Γ) and Photovoltaic Parameters of the Optimized^b TiO_2 -DSSC Sensitized with DMPZn-C2-COOH under Simulated AM1.5G Full Sun Illumination^a

dye	$\Gamma/10^{-10}$ (mol·cm $^{-2}$)	V_{OC} (mV)	J_{SC} (mA·cm $^{-2}$)	F.F. (%)	η (%)
DMPZn-C2-COOH	0.67	767	9.22	72.3	5.12
TPPZn-COOH	1.24	n/a	n/a	n/a	1.8

^aPV data of the benchmark device made with TPPZn-COOH are reported under same conditions. Data derived from ref 242. ^bPhotovoltaic performances reported under optimized conditions for DMPZn-C2-COOH/DSSC: dye immersion time of 4h, and using a 12 μm thickness TiO_2 nanoparticles film.

Table 9. Dye-Loading^b and Photovoltaic Parameters of the TiO₂-DSSCs Sensitized with PE and PES Dyes under Simulated AM1.5G Full Sun Illumination (Power 100 mW·cm⁻²)^a

dye	dye-loading ^b (nmol·cm ⁻²)	V _{OC} (mV)	J _{SC} (mA·cm ⁻²)	F.F. (%)	η (%)
PE1	176	600	5.95	63.2	2.26
PE1m	127	550	1.83	63.7	0.64
PESp	180	630	11.14	64.9	4.55
PESm	142	560	3.55	61.9	1.22

^aData derived from reference 243. ^bDye-loading data derived from the Supporting Information for ref 243.

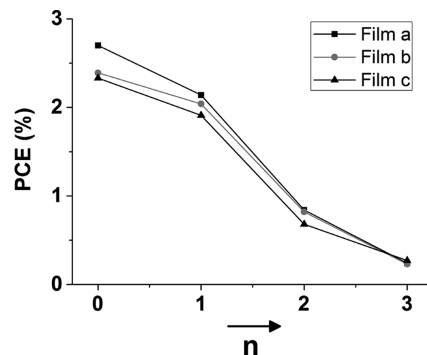
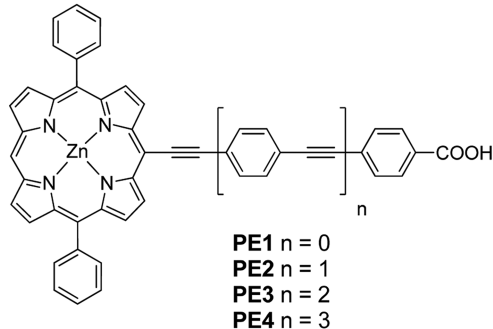


Figure 31. Molecular structures of PEn dyes (left) reported by Lin and co-workers and influence of the π -conjugation length in oligo(phenylethynyl) linked porphyrin on efficiency of TiO₂-DSSCs (right; data derived from ref 244).

Table 10. Photovoltaic Parameters of the Optimized TiO₂-DSSCs Sensitized with PEn Dyes under Simulated AM1.5G Full Sun Illumination (Power 100 mW·cm⁻²)^a

dye	V _{OC} (mV)	J _{SC} (mA·cm ⁻²)	F.F. (%)	η (%)
PE1	560 ± 10	6.6 ± 0.7	67 ± 2	2.5 ± 0.2
PE2	570 ± 20	5.5 ± 0.1	64 ± 2	2.0 ± 0.1
PE3	560 ± 10	2.0 ± 0.3	70 ± 2	0.78 ± 0.09
PE4	510 ± 20	0.70 ± 0.03	69 ± 4	0.25 ± 0.2

^aData derived from reference 244. Average values obtained for three different cells made with each dyes. Active area of the films 0.25 cm².

Based on experimental data (electrochemical and optical) and DFT computational studies, the MOs energies were found to be similar for all dyes, with the conduction band (CB) of TiO₂ located between their HOMO–LUMO levels (both localized on the porphyrin macrocycle and extended to the first PE unit only). In sight of these results, the authors proposed that the rate of electron injection might be similar for all PE1–4/TiO₂ films, which is consistent with low-distance dependence versus electron-injection rate for other PE linked systems described in the literature. As all films display very similar absorption spectra, light harvesting efficiencies (LHE) were assumed likewise to be similar for all dyes. However, although the IPCE response in the 400–800 nm range of PE1- and PE4-/TiO₂ matches with their absorption spectra, the relative IPCE values were found to be ten times higher for the former, consistent with the systematic decrease of J_{SC} and η values from PE1 to PE4. As all dyes display same LHE, and if the values of the electron injection efficiency are likewise similar, the decrease of the IPCE values can be therefore directly correlated with the decrease of charge collection efficiency at the working electrode (η_C values) from PE1 to PE4, which is dependent upon both the electron collection rate (η_{coll}) and dye regeneration efficiency (η_{reg}) according to eqs 3 and 4 (vide supra). The rate of charge recombination from reduced TiO₂ nanoparticles to the oxidized porphyrin affecting directly both J_{SC} and η_{coll} values (hence η_C , η, and IPCE values)

and the decrease of performance from PE1 to PE4 must originate mainly from an increase of CR rate for dyes with longer PE spacers. Interestingly, the V_{OC} values increase slightly from PE1 (660 mV) to PE2 (670 mV) but then systematically decreased with longer PE spacers in the order PE2 > PE3 > PE4. Recently, detailed investigations by computational studies of these dyes and similar pyrimidyl (PM) analogues have been reported.²⁴⁶ The calculations of PEn dyes evidenced that the driving forces for electron injection and regeneration gradually decrease as the distance of the π -spacer increases, which supports the drop of power conversion efficiency observed experimentally. They also evidenced that the nature of the rigid spacer (phenyl versus pyrimidyl) affects significantly the performance of optical absorption, charge separation, and the regeneration process, and hence the PCE of the device.

These results contrast with those obtained for other non-porphyrinic dyes reported in the literature, for which the V_{OC} tends to get larger and CR recombination process reduced for longer PE spacers. For instance, Gundlach et al. studied a perylene dye linked through a tripodal anchoring group via a long rigid PE spacer (**DTB-Pe-tripod**) and a similar dye through a rod-anchoring group via a shorter phenylene group (**DTB-Pe-rod**), adsorbed on TiO₂.²⁴⁷ They evidenced that a longer PE linker in **DTB-Pe-tripod** retards the electron transfer from the chromophore to the TiO₂, but on the other hand it also retards the CR rate between the TiO₂ injected electron and the oxidized perylene moiety. This phenomenon is well-known and has been studied in great deal for many porphyrin-bridge-acceptor systems, in which the efficiency of the photoinduced electron transfer and rate of charge recombination mediated through a molecular wire (bridge) are strongly dependent on the nature, length, and attenuation factor of the π -bridge.²⁴⁸ For most porphyrin dyes in DCCS, electron transfer/injection in the TiO₂–CB usually occurs very fast, typically in the 0.1–10 ps time scale, which is much faster than required, considering for instance, that dye regeneration process by I[−] ions typically occurs in nanosecond's and recombination

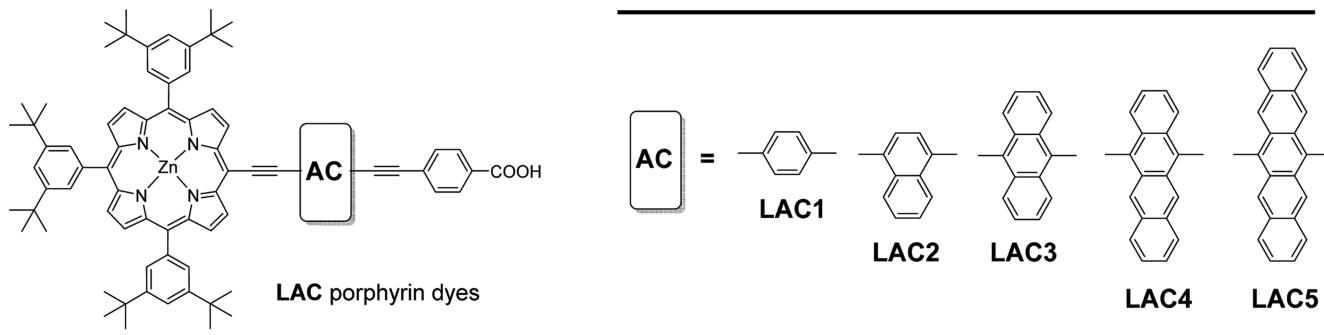


Figure 32. π -extended linkers in acene-modified zinc porphyrins: molecular structures of LAC dyes reported by Lin and co-workers. Adapted with permission from ref 252. Copyright 2010 American Chemical Society.

Table 11. Surface Coverage (Γ) and Photovoltaic Parameters^a of the TiO₂-DSSCs Sensitized with LAC Porphyrins under Simulated AM1.5G Full Sun Illumination (Power 100 mW·cm⁻²)

dye	Γ (nmol·cm ⁻²)	V_{OC} (mV)	J_{SC} (mA·cm ⁻²)	F.F. (%)	η (%)
LAC1	120	670	6.13	72	2.95 ± 0.02
LAC2	135	650	7.27	70	3.31 ± 0.06
LAC3	132	670	12.67	64	5.44 ± 0.06
LAC4	140	610	6.68	68	2.82 ± 0.14
LAC5	140	490	0.33	62	0.10 ± 0.02
N719 (Benchmark)	n/a	740	12.67	72	6.73 ± 0.10

^aAverage values obtained from three independent measurements for DSSC devices fabricated with an identical procedure. Active area of the films 0.16 cm². Data derived from ref 252.

processes in micro- to millisecond's.²⁴⁹ Thus, one can assume that upon increasing the length of an adequate and efficient spacer up to a certain limit, the retardation of the CT process will not degrade significantly the electron injection efficiency, but as a positive counterpart would slow down the CR rate between oxidized dye and TiO₂, resulting in larger J_{SC} , and according to eqs 9–11 (vide supra) in an increase of the V_{OC} . Meyer and co-workers further investigated in detail the effect of PE rigid rod linkers in tripodal Ru-bpy/PE/TiO₂ systems in DSSCs.^{250,251} They evidenced that the approach of I₃⁻ ions to the TiO₂ surface is hampered when the dye regeneration occurs at farther distance (i.e., dye with longer PE spacer) from the TiO₂ surface. As a result, charge recombination rate constants between I₃⁻ ions of the electrolyte and TiO₂-injected electrons were decreased by a factor 280 (two PE units) and 20 (one PE unit) relative to a reference dye without PE spacer, resulting in a marked increase of the open circuit photovoltage of the DSSCs. Thus, one possible attractive strategy to increase the V_{OC} of a DSSC cell would be to increase the distance between the chromophore and the surface while maintaining a high quantum yield of electron injection through an efficient spacer. In the light of the results obtained from Lin and co-workers, diverging from those of Gundlach et al. and Meyer and co-workers, one possible explanation might be that the optimal length of the spacer is reached at one PE unit for PEn porphyrin dyes.

In 2010, the same authors and co-workers developed a complementary strategy to improve further the light-harvesting capabilities of the dye PE1, incorporating acene-type linkers between the porphyrin and anchoring group²⁵² (Figure 32). Compared to the previous PEn dyes, the growing π -conjugation in a “lateral” fashion from benzene (LAC1) to pentacene spacer (LAC5) is expected to not alter electron-injection or electron-collection efficiency, because the length of the bridge between the porphyrin and anchoring group remains

the same for all dyes, but on the other hand, one can expect that it would favorably improve the LHE of the dye. Indeed, going from LAC1 to LAC5, the introduction of acene-linkers with π -extended conjugation causes systematic important redshifts and broadening of both the Soret (B) and Q bands. For LAC3 and LAC5 these bands appear much broader compared to the other dyes. Additionally, LAC4 displays two new bands for the tetracene group, and LAC5 a lowest energy band between 700–800 nm attributed to an intramolecular energy transfer porphyrin → pentacene, completing the porphyrin absorption.

The PCE of TiO₂-LAC cells gradually increased from LAC1 ($\eta = 2.95\%$) to LAC3 ($\eta = 5.44\%$) but then drastically decreased from LAC3 to LAC4 ($\eta = 2.82\%$) and LAC5 ($\eta = 0.18\%$) (Table 11). The increase of performances from LAC1 to LAC3 was attributed to larger IPCE values in the series, caused by larger broadening of the absorption bands. Although LAC5 displays much broader absorption up to 800 nm, the drastically lower performances obtained for this dye were explained in terms of poor electron-injection efficiency caused by the apparition of new deexcitation channels of the acene moiety. As confirmed by steady-state fluorescence spectroscopy, a substantial decrease of the fluorescence for LAC4 and a strong decrease for LAC5 were observed when compared to LAC1–3. Computational studies also evidenced that, while the HOMO/LUMO levels are mainly localized on the porphyrin core for LAC1 and LAC2, they become strongly delocalized over the porphyrin core and antracene moiety for LAC3 and mainly localized on the tetracene or pentacene moiety for LAC4/5. Thus, it was suggested that LAC4/5 should enable a new deactivation pathway by intersystem crossing and internal conversion, and accordingly, the strong diminishing of the fluorescence observed for these dyes should be explained by the quenching of the porphyrin excited state by energy transfer to the acene moiety, followed by nonradiative relaxation

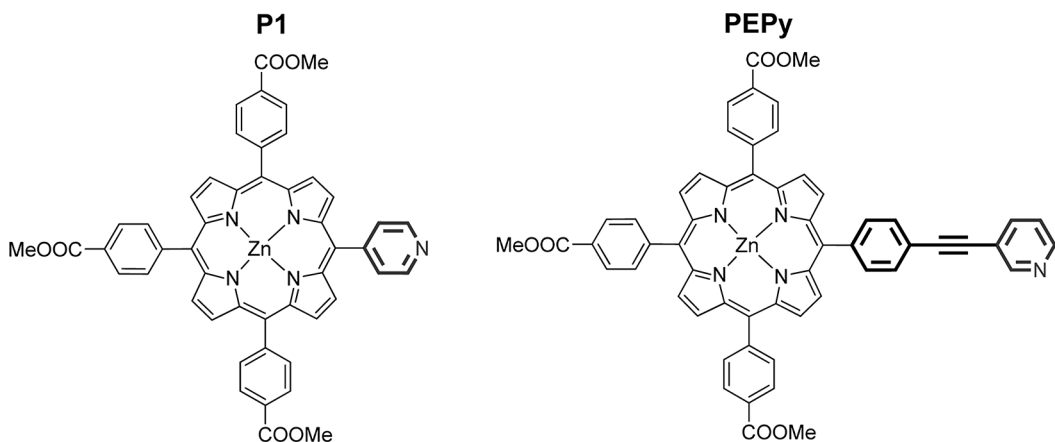


Figure 33. Molecular structures of porphyrin dyes **P1**¹⁹⁰ and **PEPy**¹⁹¹ reported by Coutsolelos and co-workers. Note: The dye depicted on the right did not have a name nor number in the article from ref 191, and was arbitrary called “**PEPy**” by us for the phenylethynyl 3-pyridyl anchoring group.

processes. This deexcitation channel must be competitive in the case of **LAC4** and major in the case of **LAC5**, which should disfavor proportionally the electron injection rate from the excited porphyrin to TiO_2 , responsible for their lower performances.

3.3. A3B-Type Porphyrin Dyes Substituted with Heteroaromatic Groups

3.3.1. A3B-Type Porphyrin Dyes Anchored through Pyridyl Groups. The use of a pyridine ring as an electron-withdrawing anchoring group^{185–194} was first reported recently by Harima and co-workers¹⁸⁵ in 2011 for a series of non-porphyrinic organic dyes, giving the same or higher efficiencies in TiO_2 -DSSCs than similar analogues tethered with a conventional carboxyphenyl group. Sharma and co-workers applied successfully this strategy to porphyrins^{121,189} and reported two dyes anchored through 4-pyridyl (**P1**)¹⁹⁰ or phenylethynyl 3-pyridyl (**PEPy**)¹⁹¹ (Figure 33 and Table 12). **PEPy/TiO₂** cell

using CDCA as coadsorbent, which significantly decreased dye aggregation and resulted in both higher J_{SC} and V_{OC} and hence higher PCE. The cell was further optimized to 5.66% using silver nanoparticles (NPs-Ag) in a modified FTO/ TiO_2 /NPs-Ag photoanode, as well as CHENO as coadsorbent. The role of NPs-Ag is to improve the absorption of the film over the entire visible region, which helps to improve the PCE of a DSSC cell.

3.3.2. A3B-Type Porphyrin Dyes Anchored through Five-Membered Ring Heteroaromatic Groups and Thienyl Appended Porphyrins. The use of five-membered ring heteroaromatic groups, either as linkers between porphyrin and anchoring group, or as secondary donors, have been scarcely considered or reported in porphyrin-DSSCs. Owing to smaller size and angle bonds, a five-membered ring substituted at the meso position of a porphyrin induces less steric hindrance with the β -pyrrolic protons than a phenyl group does. Thus, they present higher degree of conformational freedom and can adopt a more planar conformation that allows a partial overlap of their π orbitals with those of the porphyrin ring. The resulting dihedral angle formed with the porphyrin plane is therefore reduced compared to their phenyl analogues (phenyl groups are typically considered orthogonal to the porphyrin macrocycle). Consequently, these kinds of porphyrins display inherent photophysical and electrochemical properties rather different than their phenyl tetra-substituted analogues. In particular, thienyl-appended porphyrins are known to display red-shifted and broader absorption bands, as well as longer lifetime of their excited-states.²⁵³ As one of a few known examples,^{133,254} Tan and co-workers reported in 2011 a series of multialkylthienyl appended porphyrins in DSSCs using thienyl-linkers of different nature to anchor the dye through a cyanoacrylic acid group (Figure 34 and Table 13).²⁵⁴

As expected, all dyes display red-shifted (9–15 nm) and significantly broadened Soret and Q bands when compared to similar phenyl tetra-substituted zinc porphyrin analogues. The lower photovoltaic performances of **Z1** compared to **Z2**, differing only by *n*-hexyl versus methyl chains tailored at the three surrounding thiophene substituents, were explained by lower surface coverage achieved by **Z1** ($\Gamma = 29.0$ versus $48.4 \text{ nmol}\cdot\text{cm}^{-2}$). Compared to **Z2**, the molecular structure of **Z3** differs only by one additional appended hexyl chain at the 3-position of the thiophene-spacer in the anchor, while **Z4** is substituted at the 3,3'-position by an ethylenedioxy group (i.e., a 3,4-ethylenedioxythienylene group, “EDOT”). **Z3** and

Table 12. Photovoltaic Parameters of the TiO_2 -DSSCs Sensitized with **P1 and **PEPy** under Simulated AM1.5G Full Sun Illumination**

dye	coadsorbent	V_{OC} (mV)	J_{SC} ($\text{mA}\cdot\text{cm}^{-2}$)	F.F.	PCE (%)	ref
P1	none	600	9.2	56	3.10	190
PEPy	none	640	9.38	56	3.36	191
PEPy	CDCA	680	10.64	62	4.48	191
PEPy^a	CDCA	720	11.56	68	5.66	191

^aA modified photoanode (FTO/ TiO_2 /Ag-NPs) was used (see ref 191 for details).

was reported with a slightly higher PCE value than **P1/TiO₂** under standard conditions ($\eta = 3.36$ versus 3.10%, respectively). Although both cells display similar photovoltaic parameters, the device made with **PEPy** dye with a longer phenylethylene spacer displays a substantially higher V_{OC} than **P1** without using coadsorbent (640 versus 600 mV, respectively) which mainly accounts for higher PCE of the former. These results are in agreement with previous works reported by Gundlach et al.²⁴⁷ and Galoppini and co-workers,^{250,251} who observed a decrease of interfacial charge recombination rate constants when using longer phenylethylene spacers, which was manifested by an increase of the V_{OC} (vide supra, see discussion on section 3.2). The PCE of **PEPy** cell could be further increased to $\eta = 4.48\%$ when

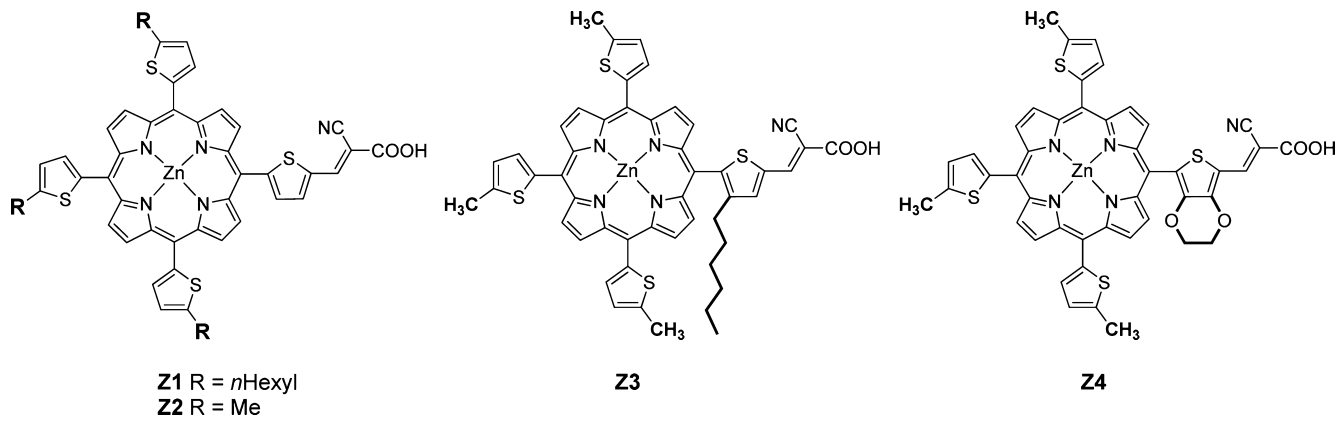


Figure 34. Multialkylthienyl appended porphyrin dyes reported by Zhou et al. (ref 254).

Table 13. Surface Coverage (Γ) and Photovoltaic Parameters of the TiO_2 -DSSCs Sensitized with Z1–4 under Simulated AM1.5G Full Sun Illumination (Power 100 mW·cm⁻²)^a

dye	Γ (nmol·cm ⁻²)	max IPCE (%)	V_{OC} (mV)	J_{SC} (mA·cm ⁻²)	F.F. (%)	η (%)
Z1	29.0	(~65) ^b	560 ± 10	12.13 ± 0.10	65 ± 1	4.44 ± 0.10
Z2	48.4	78	590 ± 10	14.18 ± 0.13	68 ± 1	5.71 ± 0.05
Z3	38.3	(~65) ^b	570 ± 10	11.37 ± 0.18	70 ± 1	4.54 ± 0.05
Z4	42.7	(~65) ^b	560 ± 10	11.56 ± 0.18	70 ± 2	4.54 ± 0.10

^aData derived from ref 254. ^bIPCE values roughly estimated from the graphs given in the article.

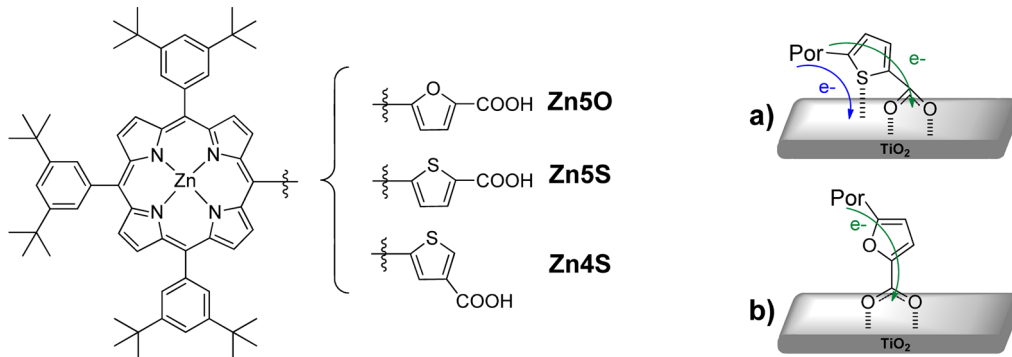


Figure 35. Left: porphyrin dyes anchored through carboxyfuranyl or carboxythienyl group; right: schematic view of adsorption geometry and electron-transfer pathways of (a) Zn5S and (b) Zn5O on TiO_2 surface, proposed by Imahori and co-workers. Figure (left and right panels) adapted with permission from ref 255. Copyright 2007 American Chemical Society.

Table 14. Surface Coverage (Γ) and Photovoltaic Parameters of the TiO_2 -DSSCs Sensitized with Zn5S, Zn4S, and Zn5O under Simulated AM1.5G Full Sun Illumination (Power 100 mW·cm⁻²)^a

dye	$\Gamma_{\text{sat}}/10^{-11}$ (mol·cm ⁻²)	max. IPCE (%)	V_{OC} (mV)	J_{SC} (mA·cm ⁻²)	F.F. (%)	η (%)
Zn5S	4.7	65	670	7.2	67	3.1 ± 0.2
Zn5O	6.9	55	620	5.8	65	2.3 ± 0.2
Zn4S	2.0	34	620	4.3	67	2.0 ± 0.02

^aData derived from ref 255.

Z4 cells display similar photovoltaic performances (J_{SC} , V_{OC} , and η), while Z2 outperformed clearly the formers, achieving a PCE of 5.71%. The authors suggested that the thiophene linker in Z2, exempt of appended group, should be able to adopt a more planar conformation with the porphyrin macrocycle, thus enhancing the electronic coupling between porphyrin and TiO_2 . This stronger coupling should promote the electron injection/collection efficiency of the dye, resulting in higher J_{SC} , IPCE values, and hence higher PCE of Z2/ TiO_2 cells. For Z3 and Z4, the hexyl chain or EDOT group appended to the thiophene spacer might hinder significantly the coplanar

orientation of the thiophene spacer so that the electronic coupling porphyrin- TiO_2 is weakened.

These results are in agreement with the work reported earlier in 2007 by Imahori and co-workers, who studied the influence of five-membered ring spacers on the structure of porphyrin films and their photovoltaic performances in TiO_2 -DSSCs (Figure 35 and Table 14).²⁵⁵

The dye Zn5S linked through a 5-carboxythien-2-yl anchoring group surpasses clearly the performances in DSSCs of both Zn5O with a 5-carboxyfuran-2-yl and the regiosiomer Zn4S with a 4-carboxythien-2-yl. Interestingly, DFT calculations

predict that the electronic structure of the porphyrin core is almost unchanged for the three dyes, but that the nature of the heteroatom (S or O), as well as the substitution position, causes considerable variations in the electron densities of the spacers, increasing in the order **Zn5S** < **Zn4S** < **Zn5O**. The smaller size of a furan than a thiophene ring making possible a larger conjugation with the porphyrin macrocycle, these calculations predict that the dihedral angle between the *meso*-heteroaromatic substituent and porphyrin plane become smaller for **Zn5O** (41°) with a furanyl than for those of **Zn4S** (80°) and **Zn5S** (73°) with a thienyl group. This larger conjugation is reflected in the absorption spectra: **Zn5O** display a broader Soret band and red-shifted Q bands in comparison with those of **Zn4S** and **Zn5S**. The three cells display similar V_{OC} values and fill factors but differ strongly from the J_{SC} , Γ , and η values. The lower dye coverage achieved by **Zn4S** ($\Gamma_{sat} = 2.0 \times 10^{-11} \text{ mol} \cdot \text{cm}^{-2}$) compared to **Zn5O** and **Zn5S** ($\Gamma_{sat} = 4.7 \times 10^{-11}$ and $6.9 \times 10^{-11} \text{ mol} \cdot \text{cm}^{-2}$, respectively) was ascribed as the main factor responsible for lower cell performances. Surprisingly, **Zn5S** and **Zn5O** differing only by the nature of the heteroatom in the bridging ring, display rather different amounts of saturated adsorbed dye. Based on ATR-FTIR and XPS spectroscopy measurements, the authors proposed that **Zn5S** should possess a 2-fold adhesive interaction with the TiO_2 surface through both the carboxylic acid and the sulfur atom, which does not occur through the oxygen atom of **Zn5O** (Figure 35, right). This “chelating-like” binding mode would imply a tilted binding geometry of the dye to the surface that explains the lower Γ_{sat} value achieved by **Zn5S**. Hence, the superior performance of the **Zn5S** cell was attributed to a possible additional electron-transfer pathway through the sulfur atom of the linker to the TiO_2 surface.

4. TRANS- AND CIS-A2B2-TYPE DESIGNS FOR MESO-SUBSTITUTED PORPHYRIN DYES

An A2B2-type porphyrin can exist under two regioisomers, namely *trans*- and *cis*-A2B2. However, the synthesis of pure

regioisomer is, by far, much easier in the case of the *trans*-type. Typically, a *trans*-A2B2 porphyrin is readily synthesized regioselectively from the condensation of an aldehyde with a dipyrromethane under acid-catalyzed conditions.^{171,256} Although some methods have been developed for the regioselective synthesis of *cis*-A2B2 porphyrins,²⁵⁶ they require, however, multi-steps and most often tedious procedures. Hence, *cis*-A2B2 porphyrins are usually obtained as secondary products from statistical reactions involving pyrrole/aldehydes condensations, and are isolated in low yields after tedious chromatographic separations of a statistical mixture of porphyrins (HPLC is most often required to separate *cis*/*trans*-A2B2 isomers under this procedure). In DSSCs, the A2B2-type design has been scarcely considered for porphyrin dyes, and relatively few examples of this type of sensitizer have been reported. In principle, this molecular design should take advantage of the A4- and A3B-type aforementioned designs, that is, the possibility to incorporate two anchoring groups for multibonds attachments, two solubilizing (or bulky) groups, and finally the relative ease to graft coupled π -conjugated spacers at the *meso* positions. Given the fact that *trans* A2B2-type porphyrins are synthetically much more accessible than *cis* type, it implies in such design, that the two anchoring groups are located in an opposite way. At first sight, this geometric orientation does not appear to be the most appealing to favor a possible multibond attachment of the dye on the TiO_2 surface, limiting somehow the interest of such design. Moreover, given the fact that the synthetic access to *trans*-A2B2-type porphyrins is similar to *trans*-A2BC (dealt with later in the next section) without any particular higher difficulties, the A2BC-type design, allowing more versatility, will be usually preferred to A2B2. As a state-of-the-art example of this design, Hupp and co-workers reported in 2010, a *trans*-A2B2-type porphyrin dye **ZnPdCA** reaching a remarkable power conversion efficiency of 5.5% in TiO_2 -DSSC (Figure 36 and Table 15).²⁵⁷

The dye **ZnPdCA** combines various favorable geometric and electronic factors: (1) a suitable length and geometry of the

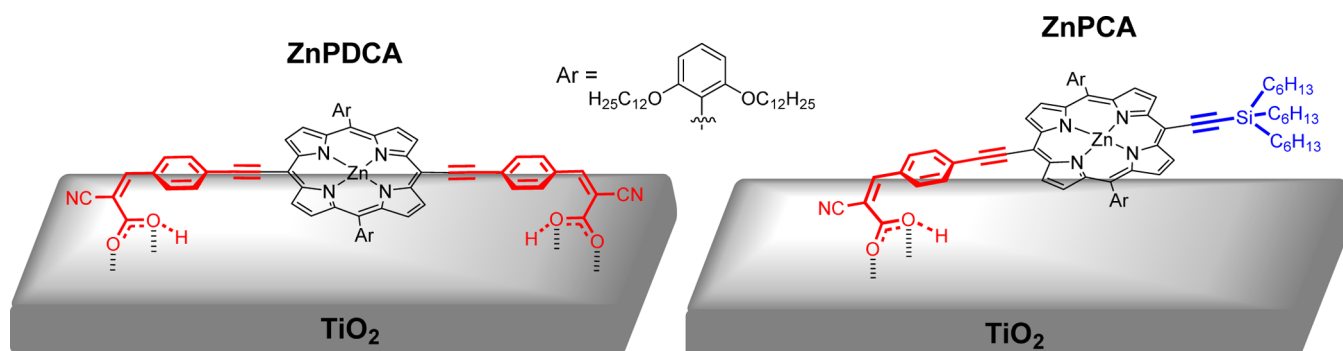


Figure 36. Molecular structures of dyes **ZnPdCA** and **ZnPCA** reported by Hupp and co-workers and schematic bonding mode attachment onto the TiO_2 surface proposed by the authors (ref 255).

Table 15. Surface Coverage (Γ), Binding Constant (K),^a and Photovoltaic Parameters of the TiO_2 -DSSCs Sensitized with **ZnPdCA and **ZnPCA** under Simulated AM1.5G Illumination (Power^b 98 mW·cm⁻²)^c**

dye	$\Gamma/10^{-8} (\text{mol} \cdot \text{cm}^{-2})$	$K/10^4 (\text{M}^{-1})$	V_{OC} (mV)	J_{SC} ($\text{mA} \cdot \text{cm}^{-2}$)	F.F. (%)	η (%)
ZnPdCA	5	11	680	11.3	70	5.5
ZnPCA	5	2	660	7.5	69	3.5

^aBinding constants of the dye to the TiO_2 surface, evaluated by monitoring changes in absorbance of the films after soaking them for 24 h in dye solutions of various concentrations in a mixture of CHCl_3 and EtOH (3:1, v/v). ^bData derived from the Supporting Information for ref 255.

^cData derived from ref 255.

spacer that can allow a double-binding mode attachment to the surface; (2) two coupled π -spacers that extend the conjugation with the porphyrin macrocycle and enhance the electronic communication dye-TiO₂ through the anchoring groups; and (3) two bulky (dodecyloxy)phenyl groups tethered at the two other (5,15)*meso*-positions protecting the porphyrin core against CR processes and aggregation. The possible double-binding mode attachment to the surface of ZnPDCA was suggested by the authors based on the following statements: in comparison with ZnPcA dye, tethered with only one anchor, ZnPDCA display (1) a 5-fold stronger binding constant to TiO₂ and (2) an important blue-shift of the Q-bands of ZnPDCA was observed going from solution to TiO₂ films, suggesting that the environment on the TiO₂ surface is distinct from that of ZnPcA. Interestingly, both dyes display similar coverage, which seems to indicate that the bridge-anchoring group must induce a coplanar/face-to-face orientation of the dye to the surface in both cases. DFT computational studies evidenced that the LUMOs of both dyes are fully delocalized over the porphyrin ring and entire ethyne-linked spacers. As expected, the extension of π -conjugation of the porphyrin macrocycle caused important broadening and redshifts of the Soret and Q bands, accompanied by higher molecular absorption coefficients, and more pronounced for ZnPDCA. The IPCE values of ZnPDCA/DSSC, higher than those of ZnPcA/DSSC by a factor ~1.6, primarily originate from higher LHE of the former by a factor ~1.3. Open-circuit photovoltage decay (OCPD) measurements suggest similar η_{coll} values for both dyes. Based on these results, the authors concluded that the differences of charge injection efficiencies (ϕ_{inj}) estimated to be 1.3 times higher for ZnPDCA than for ZnPcA are consistent with the differences in J_{SC} values by a factor ~1.5 and account most likely for the remaining difference in their IPCE values.

In 2012, Coutsolelos and co-workers reported two A2B2-type porphyrins in TiO₂-DSSCs (free base: P1 and zinc: P2), appended with two carboxyphenyl moieties acting as anchoring groups, and two *N,N*-dimethylaminophenyl moieties acting as donors²⁵⁸ (Figure 37 and Table 16). The best PCE was achieved for the zinc porphyrin dye P2 ($\eta = 4.83\%$) and could be significantly increased up to 6.07% by using CHENO as coadsorbent

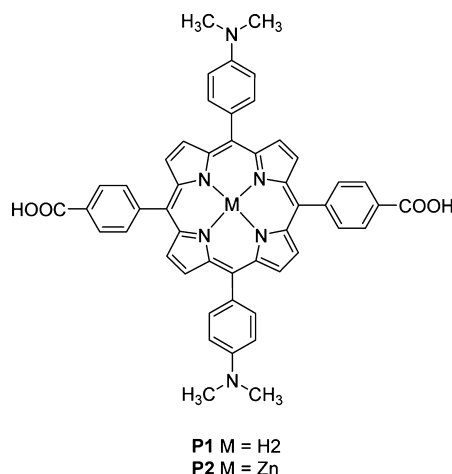


Figure 37. Molecular structures of A2B2-type porphyrin dyes P1 and P2, reported by Coutsolelos and co-workers (ref 258).

Table 16. Surface Coverage (Γ) and Photovoltaic Parameters of the TiO₂-DSSCs Sensitized with P1 and P2 under Simulated AM1.5G Full Sun Illumination (Power 100 mW·cm⁻²)^a

dye	Γ (nmol·cm ⁻²)	V_{OC} (mV)	J_{SC} (mA·cm ⁻²)	F.F. (%)	PCE (%)
P1	8.9	620	9.9	62	3.80
P2	16	660	11.1	66	4.83
P1 + CDCA ^b	n/a	700	10.6	66	4.90
P2 + CDCA ^b	n/a	720	12.4	68	6.07

^aData derived from ref 258. ^bChenodeoxycholic acid (CDCA) [10 mM] was incorporated in the dye-uptake solution for the fabrication of the device.

Although not reported in their work, one would assume that the 2-fold binding attachment of P1/2 dyes to the surface through the second carboxyphenyl group must be strongly disfavored due to geometrical issues, making the second anchoring group, somehow, useless. Presumably, the dyes should be anchored through only one of the two carboxylic acid moieties and oriented perpendicular to the surface in an “edge-to-face” geometry. The important increase of cell performances when using CHENO as coadsorbent seems indeed to be indicative of a tight staking of these dyes.

Werner et al. provided a good example and understanding on the impact and importance of the orientation of a dye toward photovoltaic parameters, photophysics, and electron transfer processes occurring at a porphyrin/metaloxide interface. Details photophysics studies using steady-state and time-resolved spectroscopic methods were carried out for two porphyrin dyes anchored through catechol groups to metaloxide surfaces (ZnO and TiO₂).²⁵⁹ The suitable length and geometry of the bridge spacer in dye 2 (*trans*-A2B2-type) allow a parallel “face-to-face” attachment to the surface, while dye 2 (A3B-type) featuring only one anchoring group binds the surface most likely perpendicular, in an “edge-to-face” fashion (Figure 38).

Both dyes were studied in ZnO- and TiO₂-DSSCs. The performances of ZnO-1 cell were slightly better than TiO₂-1, both superior than those obtained for ZnO-2 and TiO₂-2, respectively, the latter in turn, were almost the same. Although the ZnO-2 cell displayed higher V_{OC} than the ZnO-1 cell (420 mV versus 380 mV), the J_{SC} and IPCE values, in turn, were lower (Table 17). The porphyrin macrocycle of dye 2 is in tied contact with the ZnO surface because of the short distance between them in a face-to-face orientation, which perturbs significantly its electronic structure. As a result, the Zn(II)-porphyrin macrocycle in 2 is more difficult to oxidize, which widens the energy gap between ZnP^{•+}/ZnP and I₃⁻/I⁻. However, the studies of charge shift kinetics between dyes and I⁻/I₃⁻ in both ZnO/1 and ZnO/2 films did not reveal any appreciable differences, which therefore suggest that dye-regeneration efficiency (η_{reg}) must be similar in both cases. The different orientation of the dyes on the surface neither seems to influence notably the charge-transfer/charge-injection process from the excited dye to the ZnO oxide. Indeed, steady-state and time-resolved spectroscopic studies suggest that both dyes perform equally and highly efficiently, with a quantum yield of electron injection estimated to exceed 90% despite their long, nonconjugated, and fully decoupled spacer. The close proximity and tied contact between the porphyrin ring of dye 2 and the ZnO surface should increase the rate of charge recombination between oxidized dyes and ZnO injected-electrons, which

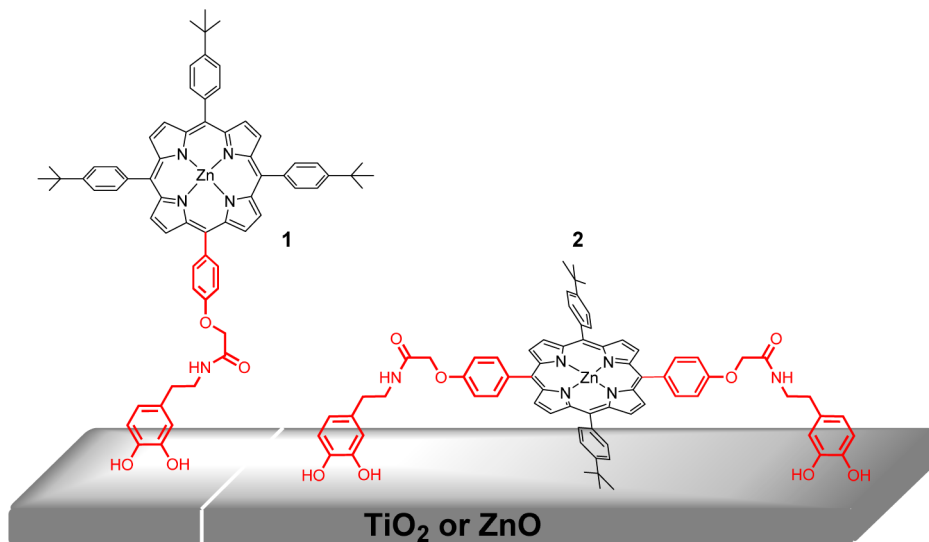


Figure 38. Molecular structures of porphyrin dyes **1** (A3B-) and **2** (A2B2-type), reported by Verener et al., and schematic binding geometry on the metaloxide surface: edge-to-face/perpendicular versus face-to-face/parallel alignment, respectively, proposed by the authors. Adapted with permission from ref 259. Copyright 2010 American Chemical Society.

Table 17. Photovoltaic Parameters of the ZnO–DSSCs Sensitized with Dyes **1 and **2**, under Simulated AM1.5G Conditions^a**

Cell	IPCE _{max} Soret (%)	V _{OC} (mV)	J _{SC} (mA·cm ⁻²)	PCE (%)
ZnO/1	(≈13.5) ^b	380	1.47	0.27
ZnO/2	(≈11) ^b	420	1.40	0.23

^aData derived from ref 259. ^bIPCE values roughly estimated from the graphs provided in the article (ref 259).

should confer to the ZnO/2 cell a lower electron-collection efficiency than ZnO/1. Moreover, the parallel attachment of **2** through two anchoring group requires a higher area to accommodate the dye on the surface, which impacts both on the adsorption kinetics ($k_{\text{ads}}\mathbf{1} = 0.057 \text{ s}^{-1}$ versus $k_{\text{ads}}\mathbf{2} = 0.037 \text{ s}^{-1}$) and on the maximum amount of adsorbed dye ($\Gamma_1 > \Gamma_2$ by a factor ~ 1.25). Because of larger dye coverage, ZnO-1 film displayed greater absorption, resulting in higher LHE. Taking into account that ϕ_{inj} and η_{reg} values are assumed likewise similar for both dyes, higher LHE and presumably higher electron-collection efficiency, hence confer to the ZnO-1 film the largest integrated IPCE value, which accounts for higher J_{SC} and accordingly a superior PCE. Similar trends were observed when turning to TiO₂-DSSCs, with a significant difference however regarding the V_{OC} that are likewise similar for both TiO₂/1 and TiO₂/2 cells, thus leading to an even lower PCE for the latter.

Interestingly, both *trans*- (upon certain geometrical restrictions) and *cis*-A2B2-type designs may allow a 2-fold binding mode of the dye to the surface. However, the difference of the resulting geometry adopted by the dye on the TiO₂ surface is drastically different: a face-to-face/parallel versus an edge-to-face/perpendicular orientation, respectively. On this line, Ambre et al. provided new insights into the understanding and rational effects of the position and number of anchoring group/substituent on a series of zinc porphyrin-DSSCs.²⁶⁰ They studied four types of porphyrin dyes, A3B/B3A-, *cis* and *trans*-A2B2-type, differently substituted with thiophenyl and carboxyphenyl moieties, the later acting as anchoring group(s) (Figure 39 and Table 18). As commented before, both *cis*-A2B2

and “B3A” (an “upside-down-fashioned” A3B-type in which three anchoring groups are tethered to the porphyrin) designs are quite rare in DSSC and worth noticing. All dyes display similar absorption spectra in solution, accompanied by broadening and slight redshifts of the porphyrin absorption bands upon increasing the number of thiophene units. For **3S1A** the presence of only one available anchoring group to attach the dye on the surface resulted in weak bonding and the lowest dye coverage on TiO₂ films of the series ($83 \text{ nmol}\cdot\text{cm}^{-2}$), with similar spectral features than in solution. *trans*-**2S2A** featuring two available anchoring groups, achieved a larger dye-coverage ($110 \text{ nmol}\cdot\text{cm}^{-2}$) thus resulting in greater absorption of the film, but for geometrical reasons only one carboxylic acid is assumed to be engaged in the attachment of the dye to the TiO₂ surface. In contrast, the suitable orientation of the two anchoring groups in *cis*-**2S2A** and **1S3A** allows a stronger attachment of these dyes to the TiO₂ surface through a 2-fold binding mode, as attested by ATR-FTIR spectroscopy experiments, and logically achieved larger dye-coverage (126 and $117 \text{ nmol}\cdot\text{cm}^{-2}$, respectively), which resulted in greater absorption of these films. Moreover, significant blueshifts of the porphyrin absorption bands going from dye-solutions to TiO₂-films were observed for *cis*-**2S2A** and **1S3A** supporting a tight packing of the dyes (H-type aggregates) that bind perpendicularly the surface. The difference of photovoltaic performances therefore primarily originates from a larger amount of dye loading (hence greater absorption of the films) in the order *cis*-**2S2A** > **1S3A** > *trans*- **2S2A** ≫ **3S1A**.

Next, the stronger attachment through a 2-fold attachment for both **1S3A** and *cis*-**2S2A** are assumed to enhance the electronic communication with the TiO₂ and thus should confer a better electron injection efficiency to these dyes, as attested by their strikingly higher J_{SC} values (6.59 and $6.08 \text{ mA}\cdot\text{cm}^{-2}$, respectively) in comparison with *trans*-**2S2A** ($J_{\text{SC}} = 4.34 \text{ mA}\cdot\text{cm}^{-2}$) or **3S1A** ($J_{\text{SC}} = 0.907 \text{ mA}\cdot\text{cm}^{-2}$). At last, despite *cis*-**2S2A** displaying higher Γ value, greater absorption in TiO₂ films, and relatively similar J_{SC} value than **1S3A** (both dyes anchored through two carboxylic moieties), the latter DSSC cell gave a significantly higher V_{OC} value than the former (546 mV and 593 mV, respectively) that contributes mostly to the superior overall PCE ($\eta = 3\%$ versus 2.5%). It was proposed that the

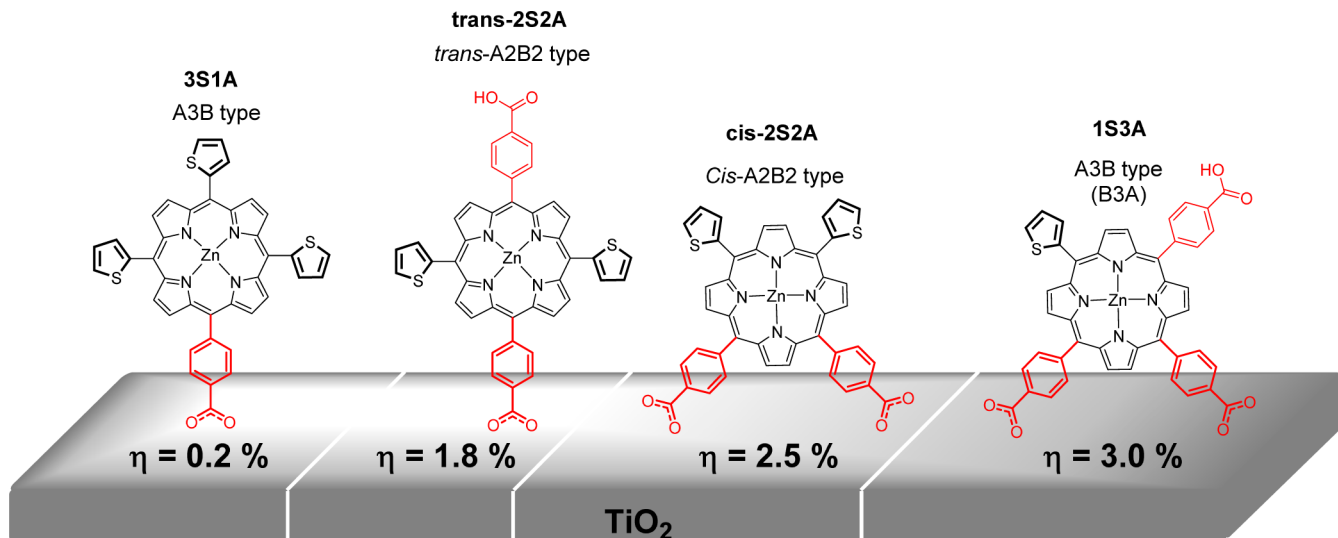


Figure 39. Molecular structures of thienyl-appended porphyrin dyes anchored through carboxyphenyl groups reported by Ambre et al.: effect of number and position of meso substituents. Adapted with permission from ref 260. Copyright 2012 American Chemical Society.

Table 18. Surface Coverage (Γ) and Photovoltaic Parameters of the Optimized TiO_2 -DSSCs^b Sensitized with 1S3A, *cis*-2S2A, *trans*-2S2A, and 3S1A, under Simulated AM1.5G Full Sun Illumination (Power 100 mW·cm⁻²)^a

dye	Γ_{Sat} (nmol·cm ⁻²)	V_{OC} (mV)	J_{SC} (mA·cm ⁻²)	F.F.	η (%)
1S3A	117	593	6.59	77	3.0
<i>cis</i> -2S2A	126	546	6.08	75	2.5
<i>trans</i> -2S2A	110	545	4.34	74	1.8
3S1A	83	455	0.907	48	0.2

^aData derived from ref 260. ^bCDCA was used as coadsorbent in the dye-uptake dye solutions: porphyrins [0.02 mM]/CDCA [0.04 mM].

heavy-atom effect of the sulfur atom must be responsible for the degradation of the V_{OC} , which indeed decreases inversely with the number of thienyl substituents in the order 1S3A (593 mV) < *cis*-2S2A ~ *trans*-2S2A (545–546 mV) < 3S1A (455 mV).

Coutsolelos and co-workers reported in 2012 a series of porphyrin dyes (**P1–3**) anchored through 4-pyridyl groups,

which is recent in porphyrin-DSSCs (Figure 40 and Table 19).¹⁹⁰ The *cis* A2B2-type porphyrin dye **P2** gave superior performances in TiO_2 -DSSC than the A3B- (**P1**) or A4-type (**P3**) analogues under same conditions. Various factors were taken into account to explain the differences of photovoltaic performances.

In contrast with **P1** bearing only one anchoring group, **P2** have a molecular structure that can allow a 2-fold binding mode, which explains well higher dye-loading for **P2**. Surprisingly, however, **P3** displays the lowest Γ value of the series despite featuring four available anchoring groups. It was assumed that the presence of numerous available free-pyridyl substituents in **P3** might increase the formation of porphyrin-porphyrin noncovalent aggregates (assembled through zinc metal-pyridine coordination) that should hinder a proper attachment of the dyes to the surface. Considering that all dyes have spectral features likewise similar in solution, the higher dye coverage in the order **P2** > **P1** > **P3** results in higher absorbance of the TiO_2 films in the same order. Additionally, **P2** displays slightly red-shifted absorption bands with respect to

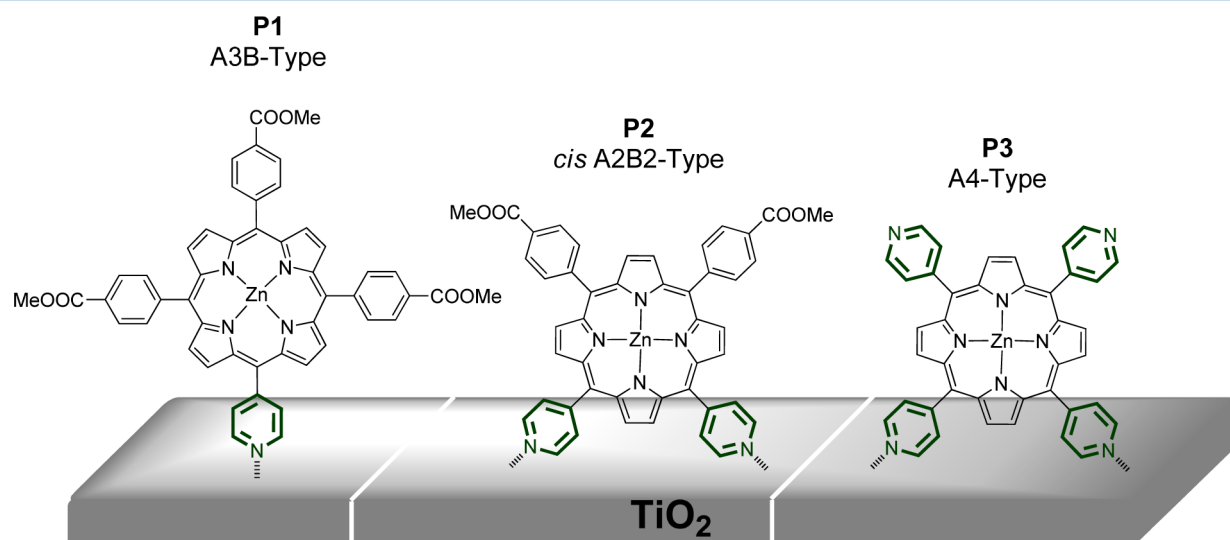


Figure 40. Molecular structures of 4-pyridyl-anchored porphyrin dyes **P1–3** reported by Coutsolelos and co-workers (ref 190).

Table 19. Surface Coverage (Γ) and Photovoltaic Parameters of the TiO_2 -DSSCs Sensitized with P1-3 under Simulated AM1.5G Full Sun Illumination (Power 100 mW·cm $^{-2}$)^a

dye	Γ (nmol·cm $^{-2}$)	film thickness (μm)	V_{OC} (mV)	J_{SC} (mA·cm $^{-2}$)	F.F. (%)	PCE (%)
P1	45	12	600	9.2	56	3.10
P2	56	12	640	10.56	60	3.90
P3	35	12	600	7.6	54	2.46
P2	64	b	640	12.04	64	5.24
P2 + DCA	52	b	680	12.86	68	6.12

^aData derived from ref 190. ^bOptimized conditions using a modified TiO_2 photoanode, pretreated with formic acid (see ref 190 for details).

the others. Consequently, both factors confer to P2 a superior LHE that contributes primarily to higher IPCE values. Next, the more suitable arrangement of the MO levels of P2 (a more negative LUMO and a slightly more positive HOMO) with respect to the potential-energy of the TiO_2 CB and I^-/I_3^- redox couple, should enhance the electron injection efficiency of P2 dye into TiO_2 and facilitate dye-regeneration, respectively. Next, the fill factor was also found to be higher for P2 (F.F. = 0.60) than the other cells (F.F. = 0.56 and 0.54 for P1 and P3, respectively), which also suggests a better electron-collection efficiency in the order P2 > P1 > P3. The superior LHE, ϕ_{inj} , n_{coll} , and η_{reg} efficiencies of P2 cell are reflected in the IPCE spectrum, which displays higher IPCE values at each wavelength than the others. To get deeper insights into the interfacial recombination processes, electrochemical impedance spectroscopy (EIS)^{224–228} analysis and photovoltaic data in the dark were carried out. On the basis of the J/V curves in the dark, it was found that P2 cell displays the lowest dark current, which decrease in the order P3 > P1 > P2. The dark current being generated mainly at the TiO_2 -electrolyte interface where no dyes are adsorbed, and considering higher dye-coverage for P2 in comparison with the others, it might be assumed a better organization and tighter packing of dyes P2 on the surface. Consequently, P2 should act as a more efficient blocking layer to hamper charge recombination between injected electron of TiO_2 and I_3^- ions, resulting in higher J_{SC} and V_{OC} values for the P2 cell. From EIS analysis in the dark, a longer electron lifetime for P2 (28 ms) than for P1 (19 ms) and P3 (14 ms) was deduced, which provides further evidence of reduced recombination rate at the TiO_2 -electrolyte interface in the P2 cell. The combination of larger V_{OC} , J_{SC} , and fill factor for P2 cell logically results in the highest PCE ($\eta = 3.90\%$) among the series. Under optimized conditions and using a modified TiO_2 -photoanode, the PCE of P2 cell was further improved to 5.24% and 6.12%, with and without using CHENO as coadsorbent, respectively.

5. TRANS-A2BC-TYPE DESIGN FOR MESO-SUBSTITUTED PORPHYRIN DYES: DONOR-BRIDGE CHROMOPHORE-ACCEPTOR (D-B-A), DONOR- π -BRIDGED CHROMOPHORE-ACCEPTOR (D- π -A OR "PUSH-PULL"), AND HYBRID SYSTEMS

Similar to A2B2-, A2BC-type porphyrins can exist in principle under two different regiosomeric forms, cis ("AABC") or trans ("ABAC"). With the exception of two recent examples of *cis*-A2BC-type porphyrin dyes reported by Kurotobi et al. (dealt in section 6), only *trans*-A2BC-type have been reported in DCCSs. This design is relatively new for porphyrin dyes and offers extremely high flexibility and versatility regarding the molecular structure of the porphyrin (electronic and geometric). In particular, the possibility to introduce a donor at the

opposite meso position of the acceptor/anchoring group allows the access to donor-bridge chromophore-acceptor (D-B-A) and donor-(π -bridged chromophore)-acceptor (D- π -A) structures, enhancing the permanent dipole moment. The donor that "pushes" the electron density toward the macrocycle, and on the opposite site the acceptor moiety that "pulls" the electron to the TiO_2 , are expected to strongly promote the electron injection process through this ballistic way. Although any *trans*A2BC-type porphyrin tethered with an acceptor and a donor at opposite sites could be in principle considered as the so-called "push-pull" porphyrins, we are making thereby a clear distinction between systems in which donor and acceptor are strongly coupled or not to the porphyrin macrocycle (typically the decoupled systems are phenyl bridged). Phenyl tetra-substituted A2BC-type porphyrins, in which all the substituents (including the donor and the acceptor) are decoupled from the porphyrin macrocycle will be considered as D-B-A systems, while A2BC-type porphyrins in which at least both donor and acceptor are strongly coupled to it (D- π -A systems), will be considered as real "push-pull" dyes. The intermediate cases, in which either the donor or the acceptor are strongly coupled to the porphyrin macrocycle, will be considered as hybrid "push-bridge-acceptor" or "donor-bridge-pull" systems, respectively. This concept is depicted in Figure 41.

5.1. "D-B-A" Systems: Phenyl Tetra-Substituted *trans*-A2BC-Type Porphyrins

The lack of absorption between 450–550 nm (green) and 600–920 nm (red and NIR), two photon-rich regions of the solar spectrum, represents a serious limitation of porphyrin sensitizers to reach higher efficiency in DSSCs. Mimicking the antennae effect of pigments in natural biological photosynthetic organisms, Odobel and co-workers reported a trichromophoric sensitizer (T) incorporating a boradiazaindacene (BODIPY), a zinc porphyrin porphyrin (ZnP) and a squaraine (SQ) unit to obtain a panchromatic dye (Figure 42 and Table 20).²⁶¹

BODIPYs²⁶² are chromophores that absorb near 500 nm, porphyrins in the 400–450 nm (strongly) and 550–600 nm (medium) regions, and squaraines strongly in the 600–700 nm, with medium, to high, extinction coefficients ($\epsilon > 10^5 \cdot \text{M}^{-1} \cdot \text{cm}^{-1}$). This complementary in absorptions thus makes them ideal partners to span a large spectral window and harvest photons over ranges that each discrete species cannot. Moreover, SQs, BODIPYs, and Zn(II)-porphyrins are pigments that display high fluorescence quantum yields, slow intersystem crossing, long excited-state lifetime, and excellent photostability, making energy-transfer processes between the three components highly efficient. In dye T, the squaraine moiety plays simultaneously the roles of light-harvesting system, energy-collector center, and sensitizer for electron injection in TiO_2 , while porphyrin and BODIPY centers act as secondary antenna. Steady-state fluorescence experiments in solution demonstrated a quantitative quenching of

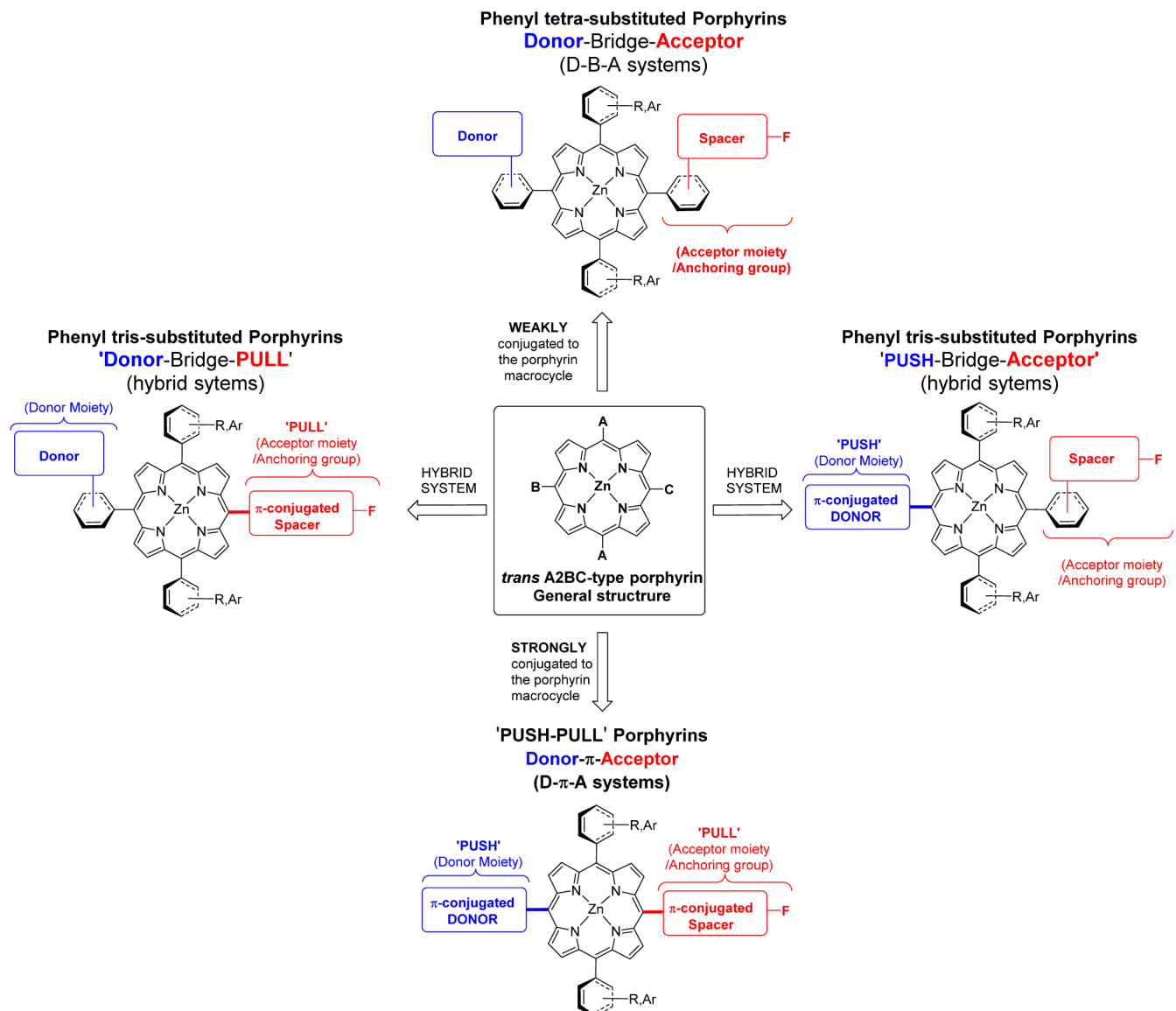


Figure 41. Common designs for *trans*-A2BC-type porphyrin dyes (F = functional binding group, R = Alkyl, alkoxy, Ar = phenyl/aryl).

the porphyrin emission in D, and those of ZnP and BODIPY in T, with an exclusive emission from the squaraine unit. Owing to a perfect matching of excitation and absorption spectra between the three components, the energy-transfer quantum yields were estimated over 98% from any antennae toward the squaraine moiety. In the DSSC cell, it enables three possible pathways for electron-injection of the squaraine moiety into the TiO₂ CB: either after direct excitation of the SQ itself (1) or mediated by an energy-transfer after absorption/excitation of the porphyrin (2) or BODIPY (3) subunits. Consequently, a 30% improvement of the PCE was gained going from SQI ($\eta = 3.0\%$), D ($\eta = 3.6\%$), to T ($\eta = 3.9\%$) DSSCs, which is consecutive to the expansion of the absorption spectrum over a broader wavelength range by porphyrin and BODIPY subunits.

In 2011, Deng and co-workers reported a series of *trans*-A2BC-type porphyrin dyes (D-B-A structured) in TiO₂-DSSCs, endowed with differently substituted phenyl groups acting as donors, and carboxyphenyl or phenylcyanoacrylic acid as acceptor/anchoring group (Dyes 1–5, Figure 43).²⁶³ The donor ability was modulated by incorporating EDG or EWG at the para position of a *meso*-phenyl, which affects the

HOMO–LUMO levels of the dye, and hence on the performances of the cell. The best performances were obtained for dyes 4 and 5, endowed with a triphenylamine-linked group (TPA) acting as an efficient secondary donor. TPA and other related arylamine groups are indeed well-known efficient EDGs that have been widely used in nonporphyrin DSSCs.^{4–6,12–18,264–266} TPA derivatives display a relative strong absorption in the 400–500 nm visible range that completes the absorption of the porphyrin and facilitate the electron charge transfer, both factors that boost the PCE of 4/TiO₂ and 5/TiO₂ cells at 1.52% and 2.38%, respectively, when compared for instance to that of the DSSC made with dye 1 with a phenyl group (i.e., an A3B-type porphyrin) of only 0.66% (Table 21, entry 1).

The same year, Kim and co-workers reported similar structured TPA-linked porphyrins (HKK-Por-3–5),²⁶⁷ and modified analogues HKK-Por-1 and HKK-Por-2 incorporating a (dicarbazole)triphenylamine moiety²⁶⁸ acting as an efficient secondary donor (Figure 43). By comparison with the dye HKK-Por-3, the performances in DSSC significantly increased upon switching the 5,15-*meso* phenyl groups by mesityls in the

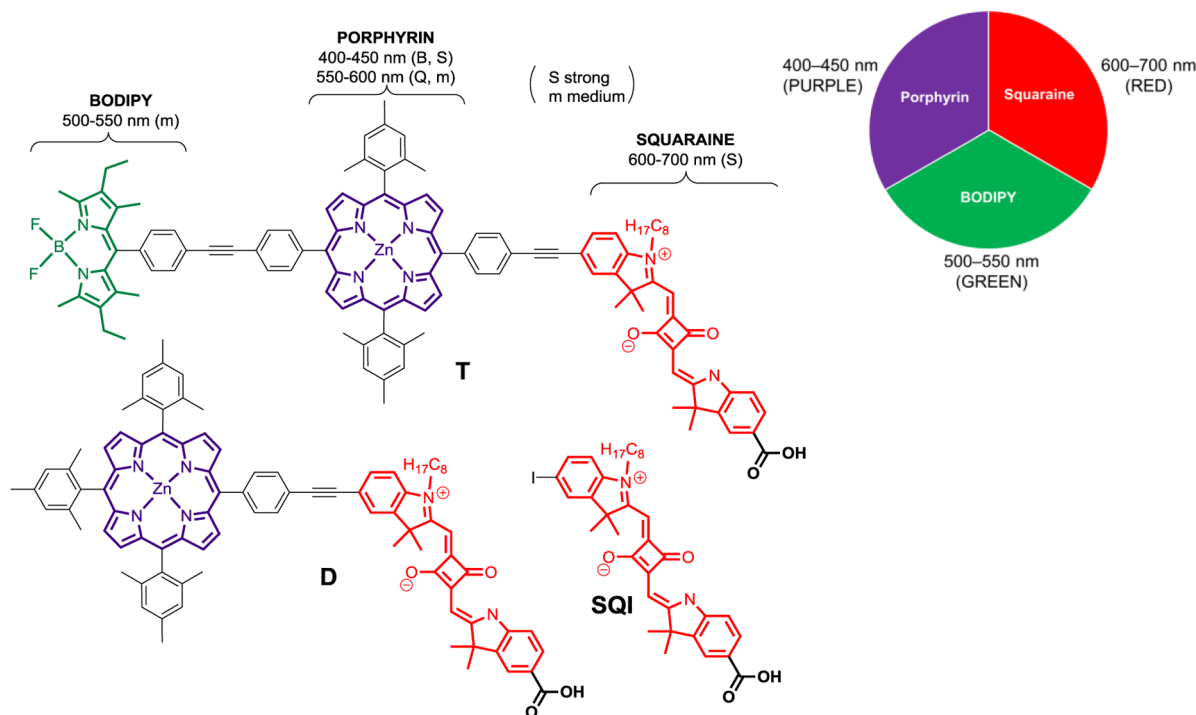


Figure 42. Molecular structures of squaraine (SQI), dichromophoric (D), and trichromophoric sensitizers (T), reported by Odobel and co-workers (ref 261).

Table 20. Photovoltaic Parameters of the TiO₂-DSSCs Sensitized with Dyes SQI, D, and T, under Simulated AM1.5G Illumination (Power 100 mW·cm⁻²)^a

dye	V _{OC} (mV)	J _{SC} (mA·cm ⁻²)	F.F. (%)	η (%)
SQI	615	6.6	73	3.0
D	635	8.0	72	3.6
T	625	8.7	71	3.9
N719 (Benchmark)	745	12.9	73	7.0

^aData collected from ref 261. PV data of the benchmark device made with the Ru(II) dye N719 are reported under same experimental conditions.

molecular structures of **HKK-Por-4/5**, and additionally incorporating ethylhexyloxy chains in **HKK-Por-5** (Table 21, entry 3). Considering that these three dyes display similar absorption features, the mesityl groups must impede more efficiently dye-aggregation than unsubstituted phenyls, and the terminal bulky alkylxylo substitutions of the TPA moiety in **HKK-Por-5** should help to both reduce charge recombination processes and increase the donor ability of the TPA unit, resulting in an increase of the PCE in the order **HKK-Por-3** ($\eta = 2.09\%$) < **HKK-Por-4** ($\eta = 2.74\%$) < **HKK-Por-5** ($\eta = 3.36\%$).

The (dicarbazole)TPA-linked porphyrins **HKK-Por-1** ($\eta = 5.01\%$) and **HKK-Por-2** ($\eta = 4.07\%$) displayed much higher PCE than their TPA analogues **HKK-Por-3** ($\eta = 2.09\%$) and **HKK-Por-4** ($\eta = 2.74\%$), respectively (Table 21, entries 2 and 3). Similar to the bulky substitution in **HKK-Por-5**, the introduction of bulkier carbazole moieties in **HKK-Por-1/2** might help to reduce charge recombination processes. Additionally the superior donor ability of a dicarbazolyl-substituted TPA group, as well as slightly improved optical properties, confers to these dyes better performances in DSSCs. It is worth to notice that dye **HKK-Por-1** flanked with two unsubstituted

phenyl groups at the 5,15-meso positions, performed almost equally ($\eta = 5.01\%$) than **HKK-Por-2** with mesityl groups ($\eta = 4.70\%$). Although it is quite counterintuitive, the difference is however rather small. The bulky dicarbazolyl-substituted TPA unit must already impede efficiently dye-aggregation, and the difference in performances might be explained by slightly lower molecular absorption coefficients and/or dye-loading dye on the TiO₂ surface for **HKK-Por-2** than **HKK-Por-1**.

5.2. Push-Bridge-Acceptor' Systems: Amino-linked Donor, Phenyl Tris-Substituted *trans*-A2BC-Type Porphyrins

In 2012, Kim and co-workers reported two structurally modified analogues of their previously reported series of dyes "**HKK-Por**" (vide supra), the sensitizers **2Flu-ZnP-COOH** and **2Flu-ZnP-CN-COOH**, endowed with a difluorenlyl amino group as secondary donor (Figure 44, entry 1).^{269–271} The use of a diarylamino group directly tethered to the porphyrin through the nitrogen atom allows a π -orbital overlap with the π -conjugated system of the porphyrin macrocycle, resulting in much stronger electronic communication than, for instance, a triphenylamino group. The best performing dye **2Flu-ZnP-CN-COOH** achieved a PCE of 4.37% and was significantly improved to 6.64% by using CHENO (Table 22, entry 1). In conjunction with the use of a new coadsorbent developed in their group (**HC-A1**; see Figure 45), the PCE of this DSSC was further improved to 7.22%. Based on these excellent performances, the same group further reported a series of structurally modified analogues dyes **HP**, **HOP**, and **EHOP**, endowed with a diphenylamino donor group differently substituted with alkyl- or alkylxylo- chains (Figure 44 and Table 22, entries 2).²⁷² The best performing dye **HOP** outperformed slightly the former **2Flu-ZnP-CN-COOH** in DSSC without using coadsorbent ($\eta = 4.7\%$ vs 4.37%) but underperformed when using the coadsorbents **CDCA** ($\eta = 5.4\%$ vs 6.64%) or **HCA-1** ($\eta = 6.9\%$ vs 7.22%). However, in conjunction with another new

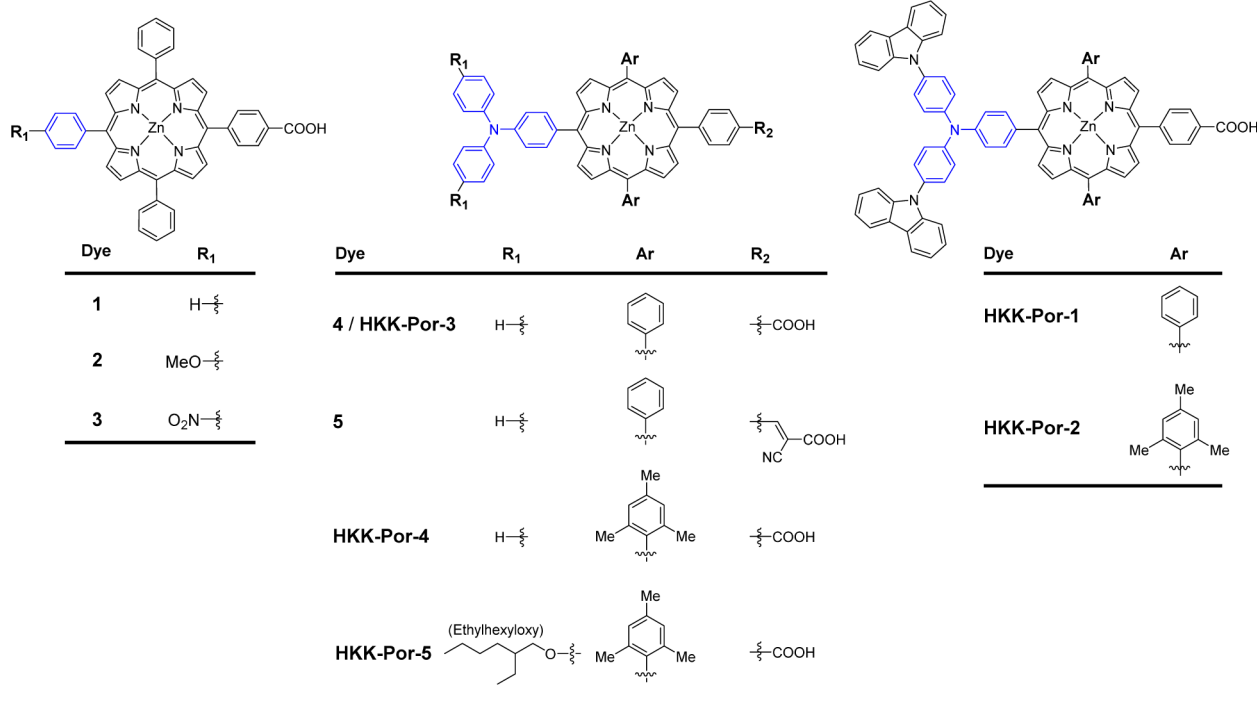


Figure 43. Molecular structures of phenyl-, triphenylamino-, and (dicarbazolyl)triphenylamino-linked donors porphyrin dyes (refs 263, 267, and 268).

Table 21. Photovoltaic Parameters of the TiO₂-DSSCs Sensitized with Dyes 1–5 Reported by Liu and Co-workers, and Dyes HKK-Por Reported by Kim and Co-workers, under Simulated AM1.5G Full Sun Illumination (Power 100 mW·cm⁻²)^a

entry	dye	V _{OC} (mV)	J _{SC} (mA·cm ⁻²)	F.F. (%)	η (%)	ref
1	1	542	2.23	54.9	0.66	263
2		553	2.90	55.5	0.89	
3		563	4.66	54.9	1.44	
4 (= HKK-Por-3)		605	4.95	50.8	1.52	
5		613	7.63	51.0	<u>2.38</u>	
2	HKK-Por-1	670	10.7	70	<u>5.01</u>	268
	HKK-Por-2	640	10.9	68	4.70	
3	HKK-Por-3 (= 4)	590	5.38	66	2.09	
	HKK-Por-4	540	7.57	67	2.74	267
	HKK-Por-5	570	9.04	66	<u>3.36</u>	

^aBest PCE value obtained in each work are underlined.

homemade coadsorbent PTZ1, HOP/DCSS achieved a superior PCE of 7.6%. Following a similar strategy, they reported in 2013 two structurally modified difluorenylaminodyes, 2,4-ZnP-CN-COOH and Hexo-ZnP-COOH, incorporating terminal hexyloxy chains or 3,4-dihexyloxyphenyl groups (Figure 44 and Table 22, entries 3).²⁷³ Under the same conditions, 2,4-ZnP-CN-COOH/DSSC displayed improved performances in comparison with their former reference cell 2Flu-ZnP-CN-COOH/DSSC, with and without coadsorbent (HCA1), achieving a maximum PCE of 8.41%. It is worth noting that all these similar-structured dyes display strikingly higher performances when using a coadsorbent, witnessing the relative strong tendency of aggregation of these kinds of porphyrins.

In 2010, Imahori and co-workers studied in detail the effect of a di-p-tolylamino group as donor(s) for porphyrin dyes

toward the photovoltaic performances of DSSCs, electrochemical and optical properties²⁷⁴ (Figure 46). The increased number of diarylamino groups enhances the light-harvesting capability of the dye by broadening and redshifting the absorption of the porphyrin, because of the extension of the effective π -conjugation over the macrocycle. Thus, the relative integrated LHE value increases in the order ZnP (1) < Mono-ZnP (1.4) < *trans*-ZnP ≈ *cis*-ZnP (1.7). In contrast, the maximum APCE (adsorbed photon-to-photocurrent efficiency) value, which correlates the electron-injection/charge-collection efficiency (APCE = $\phi_{inj} \times \eta_c$), decreases in the order ZnP (78%) ≈ Mono-ZnP (78%) > *cis*-ZnP (69%) > *trans*-ZnP (53%). Taking into account that the fill factor is rather the same for all dyes, the difference in PCE is therefore mainly explained by the difference of the IPCE values, which originates from the cumulative effect of LHE and APCE (with IPCE = LHE × APCE). Thus, the superior performance of MonoZnP/TiO₂ cell in comparison with the reference ZnP/TiO₂ (η = 6.5% vs 4.4%), mainly arises from the relative larger integrated LHE value of the former (1.7 versus 1). Although *trans*- and *cis*-ZnP display superior LHE, the significant decrease of the electron injection/charge collection efficiency (APCE = 53% and 69%, respectively) is mainly responsible for lower PCE values (η = 3.8% and 5.5%, respectively) with respect to Mono-ZnP/DSSC (η = 6.5%). The compromise between high APCE values and moderate LHE hence confer to Mono-ZnP/DSSC the highest PCE of the series, which emphasizes that the D-B-A “ballistic” structure of *trans*-A2BC-type porphyrin is one of the best design to reach optimal performances in DSSCs.

5.3. “Donor-Bridge-Pull” Systems: Phenyl Tris-Substituted *trans*-A2BC-Type Porphyrins Anchored through an Ethynylcarboxyphenyl Group

As we commented previously in section 3, the remaining concerns about the decoupling of the phenyl ring from the

The figure shows two rows of chemical structures. The left row shows a difluorenylaminolinked porphyrin dye (left) and a diphenylaminolinked porphyrin dye (right). The right row shows a diphenylaminolinked porphyrin dye (left) and an ethynylcarboxyphenyl-linked porphyrin dye (right).

Entry	Dye	R	A	Entry	Dye	R
1	2-Flu-ZnP-COOH	$\text{--}\ddot{\text{s}}\text{--H}$	$\text{--}\ddot{\text{s}}\text{--COOH}$	HP		$\text{--}\ddot{\text{s}}\text{--(n-hexyl)}$
	2-Flu-ZnP-CN-COOH	$\text{--}\ddot{\text{s}}\text{--H}$	$\text{--}\ddot{\text{s}}\text{--CH=CH--COOH}$ NC			
3	HexO-ZnP-CN-COOH	$\text{--}\ddot{\text{s}}\text{--(hexyloxy)}$	$\text{--}\ddot{\text{s}}\text{--CH=CH--COOH}$ NC	2	HOP	$\text{--}\ddot{\text{s}}\text{--(hexyloxy)}$
	2,4-ZnP-CN-COOH	$\text{--}\ddot{\text{s}}\text{--(hexyloxy)C}_6\text{H}_3\text{O--}$	$\text{--}\ddot{\text{s}}\text{--CH=CH--COOH}$ NC			
					EHOP	$\text{--}\ddot{\text{s}}\text{--(ethylhexyloxy)}$

Figure 44. Difluorenylamo- (left) and diphenylamo- (right) linked donor porphyrin dyes anchored through carboxyphenyl or phenylcynoacrylic acid groups, reported by Kim and co-workers (refs 269, 272, and 273).

porphyrin macrocycle in the traditional carboxyphenyl anchoring group has prompted the use of π -conjugated spacers that promote strong electronic coupling between the dye and TiO_2 , which is expected to favor the electron injection of the excited dye into the TiO_2 -CB.^{174–177} Additionally, the extension of π -conjugation also contributes to widen and redshift the absorption of the porphyrin, which confer potentially better light-harvesting capabilities of these systems. Although various π -conjugated spacers have been recently reported, porphyrins anchored through an ethynylcarboxyphenyl group have aroused a growing interest, considering that most of these dyes often reach superior performances than those obtained with similar structured analogues using other π -bridged anchoring groups.

Diau and co-workers reported an example of a donor-bridge-pull porphyrin dye (**YD6**), which incorporates an ethynylcarboxyphenyl as anchoring group, and a triphenylamine-based derivative (TPA) acting as secondary donor (Figure 47).²⁷⁵ In comparison with the A3B-type porphyrin dye **YD0**, the incorporation of a TPA donor group in the molecular structure of **YD6** significantly improved the performances of the DSSC, achieving an overall PCE of 5.13% versus 4.34% for the former (Table 23).

Another example of this class of dye was reported by Palomares and co-workers, the indoline-linked dye **VC-70** anchored through an ethynylcarboxyphenyl (Figure 48).²⁷⁶ Interestingly, the photovoltaic performances of the device made with dye **VC-70** were relatively well-below those of the benchmark cell **YD2-o-C8/DSSC** before light soaking, achieving a modest PCE of 5.59% (Table 24). However, all photovoltaic

characteristics of the **VC-70** cell significantly improved after 90 min of illumination, while those of the benchmark slightly decreased. Under same experimental conditions, **VC70/DSSC** reached a maximum PCE of 7.31% which is comparable to that obtained with the device made with the former champion dye **YD2-o-C8** ($\eta = 7.60\%$). As commented before for **PZn-hT** cell in section 3.1 (vide supra), the evolution of the performances of a DSSC upon illumination was reported in some cases, but elucidated only quite recently. In agreement with previous works,^{234–236} the authors evidenced that the increase of the V_{OC} was due to an increase of the electron lifetime in the device, as a result of cations exchange in the electrolyte and their migration to the TiO_2 surface (Li^+ and DMPI^+ are counterions of I^-/I_3^-), and suggested that the low densely packing of the molecule dyes should favor such phenomena. From charge extraction and transient photovoltage data, the increase of the J_{SC} was ascribed to a downward shift of the TiO_2 conduction band.

5.4. D- π -A Systems: “Push–Pull” Porphyrins

In the state-of-the-art design for *trans*-A3B-type “push–pull” porphyrins, Diau and co-workers pioneered the incorporation of π -conjugated donors (ethyne- or amino-linked), ethynylcarboxyphenyl as an efficient acceptor/anchoring group, both strongly coupled to the porphyrin ring and 3,5-di-*tert*-butylphenyl bulky groups, well-known to impede efficiently the π - π stacking aggregation of porphyrins (Figure 49). These remarkable and highly sophisticated designs lead to the best-performing porphyrin dyes to date in TiO_2 -DSSCs.

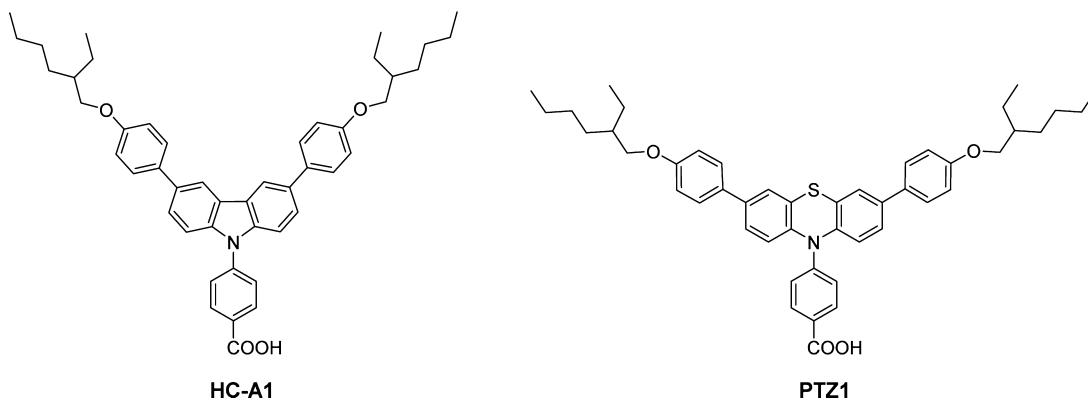
5.4.1. Ethyne-Linked Donor “Push–Pull” Porphyrins Anchored through an Ethynylcarboxyphenyl Group.

Table 22. Dye-Loading and Photovoltaic Parameters of the TiO₂-DSSCs Sensitized with the Porphyrin Dyes Reported by Kim and Co-workers under Simulated AM1.5G Full Sun Illumination (Power 100 mW·cm⁻²)^a

entry	dye	coadsorbent ^b	dye-loading (nmol·cm ⁻²)	V _{OC} (mV)	J _{SC} (mA·cm ⁻²)	F.F. (%)	η (%)	ref
1 ^c	2Flu-ZnP-CN-COOH	none	n/a	579	10.0	75	4.37	269
		CDCA	99.1	628	14.6	72	6.64	
		HC-A1	121.7	669	15.3	71	<u>7.22</u>	
	2Flu-ZnP-COOH	none	n/a	558	7.31	77	3.16	
		CDCA	11.3	580	11.1	73	4.7	
	N719 (Benchmark)	none	n/a	708	16.7	73	8.64	
2 ^c	HP	none	179	546	4.9	74.3	2.0	272
		CDCA	152	531	7.8	74.0	3.1	
		HC-A1	124	569	8.5	75.9	3.7	
		PTZ1	111	593	10.9	76.6	5.0	
	HOP	none	267	617	11.8	65.1	4.7	
		CDCA	239	620	13.2	66.2	5.4	
		HC-A1	189	675	15.2	67.5	6.9	
		PTZ1	165	678	15.9	70.3	<u>7.6</u>	
	EHOP	none	245	548	9.6	68.9	3.6	
		CDCA	214	554	10.1	70.5	4.0	
		HC-A1	161	613	12.7	70.6	5.5	
		PTZ1	131	632	13.4	72.2	6.1	
3	N719 (Benchmark)	none	n/a	701	16.7	73.6	8.6	
	2Flu-ZnP-CN-COOH (Reference dye)	none	n/a	579	9.67	71	3.95	273
		HC-A1	n/a	671	14.6	74	7.30	
	2,4-ZnP-CN-COOH	none	n/a	629	10.9	71	4.88	
		HC-A1	n/a	739	15.4	74	<u>8.46</u>	
	HexO-ZnP-CN-COOH	none	n/a	602	10.4	73	4.53	
		HC-A1	n/a	686	13.7	75	7.02	
	N719 (Benchmark)	none	n/a	700	17.7	73	9.09	

^aUnderlined values correspond to the best PCE obtained in each work. PV data of the benchmark devices made with the Ru(II) complex N719 were reported under same experimental conditions. ^bCDCA = chenodochylic acid; for HC-A1 and PTZ1, see molecular structures in Figure 45.

^cData derived from both the main article and Supporting Information.

**Figure 45.** Molecular structures of coadsorbents HC-A1 and PTZ1 developed by Kim and co-workers (refs 88 and 272).

Between 2009 to present, Diau and collaborators reported various “push–pull” porphyrin dyes achieving remarkably high efficiencies in DSSCs, which incorporate in their molecular structure an ethynylcaboxyphenyl as anchoring group, and ethyne-linked EDG or EWG, including aryl/phenyl, *N,N*-dialkylaminophenyl or triphenylamine derivatives (Figure 50 and Table 25).^{241,275,277–281} Upon incorporation of these different substituents, the relationship between molecular structures, electronic effect and donor capability toward the photovoltaic performances of these dyes in DSSCs were systematically investigated in details. Among all these similar structured porphyrins, it is worth noting that dyes tethered with even one of the simplest donor, an ethynyl-linked -phenyl

(LD1) or -biphenyl (LD21), reach remarkably high PCE of 5.11% and 6.3%, respectively (Table 25, entries 1 and 2). The presence of an electron-withdrawing nitro group at the para position of the phenyl group in PEINO2 reverses the driving force and pulls back the electron, process that competes with the electron injection of the dye in TiO₂ thus leading to a very low PCE of only 1.09% (Table 25, entry 5). On the contrary, the dialkylaminophenyl group in PE1NMe2/LD13 or LD15 enhances the driving force to push the electron toward the dye, which increases the “push–pull effect” (Table 25, entries 5–7). In combination with other favorable factors (electrochemical and optical properties), these dialkylaminophenyl-linked dyes achieved the highest PCE in DSSC of this series. The dye

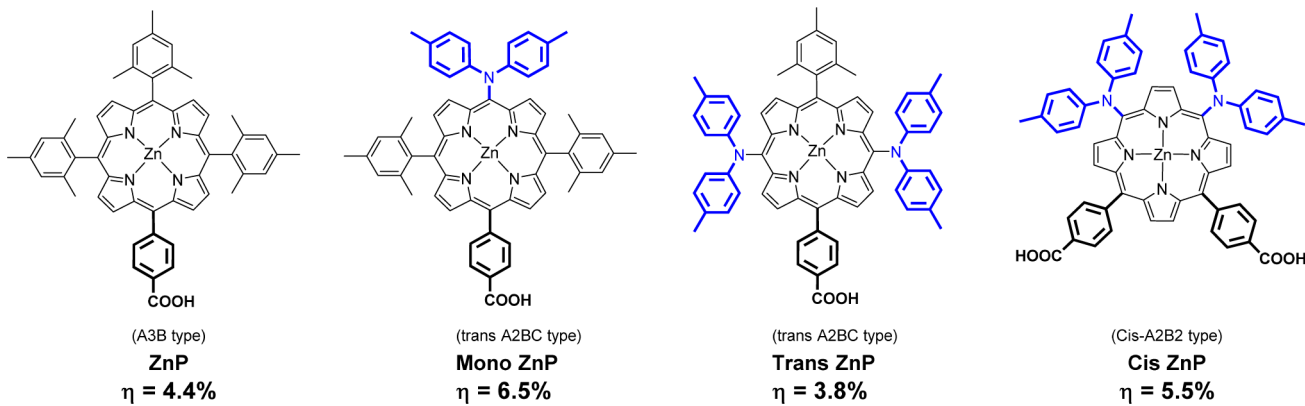


Figure 46. Molecular structures of carboxyphenyl-anchored porphyrin dyes reported by Imahori et al. (ref 274): effect of the number and position of *meso*-diarylaminodonor groups on the photovoltaic performances in TiO₂-DSSCs (PCE values were obtained under optimized conditions using CHENO as coadsorbent).

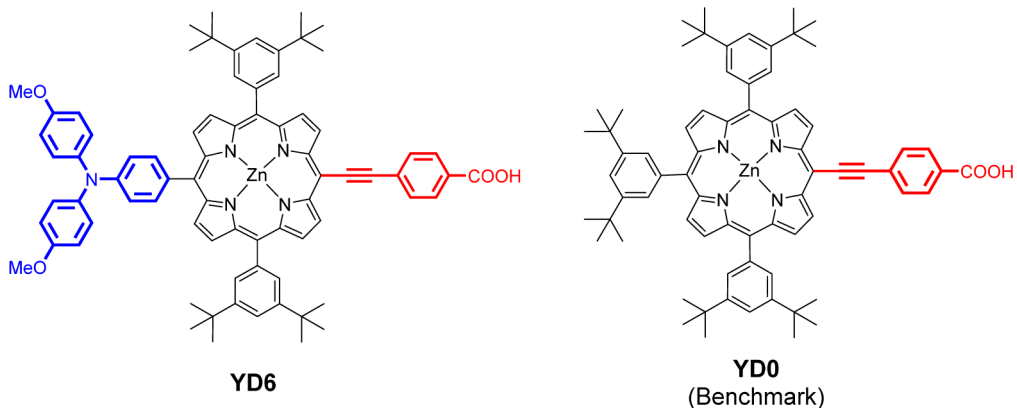


Figure 47. Molecular structures of YD6 (left) and benchmark YD0 (right), reported by Diau and co-workers (ref 275).

Table 23. Photovoltaic Parameters of the TiO₂-DSSCs Sensitized with YD6 and Benchmark YD0 under Simulated AM1.5G Full Sun Illumination (Power 100 mW·cm⁻²)^a

dye	V_{OC} (mV)	J_{SC} (mA·cm ⁻²)	F.F. (%)	η (%)
YD0	675	9.45	68	4.34
YD6	708	10.81	67	5.13

^aData derived from ref 275.

Table 24. Photovoltaic Parameters of the TiO₂-DSSCs Sensitized with VC-70 and Benchmark YD2-o-C8 under Simulated AM1.5G Full Sun Illumination (Power 100 mW·cm⁻²)^a

dye	illumination time	V_{OC} (mV)	J_{SC} (mA·cm ⁻²)	F.F. (%)	η (%)
YD2-o-C8	0 min	774	13.48	73	7.60
	90 min	774	12.83	75	7.43
VC-70	0 min	674	12.20	67	5.59
	90 min	699	14.47	72	7.31

^aData derived from ref 276.

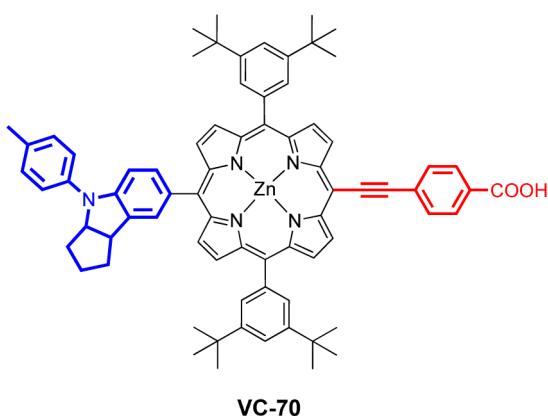


Figure 48. Molecular structure of indoline-linked porphyrin dye VC-70 anchored through the ethynylcarboxyphenyl group, reported by Palomares and co-workers (ref 276).

PEINMe₂ was first reported by Lin and co-workers in 2010, achieving a PCE of 6.12% in DSSC²⁸⁰ which was successively improved by the same authors up to a maximum reported value of 9.34% in 2011 (LD13).²⁷⁷

5.4.2. Amino-Linked Donor “Push–Pull” Porphyrins Anchored through an Ethynylcarboxyphenyl Group. In 2009, Yeh and co-workers reported a diarylaminosubstituted “push–pull” porphyrin, (Dye 1, latter known as the “green dye YD1”) reaching remarkably high PCE in TiO₂-DSSCs with maximum PCE values of 5.4% and 6.0% without and with coadsorbent (CHENO), respectively (Figure 51 and Table 26, entry 1).²⁴¹ Noteworthy, this dye outperformed the best porphyrin sensitizer at the time, and displayed comparable performances than those of the Ru(II) dye N3 (Ru(II) polypyridyl complex) under same conditions. Diarylaminogroups revealed

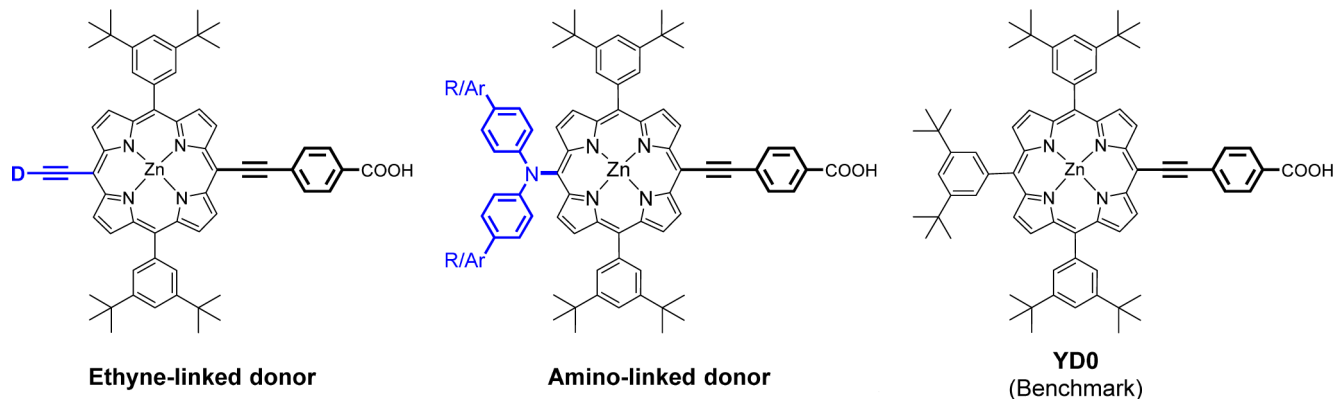


Figure 49. General structures of ethyne- and (diaryl)amino-linked donors “push–pull” porphyrins dyes anchored through an ethynylcarboxyphenyl group, and benchmark **YD0**, reported by Diau and collaborators (D = donor, R/Ar = alkyls, phenyl, or aryl groups).

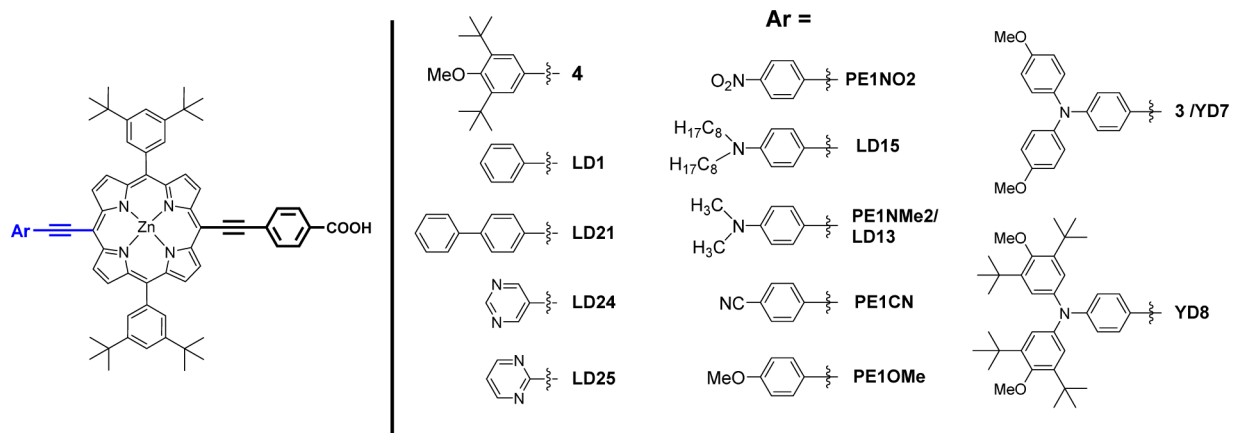


Figure 50. Ethyne-linked EDG (or EWG), ethynylcaboxyphenyl anchored, “push–pull” porphyrins reported by Diau and collaborators (refs 241, 275, and 277–281).

Table 25. Photovoltaic Parameters of the TiO₂-DSCCS Sensitized with LD, YD, and PE1 Porphyrins (PV Data of the Devices Made the Ru(II) Polypyridyl Complex N719 are Reported under Same Experimental Conditions in Each Work)

entry	dye	V _{OC} (mV)	J _{SC} (mA·cm ⁻²)	F.F. (%)	η (%)	ref
1	LD1	660	10.56	73.3	5.11	278
	N719	n/a	n/a	n/a	9.27	
2	LD21	682	12.92	71.7	6.3	279
	LD24	644	11.78	70.8	5.4	
	LD25	624	9.07	72.7	4.1	
	N719	836	14.79	74.6	9.2	
3	YD7 (= 3)	650	10.05	67	4.38	275
	YD8	651	9.94	66	4.27	
4	3 (= YD7)	546	3.76	67.2	1.4	241
	4	544	3.17	68.0	1.2	
5	PE1NMe2	680	13.08	68	6.12	280
	PE1NO2	570	2.53	74	1.09	
	PE1CN	650	8.59	72	4.05	
	PE1OMe	560	10.13	69	4.76	
	N719	750	13.48	70	7.03	
6	LD13	697	18.44	72.7	9.34	277
7	LD13 ^a	676	17.43	71.0	8.37	281
	LD15 ^a	676	17.87	72.60	8.77	
	LD15 ^b	669	18.56	71.8	8.92	

^aDye-uptake solvent THF. ^bDye-uptake solvent: toluene/EtOH 1:1 (v/v).

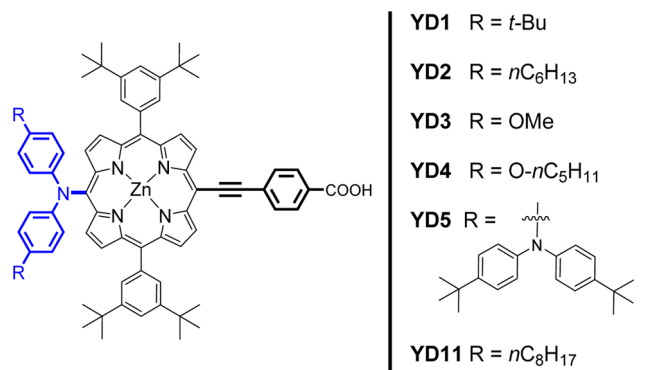


Figure 51. Diarylamino-linked donor, ethynylcarboxyphenyl anchored, “push–pull” porphyrin dyes **YD1–5** and **YD11** reported by Yeh and co-workers (refs 241, 275, and 282–285).

to be one of the best efficient donors to date in push–pull porphyrin dyes, allowing strong conjugation with the π-conjugated porphyrin macrocycle and a strong “electron-pushing” effect. It was evidenced that diarylamino groups, directly N-bonded at the *meso*-position of the porphyrin, allow a delocalization of the positive charge of the oxidized dye over both the diarylamino moiety and porphyrin ring. Moreover, the extension of π-conjugation of the porphyrin over both the donor (diarylamino group) and acceptor part (ethynylcarboxyphenyl), both strongly coupled to the macrocycle, significantly widens and redshifts the absorption bands of the dye.

Table 26. Photovoltaic Parameters of the TiO₂-DSSCs Sensitized with YD-1–5 and YD11 under Simulated AM1.5G Full Sun Illumination (Power 100 mW·cm⁻²)^a

entry	dye	[dye]/[CDCA] ratio ^b	TiO ₂ film thickness (μm) ^c	V _{OC} (mV)	J _{SC} (mA·cm ⁻²)	F.F. (%)	η (%)	ref
1	YD1 ^d	1:0	9	686	12.2	64.5	5.4	241
		1:1	9	710	14.3	59.4	6.0	
		1:2	9	708	13.2	64.0	6.0	
		1:4	9	710	12.05	66.2	5.7	
		1:10	9	701	11.23	66.8	5.3	
		1:1	9	701 ^e	13.6 ^e	62.9 ^e	6.0 ± 0.06 ^e	
	N3 (benchmark)	n/a	9	756	12.08	66.6	6.1	
2	YD0 ^f (benchmark)	1:2	[10 + 4]	675	9.45	68	4.34	275
		1:2	[10 + 4]	710	12.73	68	6.15	
		1:2	[10 + 4]	710	13.40	69	6.56	
		1:2	[10 + 4]	713	10.85	69	5.34	
		1:2	[10 + 4]	711	11.68	68	5.65	
		1:2	[10 + 4]	651	5.05	64	2.10	
3 ^g	YD11	1:0	10	714	13.43	69	6.62	282
		1:2	10	721	13.17	69	6.55	
		1:0	5	723 ^h	10.54 ^h	73 ^h	5.54 ± 0.11 ^h	
		1:0	10	715 ^h	12.99 ^h	71 ^h	6.56 ± 0.09 ^h	
		1:0	[10 + 4]	716 ^h	14.01 ^h	68 ^h	6.79 ± 0.12 ^h	
		1:2	7	650	6.92	73	3.29 (3.58 ⁱ)	283
4	YD2	1:0	7	660	15.4	62	6.36 (7.41 ⁱ)	
		1:2	[10 + 4]	697	10.42	69	5.0	284
5	YD0 ^f (benchmark)	1:2	[10 + 4]	714	14.80	67	7.1	
		1:2	[10 + 4]	755	10.5	71.2	5.6	285
		1:2	2.4	750	13.3	69.8	6.9	
		1:2	4.5	739	15.0	70.9	7.9	
		1:2	6.7	732	16.3	71.0	8.4	
		1:2	8.9	735	16.7	71.5	8.8	
6	YD2	1:2	11.5	770	18.6	76.4	10.9	
		1:2	[11 + S ^j]					

^aDevices made with porphyrin YD0, or Ru(II) complex N3, were used as benchmarks. ^bRatio of [Dye]/[CDCA] in the dye-uptake solution.

^cThickness of the TiO₂ active layer; the second value in brackets refers to the scattering layer. ^dYD1 was previously called “Dye 5” in the main article of ref 241. ^eAverage value obtained for two devices under optimized conditions. ^fSee molecular structure of the benchmark YD0 in Figure 49.

^gData derived from both the main article and Supporting Information for ref 282. ^hAverage values obtained for four devices. ⁱInternal PCE value.

^jThe scattering layer is made of a 5 μm thin layer of 400 nm reflecting particles.

At the end of 2009, beginning of 2010, the same authors further modified the molecular structure of YD1 dye in analogues YD2–5,11 (Figure 51 and Table 26, entry 2).²⁷⁵ The best performances in TiO₂-DSSCs were obtained for the well-known dye YD2 achieving a PCE of 6.56%, which is higher than the optimized TiO₂/YD1 cell ($\eta = 6.15\%$) under the same conditions. They further reported another green dye analogue YD11 achieving higher efficiencies under modified and optimized conditions, with and without scattering layer: $\eta = 5.5$ –6.6 and 6.79%, respectively (Table 26, entry 3).²⁸² The performance of YD2 in TiO₂-DSSCs was successively improved between 2010–2011 ($\eta = 6.36\%$,²⁸³ 7.1%²⁸⁴) and an achievement of 10.9% solar-to-electric power conversion efficiency was achieved under optimized and standard conditions (Table 26, entry 4–6).²⁸⁵

5.4.3. Polycyclic Aromatic Hydrocarbons-Modified Analogues of LD1 and YD11. As previously discussed in section 3.2 for A3B-type LAC porphyrins (vide supra), the use of polycyclic aromatic hydrocarbons as π -extended linkers is one complementary strategy to improve the light-harvesting capabilities of a porphyrin dye and was applied successfully to push–pull porphyrins. Similar to LAC1–5 porphyrins, the dyes YD12 and YD13, analogues of YD11/YD2, incorporate extended acene in the bridge linking porphyrin and carboxyl binding group (Figure 52 (top) and Table 27 (right)).^{282,286}

For the previous LAC porphyrins, the growing conjugation of the acene moiety, from phenyl in LAC1 to anthracene in LAC5, widened and red-shifted the Soret and Q bands absorption of the porphyrin. Accordingly, the photovoltaic performances increased from LAC1 to LAC3 with a maximum PCE for LAC3 (anthracene), but then decreased for LAC4/5 (tetracene or pentacene, respectively) due to the predominance of porphyrin-acene deexcitation pathway for higher-order acene. In the case of dyes YD12 and YD13, the performances of YD12 in TiO₂ cell ($\eta = 6.69$ –6.91%) with the smaller acene bridge (naphthalene) were slightly improved in comparison with the reference YD11 ($\eta = 6.56$ –6.79%) but then drastically decreased for YD13 with a larger anthracene spacer ($\eta = 1.76$ –1.86%). A similar approach has been applied to LD2–4 and LD22/23 modified analogues of LD21, by incorporating ethyne-linked acenyl and other related polycyclic aromatic hydrocarbons systems, acting as donors (Figure 52 (down) and Table 27 (left)).^{278,279} In comparison with dye LD1 that incorporates a phenylethyne donor group ($\eta = 5.11\%$), remarkably higher performances were obtained for the dyes LD22 ($\eta = 8.1\%$), LD3b ($\eta = 8.26\%$), and LD4 ($\eta = 10.06\%$) incorporating fluorenyl-, phenanthrenyl-, or pyrenyl-ethyne linked donors, respectively.

5.4.4. Alkoxy Wrapped Push–Pull Porphyrins. Based on the excellent performances obtained for the dye YD2 in

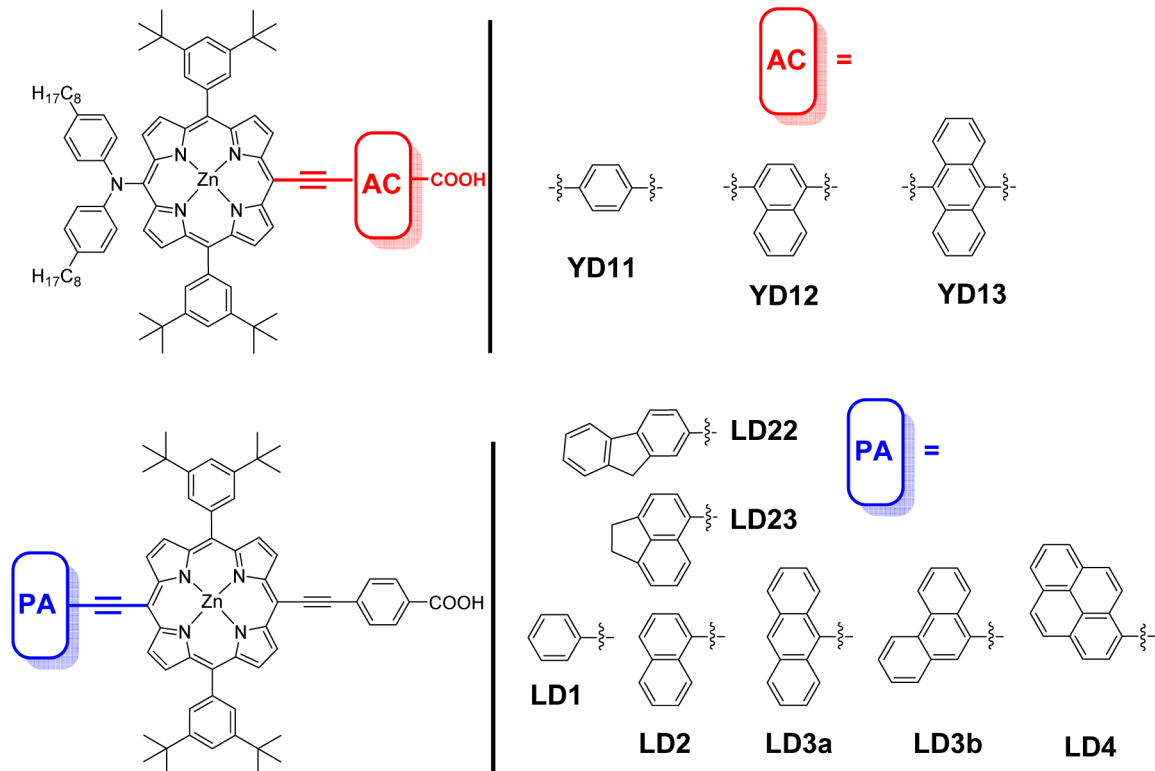


Figure 52. Molecular structures of dyes YD11–13, LD1–4, and LD22–23 reported by Diau and collaborators (refs 278, 279, 282, and 287).

Table 27. Photovoltaic Parameters of the TiO₂-DSSCs Sensitized with LD1–4, LD22–23, and YD11–13 under Simulated AM1.5G Full Sun Illumination (Power 100 mW·cm⁻²)^a

dye	<i>V_{OC}</i> (mV)	<i>J_{SC}</i> (mA·cm ⁻²)	F.F. (%)	<i>η</i> (%)	ref	dye	<i>V_{OC}</i> (mV)	<i>J_{SC}</i> (mA·cm ⁻²)	F.F. (%)	<i>η</i> (%)	ref
LD1	660	10.56	73.3	5.11	278	YD11	715	12.99	71	6.56	282
LD2	682	15.92	72.1	7.83		YD12 ^b	714	13.77	68	6.69	
LD3a	654	14.04	73.1	6.62		YD13 ^b	618	3.97	72	1.76	
LD3b	678	17.02	71.6	8.26		N719 ^b	769	10.97	73	6.16	
LD4	711	19.63	72.1	10.06		YD11 ^c	716	14.01	68	6.79	282
N719	n/a	n/a	n/a	9.27		YD12 ^c	717	14.23	68	6.91	
					279	YD13 ^c	630	4.12	72	1.86	
LD22	689	17.26	68.1	8.1		N719 ^c	786	13.08	71	7.27	
LD23	685	15.51	70.0	7.4							
N719	836	14.79	74.6	9.2							

^aDevices made with the Ru(II) complex N719 were used as benchmarks. ^bPerformances obtained with a 10 μm film without scattering layer.

^cPerformances obtained with a 10 μm film and an additional 4 μm scattering layer.

TiO₂-DSSCs, Yella et al. reported in 2011 a structurally modified analogue, YD2-o-C8, in which the 3,5-di-*tert*-butylphenyl groups have been replaced by 2,6-dioctyloxyphenyls^{65,287,288} (Figures S3 and S4 and Table 28). In conjunction with a novel iodine-free electrolyte (coded AY1) using the Co^{III/II} tris(2,2'-bipyridine) complex as redox couple, YD2-o-C8/DSSC strikingly outperformed YD2/DSSC under the same conditions ($\eta = 11.9\%$ versus 8.4%, respectively), which had been the best performance ever obtained in DSSCs until 2014. The use of a cobalt complex as the redox shuttle offers a main advantage in terms of attainable open-circuit potential due to the flexibility it offers in tuning the redox potential by varying the ligands.^{50,51,65–73} In addition, the overpotential needed for dye regeneration is considerably less compared to the standard iodide/tri-iodide redox mediators. Co-sensitization of YD2-o-C8 with another organic dye (Y123) and using the Co^{III/II} tris(2,2'-bipyridine) redox couple in the AY1 electrolyte, further

enhanced the PCE of the DSSC to 12.3%, which exceeds those obtained for the best Ru(II)-polypyridyl sensitizers.

In the molecular structure of YD2-o-C8, two sets of long alkoxy chains located at the ortho positions of the (5,15-meso)phenyls groups are favorably ortho directed atop and above both faces of the porphyrin, enveloping efficiently the macrocycle. Diau and collaborators introduced later this structural design under the general concept of “alkoxy-wrapped” push–pull porphyrin dyes (Figure S3).^{287,289} As we commented in the introduction of this review, Zn(II)-porphyrin dyes most usually outperform their free base- and other metallo-porphyrins analogues. However, the positively charged zinc metal ion directly exposed to the electrolyte tends to trap more easily the I₃⁻ ions, which may increase drastically charge recombination processes, and hence represent a limiting factor for the performances of the dye in the DSSC. As known for YD2 and other porphyrins, the 3,5-di-*tert*-butylphenyl bulky groups

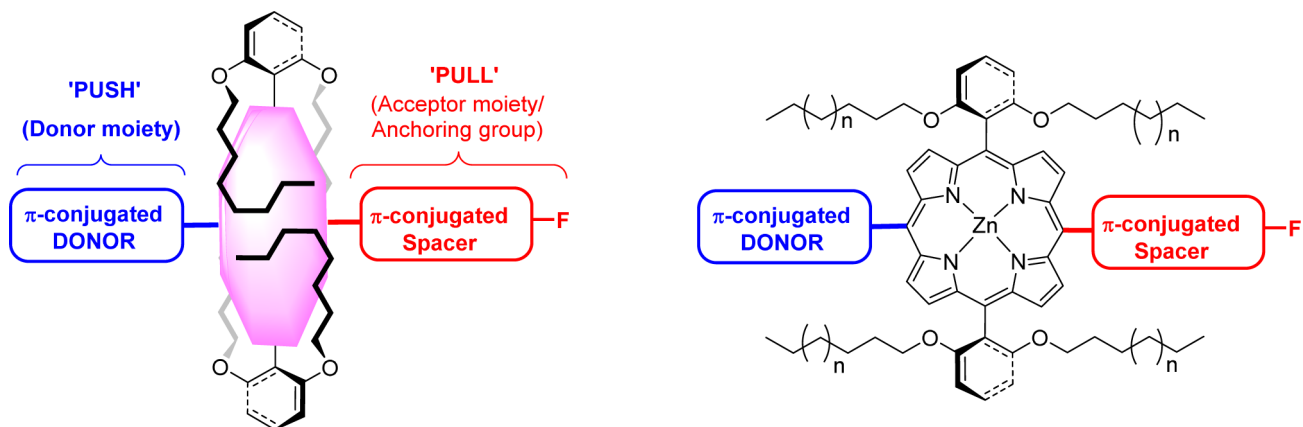


Figure 53. Schematic view (left) and general structure (right) of “alkoxy-wrapped push–pull” porphyrins (F = functional binding group).

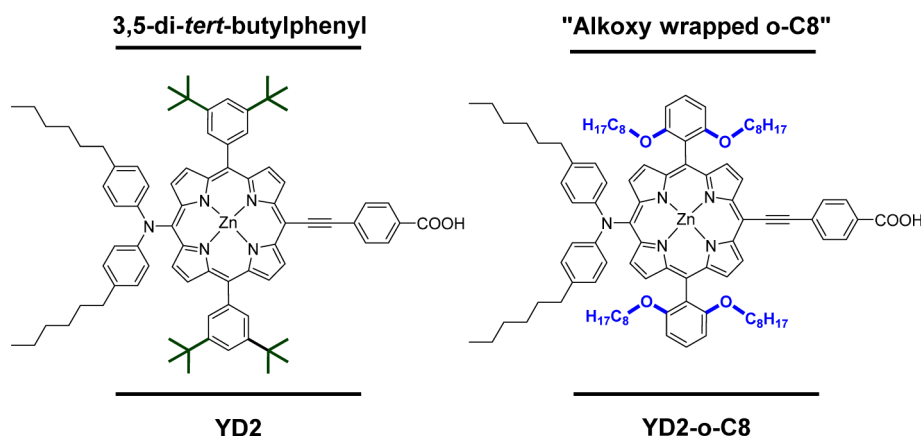


Figure 54. Molecular structures of dyes YD2 and YD2-o-C8 reported by Yella et al. (ref 65).

Table 28. Detailed Photovoltaic Parameters of the Devices Made with the Dyes YD2 and YD2-o-C8 and Cobalt-Based AY1 Electrolyte at Different Light Intensities^a

dye	P_{in} (mW·cm ⁻²)	V_{OC} (mV)	J_{SC} (mA·cm ⁻²)	F.F.	PCE (%)
YD2	9.4	745	1.5	82	9.5
	51.3	805	8.0	76	9.5
	99.8	825	14.9	69	8.4
YD2-o-C8	9.4	875	1.7	77	12.5
	51.2	940	9.3	74	12.7
	99.5	965	17.3	71	11.9
YD2-o-C8	9.4	840	1.83	79	13.0
+Y123	50.8	910	9.72	76	13.1
	99.5	935	17.66	74	12.3

^a P_{in} incident intensity of AM1.5 solar light. J_{SC} = photocurrent density, V_{OC} = open circuit potential, F.F. = fill factor, PCE = solar-to-electric power conversion efficiency. Data derived from ref 65.

impede efficiently $\pi-\pi$ -aggregation of porphyrins, but one can expect that they cannot protect efficiently the porphyrin core from the electrolyte in the DSSC. On this line, the long and judiciously tailored alkoxy chains of YD2-o-C8 present a 2-fold advantage: they also impede efficiently the $\pi-\pi$ aggregation, which reduce dipole–dipole deexcitation channels (hence improving the charge injection of the dye) and additionally protect the porphyrin core against the electrolyte, which on the other hand retards the charge recombination process with the oxidized species of the redox shuttle. Moreover, the introduction

of two alkoxy chains at the ortho positions of the *meso*-phenyls also confers them a slightly better electron-donating character than for *meta*-substituted 3,5-di-*tert*-butylphenyl groups in YD2. As a result, computational studies predict an increase of the electron density of the porphyrin ring for YD2-o-C8, lifting the LUMO/LUMO(-1) and HOMO levels higher than those of YD2, and with a larger HOMO/LUMO gap. These calculations agree the experimental data, YD2-o-C8 being more easily oxidized ($E^1_{ox} = +0.82$ V vs NHE) and more hardly reduced ($E^1_{red} = -1.29$ V vs NHE) than YD2 ($E^1_{ox} = +0.89$ V, $E^1_{red} = -1.10$ V vs NHE), reflecting a better electron-rich character. Additionally, YD2-o-C8 displays slightly red-shifted Soret and narrowed Q-bands, with comparable molar absorption coefficients. Detailed photophysical studies were carried out to shed light on the difference of photovoltaic performance observed for the two dyes in TiO₂/DSSCs under the same conditions, using the AY1 electrolyte. YD2-o-C8 cell displays much larger J_{SC} and V_{OC} values than YD2 (Figure 55a) even at low light intensities, and shows impressive IPCE values over the full visible range (exceeding 80% from ~425 to 675 nm, and extending up to ~725 nm), and despite similar molar coefficient absorptions, exceed by 20–30% the absolute IPCE values of YD2 (Figure 55b). The lower IPCE values obtained from YD2 result of lower APCE values in the 420–700 nm wavelength range (60–90%) in comparison with those of YD2-o-C8 (80–100%). The LHE being very similar and highly efficient for both dyes (close to unity for the Soret and Q bands), as well as dye-regeneration efficiency (η_{reg}) and electron-injection quantum yield (ϕ_{inj}), the superior IPCE values of YD2-o-C8/DSSC were therefore

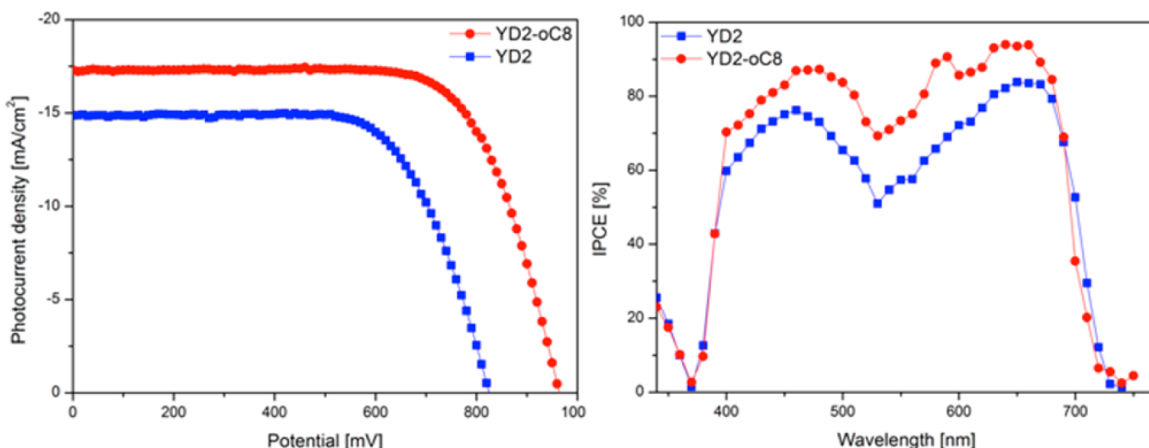


Figure 55. (a) Comparison of the photocurrent–voltage (J – V) curves of YD2-o-C8 and YD2 sensitized solar cells under full AM1.5G solar intensity. (b) Incident photon to current conversion efficiencies as a function of wavelength for the two dyes (YD2-o-C8, red and YD2, blue). TiO_2 film thickness: a 5 μm transparent layer and on top 5 μm scattering layer. From ref 65. Reproduced with permission from AAAS, copyright 2011.

assigned to a better efficiency of the photogenerated charge carriers collection (η_{coll}), matching well with the larger J_{SC} (Table 28). These results highlight that the alkoxy-wrapped structure of YD2-o-C8 protect efficiently the porphyrin core from charge recombination process with the electrolyte redox couple. Next, the strikingly high V_{OC} values obtained for YD2-o-C8/ TiO_2 cells (965 mV at 1 sun) witness that this kind of structure also impede the access of the bulky cobalt complexes to the TiO_2 surface by forming an efficient blocking layer, resulting in a decrease of charge recombination rates $\text{TiO}_2(\text{e}^-)/\text{Co(III)}$ which increases the open circuit voltage. This is also supported by the strong drop of both V_{OC} and J_{SC} values observed in YD2-o-C8/ TiO_2 cell when using iodine-based electrolytes (AY2 or Z959; Table 29).

Table 29. Effect of the Electrolyte on the Photovoltaic Parameters of the TiO_2 -DSSCs Sensitized with YD2-o-C8 under Simulated AM1.5G Full Sun Illumination (Power 100 $\text{mW}\cdot\text{cm}^{-2}$)^a

electrolyte	V_{OC} (mV)	J_{SC} ($\text{mA}\cdot\text{cm}^{-2}$)	F.F. (%)	PCE (%)
AY1	965	17.3	71	11.9
AY2	772	15.0	66	7.6
Z959	832	15.8	71	9.4

^aAY1 is the $\text{Co}^{\text{III}/\text{II}}$ tris(2,2'-bipyridine) based electrolyte, AY2 and Z959 are standard I_3^-/I^- based electrolytes. Data derived from ref 65.

Based on the strikingly outperformances of the “alkoxy-wrapped” YD2-o-C8 push–pull porphyrin compared to the YD2 analogue, many works have been logically devoted to apply this design to other porphyrin dyes (Table 30). For instance, alkoxy-wrapped O–C12 dyes LD14 and LD16 reported by Lin and co-workers in TiO_2 -DSSCs outperform clearly their 3,5-di-*tert*-butylphenyl analogues PE1NMe2/LD13 and LD15, respectively.

5.4.5. Panchromatic Response Toward the Near-IR Region through π -Extended Donor Systems in “Push–Pull” Porphyrins. In order to expand the spectral window and improve the light-harvesting properties of a “push–pull” porphyrin dye (especially in the visible (red) and NIR regions, where porphyrins lack of absorption), many strategies have been attempted. For instance, the expansion of π -conjugation by fusion or annulation of a porphyrin with aromatic systems

such as naphtalene,¹³⁸ anthracene,^{139–142} perylene,¹⁴³ or another porphyrin¹²⁸ confers to the resulting system wider and broader absorption in the visible and/or NIR regions. Although these dyes feature much better light-harvesting properties than their respective unfused analogues, their performances in DSSCs, however, tend to be disappointing and drastically lower in comparison (this is particularly true in the case of fused porphyrin dimers¹²⁸). Besides possible mismatches of the MO levels (in particular low lying LUMO levels), the extension of aromaticity over the porphyrin core most often causes drastic aggregation issues because of the strong π -electron rich character of these large and flat aromatic systems, and represent a serious limitation for their use in DSSCs. Incorporation of additional strong chromophores (acting as antenna/secondary energy donor) covalently linked to the porphyrin is another alternative to get a panchromatic response of the sensitizer. Although some interesting results were obtained following this strategy, such as the trichomophoric sensitizer BODIPY-Porphyrin-Squarene reported by Odobel and co-workers,²⁶¹ or ethynyl-linked porphyrin dimers,^{128–133} or trimers/tryad^{134–136} this approach seemed, until now, hardly transposable to the “push–pull” framework. This was attempted in some push–pull porphyrins incorporating diketopyrrolopyrrole (DPP),²⁹⁰ BODIPY²⁹¹ subunits, or another porphyrin (dimer¹²⁸ or triad¹²⁹) but achieved relatively low PCE in DSSCs despite broad and strong absorption in the visible and/or in the near-IR regions (dimer YDD1:¹²⁸ PCE = 5.21%; triad DTBC:¹²⁹ PCE = 5.2%). This year (end of 2013–beginning of 2014), Luo et al. demonstrated the feasibility of this concept by using an ethyne-linked N-annulated perylene (NP) acting as secondary light-harvester and donor (Figure 56).^{292,293} In conjunction with the electrolyte based on the $\text{Co}^{\text{III}/\text{II}}$ tris(2,2'-bipyridine) complex, $[\text{Co}(\text{bipy})_3]^{3+/2+}$, the TiO_2 /DSSCs devices made with WW-5 or WW-6 dyes showed impressive photovoltaic performances (Table 31), achieving a PCE of 10.3% and 10.5% respectively, under AMG 1.5 standard conditions, equaling those of YD2-o-C8 under same conditions ($\eta = 10.5\%$), and were even slightly higher under half-sun illumination ($\eta = 11.1\%$, 11.3%, and 10.8% under 50 $\text{mW}\cdot\text{cm}^{-2}$ irradiance, respectively). Various factors were considered for the design of these dyes. The skeleton of the push–pull porphyrins takes up some design aspects of YD2, YD2-o-C8, and LD1 dyes, previously commented in this section. First, the ethynylcarboxyphenyl

Table 30. Comparative PCE Values of TiO_2 -DSSCs Sensitized with Alkoxy Wrapped O-C8 or O-C12 Push-Pull Porphyrin Dyes, and Their 3,5-Di-*tert*-butylphenyl Analogue under Simulated AM1.5G Full Sun Illumination, Reported by Diau and Collaborators (*AY1: Electrolyte Using the $\text{Co}^{\text{III/II}}$ Tris(2,2'-bipyridine) Complex As Redox Couple)

3,5-di- <i>tert</i> -butylphenyl	"Alkoxy Wrapped o-C8"	"Alkoxy Wrapped o-C12"
 D =		
 YD2 $\eta = 6.6\text{--}10.9\%$ (Refs 275, 283-285)	 YD2-o-C8 $\eta = 7.6\text{--}9.4\%$ (Ref 65)	 LD12 $\eta = 7.43\%$ (Ref 277)
 YD2/AY1* $\eta = 8.4\%$ (Ref 65)	 YD2-o-C8/AY1* $\eta = 11.9\%$ (12.3 % with Y123) (Ref 65)	—
 YD3 $\eta = 5.34\%$ (Ref 275)	 YD22 $\eta = 6.6\%$ (Ref 289)	—
 PE1NMe2 $\eta = 6.12\%$ (Ref 280)	 YD20 $\eta = 8.1\%$ (Ref 289)	—
 LD13 $\eta = 8.37\text{--}9.34\%$ (Refs 277, 281)	 LD14-C8 $\eta = 6.39\text{--}8.94\%$ (Ref 281)	 LD14 $\eta = 10.05\text{--}10.17\%$ (Refs 277, 281)
 LD15 $\eta = 8.77\text{--}8.92\%$ (Ref 281)	—	 LD16 $\eta = 10.24\%$ (Ref 281)

group was chosen as the acceptor/anchor moiety, well-known as an efficient π -conjugated anchor that enhances the electronic communication between the excited dye and the semiconductor and confers to the porphyrin better optical and electrochemical properties. Next, the 3,5-di-*tert*-butylphenyl bulky groups

impede efficiently dye-aggregation, similarly than in **YD1**, while the O-C12 alkoxy phenyls remind the O-C8 alkoxy wrapped structure of **YD2-o-C8**. Similarly than polycyclic aromatic hydrocarbon modified analogues of **LD1** previously reported by Diau and collaborators (Section 5.4.3 *vide supra*),

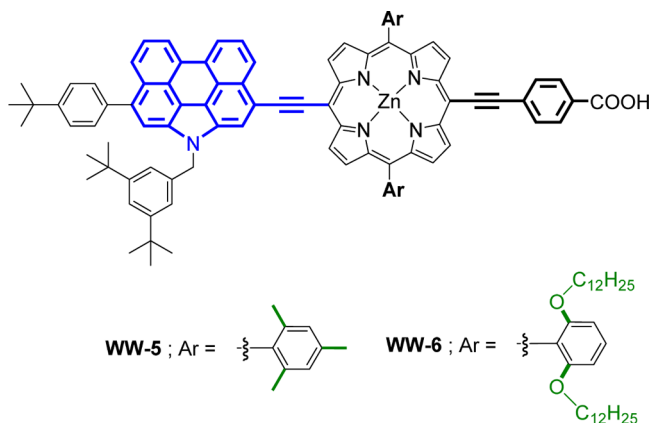


Figure 56. N-Annulated perylene ethyne-linked donor, ethynylcarboxyphenyl anchored, push–pull porphyrin dyes, reported by Luo et al. (ref 292).

Table 31. Dye Loading Densities and Photovoltaic Parameters of the TiO_2 -DSSCs Sensitized with WW-5, WW-6 and Benchmark YD2-o-C8 under Simulated AM1.5G Full Sun Illumination (Power 100 $\text{mW}\cdot\text{cm}^{-2}$) Using the Cobalt (III/II) Tris(2,2'-bipyridine) Complex in the Electrolyte^a

dye	dye-loading density/ $10^{-8} (\text{cm}^{-2}\cdot\mu\text{m}^{-1})$	V_{OC} (mV)	J_{SC} ($\text{mA}\cdot\text{cm}^{-2}$)	F.F. (%)	PCE (%)
WW-5	1.81	766	18.43	73.3	10.3
WW-6	1.62	809	17.69	73.5	10.5
YD2-o-C8	1.38	868	16.33	74.3	10.5

^aData derived from reference 292.

the ethyne linkage between the NP-donor and porphyrin allows an effective π -conjugation over both components, which strongly widen, increase and extend to the red the absorption of the dye. N-Annulated perylenes (NPs), a subclass of perylene, are π -extended aromatic systems that display strong absorption in the visible region ($\lambda_{\text{max}} = 430 \text{ nm}$), high fluorescence quantum yield and strong electron-donor capability. These excellent properties of NPs thus make them also suitable candidates as electron-rich donors to reinforce the “pushing effect” in porphyrin dyes. Moreover, they also feature strong thermal, chemical, and photochemical robustness. An important issue for the preparation of perylenes and related polyphenylenes compounds²⁹⁴ with given physical and chemical properties remains the control of regioselective functionalization at

the *peri* or *bay* positions. On this line, the unique structure of NP containing a nitrogen atom annulated in its structure made possible such control in the functionalization, allowing the incorporation of solubilizing and bulky 3,5-di-*tert*-butylbenzyl or 4-*tert*-butylphenyl groups in the NP structure to overcome solubility and aggregation issues. Additionally, these bulky groups at the tips of the dye must also participate to reduce interfacial charge-recombination between photojected electrons $\text{TiO}_2(\text{e}^-)$ and oxidized mediator ($[\text{Co}(\text{bipy})_3]^{3+}$) in the electrolyte.

The photovoltaic performances of the DSSCs sensitized with WW-5, WW-6, and those of the benchmark YD2-o-C8 used for comparison, are summarized in Table 31. The current–voltage characteristics and the corresponding IPCE action spectra are depicted in Figure 57a,b, respectively. DSSC devices made with WW-5 and WW-6 sensitizers display impressive J_{SC} values of 18.43 and 17.69 $\text{mA}\cdot\text{cm}^{-2}$, respectively, which are significantly higher than the device made with YD2-o-C8 ($J_{\text{SC}} = 16.33 \text{ mA}\cdot\text{cm}^{-2}$). In turn, however, the V_{OC} values were significantly lower in comparison ($\Delta V = -102$ and -59 mV , respectively). In conjunction with the cobalt-based electrolyte using the $[\text{Co}(\text{bipy})_3]^{3+/2+}$ complex as redox shuttle, WW-5 and WW-6 cells achieved similar overall PCE ($\eta = 10.3\text{--}10.5\%$) than YD2-o-C8 ($\eta = 10.5\%$) under AMG 1.5 standard conditions. It is important to notice that, despite lower dye-coverage, the YD2-o-C8-cell reached a similar overall PCE as the two others, which primarily indicates that this dye perform more efficiently, and the remarkable difference of photovoltaic performances are worth being detailed.

As illustrated in Figure 58, the LUMO level of WW-5 and WW-6 lie below than that of YD2-o-C8 resulting in smaller driving-force for electron injection, which may render this process less effective for the formers. Because of the extended π -conjugation, the absorption of WW-5 and WW-6 were considerably widened, more intense and red-shifted in comparison with YD2-o-C8, and together with less, but still very efficient electron injection, resulted in larger integrated IPCE values which significantly improved the J_{SC} relative to YD2-o-C8. This is reflected in the IPCE action spectra (Figure 57b), WW-5 and WW-6 cells reaching inferior absolute IPCE(λ) values than the benchmark in the 400–700 nm region, and slightly lower FF. However, whereas the IPCE action spectra ends at $\sim 725 \text{ nm}$ for YD2-o-C8, those of WW-5 and WW-6 shift up to 815 nm (+ 90) and 785 nm (+ 60), respectively, with high IPCE values (>65% in the 400–760 nm range for WW-5), which explain the

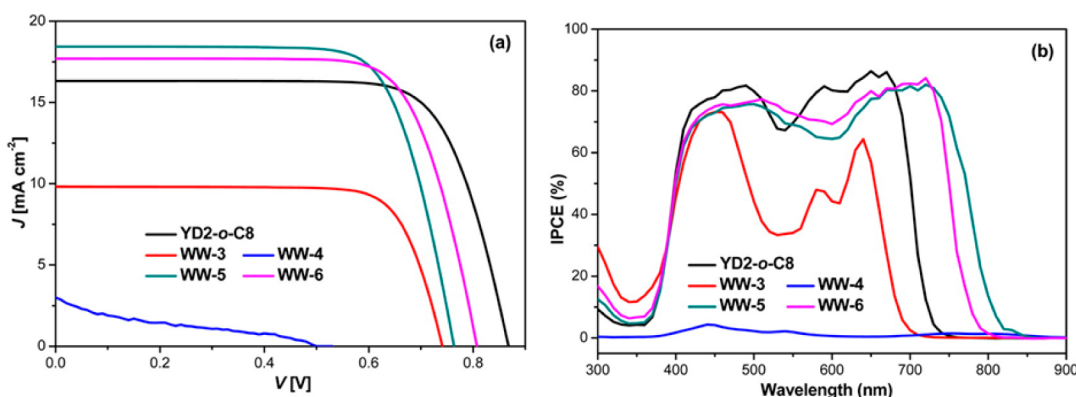


Figure 57. (a) Current–voltage characteristics of WW3–6 and YD2-o-C8 sensitized solar cells cell and (b) corresponding IPCE action spectra. Reproduced with permission from ref 292. Copyright 2014 American Chemical Society.

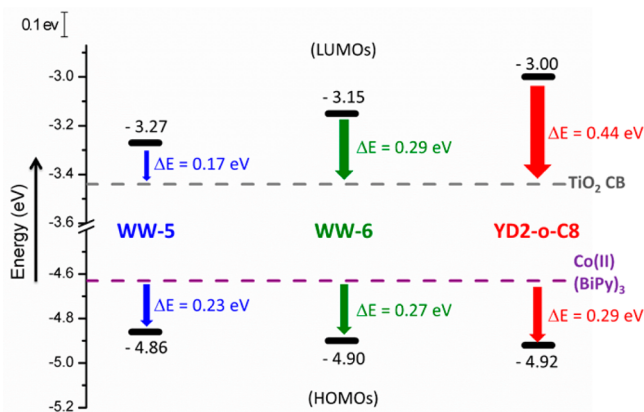


Figure 58. Schematic energy diagram of the MOs levels of dyes WW-5, -6 and benchmark YD2-o-C8 (data derived from ref 292).

increase of the J_{SC} values in the order YD2-o-C8 ($16.33 \text{ mA}\cdot\text{cm}^{-2}$) < WW-6 ($17.69 \text{ mA}\cdot\text{cm}^{-2}$) < WW-5 ($18.43 \text{ mA}\cdot\text{cm}^{-2}$). On the other hand, the OC12 alkoxy wrapped structure in WW-6 must act as more efficient blocking layer than the mesityl groups in WW-5, to keep the bulky $[\text{Co}(\text{bipy})_3]^{3+}$ oxidized species away from the TiO_2 surface, which explain the higher V_{OC} reach for the former (809 mV vs 766 mV , respectively) by the virtue of reduced charge recombination. The diminishing driving-force for dye-regeneration from YD2-o-C8 ($\Delta G_{reg} = 0.29 \text{ eV}$) > WW-6 ($\Delta G_{reg} = 0.27 \text{ eV}$) > to WW-6 ($\Delta G_{reg} = 0.23 \text{ eV}$), as a result of upper-lying HOMO levels, may also contribute to decrease the V_{OC} in the same order.

Based on their two previous best performing dyes, the ethyne-linked donors push pull porphyrins containing either a pyrenyl (**LD4**, $\eta = 10.1\%$) or a *N,N*-dialkylaminophenyl (**LD13–16**, $\eta_{max} = 10.2\%$) group (vide supra), Lin and collaborators further extended the π -conjugation of the donor moiety by incorporating an additional ethynylantracenyl spacer to develop efficient near-IR sensitizers, the dyes **LD31**, **LWP3**, and **LWP4** (Figure 59 and Table 32).^{295,296} In comparison with the benchmark **LD14**, the π -extended conjugation in **LD31** and **LWP3** though an additional ethynylantracenyl spacer significantly broadened the Soret and Q bands, red-shifted by about 50–60 to 20–25 nm, respectively. Both dyes display extended and shifted absorption toward the red and near-IR region over $\sim 750 \text{ nm}$. Consequently, while the IPCE response of **LD14** collapse from $\sim 650 \text{ nm}$ to end at $\sim 750 \text{ nm}$, those of **LD31** and **LWP3** collapse from $\sim 700 \text{ nm}$ to end up at $\sim 800 \text{ nm}$. However, the π -extended conjugation in **LWP3/LD31** caused significant lowering of their energy excited states (LUMO/LUMO-1) with respect to the analogue **LD14**, resulting in a less favorable electron-injection process of these dyes into the TiO_2 conduction band. In addition to higher tendency of aggregation, this factor mostly contributes to the inferior IPCE values observed in the 400–675 nm region for **LWP3** with respect to **LD14** despite improved light harvesting properties and is in agreement with the decrease of J_{SC} ($17.76 \text{ mA}\cdot\text{cm}^{-2}$ versus $18.82 \text{ mA}\cdot\text{cm}^{-2}$). In the case of **LD31**, the three components electron-injection/LHE/aggregation are better balanced, leading to similar or slightly higher IPCE values than **LD14** in the 400–700 nm region (presumably due to reduced aggregation and better solubility of **LD31** owing to the additional terminal *N*-octyl chains versus *N*-methyl groups in **LWP3**). Hence, the additional shift of the IPCE response over 800 nm for **LD31** mostly contribute to the superior overall

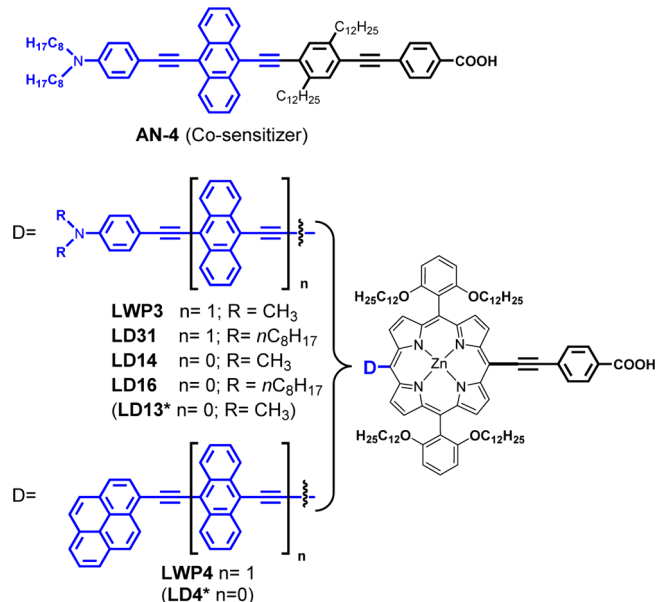


Figure 59. Molecular structures of the cosensitizer **AN-4** (top; ref 295), benchmarks **LD4*/13*/14/16** (refs 277, 278, and 281), and dyes **LD31**, **LWP3**, and **LWP4** (bottom; refs 295 and 296), reported by Lin and collaborators (*for the sake of clarity the molecular structure of **LD4** and **LD13** are not fully depicted and simplified: these dyes have (3,5-di-*tert*-butyl)phenyl groups at the (5,15)meso positions instead bis(dodecyloxy)phenyls; see molecular structures on Figures S2 and S0, respectively).

integrated IPCE value with respect to **LD14**, matching well with the larger J_{SC} observed for the former ($J_{SC} = 20.02 \text{ mA}\cdot\text{cm}^{-2}$ vs $17.50 \text{ mA}\cdot\text{cm}^{-2}$). With slightly lower V_{OC} and F.F. than **LD14/DSSC**, but overcompensated by higher J_{SC} , the overall PCE of **LD31/DSSC** was improved to 9.95% (vs 9.34% for **LD14** under same conditions). Finally, cosensitization of porphyrin **LD31** with the nonporphyrinic sensitizer **AN-4** further improved slightly the PCE to 10.26%.

By following the same strategy, the ethyne-linked pyrenyl dye **LD4** was modified to the ethynylantracenyl-bridged analogue **LWP4**. However, the performances of **LWP4/DSSC** were relatively low, achieving a PCE of only 6.70% (for comparison **LD4/DSSC** previously reported achieved a PCE of 10.06%;²⁷⁸ note that **LD4** has 3,5-di-*tert*butylphenyl groups instead the OC12 alkoxy wrapped structure). As observed for dyes **LWP3** and **LD31**, **LWP4** displays improved light harvesting properties with respect to the benchmarks **LD4** or **LD14**, with absorption displaced to the red and near-IR region over $\sim 750 \text{ nm}$, and accordingly the IPCE response was also extended over $\sim 800 \text{ nm}$. **LWP4** displays LUMO levels lower than its analogue **LWP3**, which should degrade even more the electron injection process with respect to **LD4** and **LD14**. Moreover, based on their EIS studies, solubility and aggregation issues due the large aromatic hydrocarbon structure are more pronounced for **LWP4** than **LWP3**. Thus, these two factors should explain the lower IPCE values of **LWP4** with respect to **LWP3** in the whole spectral region, and accordingly explain the poorer J_{SC} ($14.20 \text{ mA}\cdot\text{cm}^{-2}$ vs $17.76 \text{ mA}\cdot\text{cm}^{-2}$). Finally, the authors also suggested that dye-regeneration of the oxidized dyes in the polar media of the electrolyte, may be less effective in the case of **LWP4** that has a nonpolar pyrene group than for **LWP3** with a 4-dimethylaminophenyl polar tail. It is important to notice that the two near-IR sensitizers **LWP4** and **LD31**

Table 32. Dye-Loading and Photovoltaic Parameters of the TiO₂-DSSCs Sensitized with Porphyrins LD31, LWP3, LWP4, and LD14 (Benchmark), Co-Sensitizer AN-4, and Ru(II) Dye N179 (Benchmark), under Simulated AM1.5G Full Sun Illumination (Power 100 mW·cm⁻²)^a

entry	dye	dye-loading (nmol·cm ⁻²)	V _{OC} (mV)	J _{SC} (mA·cm ⁻²)	F.F. (%)	PCE (%)	Reference
1 ^{b,c,d}	LD31	n/a	699	20.02	71.1	9.95 ± 0.04	295
	AN-4	n/a	692	8.85	72.6	4.44 ± 0.01	
	(LD31+AN-4) ^e	n/a	704	20.27	71.8	10.26 ± 0.07	
	LD14	n/a	738	17.50	72.3	9.34 ± 0.06	
2 ^{b,f}	LWP3	120	720	17.76	74	9.51 ± 0.11	296
	LWP4	114	680	14.20	69	6.70 ± 0.07	
	LD14	133	720	18.82	74	10.03 ± 0.02	
	N719	n/a	730	16.74	73	8.96 ± 0.10	
3	LD4	n/a	711	19.63	72.1	10.06	278
	LD13	n/a	697	18.438	72.7	9.34	277
	LD14	n/a	736	19.167	72.1	10.17	277
	LD13	n/a	676	17.432	71.0	8.37	281
	LD14	n/a	710	20.397	69.4	10.05	281
	LD16	n/a	707	20.587	70.4	10.24	281

^aPV data of LD4-, LD13-, and LD14-/DSSCs previously reported are reminded for comparison purpose (entry 3). ^bAverage values obtained from three devices under identical conditions. ^cOptimized performances of the devices made with octahedron-like TiO₂ nanocrystal photoanode and a scattering layer (total film thickness: 26 μm (TiO₂ film with an active area of 0.16 cm⁻²). ^dCHENO was used as coadsorbent ([7.5 × 10⁻⁴ M]). ^eFor the co-sensitized system, the cocktail solution contained LD31 and AN-4 in a molar ratio of 2:1. ^fTiO₂ film with an active area of 0.096 cm⁻².

achieved comparable efficiencies (~10%) with respect to dyes LD4/13–16 (entry 3), providing other examples of the feasibility to convert energy in the near-IR region (up to 800 nm) with a porphyrin sensitizers without deep sacrifice of the PCE.

5.4.6. Panchromatic Response Toward the Near-IR Region and Improvement of Charge-Transfer Ability through Modification of the Acceptor Moiety in “Push–Pull” Porphyrins. In the great majority, the best performing push–pull porphyrin dyes to date are A2BC-type anchored through an ethynylcarboxyphenyl group, which still show lack of absorption in the green (500–600 nm), red, and NIR regions (600–920 nm). If systematic investigations concerning the molecular structure and nature of the donor moiety (“pushing effect”), as well as the effect of the lateral 5,15-meso substituents, have been reported extensively in push–pull porphyrins, very few works, however, have been addressed to the acceptor/anchor moiety (exception made of the acene-modified ethynylcarboxyphenyl dyes YD11–13 described previously in this section, which display superior performances than their ethynylcarboxyphenyl analogues due to better optical properties; namely, red-shifted and broadened absorptions. For instance, the ethynylcarboxyphenyl anchoring group could be logically modified to lower slightly the LUMO to get a panchromatic response, and design new generations of efficient porphyrin dyes. Moreover, the concerns about improving the charge transfer ability (“pulling effect”) of the acceptor/anchor moiety have been scarcely considered so far. On this scope, Imahori and co-workers reported in 2011 two similar-structured push–pull porphyrins ZnPF and ZnPH, differing only by the nature of the phenylene spacer of the acceptor moiety (i.e., an ethynylcarboxytetrafluorophenyl or ethynylcarboxyphenyl anchoring group, respectively) and studied the electron-withdrawing effect on the performances of these dyes in TiO₂-DSSCs (Figure 60 and Table 33).²⁹⁷

The introduction of a diarylamino donor group on one hand, and electron-withdrawing fluorine atoms in the phenylene bridge of the acceptor moiety in ZnPF on the other hand, enhances the CT character (“push–pull effect”) of this dye. Consequently, the fluoro-substituted porphyrin ZnPF displays

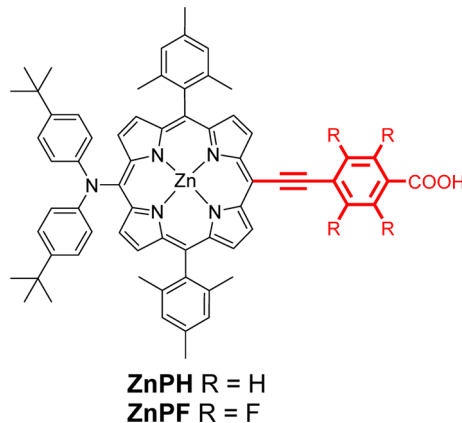


Figure 60. Molecular structures of dyes ZnPH and ZnPF, reported by Imahori and co-workers (ref 297).

slightly improved light-harvesting properties in solution compared to ZnPH, due to a stronger charge-transfer effect. However, it was found that the TiO₂/ZnPF+CDCA cell displays much lower PCE than the corresponding TiO₂/ZnPH + CDCA cell (η = 4.6% and 6.9% respectively). Supported by FTIR and XPS measurements, the authors proposed that ZnPH must bind the surface perpendicularly through a bidentate chelating mode of the carboxylic group and adopt a densely packed organization, whereas the analogue dye ZnPF should adopt a strongly tilted orientation (relatively parallel to the surface) and loosely anchored through an ester-like, monodentate mode of the carboxylic acid group. Moreover, based on the porphyrin densities adsorbed on the TiO₂ film, dye-loading experiments, and estimation of the corresponding surface coverage for each dyes, ZnPF was found to achieve much lower surface coverage than ZnPH (Γ = 6.2 × 10⁻¹¹ and 15 × 10⁻¹¹ mol·cm⁻², respectively). To explain such difference of behavior, the authors suggested the possible existence of additional interactions between fluorine atoms of ZnPF and TiO₂.²⁹⁸ Despite lower surface coverage of ZnPF than ZnPH, the LHE values of the TiO₂/ZnPF+CDCA and TiO₂/ZnPH + CDCA cells were comparable, considering the effect of the

Table 33. Dye Coverage (Γ) and Photovoltaic Parameters of the Optimized TiO_2 -DSSCs Sensitized with ZnPH and ZnPf under Simulated AM1.5G Full Sun Illumination (Power 100 $\text{mW}\cdot\text{cm}^{-2}$)^a

dye	coadsorbent	optimized immersion time (h)	$\Gamma_{\text{sat}}/10^{-11}$ ($\text{mol}\cdot\text{cm}^{-2}$)	V_{OC} (mV)	J_{SC} ($\text{mA}\cdot\text{cm}^{-2}$)	F.F. (%)	PCE (%)
ZnPf	CDCA (2eq)	0.5	6.2	650	10.6	66	4.6
ZnH	CDCA (2eq)	2	15	660	16.2	65	6.9

^aData derived from reference 297.

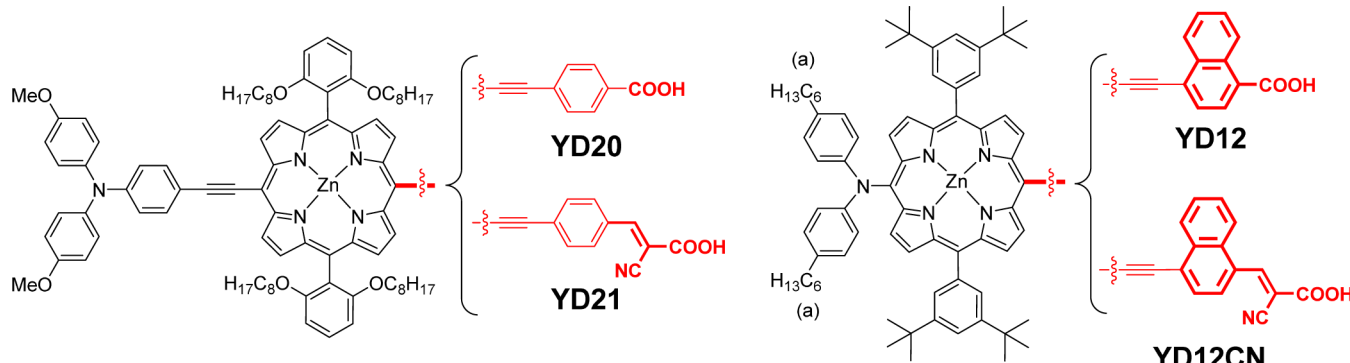


Figure 61. Molecular structures of dyes YD20, YD12^a anchored through ethynylcarboxyphenyl or ethynylcarboxynaphthyl group, and their respective cyanoacrylic acid analogues YD21 and YD12CN^a, reported by Yeh and co-workers (refs 289 and 299; ^anote that YD12 and YD12CN were reported with *n*-hexyl chains at the amine moiety in the main article of ref 299, although there is a certain confusion between *n*-octyl or *n*-hexyl chains in the Supporting Information of the same article, and elsewhere published by the same authors, see refs 148, 282, and 286).

Table 34. Dye-Loading and Photovoltaic Parameters of the TiO_2 -DSSCs Sensitized with YD12/12CN and YD20/21 under Simulated AM1.5G Full Sun Illumination (Power 100 $\text{mW}\cdot\text{cm}^{-2}$)

dye	dye-loading ($\text{nmol}\cdot\text{cm}^{-2}$)	V_{OC} (mV)	J_{SC} ($\text{mA}\cdot\text{cm}^{-2}$)	F.F. (%)	PCE (%)	ref
YD20	161	676	17.43	68.6	8.1	289
YD21	132	631	12.05	72.1	5.5	
YD12	255	550	17.65	64.3	6.2	299
YD12CN	213	544	16.45	64.2	5.8	
YD12+TBP ^a	255	729	17.19	67.7	8.5	
YD12CN+TBP ^a	213	636	9.78	71.6	4.5	

^aTBP = 4-*tert*-butylpyridine additive in the electrolyte.

light-scattering TiO_2 layer. Thus, taking into account that V_{OC} and fill factor values are rather similar for both cells, the difference of PCE mainly originates from the strikingly lower J_{SC} value obtained for ZnPf cell ($J_{\text{SC}} = 10.6 \text{ mA}\cdot\text{cm}^{-2}$) than for ZnPH ($J_{\text{SC}} = 16.2 \text{ mA}\cdot\text{cm}^{-2}$). Based on fluorescence measurements, it was assumed that the electron injection (ϕ_{inj}) must be highly and equally efficient for both dyes. In sight of these results, the authors concluded that the lower η_{col} value of ZnPf must be mainly responsible of the lower IPCE values. Supposedly, the titled geometry of ZnPf should allow a closer distance between the porphyrin ring and TiO_2 surface, and thus open additional through-space, in addition to through-bond, deexcitation channels, in agreement with the work of D'Souza and co-workers (see discussion on section 3.1). Consequently, the electron recombination rate between oxidized dyes and injected TiO_2 electrons should be increased in ZnPf/DSSC with respect to ZnPH/DSSC, which explain well the lower η_{col} value and smaller ratio of long-lived porphyrin radical cation (the latter being subsequently quenched by the I^- ions of the electrolyte to generate the photocurrent of the cell), responsible for lower J_{SC} and hence lower PCE.

Diau and co-workers reported a series of porphyrin dyes anchored through ethynylcarboxyphenyl (YD20²⁸⁹) or ethynylcarboxynaphthyl groups (YD12²⁹⁹) and their corresponding cyanoacrylic acid analogues (YD12CN²⁹⁹ and YD21,²⁸⁹

respectively; Figure 61 and Table 34) and drew similar conclusions regarding the relationship geometry-performances.

They evidenced that the introduction of a cyanoacrylic acid moiety causes slight redshifts of the porphyrin absorption bands but diminished the absorption coefficients, decreased the amount of adsorbed dye (Γ), IPCE and J_{SC} , and accordingly achieved lower overall PCE in comparison with their carboxylic acid analogues. They suggested that the flexible double bond of the cyanoacrylic spacer might induce a more tilted and loosely orientation, while the rigidly and linearly oriented ethynylcarboxyacetyl groups must allow a densely packed and well-organized arrangement of the dyes on the surface. Thus, the titled and relatively planar orientation of dyes YD12CN and YD21, and the short distance between the porphyrin ring and TiO_2 surface, should increase the electron recombination rates through space between oxidized dyes and TiO_2 -injected electrons leading to poorer charge collection efficiencies. The lower η_{coll} values were also ascribed as the main factor responsible of the drastically lower J_{SC} and hence lower η values than their corresponding carboxyl analogues YD12 and YD20. Additionally, the lower coverage and more flexible attachment of dyes YD12CN and YD21 should induce more available free space on the surface, therefore increasing recombination rate between injected electron in the CB of TiO_2 and the I_3^- ions from the electrolyte, as attested by the lower V_{OC} values than

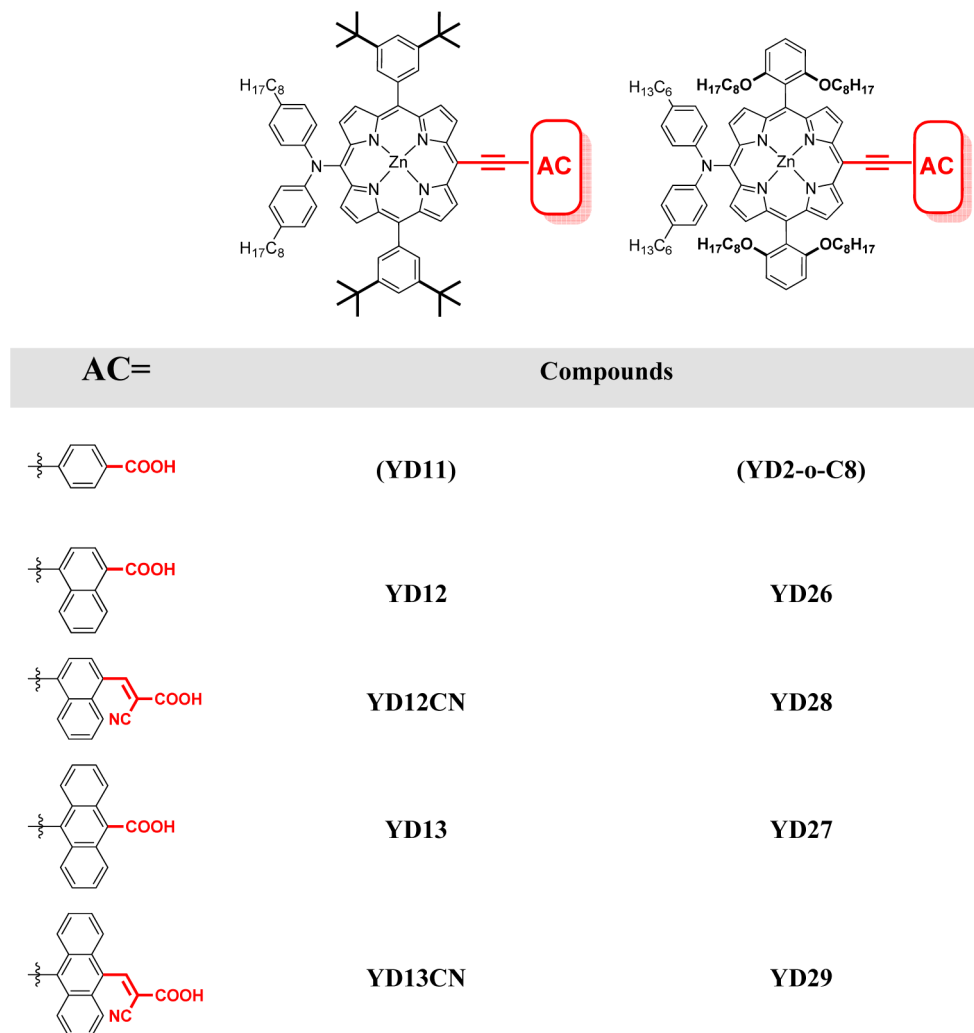


Figure 62. Modification of the anchoring group of YD11 and YD2-o-C8: molecular structures of analogues dyes YD12, YD13, YD26, and YD27 anchored through ethynyl carboxyacene groups, and their respective cyanoacrylic acid analogues YD12CN, YD13CN, YD28, and YD29, reported by Diau and co-workers (ref 286).

their respective analogues YD12 and YD20, a factor that should also decrease the overall PCE of these cells. Interestingly, YD12/ and YD12CN/TiO₂-DSSCs display remarkably different behavior upon addition of TBP (4-*tert*-butylpyridine) in the electrolyte. TBP is a well-known additive that can increase remarkably the V_{OC} of a cell by modifying the TiO₂ surface.^{77–81} In the presence of TBP, the V_{OC} was considerably boosted in both cases, which was mainly ascribed to a large upward shift of the TiO₂–CB level (i.e., shifted to lower potential) and a significant retardation of charge recombination. In turn, however, the J_{SC} decreased, only slightly for YD12 cell and drastically for YD12CN, because of lower electron-injection efficiencies of the dyes (ϕ_{inf}) into the upper-lying TiO₂ CB. As a result, while the DSSC device made with YD12 dye outperformed slightly the YD12CN analogue without TBP ($\eta = 6.2\%$ versus 5.8% , respectively), the PCE of the former increased strongly upon addition of additive (from $\eta = 6.2\%$ to 8.5%) while the latter decreased notably (from $\eta = 5.8\%$ to 4.5%). The same authors reported some other acene-extended modified analogues of YD11 and YD2-o-C8, (namely YD13/13CN, and YD26–29, respectively) anchored through carboxylic or cyanoacrylic acid (Figure 62 and Table 35).²⁸⁶ Exception made of YD13 device ($\eta = 2.57\%$) which

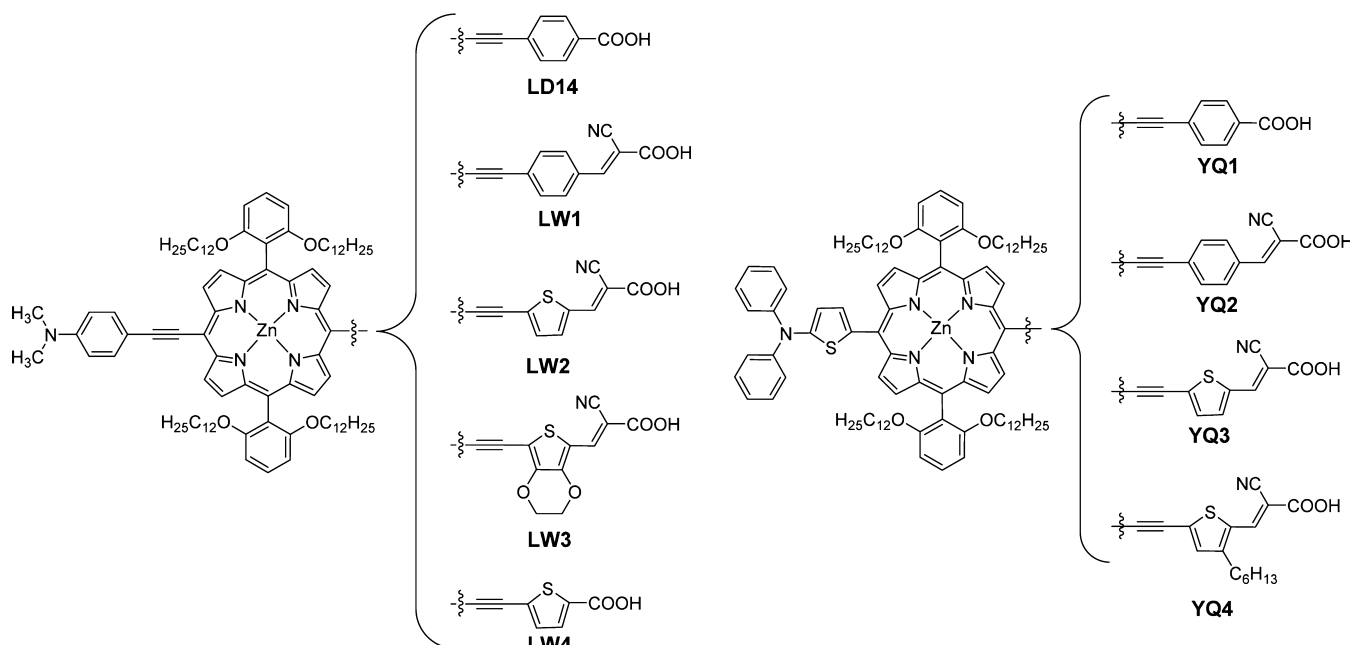
underperformed slightly YD13CN ($\eta = 2.86\%$), the carboxylic-anchored dyes also always tend to give significantly superior performances in DSSC than the corresponding cyanoacrylic acid-anchored analogues.

Following the same trend as previously discussed in section 5.4.4, all alkoxy wrapped OC8 dyes performed better than their 3,5-di-*tert*-butylphenyl analogues, and in particular YD27/DSSC ($\eta = 6.03\%$) versus YD13/DSSC ($\eta = 2.57\%$). Moreover, following the same trend than LAC-porphyrins (vide infra, see section 3.2) and modified analogues of YD11 (vide infra, see section 5.4.3) previously discussed, dyes with a smaller naphthalene spacer in the anchoring group always performed better than those with a larger antracene. YD26 combining all the favorable structural components (naphthalene spacer, alkoxy wrapped structure, and carboxyl binding group) logically achieved the best PCE of the series ($\eta = 8.04\%$). Although cyano- and (cyano)phenyl-acrylic acid groups have been widely used as efficient anchors for a great variety of organic dyes,^{4–18} including porphyrins (vide infra, see discussion on section 3.1) this conceptual design in the light of these results, seems, however, not working well when transposed to “push–pull” porphyrins anchored through ethynylphenyl cyanoacrylic acid, which underperform clearly their ethynylcarboxyphenyl analogues.

Table 35. Photovoltaic Parameters of the TiO₂-DSSCs Sensitized with YD12/12CN, YD13/13CN, and YD26–29 under Simulated AM1.5G Full Sun Illumination (Power 100 mW·cm⁻²)^a

dye	5,15-meso groups ^b	type of anchor	V _{OC} (mV)	J _{SC} (mA·cm ⁻²)	F.F. (%)	PCE (%)
YD12	3,5-DTBP	COOH	713	14.06	72.1	7.23
YD12CN	3,5-DTBP	cyanoacrylic acid	651	8.79	74.8	4.28
YD13	3,5-DTBP	COOH	679	5.09	74.3	2.57
YD13CN	3,5-DTBP	cyanoacrylic acid	632	6.03	75.2	2.86
YD26	2,6-OC8Ph	COOH	745	15.37	70.2	8.04
YD28	2,6-OC8Ph	cyanoacrylic acid	696	11.30	73.7	5.80
YD27	2,6-OC8Ph	COOH	720	11.59	72.3	6.03
YD29	2,6-OC8Ph	cyanoacrylic acid	673	7.17	75.5	3.64

^aData derived from ref 286. ^b3,5-DTBP = 3,5-di-*tert*-butylphenyl; 2,6-OC8Ph = 2,6-diocetylxylophenyl.

**Figure 63.** Molecular structures of alkoxy wrapped push–pull porphyrin dyes LW1–4 and benchmark LD14 reported by Lu et al. (left; ref 300), and YQ1–4 reported by Xie and co-workers (right; ref 301).**Table 36.** Photovoltaic Parameters of the TiO₂-DSSCs Sensitized with LW1–4 and Benchmark LD14 (Left; Data Derived from ref 300), and YQ1–4 (Right; Data Derived from ref 301), under Simulated AM1.5G Full Sun Illumination (Power 100 mW·cm⁻²)

dye	V _{OC} (mV)	J _{SC} (mA·cm ⁻²)	F.F. (%)	PCE (%)	dye	V _{OC} (mV)	J _{SC} (mA·cm ⁻²)	F.F. (%)	PCE (%)
LW1	648	15.70	70	7.12	YQ1	680	14.27	62	6.01
LW2	685	15.36	70	7.37	YQ2	630	12.51	54	4.23
LW3	657	16.35	71	7.63	YQ3	580	12.76	59	4.38
LW4	750	17.65	72	9.53	YQ4	600	13.61	62	5.00
LD14	730	17.38	71	9.01					

Lu et al. recently reported some modified push–pull porphyrins wrapped OC12 analogues of LD14, using ethynylthienyl or ethynylphenyl π -bridged anchors³⁰⁰ (Figure 63 and Table 36, left). Similarly, they obtained significantly lower photovoltaic performances for the cell sensitized with LW1 dye, anchored through an ethynylphenyl cyanoacrylic acid group ($\eta = 7.12\%$), than the carboxylic acid analogue LD14 ($\eta = 9.01\%$). Switching the phenyl spacer in LW1 to a thiényl- (LW2) or EDOT- (LW3) π -spacer, increased slightly the overall PCE of these cells to 7.37% and 7.63%, respectively, as a result of better spectral response in the NIR region (up to 850 nm). The best performing DSSC device of the series was obtained with the carboxythienyl-anchored analogue dye LW4, reaching a PCE of

9.53% despite lower spectral response in the NIR region than LW2 or LW3. In comparison with the carboxythienyl-anchored dye LW4, the lower performances of the cyanoacrylic acid analogues LW2 or LW3 were attributed to faster charge recombination rate at the dye-sensitized heterojunction interface. Under same experimental conditions, dye LW4 displayed superior photovoltaic performances in DSSC than the ethynyl carboxyphenyl analogue LD14 ($\eta = 9.01\%$), achieving an overall PCE of 9.53%. Thus, the ethynyl carboxythienyl group stands out as a new efficient π -bridged anchoring group and potential challenger to the more traditional ethynylcarboxyphenyl to design future generation of efficient “push–pull” porphyrin dyes.

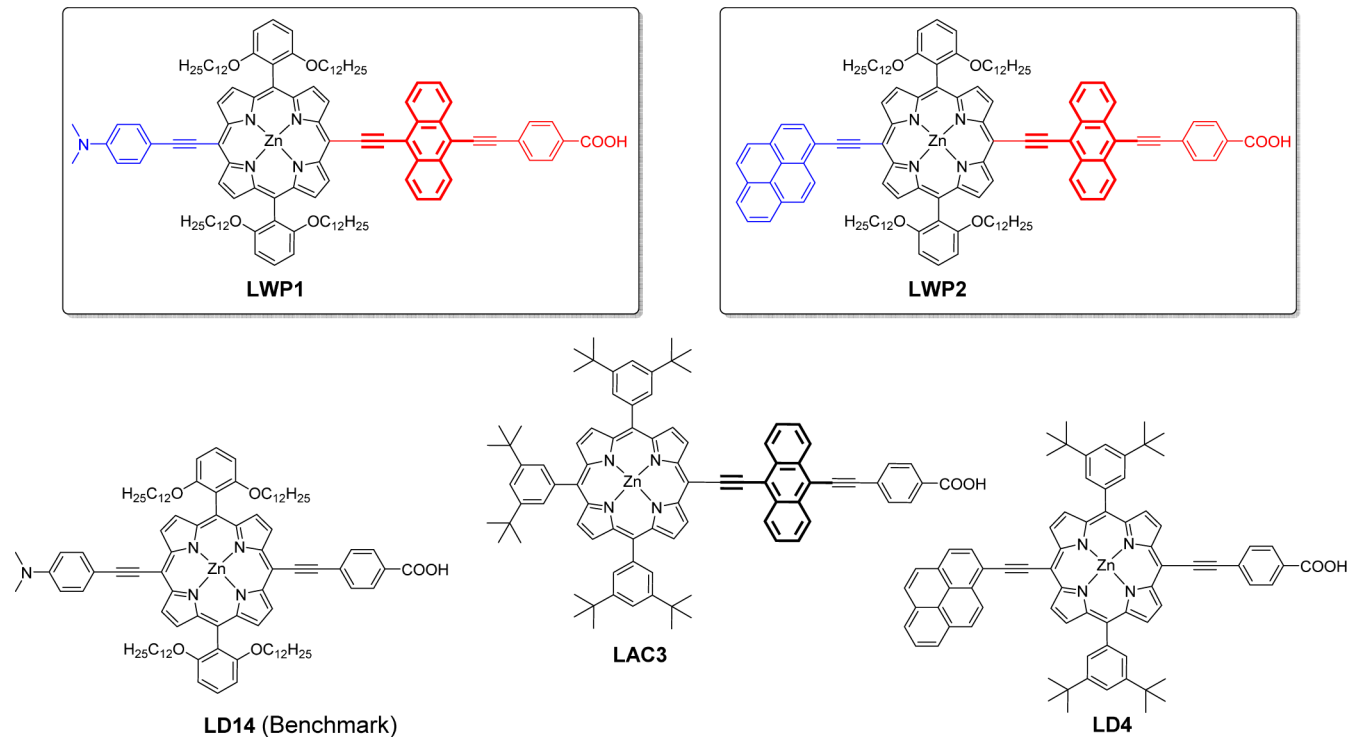


Figure 64. Molecular structures of acene modified push–pull porphyrins **LWP1** and **LWP2**, reported by Lin and co-workers (ref 296); molecular structures of **LAC3**, **LD4**, and **LD14** are reminded for comparison (note that **LD4** and **LAC3** have a 3,5-di-*tert*-butylphenyl substitution instead of an alkoxy wrapped O–C₁₂ structure).

Table 37. Dye-Loading and Photovoltaic Parameters of the TiO₂-DSSCs Sensitized with LWP2, LWP3, and Benchmark LD14, under Simulated AM1.5G Full Sun Illumination (Power 100 mW·cm⁻²)^a

dye	dye-loading (nmol·cm ⁻²)	J _{SC} (mA·cm ⁻²)	V _{OC} (mV)	F.F. (%)	PCE (%)	ref
LWP1	165	17.77	730	75	9.73 ± 0.03	296
LWP2	161	14.17	680	72	6.97 ± 0.02	
LD14	133	18.82	720	74	10.03 ± 0.02	
N719	n/a	16.74	730	73	8.96 ± 0.10	
LAC3	132	12.67	670	64	5.44 ± 0.06	252
LD4	n/a	19.63	711	72.1	10.06	277

^aPV data of **LAC3**- and **LD4**- DSSCs are reminded for comparison.

Xie and co-workers reported latter various push–pull porphyrin dye wrapped OC12 using a 2-diphenylaminothiophene at the donor part, and similar ethynylthienyl- or ethynylphenyl- π -bridged cyanocrylic acid anchors.³⁰¹ Similar trends in the photovoltaic performances were observed for the dyes **YQ1–4**: the ethynyl carboxyphenyl anchored dye **YQ1** achieved the best performances and PCE of the series ($\eta=6.01\%$), which outperformed clearly the cyanoacrylic acid anchored analogue **YQ2** ($\eta=4.23\%$). Switching the π -bridge from phenyl- (**YQ2**) to thiophene linkers in **YQ3** and **YQ4**, resulted as well in a superior overall PCE (from $\eta=4.23\%$ to 4.38% and 5.00%, respectively).

Following a similar strategy used in their previous work for **LAC** dyes incorporating π -extended acene-bridges (Section 3.2, *vide supra*), Lin and collaborators reported two other modified analogues of **LD14** and **LD4**, the dyes **LWP1** and **LWP2**, respectively, incorporating an additional ethynylanthracenyl spacer in the acceptor part (Figure 64 and Table 37).²⁹⁶ Similarly than **LWP3** and **LWP4** dealt in the previous section 5.4.5 (Figure 59 and Table 32, *vide supra*) which also incorporate this spacer but at the donor part, significant redshift and broadening of the

Soret- and Q-bands were observed for **LWP1** and **LWP2**, with absorption over 700–750 nm, with respect to the benchmark analogues **LD14** and **LD4**. Similar trends were also observed for **LWP2**/DSSC (pyrenyl donor type) achieving a modest PCE of only $\eta=6.97\%$ due to strong dye-aggregation issues (for comparison **LD4**/DSSC previously reported, achieved a PCE of 10.06%; note that **LD4** has a 3,5-di-*tert*-butylphenyl substitution instead of an alkoxy OC12wrapped structure in **LWP2**). In turn, **LWP1** displayed fewer tendencies to aggregate in comparison with **LWP4** (ethynylanthracenyl spacer at the donor part). Thus, despite a reduced V_{OC} and similar F.F. but overcompensated by higher J_{SC} , **LWP2** device performed almost equally under same conditions than the benchmark device made with **LD14**, without significant losses in the overall PCE ($\eta=9.73$ and 10.03%, respectively). As well, the shift of the IPCE response toward the NIR-region for **LWP2**/DSSC compensated a less efficient electron-injection than that of **LD14** resulting in a larger integrated IPCE value and accordingly, to a larger J_{SC} .

Grätzel, Nazzeeruddin, and co-workers recently reported two modified analogues of **YD2-o-C8**, the dyes **SM371** and **SM315**

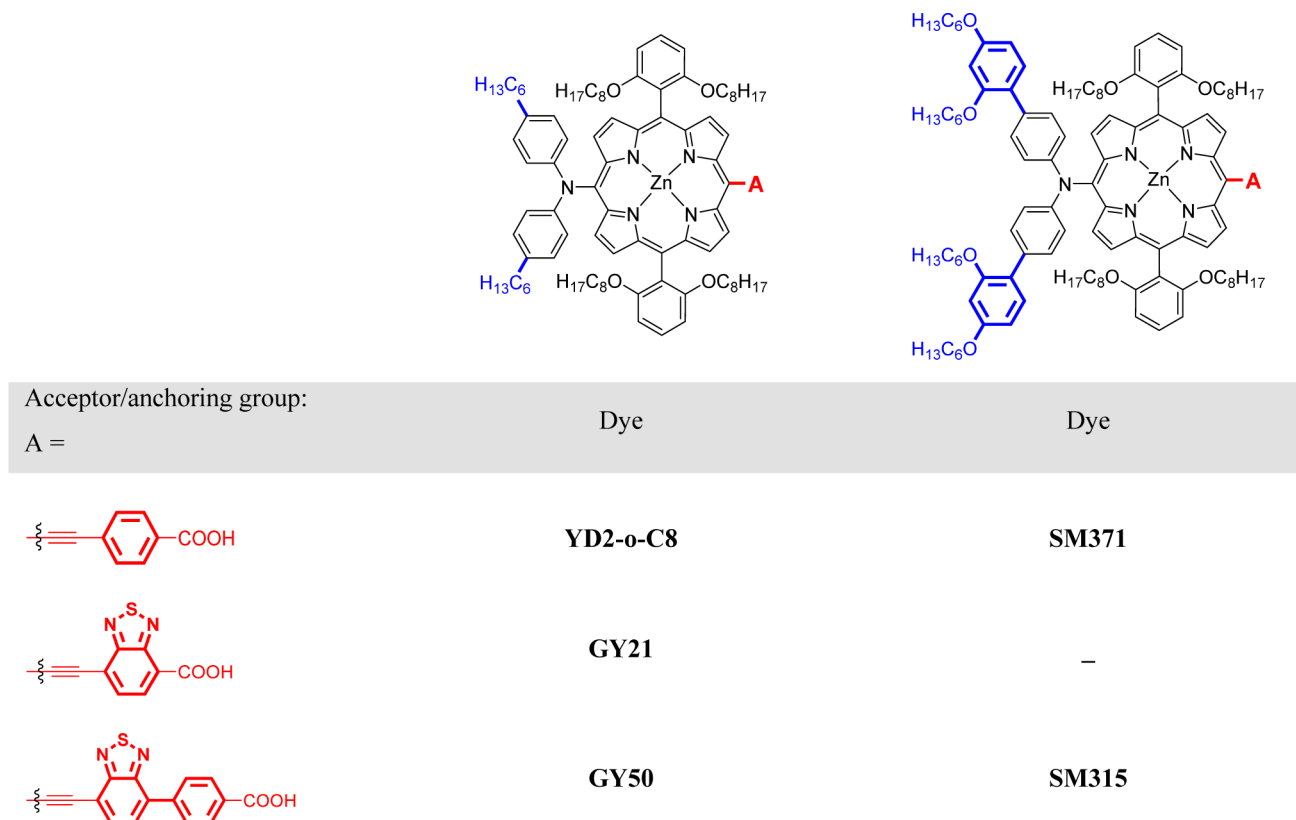


Figure 65. Molecular structures of dyes SM315, SM371 (ref 159), GY21, GY50 (ref 302), and benchmark YD2-o-C8 (ref 65), reported by Grätzel and collaborators.

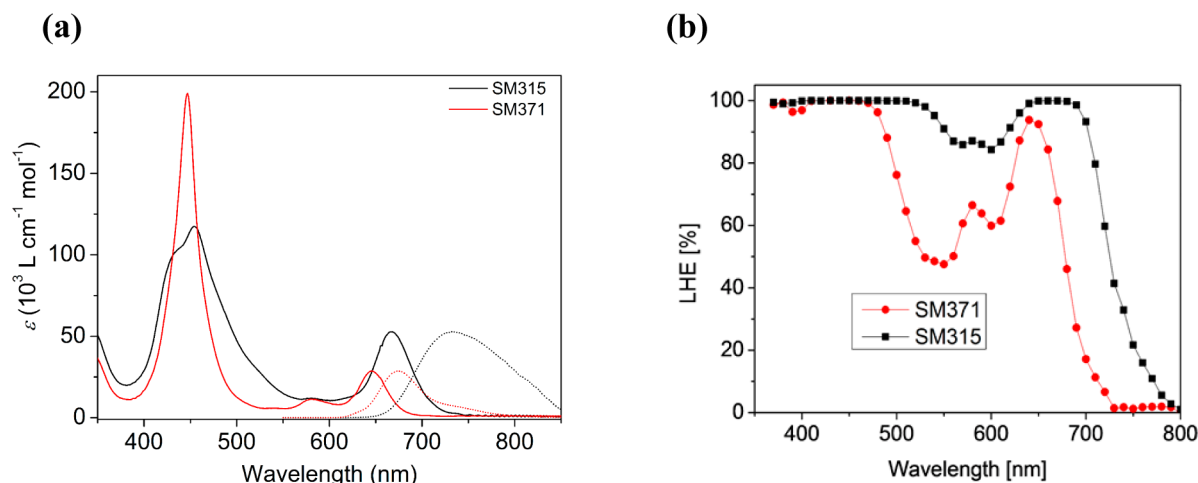


Figure 66. (a) Absorption (solid line) and normalized emission ($\lambda_{ex} = 440$ nm dashed line) spectra for SM371 (red) and SM315 (black) in THF solution. (b) Light harvesting efficiency of SM371 (red) and SM315 (black) on transparent 3.5 μ m TiO₂. Reprinted by permission from Macmillan Publishers Ltd. *Nature Chem.* (ref 159), copyright 2014.

exhibiting unprecedented solar-to-electric conversion efficiencies under standard AM 1.5G illumination of 12% and 13%, respectively, in conjunction with the cobalt-based electrolyte using the Co^{III/II} tris(2,2'-bipyridine) complex as redox couple (Figures 65–67 and Table 38).¹⁵⁹ At the same time, Yella et al. from the same group reported two similar structured dyes GY21 and GY50, modified analogues of YD2 (Figure 65 and Table 38, entry 2).³⁰² To date, SM315 and GY50 represent the best performing dyes all categories ever reported in DSSCs without the need of cosensitization, and establishes the actual new record of efficiency with a ~13% PCE achievement under

standard AM1.5G illumination. The dyes SM315 and SM371 take up the design of the OC8 alkoxy wrapped structure of YD2-o-C8. The donor moiety was modified to a bis(2',4'-bis(hexyloxy)-[1,1'-biphenyl]-4-yl)amino group, which previously demonstrated its remarkable compatibility with cobalt-complex redox mediators in DSSCs.⁶⁶ While SM371 is tethered with the same ethynylcarboxyphenyl group than YD2-o-C8, the acceptor moiety was modified in SM371 by introduction of a benzothiadiazole (BTD) π -spacer. Therien and co-workers previously reported that the use of proquinoidal spacer units such as BTD in π -bridged ethyne–ethyne linked porphyrin

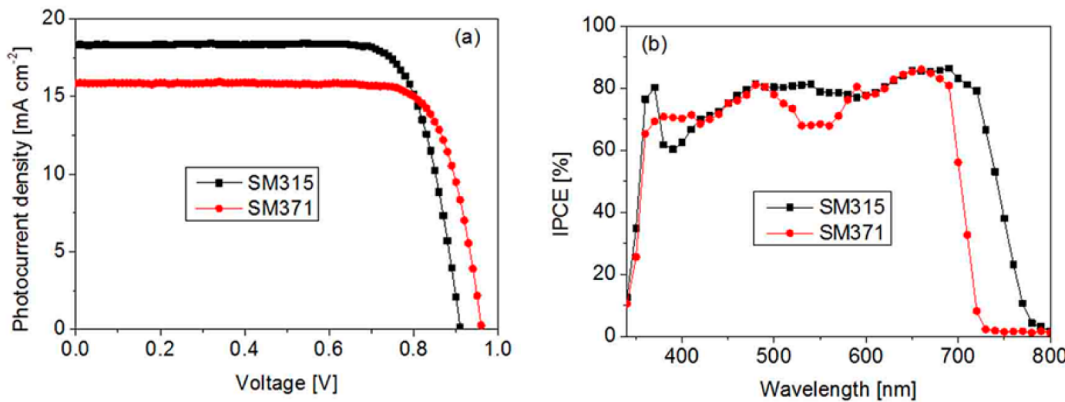


Figure 67. Comparison of (a) J – V curve under AM 1.5 G illumination ($1000 \text{ W}\cdot\text{m}^{-2}$) and (b) photocurrent action spectrum of SM371 (red) and SM315 (black). Reprinted by permission from Macmillan Publishers Ltd. *Nature Chem.* (ref 159), copyright 2014.

Table 38. Photovoltaic Parameters of the TiO₂-DSSCs Sensitized with SM371, SM315, GY21, and GY50 under Simulated AM1.5G Full Sun Illumination (Power 100 mW·m⁻²)^a

entry	dye	electrolyte	redox couple	V_{OC} (mV)	J_{SC} (mA·cm ⁻²)	F.F. (%)	PCE (%)	ref
1	SM315	(cobalt)	[Co(bipy) ₃] ^{3+/2+}	910	18.1	78	13	159
	SM371	(cobalt)	[Co(bipy) ₃] ^{3+/2+}	960	15.9	79	12	
2	GY21	(cobalt)	[Co(bipy) ₃] ^{3+/2+}	615	5.03	79.8	2.52	302
	GY21	PMMII	I ₃ ⁻ /I ⁻	552	11.50	75.1	4.84	
	GY50	(cobalt)	[Co(bipy) ₃] ^{3+/2+}	885	18.53	77.3	12.75	
	GY50	PMMII	I ₃ ⁻ /I ⁻	732	18.45	65.7	8.90	
3	YD2-o-C8	AY1	[Co(bipy) ₃] ^{3+/2+}	965	17.3	71	11.9	65
	YD2-o-C8	AY2	I ₃ ⁻ /I ⁻	772	15.0	66	7.6	
	YD2-o-C8	Z959	I ₃ ⁻ /I ⁻	832	15.8	71	9.4	

^aPV data of YD2-o-C8/DSSCs are reminded for comparison.

dimers strongly increases the magnitude of the electronic interaction between the two components that facilitate an extensive electronic delocalization and strongly perturb the electronic structures of the porphyrins.³⁰³ In particular, these systems display much broader absorption accompanied by a splitting of the Soret (B) band characteristic of extensive excitonic interactions,³⁰⁴ and more intense Q-bands strongly shifted to the NIR. These excellent properties thus make BTD an ideal component in push–pull porphyrin to obtain a panchromatic response of the dye. The optical changes induced by the BTD bridge can be appreciated in the absorption spectrum of SM315 (Figure 66a), displaying a broader and split Soret band ($\lambda_{max} = 440$ and 454 nm), a broader absorption in the 500–600 nm range, and a more intense Q-band of lowest-energy ($\lambda_{max} = 668$ nm, $\epsilon = 53\,000 \text{ M}^{-1}\cdot\text{cm}^{-1}$) significantly red-shifted in comparison with that of SM371 ($\lambda_{max} = 646$ nm, $\epsilon = 29\,000 \text{ M}^{-1}\cdot\text{cm}^{-1}$).

In comparison with SM371, the light-harvesting properties of SM315 were strongly improved, bridging better the gap of the green region (LHE > ~85% in the 500–600 nm range) and extended to the red up to 800 nm (Figure 66b). This superior light harvesting efficiency and capability of SM315 is reflected in the IPCE spectra (Figure 67b), displaying similar and high IPCE values than those of SM371 in the 300–500 and 600–700 nm regions, slightly higher in the green-region (500–600 nm), and most importantly high values reached in the 725–800 nm red-region where those of SM371 are already extinct. Based on fluorescence experiments, the electron-injection efficiency was assumed to be close to unity for both SM371 and SM315, and on the other hand, intensity-modulated photo-induced absorption (PIA) experiments also indicate highly

efficient dye regeneration in both cases. Thus, assuming quantum-yields close to unity for both of these processes, the larger cumulated integrated IPCE value of SM315 relative to SM371 therefore accounts for higher J_{SC} for the former cell ($J_{SC} = 18.1$ and $15.9 \text{ mA}\cdot\text{cm}^{-2}$, respectively). In turn, the V_{OC} of SM315 was slightly lower than SM371. A decrease in the V_{OC} can be caused by two different factors (see the Introduction section, *vide supra*): either a downward shift of the TiO₂–CB (i.e., shifted at higher potential) and/or an increase of recombination process between photojected electrons and oxidized redox species in the electrolyte (i.e., [Co(bipy)₃]³⁺). Chemical capacitances^{224,305} were found likewise similar for both devices, thus ruling out a downward shift of the TiO₂–CB. On the other hand, the measurement of the electron lifetime was found to be six time shorter for SM315 than for SM371, indicative of faster recombination rate at the TiO₂–electrolyte interface. As supported further by PIA experiments, the decrease of the V_{OC} in SM315 cell therefore originate from enhanced electron recombination between photojected electrons and oxidized [Co(bipy)₃]³⁺ complex. In previous works on non-porphyrinic dyes in DSSCs, it was clearly demonstrated that the strongly electro-deficient BTD π -bridge enhanced the intramolecular charge transfer (ICT) of the dye excited-state, but on the other hand accelerate the back electron transfer of the charge-separated state. The ultimate phenyl spacer between the BTD unit and the terminal carboxylic acid anchoring group was found to be of high importance to slow down such recombination process, while maintaining an efficient electron injection Dye* → TiO₂.³⁰⁶ With regard to the PIA experiments and the six-time shorter electron lifetime measured in SM315, the authors clearly demonstrated that the accelerating effect of

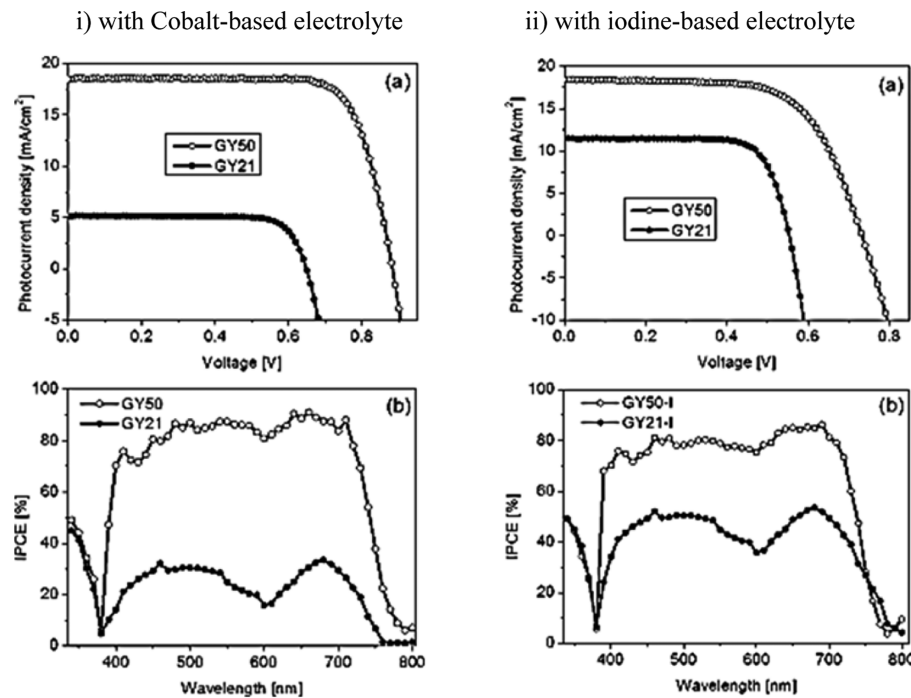


Figure 68. (a) J - V characteristics of the devices made with the **GY50** and **GY21** and (b) photocurrent action spectrum IPCE using either (i) the cobalt- (left) or (ii) the iodine-based (right) electrolyte. Reproduced with the permission from ref 302. Copyright 2014 Wiley-VCH.

the BTD bridge is not fully attenuated by the phenyl group, resulting in larger recombination process responsible of the 50 mV drop in V_{OC} relative to SM371 cell. This loss in V_{OC} for SM315/DSSC is, however, overcompensated by a gain of 2.2 mA·cm⁻² in the J_{SC} , and considering similar F.F., leads to a higher PCE ($\eta = 13\%$) than for SM371/DSSC ($\eta = 12\%$). The importance of the ultimate phenyl spacer toward reduced back-electron transfer can be clearly appreciated by comparing the performances of the two similar structured BTD-bridged dyes **GY21** (without) and **GY50** (with a phenyl spacer) reported at the same type by Yella et al. from the same group (Table 38).³⁰² Regardless to the electrolyte (iodine- or cobalt-based), the photovoltaic performances and overall PCE are strikingly higher for dye **GY50** than **GY21** (Figure 68). As depicted in Figures 68 i.b and ii.b, the IPCE values of **GY50** are much higher at any wavelength in the whole \sim 400–800 nm region (>80%). To shed light on the exact reasons of such impressive difference in the IPCE, V_{OC} , and J_{SC} values, each DSSC processes were studied separately in details. Dye regeneration (η_{reg}), electron-injection (ϕ_{inj}), and light-harvesting (LHE) were found to be highly efficient, and likewise similar for both DSSC, thus pointing that charge-collection efficiency (η_{coll}) is the main factor responsible of the difference observed in the IPCE values (vide supra, see eq 4, Figure 4). The J_{SC} being directly proportional to the integrated IPCE value (vide supra, see eq 2 (Figure 4)), and considering similar absorption window, η_{reg} , ϕ_{inj} and LHE for both dyes, the drop of J_{SC} from **GY50** to **GY21** can be directly assigned to lower IPCE values caused by poorer charge-collection efficiency. This was confirmed by transient photocurrent decay experiments, which evidenced a charge-collection efficiency >90% at any given charge density for **GY50** cell, whereas that of **GY50** quickly drop to 50% as the charge densities increased. Next, the reasons for the drop in V_{OC} were analyzed by transient photovoltage decay experiments. The lifetime of the injected electron from TiO_2 to the electrolyte was found longer for **GY50** at any given charge-density than for

GY21 (up to 100 times longer when using the cobalt-based electrolyte). In other words, it means that recombination rate at the TiO_2 -electrolyte interface is faster in the case of **GY21** than for **GY50**. Additionally, the chemical capacitance was found to be lower for **GY21**, indicative of a downward shift of the TiO_2 -CB (shifted to higher potential). The loss of V_{OC} from **GY50**/DSSC ($V_{OC} = 732$ mV (iodine) and 885 mV (cobalt)) to **GY21**/DSSC ($V_{OC} = 552$ mV (iodine) and 549 mV (cobalt)) can be therefore ascribed to both a downward shift of the TiO_2 -CB, and faster recombination rates at the TiO_2 -electrolyte interface for the latter DSSC. As for the **YD2-o-C8** cell (Table 38, entry 3), the perfect harmony between **GY50** sensitizer and the $[Co(bipy)]^{3+/2+}$ redox couple in the electrolyte can be clearly appreciated by the 162 mV improvement in the V_{OC} when compared to the iodine-based electrolyte (723 mV \rightarrow 885 mV), factor that mainly contribute to the 43% improvement of PCE for **GY50**/DSSC ($\eta = 8.90\% \rightarrow 12.75\%$).

6. ASYMMETRICAL, MULTI-DONORS, AND HIGHLY CONJUGATED, MESO-SUBSTITUTED “PUSH–PULL” PORPHYRIN DYES

In the state-of-the-art design for A2BC push–pull porphyrin dyes, the donor and acceptor moieties are located at two opposite *meso*-positions of the porphyrin, while the two others are occupied by bulky groups (decoupled systems). The role of these latter is to impede dye aggregation, protect the zinc center metal ion of the porphyrin core against the electrolyte, and reduce recombination rate between oxidized species of the redox shuttle and photojected electron into the TiO_2 . In order to take a maximum advantage and optimize the four *meso*-positions of a porphyrin, one could wonder why the two extra 5,15-*meso*-positions are not occupied by additional donor groups that would increase the electronic density and/or light-harvesting capability of the porphyrin dye. In an ideal case, these donors would be additionally systems that are strongly

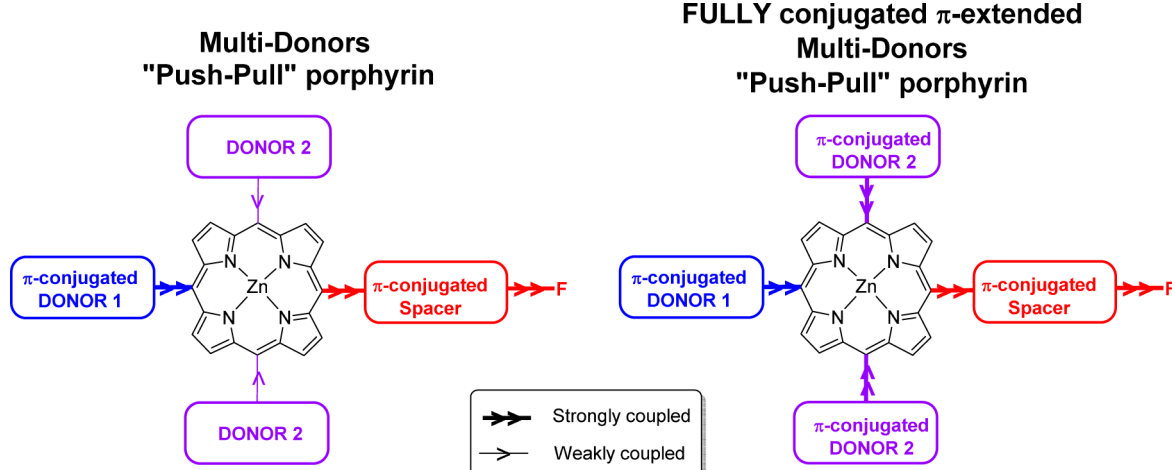


Figure 69. Schematic representation of multidonor and highly conjugated porphyrins dyes (F = functional binding group: COOH).

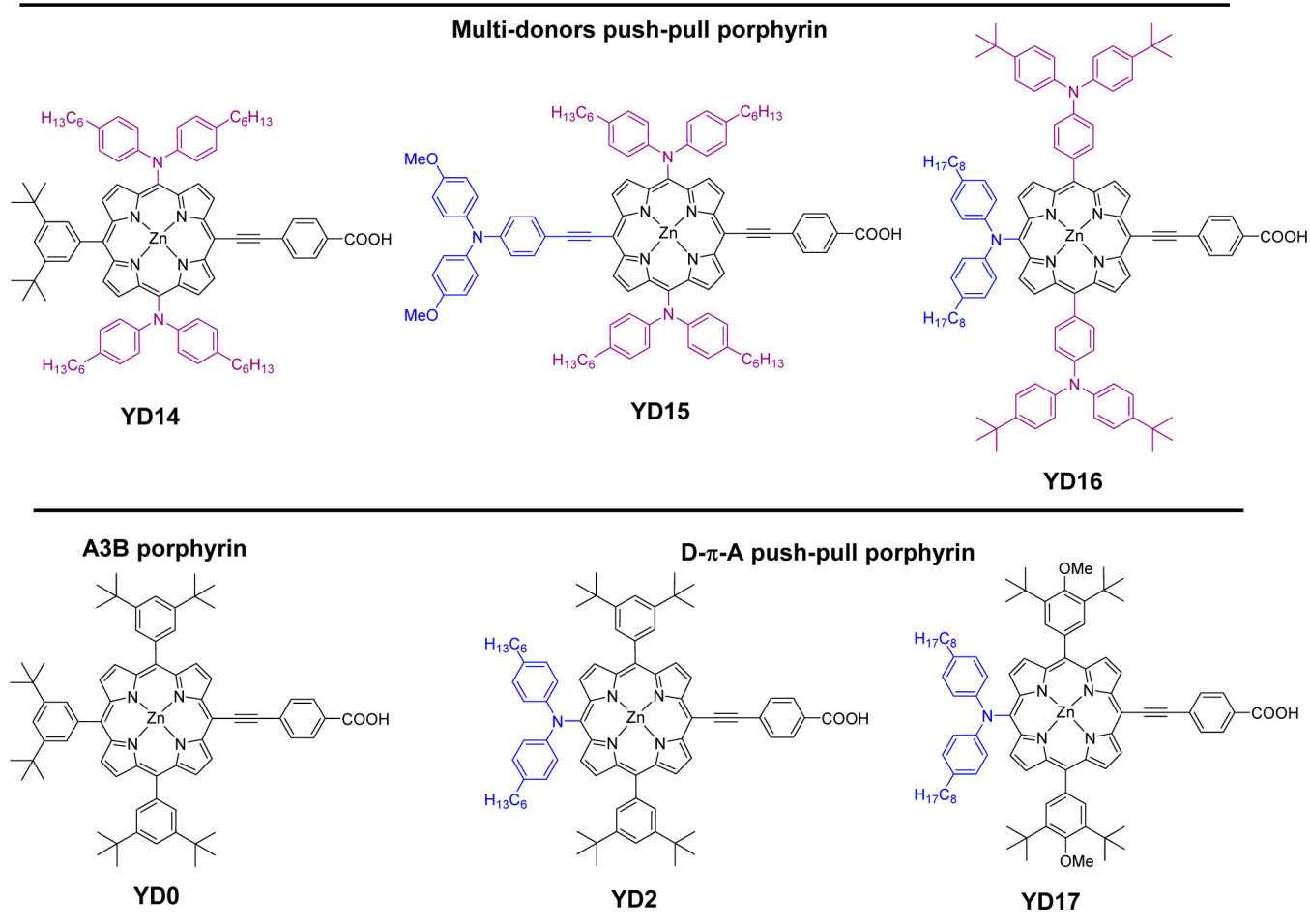


Figure 70. Molecular structures of dyes YD0, YD2, and YD14–17, reported by Diau and co-workers (ref 284).

π -coupled to the porphyrin, and bulky enough to impede aggregation and decrease recombination processes (Figure 69). The complexity of synthesis of such architectures, including fully conjugated multi donors- and acceptor- components in the same porphyrin dye, is however challenging and admirable.

Diau and co-workers have demonstrated the feasibility of this concept and reported in 2010 the only known examples to date (to the best of our knowledge) of fully coupled

π -conjugated- (YD15) and partially coupled- (YD14, YD16) multidonors push–pull porphyrin dyes (Figure 70, Table 39).²⁸⁴ The designs of YD14–17 dyes were inspired by the molecular structure of YD2, to study the influence on the optical, electrochemical and photovoltaic properties upon incorporation of additional diarylaminophenyl or triphenylamino-EDGs at different meso positions of the porphyrin. YD17 incorporates an additional OMe group at the para position of the 3,5-di-*tert*-butyl

Table 39. Dye-Loading and Photovoltaic Parameters of the TiO_2 -DSSCs Sensitized with YD0, YD2, and YD14–17 under Simulated AM1.5G Full Sun Illumination (Power 100 $\text{mW}\cdot\text{cm}^{-2}$) and an Active Area of 0.16 cm^2 . Data Derived from Ref 284

dye	dye-loading (nmol·cm ⁻²)	Voc (mV)	J _{sc} (mA·cm ⁻²)	F.F. (%)	η (%)
YD0	140	697	10.42	69	5.0
YD2	148	714	14.80	67	7.1
YD17	142	722	13.99	69	7.0
YD14	131	712	14.27	67	6.8
YD16	111	704	12.21	64	5.5
YD15	128	623	9.42	71	4.2

meso-phenyl groups, acting as weak (decoupled) donors, whereas YD14–16 incorporate either weakly coupled (triphenylamino groups) and/or strongly coupled -EDGs (diaryl amino or ethynyl triphenyl amino groups), which are expected to improve the donor ability of these dyes with respect to YD2.

In comparison with the benchmark dye YD0, the incorporation of strongly coupled EDG groups in the molecular structure of YD2/17 (one), YD14 (two), YD16 (two medium and one strongly coupled), and YD15 (three), results in drastic changes of their spectral features (in particular redshifts and broadening of absorption bands) and redox potentials. In particular, YD14 and YD15 display a split Soret band accompanied by a redshift of the second one ($\lambda_{\text{max}} = 488$ nm for YD15 versus 442 nm for YD0), much broadened and redshifted Q bands ($\lambda_{\text{max}} = 707$ nm for YD15 versus 579 and 627 nm for YD0), thus covering a wider range of the visible range and fulfilling the absorption gap of common porphyrins between 450–550 nm and 650–800 nm. The number of EDGs also affects notably the redox potentials of the porphyrin.

Table 41. PCE Values of Some of the Best Efficient and Representative Photosensitizers Based on Ru(II)-Polypyridyl Complex in TiO_2 /DSSCs under Simulated AM1.5G Full Sun Illumination

year	author(s)	sensitizer	max. PCE (%)	ref
2001	Nazeeruddin, Grätzel	black dye	10.4	309
2005/06	Nazeeruddin, De Angelis	N719	11.18	310
2008	Wang, Zakeeruddin, Grätzel	C101	11.0	311
2009	Wu, Zakeeruddin, Grätzel	CYCB11	11.5	312
2010	Wang	C106	11.7	313
2012	Han	black dye	11.4	314

Indeed, the porphyrin radical cation being more stabilized with an increase number of strongly coupled EDGs from YD0 (none) to YD15 (three), the first oxidation potential decreases following the same order YD0 (+1.04 V) \gg YD17 (+0.91 V) \sim YD2 (+0.89 V) $>$ YD14 (+0.86 V) \sim YD16 (+0.85 V) $>$ YD15 (+0.81 V). Although the multidonors appended porphyrins (YD14–16) display superior light harvesting properties and stronger donor ability than YD2/17, they surprisingly display PCE in the reverse order of the number of strongly conjugated donors YD15 ($\eta = 4.2\%$, three) $<$ YD16 ($\eta = 5.5\%$, one strong and two medium) $<$ YD14 ($\eta = 6.8\%$, two) $<$ YD2, YD17 ($\eta \sim 7\%$, one). The low performance of YD16 was explained by the presence of the two bulky triphenyl amino substituents that reduce significantly the amount of adsorbed dyes (111 versus 148 nmol·cm⁻² for YD2) which result in a degradation of the J_{sc} (12.21 versus 14.80 mA·cm⁻² for YD2). The dye YD15, fully conjugated with three strong donor groups, displays the lowest PCE of the series ($\eta = 4.2\%$), which is even lower than YD0 ($\eta = 5.0\%$) without strong donors. The poor performances of YD15 is

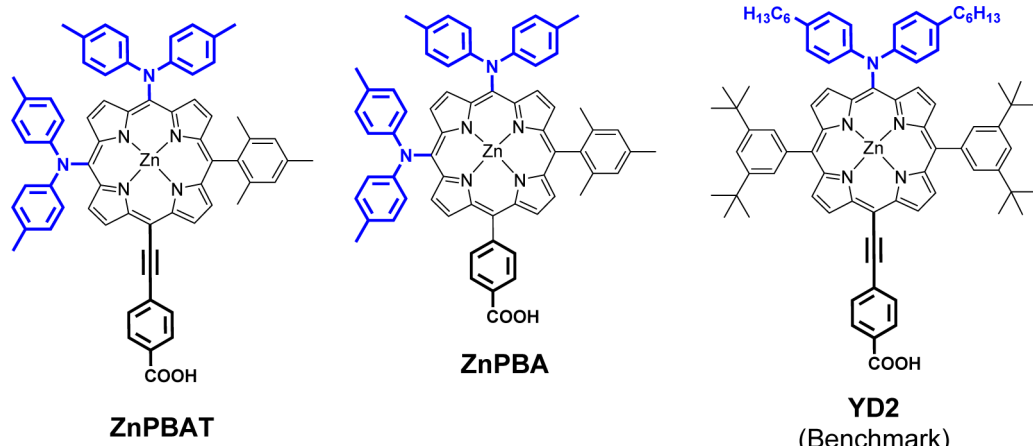


Figure 71. Molecular structures of *cis*-A2BC-type (“AABC”) porphyrin dyes ZnPBA, ZnPBAT, and benchmark YD2 reported by Sundström and co-workers (ref 307).

Table 40. Aging, Surface Coverage (Γ), and Photovoltaic Parameters of Optimized^b TiO_2 -DSSCs Sensitized with ZnPBA, ZnPBAT and Benchmark YD2 under Simulated AM1.5G Full Sun Illumination (Power 100 $\text{mW}\cdot\text{cm}^{-2}$)^a

dye	aging (days)	$\Gamma_{\text{sat}}/10^{-11}$ (mol·cm ⁻²)	coadsorbent CDCA (equivalents)	Voc (mV)	J _{sc} (mA·cm ⁻²)	F.F. (%)	η (%)
ZnPBA	1.5	9.2	10	719	19.33	72.4	10.1
ZnPBA	8	8.7	5	713	16.26	71.9	8.3
YD2 (Benchmark)	2	8.9	2	742	17.05	71.8	9.1

^aData derived from ref 307. ^bPhotovoltaic parameters reported in the table were obtained for the highest η values after aging of the cells (see details in the second column of the table).

reflected by the smallest J_{SC} ($9.41 \text{ mA}\cdot\text{cm}^{-2}$) and V_{OC} (623 mV) values among all DSSCs of this series. The authors

Table 42. Best PCE Values for n-Type TiO₂/DSSCs Sensitized with A4-Type meso-Substituted Porphyrins (under Simulated AM1.5G Full Sun Illumination, unless Otherwise Noted)

year	author(s)	sensitizer	max. PCE (%)	ref
1996	Goosens	ZnpTCPP	(1.1) ^a	212
2000	Wamser	H2-pTCPP	(3.5) ^b	208
2002	Ma	H2-pTCPP	0.36	205
		H2-pTSPP	0.04	205
2004	Waclawik	H2-pTCPP	(0.69) ^c	207
2007	Galoppini	Zn-pTCPP-[S]	0.09 ^d	213
		Zn-mTCPP-[S]	0.70 ^d	213
		Zn-mTCP2P-[S]	0.78 ^d	213
		Zn-mTC(PEP)P-[S]	0.26 ^d	213
2012	Sharma, Coutsolelos	P3	2.46	190

^aUnder low light intensity ($16 \text{ mW}\cdot\text{cm}^{-2}$). ^bUnder low light intensity ($1.4 \text{ mW}\cdot\text{cm}^{-2}$). ^cUnder low light intensity ($37.85 \text{ mW}\cdot\text{cm}^{-2}$); reported values were corrected for 24% power loss due to attenuation caused by the FTO glass. ^dPCE values (η) were not reported, and calculated from eq 1 and the information given in the article for ref 213.

suggested that dye YD15 must strongly aggregate, which would explain the poor photovoltaic performances. The planar and π -electron rich conjugated system fully delocalized over the porphyrin ring, the three donors and the acceptor moiety, must indeed strongly favor a coplanar organization of the porphyrins by π - π stacking. The strikingly difference of photovoltaic performances between similar-structured dyes YD15 and YD14, which differ only by a 3,5-di-*tert*-butylphenyl group for the latter (well-known to impede efficiently aggregation

Table 44. Best PCE Values for n-Type TiO₂/DSSCs Sensitized with A2B2-Type meso-Substituted Porphyrins under Simulated AM1.5G Full Sun Illumination

year	author(s)	sensitizer	max. PCE (%)	ref
2010	Hupp	ZnPdCA	5.5	257
	Imahori	cis-ZnP	5.5	274
2012	Coutsolelos	P1 ^a	4.90	258
		P2 ^a	6.07	258
		P2 ^a	6.12	190
	Luo, Diau, Hung	trans-2S2A	1.8	260
		cis-2S2A	2.5	260

^aVarious dyes with different molecular structures were reported under the same name by the same authors and/or others.

Table 43. Best PCE Values for n-Type TiO₂/DSSCs Sensitized with A3B-Type meso-Substituted Porphyrins under Simulated AM1.5G Full Sun Illumination

year	author(s)	sensitizer	max. PCE (%)	ref	year	author(s)	sensitizer	max. PCE (%)	ref
2006	Imahori, Yoshikawa	ZnP (=2,4,6-Me)	3.5	218	2011	Tan	Z1	4.44	254
2007	Imahori	ZnSS	3.1	255			Z2	5.71	254
		ZnSO	2.3	255			Z3	4.54	254
		Zn4S	2.0	255			Z4	4.54	254
2008	Imahori	Zn-3 (= 2,4,6-Me)	4.6	138	2012	Lin, Diau	LD11 ^b	4.78	277
2009	Imahori	4H	1.2	216			LD12	7.43	277
		BP	2.6	216		Barea, Diau, Bisquert	YD0	3.29	283
		4CF3	3.0	216		Mori, Mozer	P199	2.59	160
		4OMe	3.5	216		Luo, Diau, Hung	3S1A	0.2	260
		2,4,6Et	3.7	216			1S3A	3.0	260
		4Me	3.8	216		He	DMPZn- C2-COOH	5.12	242
		2,4,6-Me (= ZnP)	4.6	216			TPPZn- COOH	1.8	242
	Tan	PZn-T	4.25	232		Coutsolelos	P1 ^a	3.10	190
		PZn-oT	4.55	232	2013	Sharma, Coutsolelos	(PEPy) ^c	5.66	191
		PZn-hT	5.14	232		D'Souza	1o	0.11	223
	Yeh, Diau	1 (=YD0)	2.4	241			1o-Zn	0.37	223
		2	1.2	241			1m	0.71	223
		6	2.2	241			1m-Zn	4.17	223
		7	0.93	241			1p	0.42	223
	Lin, Diau	PE1 ^a	2.5	244			1p-Zn (=4-Me)	3.13	223
		PE2	2.0	244			2m	0.65	223
		PE3	0.78	244			2m-Zn	2.45	223
		PE4	0.25	244			2p	0.65	223
2010	Lin, Diau	LAC1	2.95	252			2p-Zn	2.42	223
		LAC2	3.31	252			3m	0.30	223
		LAC3	5.44	252			3m-Zn	1.99	223
		LAC4	2.82	252			3p-Zn	2.09	223
		LAC5	0.1	252		Yeh, Diau	YD30	3.6	287
	Imahori	ZnP	4.4	274	2014	Jing, Zhu	PE1m	0.64	243
	Yeh, Diau	YD0	4.34	275			PESm	1.22	243
	Yeh, Diau	YD0	5.0	284			PE1 ^a	2.26	243
							PESP	4.55	243

^aVarious dyes with different molecular structures were reported under the same name by the same authors and/or others. ^bDye LD11 was not reported in this review. ^cThis dye did not have a name in the article, and was called "PEPy".

Table 45. Best PCE Values for n-Type TiO₂/DSSCs Sensitized with A2BC-Type *meso*-Substituted Porphyrins under Simulated AM1.5G Full Sun Illumination (*Denotes the Use of the Co^{III/II} Tris(2,2'-bipyridine) Complex As Redox Shuttle in the Electrolyte of the DSSC)

year	author(s)	sensitizer	max. PCE (%)	ref	year	author(s)	sensitizer	max. PCE (%)	ref		
2009	Yeh, Diau	YD11	2009	6.79	282	Lin, Diau, Kuo	LD23	2012	7.4	279	
		YD12	2009	6.91	282		LD24	2012	5.4	279	
		YD13	2009	1.86	282		LD25	2012	4.1	279	
	Yeh, Diau	3 (= YD7)	2009	1.4	241		LD13	2012	8.37	281	
		4	2009	1.2	241		LD14	2012	10.05	281	
		5 (= YD1)	2009	6.0	241		LD14-C4 ^a	2012	5.91	281	
	Imahori	mono ZnP	2010	6.5	274		LD14-C8	2012	8.94	281	
		Trans ZnP	2010	3.8	274		LD15	2012	8.92	281	
	Yeh, Diau	YD1	2010	6.15	275		LD16	2012	10.24	281	
		YD2	2010	6.56	275		Bisquert, Yeh, Diau	YD20	2012	8.1	289
		YD3	2010	5.34	275		YD21	2012	5.5	289	
		YD4	2010	5.65	275		YD22	2012	6.6	289	
		YD5	2010	2.10	275		Kim	HP	2013	5.0	272
		YD6	2010	5.13	275		HOP	2013	7.6	272	
		YD7	2010	4.38	275		EHOP	2013	6.1	272	
		YD8	2010	4.27	275		Kim	2Flu-ZnP-CN-COOH	2013	7.30	273
		YD11	2010	6.62	275		2,4-ZnP-CN-COOH	2013	8.46	273	
		PE1NMe2	2010	6.12	280		HexO-ZnP-CN- COOH	2013	7.02	273	
	Lin, Diau	PE1NO2	2010	1.09	280		YD12	2013	7.23	286	
		PE1CN	2010	4.05	280		YD12CN	2013	4.28	286	
		PE1OMe	2010	4.76	280		YD13	2013	2.57	286	
		YD14	2010	6.8	284		YD13CN	2013	2.86	286	
	Yeh, Diau	YD15	2010	4.2	284		YD26	2013	8.04	286	
		YD16	2010	5.5	284		YD27	2013	6.03	286	
		YD17	2010	7.0	284		YD28	2013	5.80	286	
		YD2	2010	7.1	284		YD29	2013	3.64	286	
		YD2	2010	10.9	285		Yeh, Diau	YD2	2013	4.8	287
	Grätzel	YD2	2010	10.9	285		YD2-oC8	2013	5.1	287	
		YD2*	2011	8.4*	65		YD12	2013	8.5	299	
2011	Diau, Yeh, Zakeerud-din, Grätzel	YD2-O-C8*	2011	11.9*	65		YD12CN	2013	5.8	299	
		[YD2-O-C8+Y123]*	2011	12.3*	65		Sundström, Imahori	ZnPBAT	2013	10.1	307
		D	2011	3.0	261		ZnPBA	2013	8.3	307	
	Odobel	T	2011	3.9	261		YD2	2013	9.1	307	
		1	2011	0.66	263		Nazeeruddin, Grätzel	SM315*	2014	13*	159
	Deng, Liu	2	2011	0.89	263		SM371*	2014	12*	159	
		3	2011	1.44	263		Palomares	VC70	2014	7.31	276
		4 (=HKK-Por3)	2011	1.52	263		Wang, Wu	WW5*	2014	10.3*	292
		5	2011	2.38	263		WW6*	2014	10.5*	292	
		HKK-Por1	2011	5.01	268		YD2-o-C8*	2014	10.5*	292	
	Kim	HKK-Por2	2011	4.70	268		Yeh, Diau	LD31	2014	9.95	295
		HKK-Por3	2011	2.09	267		(LD31+AN-4)	2014	10.26	295	
		HKK-Por4	2011	2.74	267		LD14	2014	9.34	295	
		HKK-Por5	2011	3.36	267		Lin, Wu	LWP1	2014	9.73	296
		LD13	2011	9.34	277		LWP2	2014	6.07	296	
	Lin, Diau	LD14	2011	10.17	277		LWP3	2014	9.51	296	
		LD1	2011	5.11	278		LD14	2014	9.01	300	
	Lin, Diau	LD2	2011	7.83	278		LWP4	2014	6.70	296	
		LD3a	2011	6.62	278		LD14	2014	10.03	296	
		LD3b	2011	8.26	278		LW3	2014	7.63	300	
		LD4	2011	10.06	278		LW4	2014	9.53	300	
		YD2	2011	6.36	283		LD14	2014	9.01	300	
	Barea, Diau, Bisquert	ZnPH	2011	6.9	297		Xie	YQ1	2014	6.01	301
		ZnPF	2011	4.6	297		YQ2	2014	4.23	301	
	Kim	2Flu-ZnP-CN-COOH	2012	7.22	269		YQ3	2014	4.38	301	
		2Flu-ZnP-COOH	2012	4.7	269		YQ4	2014	5.00	301	
	Lin, Diau	LD21	2012	6.3	279		Zakeeruddin, Grätzel	GY21*	2014	2.52*	302
		LD22	2012	8.1	279		GY21	2014	4.84	302	
							GY50*	2014	12.75*	302	
							GY50	2014	8.90	302	

^aDye LD14-C4 was not reported in the current review.

between porphyrin) instead of an ethynylamino group for the former, clearly seems to point that way. Additionally, one could wonder about the influence of additional donor groups on the resulting direction of the interfacial dipole moment in these kinds of systems. Indeed, it is known that the orientation and the magnitude of the dipole moment at the dye/TiO₂ interface affect the TiO₂ ECB.^{1,6} Typically, D-B-A organic dyes endowed with an electron-donor moiety and an anchor acting as an electron-withdrawing group are anchored perpendicularly/vertically to the surface and display a dipole moment oriented in ballistic way D → A → TiO₂, which results in a negative shift of the Fermi level (*n*Ef) of TiO₂ and hence provide higher *V*_{OC} of the TiO₂ cell. Thus, the opposite location of the donor and acceptor moieties in push–pull porphyrins **YD2** and **YD17** must result in a strong dipole moment oriented in a ballistic way, while for **YD14–16** the orientation and magnitude must be strongly affected by the additional donors at the 5,15 meso positions, orientated parallel to the surface. This might be an additional factor that contributes to the lower *V*_{OC} values observed for **YD14–16** dyes (623–712 mV) than for **YD2** and **YD17** (714 and 722 mV, respectively). With regard to the superior light-harvesting capabilities and lower redox potentials (i.e., stronger donor ability) of these multidonor and fully conjugated push–pull porphyrins, the incorporation of additional donors clearly seems an appealing strategy to produce new generation of efficient porphyrin sensitizers. However, a major drawback of this molecular design lies in the fact that switching the bulky groups by π -conjugated donors result in strong aggregation issues (because of gaining more planarity), which unfortunately causes much larger degradation of the photovoltaic performances of the DSSC than it brings benefits. Therefore, one future challenge might come from being able to combine these two properties in a same dye, that is, the incorporation of multi π -conjugated donors judiciously tailored in such a way that they also impede efficiently dye aggregation.

As commented in the introduction of the previous section, the *cis*-A2BC-type (or “AABC”) design had never been used for porphyrin dyes until recently. Sundström, Imahori and co-workers provided in November 2013,³⁰⁷ the two only known examples, to the best of our knowledge, of highly asymmetrical, *cis*-A2BC-type porphyrin dyes in DSSC (Figure 71). **ZnPBAT** is a *cis*-A2BC-type porphyrin with an enhanced “push–pull” character owing to the two diphenylamino groups as strong π -coupled donors. The acceptor part is an ethynylcarboxyphenyl, and the last remaining meso position occupied by a mesityl group to prevent dye-aggregation. To study the influence of the anchoring group, loss of symmetry and effect of an additional diphenylamino donor group in the dye **ZnPBAT** toward the photovoltaic performances in DSSC, two other devices were made either with the benchmark **YD2** or with the carboxyphenyl anchored analogue **ZnPBA** for comparison purpose. In comparison with **YD2** (one diphenylamino donor), the introduction of a second donor in **ZnPBAT** significantly broadened and red-shifted the porphyrin absorption bands. As expected, the LUMO level of **ZnPBAT** and **YD2** are relatively similar and largely delocalized over both the macrocycle and ethynylcarboxyphenyl moieties, in comparison with that of the carboxyphenyl anchored **ZnPBA** dye. The combination of two diphenylamino donors and an ethynylcarboxyphenyl acceptor confers to **ZnPBAT** improved light-harvesting properties with respect to the two other dyes. The three dyes achieved similar saturation dye-coverage (Table 40), and in agreement with calculation predictions, it is assumed a tight packing of the molecules onto the TiO₂ surface.

Table 46. Best Performing *meso*-Substituted Porphyrins in TiO₂/DSSCs Achieving a PCE Superior at 8% under Simulated AM1.5G Full Sun Illumination (*Denotes the Use of the Co^{III/II} Tris(2,2'-bipyridine) Complex As Redox Shuttle in the Electrolyte)

entry	author(s)	sensitizer	year	max. PCE (%)	ref
1	Nazeeruddin, Grätzel	SM315*	2014	13*	159
2	Zakeeruddin, Grätzel	GY50*	2014	12.75*	302
3	Diau, Yeh, Zakeeruddin, Grätzel	[YD2-o-C8+Y123]*	2011	12.3*	65
4	Nazeeruddin, Grätzel	SM371*	2014	12*	159
5	Diau, Yeh, Zakeeruddin, Grätzel	YD2-o-C8*	2011	11.9*	65
6	Yeh, Diau, Grätzel	YD2	2010	10.9	285
7	Wang, Wu	WW6*	2014	10.5*	292
8	Wang, Wu	YD2-o-C8*	2014	10.5*	292
9	Wang, Wu	WW5*	2014	10.3*	292
10	Lin, Diau	(LD31+AN-4)	2014	10.26	295
11	Lin, Diau	LD16	2012	10.24	281
12	Lin, Diau	LD14	2011	10.17	277
13	Sundström, Imahori	ZnPBAT	2013	10.1	307
14	Lin, Diau	LD4	2011	10.06	278
15	Lin, Wu	LD14	2014	10.03	296
16	Lin, Diau, Kuo	LD14	2012	10.05	281
17	Lin, Diau	LD31	2014	9.95	295
18	Lin, Wu	LWP1	2014	9.73	296
19	Liao, Wang	LW-4	2014	9.53	300
20	Lin, Wu	LWP3	2014	9.51	296
21	Lin, Diau	LD13	2011	9.34	277
22	Diau, Lin	LD14	2014	9.34	295
23	Sundström, Imahori	YD2	2013	9.1	307
24	Liao, Wang	LD14	2014	9.01	300
25	Lin, Diau, Kuo	LD14-C8	2012	8.94	281
26	Lin, Diau, Kuo	LD15	2012	8.92	281
27	Zakeeruddin, Grätzel	GY-50	2014	8.90	302
28	Yeh, Diau	YD12	2013	8.5	299
29	Kim	2,4-ZnP-CN-COOH	2013	8.46	273
30	Diau, Yeh, Zakeeruddin, Grätzel	YD2*	2011	8.4*	65
31	Lin, Diau, Kuo	LD13	2012	8.37	281
32	Sundström, Imahori	ZnPBA	2013	8.3	307
33	Lin, Diau	LD3b	2011	8.26	278
34	Lin, Diau	LD22	2012	8.1	279
35	Yeh, Diau, Bisquert	YD20	2012	8.1	289
36	Yeh, Diau	YD26	2013	8.04	286

By following the evolution of the cell performances versus immersion time, and regarding the higher amount of CDCA needed to reach the maximum IPCE response and photovoltaic performances, it was concluded that the affinity for dye-aggregation follows the order **YD2** < **ZnPBA** < **ZnPBAT**. The relative cumulated integrated IPCE value increases in the order **ZnPBA** (1) < **YD2** (1.11) < **ZnPBAT** (1.28), and APCE values in the order **YD2** (88%) < **ZnPBA** (92%) < **ZnPBAT** (95%). The rather small difference in the APCE values between **YD2** and **ZnPBAT**, and assuming highly efficient electron-injection for both dyes, witness only slight differences in their *n*_{coll} and ϕ_{inj} values. Thus, the superior LHE of **ZnPBAT** with regard to **YD2** cell, mostly contribute to higher IPCE values, and hence a larger *J*_{SC}. **ZnPBAT** and **ZnPBA** achieved similar *V*_{OC} significantly lower than that of **YD2** cell. From electrochemical impedance spectroscopy experiments (EIS),^{224–228} this loss

of V_{OC} was attributed to faster recombination rate at the TiO_2 electrolyte interface in **ZnPBAT**- and **ZnPBA**- than in **YD2**/DSSC. Considering similar fill factor, this loss of V_{OC} is however overcompensated by a larger J_{SC} in the case of **ZnPBAT** cell, achieving a PCE of 10.1%, which is superior to that of **YD2** ($\eta = 9.1\%$) under optimized and similar conditions.

7. CONCLUSION

In summary, we have discussed the molecular engineering aspect of meso-substituted porphyrins, in particular donor- π -bridged chromophore-acceptor porphyrin sensitizers (“push-pull”), and their photovoltaic performance in DSSCs. To date, the great majority of the best performing porphyrin sensitizers are A2BC-type, “push–pull” meso-substituted porphyrins (Figures 72 and 73) anchored through an ethynylcarboxyphenyl group, and tailored with a strong donor group at the opposite site. The two 5,15-meso positions ('A' positions) consisting of alkoxy substituted phenyl ring, are also of high-importance to reduce aggregation and recombination processes. As demonstrated for **SM315** and **GY50**, the best performing dyes to date in DSSCs, further molecular engineering of porphyrins³⁰⁸ should come from the acceptor part, to lower slightly the LUMO level of the dye and get a panchromatic response leading to over 20 mA·cm⁻² of short circuit current. The arrival and further developments of redox shuttles, more flexible in terms of redox potential, should benefit to another class of sensitizers than porphyrins through a better matching with the HOMO level of a given dye. Redox mediators with higher redox potential can allow attaining greater V_{OC} in DSSC, but must fulfill the compromise to satisfy a minimum overpotential needed for an efficient dye-regeneration. So far, this harmony was realized between the cobalt(III/II)

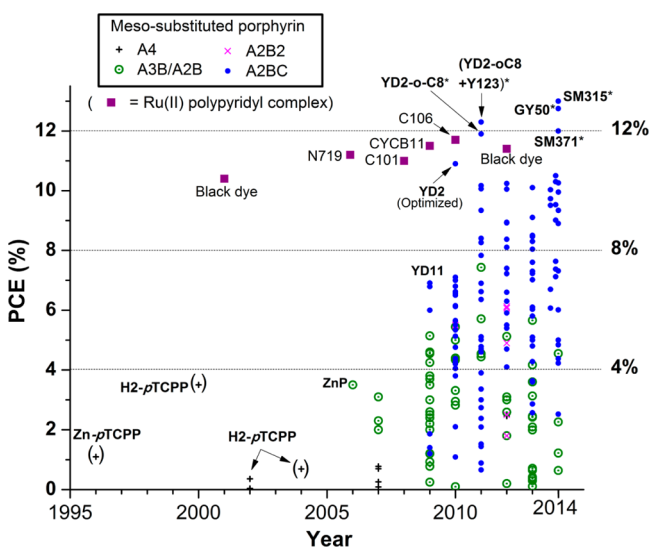


Figure 72. Evolution of PCE in n-type TiO₂/DSSCs photosensitized with meso-substituted porphyrins from 1995 to 2014 (nonexhaustive list; “year” refers to the time of publication in the journal). For comparison, some of the best efficient and representative photosensitizers based on ruthenium(II)-polypyridyl complex are also noted (rectangles). Symbols in parentheses refer to PCE values determined under low-light intensity; all other values are reported under simulated AM1.5G full sun illumination, see Tables 41–45 for details and references (PCE = solar-to-electric power conversion efficiency, *refers to the cobalt(III/II) tris(2,2'-bipyridine) complex in the electrolyte of the DSSC).

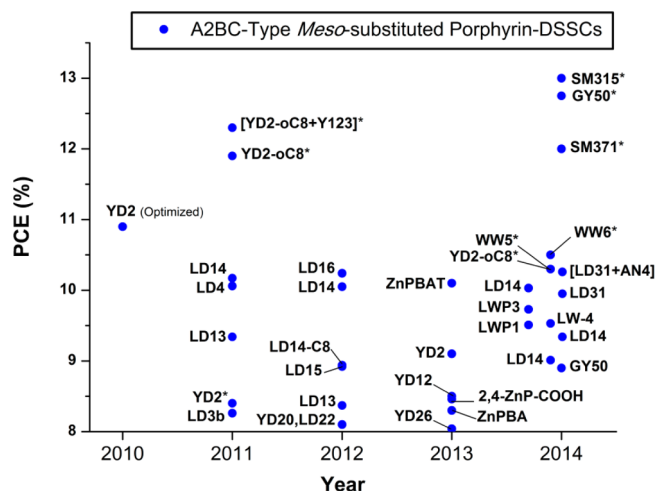


Figure 73. Best performing meso-substituted porphyrins in TiO₂/DSSCs achieving a PCE superior at 8% under simulated AM1.5G full sun illumination, see Table 46 for details and references (* denotes the use of the Co^{III/II} tris(2,2'-bipyridine) complex as redox shuttle in the electrolyte of the DSSC; PCE = solar-to-electric power conversion efficiency).

tris(2,2'-bipyridine) complex and some porphyrin dyes, achieving impressive V_{OC} close to 1 V. To optimize further the use of cobalt complexes as redox couples, a molecularly designed donor group should be incorporated into the porphyrin to reduce recombination and increase open circuit potential to 1 V. Armed with $20 \text{ mA}\cdot\text{cm}^{-2}$ short circuit current, 1 V open circuit potential and a fill factor of 75%, future generations of porphyrin dyes should be able to achieve soon a power conversion efficiency beyond 15% at full sun illumination (AM 1.5 G, $1000 \text{ W}\cdot\text{m}^{-2}$).

AUTHOR INFORMATION

Corresponding Authors

*E-mail: mdkhaja.nazeeruddin@epfl.ch.

*E-mail: tomas.torres@uam.es.

Notes

The authors declare no competing financial interest.

Biographies



Maxence Urbani was born in Langres (France) in 1980, and graduated in organic chemistry in 2003 at the University Henry Poincaré (Nancy, France). The same year he joined the Prof. Jean-François Nierengarten's group, where he received his M. Sc. (2004) in analytic

and material chemistry at the University of Louis Pasteur (Strasbourg, France), and his Ph.D. (2007) in Macromolecular and Supramolecular Chemistry at the university Paul Sabatier (Toulouse, France), working on Fullerene-Porphyrin ensembles. After that, he carried out a two-year postdoctoral stay (2008–2010) in the group of Prof. Fernando Langa, at the University of Castilla-la-mancha (Toledo, Spain) working on oligothienylene vinylene, fullerene, and porphyrin ensembles. Since 2010, he is now a postdoctoral researcher in the Prof. Tomas Torres's group at the University Autonoma de Madrid and IMDEA-Nanociencia (Madrid, Spain). His current research interests include the preparation and study of bipyridine-ruthenium complexes and porphyrin dyes for their application in DSSCs.



Tomás Torres is Full Professor of Organic Chemistry at the Autonoma University of Madrid (UAM) and Associated Senior Scientist at the IMDEA-Nanoscience. In addition to various aspects of synthetic and supramolecular chemistry his current research interests include the preparation and study of optical properties of organic functional materials. His group, that presently consists of 25 researchers, is currently exploring several areas of basic research and applications of phthalocyanines, porphyrins and carbon nanostructures (fullerenes, carbon nanotubes, and graphene), including organic and hybrid solar cells, with a focus on nanotechnology.



Md. K. Nazeeruddin is a Senior Scientist at EPFL and also professor at world class university Korea. He has published over 380 peer reviewed scientific publications, 10 review/invited book chapters and inventor or coinventor of 45 patents, with an h index of 84. He is an expert in the design, synthesis, and characterization of platinum group metal complexes associated with dye-sensitized solar cells and organic light emitting diodes.



Michael Grätzel directs the Laboratory of Photonics and Interfaces at EPFL. He pioneered the use of mesoscopic materials in energy conversion systems, in particular photovoltaic cells, lithium ion batteries, and photoelectrochemical devices for the splitting of water into hydrogen and oxygen by sunlight. He discovered a new type of solar cell based on dye sensitized nanocrystalline oxide films, and acting as a reference group in the world. He published 1060 peer-reviewed scientific publications, 40 review/invited book chapters, and inventor or coinventor of over 50 patents and h index of >154.

ACKNOWLEDGMENTS

We are grateful for the financial support of the MEC and the MICINN, Spain (CTQ2011-24187/BQU), Comunidad de Madrid, Spain (FOTOCARBON, S2013/MIT-2841), and the European Union within the FP7-ENERGY-2012 -1, Nr. 309194 -2, GLOBALSOL Project.

REFERENCES

- (1) O'Regan, B.; Grätzel, M. *Nature* **1991**, *353*, 737.
- (2) Grätzel, M. *Acc. Chem. Res.* **2009**, *42*, 1788.
- (3) O'Regan, B. C.; Durrant, J. R. *Acc. Chem. Res.* **2009**, *42*, 1799.
- (4) Hagfeldt, A.; Boschloo, G.; Sun, L.; Kloo, L.; Pettersson, H. *Chem. Rev.* **2010**, *110*, 6595.
- (5) Clifford, J. N.; Martínez-Ferrero, E.; Viterisi, A.; Palomares, E. *Chem. Soc. Rev.* **2011**, *40*, 1635.
- (6) Mishra, A.; Fischer, M. K. R.; Bäuerle, P. *Angew. Chem., Int. Ed.* **2009**, *48*, 2474.
- (7) Listorti, A.; O'Regan, B.; Durrant, J. R. *Chem. Mater.* **2011**, *23*, 3381.
- (8) Zhang, S.; Yang, X.; Numata, Y.; Han, L. *Energy Environ. Sci.* **2013**, *6*, 1443.
- (9) Jung, H. S.; Lee, J.-K. *J. Phys. Chem. Lett.* **2013**, *4*, 1682.
- (10) Yen, Y.-S.; Chou, H.-H.; Chen, Y.-C.; Hsu, C.-Y.; Lin, J. T. *J. Mater. Chem.* **2012**, *22*, 8734.
- (11) Nazeeruddin, M. K.; Ko, J.; Grätzel, M. Mesoscopic Dye-Sensitized Solar Cells. In *Organic Nanomaterials: Synthesis, Characterization, and Device Applications*; Torres, T., Bottari, G., Eds.; John Wiley & Sons, Inc.: Hoboken, NJ, 2013; p 579.
- (12) Kim, B.-G.; Chung, K.; Kim, J. *Chem.—Eur. J.* **2013**, *19*, 5220.
- (13) Martinson, A. B. F.; Hamann, T. W.; Pellin, M. J.; Hupp, J. T. *Chem.—Eur. J.* **2008**, *14*, 4458.
- (14) Ooyama, Y.; Harima, Y. *Eur. J. Org. Chem.* **2009**, *2009*, 2903.
- (15) Balasingam, S. K.; Lee, M.; Kang, M. G.; Jun, Y. *Chem. Commun.* **2013**, *49*, 1471.
- (16) Ooyama, Y.; Harima, Y. *ChemPhysChem* **2012**, *13*, 4032.
- (17) Ooyama, Y. Dyes, Solar cells. In *Kirk-Othmer Encyclopedia of Chemical Technology*; Seidel, A., Bickford, M., Eds.; John Wiley & Sons, Inc.: New York, 2000; p 1.
- (18) Giribabu, L.; Kanaparthi, R. K.; Velkannan, V. *Chem. Rec.* **2012**, *12*, 306.

- (19) Bisquert, J.; Cahen, D.; Hodes, G.; Rühle, S.; Zaban, A. *J. Phys. Chem. B* **2004**, *108*, 8106.
- (20) Ribó, J. M.; Bofill, J. M.; Crusats, J.; Rubires, R. *Chem.—Eur. J.* **2001**, *7*, 2733.
- (21) Huijser, A.; Savenije, T. J.; Kroese, J. E.; Siebbeles, L. D. A. *J. Phys. Chem. B* **2005**, *109*, 20166.
- (22) Bai, Y.; Mora-Sero, I.; Nabuillun, J.; De Angelis, F.; Bisquert, J.; Wang, P. *Chem. Rev.* **2014**, *10*.1021/cr400606n.
- (23) Chen, X.; Mao, S. S. *Chem. Rev.* **2007**, *107*, 2891.
- (24) Sang, L.; Zhao, Y.; Burda, C. *Chem. Rev.* **2014**, *10*.1021/cr400629p.
- (25) Liu, G.; Yang, H. G.; Pan, J.; Yang, Y. Q.; Lu, G. Q.; Cheng, H.-M. *Chem. Rev.* **2014**, *10*.1021/cr400621z.
- (26) Lopez-Lopez, C.; Colodrero, S.; Raga, S. R.; Lindstrom, H.; Fabregat-Santiago, F.; Bisquert, J.; Miguez, H. *J. Mater. Chem.* **2012**, *22*, 1751.
- (27) Mora-Seró, I.; Bisquert, J. *Nano Lett.* **2003**, *3*, 945.
- (28) Bertoluzzi, L.; Herraiz-Cardona, I.; Gottesman, R.; Zaban, A.; Bisquert, J. *J. Phys. Chem. Lett.* **2014**, *5*, 689.
- (29) Akimov, A. V.; Neukirch, A. J.; Prezhdo, O. V. *Chem. Rev.* **2013**, *113*, 4496.
- (30) Lindstrom, C. D.; Zhu, X. Y. *Chem. Rev.* **2006**, *106*, 4281.
- (31) Boschloo, G.; Hagfeldt, A. *Acc. Chem. Res.* **2009**, *42*, 1819.
- (32) Yu, Z.; Gorlov, M.; Nissfolk, J.; Boschloo, G.; Kloo, L. *J. Phys. Chem. C* **2010**, *114*, 10612.
- (33) Wang, H.; Bell, J.; Desilvestro, J.; Bertoz, M.; Evans, G. *J. Phys. Chem. C* **2007**, *111*, 15125.
- (34) Nakade, S.; Kanzaki, T.; Kubo, W.; Kitamura, T.; Wada, Y.; Yanagida, S. *J. Phys. Chem. B* **2005**, *109*, 3480.
- (35) Paulsson, H.; Kloo, L.; Hagfeldt, A.; Boschloo, G. *J. Electroanal. Chem.* **2006**, *586*, 56.
- (36) Richards, C. E.; Anderson, A. Y.; Martiniani, S.; Law, C.; O'Regan, B. C. *J. Phys. Chem. Lett.* **2012**, *3*, 1980.
- (37) Boschloo, G.; Gibson, E. A.; Hagfeldt, A. *J. Phys. Chem. Lett.* **2011**, *2*, 3016.
- (38) Farnum, B. H.; Ward, W. M.; Meyer, G. *J. Inorg. Chem.* **2013**, *52*, 840.
- (39) Jono, R.; Sumita, M.; Tateyama, Y.; Yamashita, K. *J. Phys. Chem. Lett.* **2012**, *3*, 3581.
- (40) Yanagida, S.; Yu, Y.; Manseki, K. *Acc. Chem. Res.* **2009**, *42*, 1827.
- (41) Cong, J.; Yang, X.; Kloo, L.; Sun, L. *Energy Environ. Sci.* **2012**, *5*, 9180.
- (42) Hamann, T. W.; Ondersma, J. W. *Energy Environ. Sci.* **2011**, *4*, 370.
- (43) Wang, P.; Zakeeruddin, S. M.; Moser, J.-E.; Humphry-Baker, R.; Grätzel, M. *J. Am. Chem. Soc.* **2004**, *126*, 7164.
- (44) Wang, M.; Chamberland, N.; Breau, L.; Moser, J.-E.; Humphry-Baker, R.; Marsan, B.; Zakeeruddin, S. M.; Grätzel, M. *Nat. Chem.* **2010**, *2*, 385.
- (45) Moia, D.; Vaissier, V.; Lopez-Duarte, I.; Torres, T.; Nazeeruddin, M. K.; O'Regan, B. C.; Nelson, J.; Barnes, P. R. F. *Chem. Sci.* **2014**, *5*, 281.
- (46) Knupfer, M. *Appl. Phys. A: Mater. Sci. Process.* **2003**, *77*, 623.
- (47) Verma, S.; Ghosh, H. N. *J. Phys. Chem. Lett.* **2013**, *3*, 1877.
- (48) Zhang, B.; Xu, X.; Zhang, X.; Huang, D.; Li, S.; Zhang, Y.; Zhan, F.; Deng, M.; He, Y.; Chen, W.; Shen, Y.; Wang, M. *ChemPhysChem* **2014**, *15*, 1182.
- (49) Daeneke, T.; Mozer, A. J.; Uemura, Y.; Makuta, S.; Fekete, M.; Tachibana, Y.; Koumura, N.; Bach, U.; Spiccia, L. *J. Am. Chem. Soc.* **2012**, *134*, 16925.
- (50) Xie, Y.; Hamann, T. W. *J. Phys. Chem. Lett.* **2013**, *4*, 328.
- (51) Feldt, S. M.; Wang, G.; Boschloo, G.; Hagfeldt, A. *J. Phys. Chem. C* **2011**, *115*, 21500.
- (52) Lobato, K.; Peter, L. M. *J. Phys. Chem. B* **2006**, *110*, 21920.
- (53) Hagfeldt, A.; Grätzel, M. *Chem. Rev.* **1995**, *95*, 49.
- (54) Koval, C. A.; Howard, J. N. *Chem. Rev.* **1992**, *92*, 411.
- (55) Nayak, P. K.; Garcia-Belmonte, G.; Kahn, A.; Bisquert, J.; Cahen, D. *Energy Environ. Sci.* **2012**, *5*, 6022.
- (56) Zhang, S.; Yang, X.; Zhang, K.; Chen, H.; Yanagida, M.; Han, L. *Phys. Chem. Chem. Phys.* **2011**, *13*, 19310.
- (57) Zhang, Z.; Yates, J. T. *Chem. Rev.* **2012**, *112*, 5520.
- (58) Kamat, P. V.; Tvrdy, K.; Baker, D. R.; Radich, J. G. *Chem. Rev.* **2010**, *110*, 6664.
- (59) Kubacka, A.; Fernández-García, M.; Colón, G. *Chem. Rev.* **2012**, *112*, 1555.
- (60) Daeneke, T.; Kwon, T.-H.; Holmes, A. B.; Duffy, N. W.; Bach, U.; Spiccia, L. *Nat. Chem.* **2010**, *3*, 211.
- (61) Daeneke, T.; Mozer, A. J.; Kwon, T.-H.; Duffy, N. W.; Holmes, A. B.; Bach, U.; Spiccia, L. *Energy Environ. Sci.* **2013**, *5*, 7090.
- (62) Hamann, T. W.; Farha, O. K.; Hupp, J. T. *J. Phys. Chem. C* **2008**, *112*, 19756.
- (63) Hattori, S.; Wada, Y.; Yanagida, S.; Fukuzumi, S. *J. Am. Chem. Soc.* **2005**, *127*, 9648.
- (64) Li, T. C.; Spokoyny, A. M.; She, C.; Farha, O. K.; Mirkin, C. A.; Marks, T. J.; Hupp, J. T. *J. Am. Chem. Soc.* **2010**, *132*, 4580.
- (65) Yella, A.; Lee, H.-W.; Tsao, H. N.; Yi, C.; Chandiran, A. K.; Nazeeruddin, M. K.; Diau, E. W.-G.; Yeh, C.-Y.; Zakeeruddin, S. M.; Grätzel, M. *Science* **2011**, *334*, 629.
- (66) Yum, J.-H.; Baranoff, E.; Kessler, F.; Moehl, T.; Ahmad, S.; Bessho, T.; Marchioro, A.; Ghadiri, E.; Moser, J.-E.; Yi, C.; Nazeeruddin, M. K.; Grätzel, M. *Nat. Commun.* **2012**, *3*, 631.
- (67) Feldt, S. M.; Gibson, E. A.; Gabrielson, E.; Sun, L.; Boschloo, G.; Hagfeldt, A. *J. Am. Chem. Soc.* **2010**, *132*, 16714.
- (68) Chandiran, A. K.; Tetraeault, N.; Humphry-Baker, R.; Kessler, F.; Baranoff, E.; Yi, C.; Nazeeruddin, M. K.; Grätzel, M. *Nano Lett.* **2012**, *12*, 3941.
- (69) Amit Kumar, S.; Urbani, M.; Medel, M.; Ince, M.; González-Rodríguez, D.; Chandiran, A. K.; Bhaskarwar, A. N.; Torres, T.; Nazeeruddin, M. K.; Grätzel, M. *J. Phys. Chem. Lett.* **2014**, *501*.
- (70) Koh, T. M.; Nonomura, K.; Mathews, N.; Hagfeldt, A.; Grätzel, M.; Mhaisalkar, S. G.; Grimsdale, A. C. *J. Phys. Chem. C* **2013**, *117*, 15515.
- (71) Polander, L. E.; Yella, A.; Curchod, B. F. E.; Ashari Astani, N.; Teuscher, J.; Scopelliti, R.; Gao, P.; Mathew, S.; Moser, J.-E.; Tavernelli, I.; Rothlisberger, U.; Grätzel, M.; Nazeeruddin, M. K.; Frey, J. *Angew. Chem., Int. Ed.* **2013**, *52*, 8731.
- (72) Palomaki, P. K. B.; Civic, M. R.; Dinolfo, P. H. *ACS Appl. Mater. Interfaces* **2013**, *5*, 7604.
- (73) Aljarilla, A.; Clifford, J. N.; Pelleja, L.; Moncho, A.; Arrechea, S.; de la Cruz, P.; Langa, F.; Palomares, E. *J. Mater. Chem. A* **2013**, *1*, 13640.
- (74) Barea, E. M.; Bisquert, J. *Langmuir* **2013**, *29*, 8773.
- (75) Pascoe, A. R.; Bourgeois, L.; Duffy, N. W.; Xiang, W.; Cheng, Y.-B. *J. Phys. Chem. C* **2013**, *117*, 25118.
- (76) Ito, S.; Liska, P.; Comte, P.; Charvet, R.; Pechy, P.; Bach, U.; Schmidt-Mende, L.; Zakeeruddin, S. M.; Kay, A.; Nazeeruddin, M. K.; Grätzel, M. *Chem. Commun.* **2005**, 4351.
- (77) Boschloo, G.; Häggman, L.; Hagfeldt, A. *J. Phys. Chem. B* **2006**, *110*, 13144.
- (78) Shi, C.; Dai, S.; Wang, K.; Pan, X.; Kong, F.; Hu, L. *Vib. Spectrosc.* **2005**, *39*, 99.
- (79) Schlichthörl, G.; Huang, S. Y.; Sprague, J.; Frank, A. J. *J. Phys. Chem. B* **1997**, *101*, 8141.
- (80) Hara, K.; Dan-oh, Y.; Kasada, C.; Ohga, Y.; Shinpo, A.; Suga, S.; Sayama, K.; Arakawa, H. *Langmuir* **2004**, *20*, 4205.
- (81) Liu, Y.; Lin, H.; Dy, J. T.; Tamaki, K.; Nakazaki, J.; Nishiyama, C.; Uchida, S.; Segawa, H.; Li, J. *J. Phys. Chem. C* **2014**, *118*, 1426.
- (82) Sun, Z.; Zhang, R.-K.; Xie, H.-H.; Wang, H.; Liang, M.; Xue, S. *J. Phys. Chem. C* **2013**, *117*, 4364.
- (83) Zhang, C.; Huang, Y.; Huo, Z.; Chen, S.; Dai, S. *J. Phys. Chem. C* **2009**, *113*, 21779.
- (84) Kopidakis, N.; Neale, N. R.; Frank, A. J. *J. Phys. Chem. B* **2006**, *110*, 12485.
- (85) Kim, M.-J.; Lee, C.-R.; Jeong, W.-S.; Im, J.-H.; Ryu, T. I.; Park, N.-G. *J. Phys. Chem. C* **2010**, *114*, 19849.
- (86) Neale, N. R.; Kopidakis, N.; van de Lagemaat, J.; Grätzel, M.; Frank, A. J. *J. Phys. Chem. B* **2005**, *109*, 23183.

- (87) Lee, K.-M.; Suryanarayanan, V.; Ho, K.-C.; Justin Thomas, K. R.; Lin, J. T. *Sol. Energy Mater. Sol. Cells* **2007**, *91*, 1426.
- (88) Choi, I. T.; Ju, M. J.; Song, S. H.; Kim, S. G.; Cho, D. W.; Im, C.; Kim, H. K. *Chem.—Eur. J.* **2013**, *19*, 15545.
- (89) Jiang, D.; Hao, Y.; Shen, R.; Ghazarian, S.; Ramos, A.; Zhou, F. *ACS Appl. Mater. Interfaces* **2013**, *5*, 11906.
- (90) Kumar, A.; Madaria, A. R.; Zhou, C. *J. Phys. Chem. C* **2010**, *114*, 7787.
- (91) Guo, W.; Xu, C.; Wang, X.; Wang, S.; Pan, C.; Lin, C.; Wang, Z. *L. J. Am. Chem. Soc.* **2012**, *134*, 4437.
- (92) Zheng, Q.; Kang, H.; Yun, J.; Lee, J.; Park, J. H.; Baik, S. *ACS Nano* **2011**, *5*, 5088.
- (93) Dong, C.; Li, X.; Zhao, W.; Jin, P.; Fan, X.; Qi, J. *Chem.—Eur. J.* **2013**, *19*, 10046.
- (94) Wang, X.; Li, Z.; Shi, J.; Yu, Y. *Chem. Rev.* **2014**, *10*, 10121/cr400633s.
- (95) Chang, S.; Wang, H.; Hua, Y.; Li, Q.; Xiao, X.; Wong, W.-K.; Wong, W. Y.; Zhu, X.; Chen, T. *J. Mater. Chem. A* **2013**, *1*, 11553.
- (96) Brennan, T. P.; Tanskanen, J. T.; Bakke, J. R.; Nguyen, W. H.; Nordlund, D.; Toney, M. F.; McGehee, M. D.; Sellinger, A.; Bent, S. F. *Chem. Mater.* **2013**, *25*, 4354.
- (97) Jiao, Y.; Zhang, F.; Grätzel, M.; Meng, S. *Adv. Funct. Mater.* **2013**, *23*, 424.
- (98) Thompson, D. W.; Kelly, C. A.; Farzad, F.; Meyer, G. J. *Langmuir* **1999**, *15*, 650.
- (99) Wang, P.; Wenger, B.; Humphry-Baker, R.; Moser, J.-E.; Teuscher, J. I.; Kantlehner, W.; Mezger, J.; Stoyanov, E. V.; Zakeeruddin, S. M.; Grätzel, M. *J. Am. Chem. Soc.* **2005**, *127*, 6850.
- (100) Splan, K. E.; Massari, A. M.; Hupp, J. T. *J. Phys. Chem. B* **2004**, *108*, 4111.
- (101) Gardner, J. M.; Giaimuccio, J. M.; Meyer, G. J. *J. Am. Chem. Soc.* **2008**, *130*, 17252.
- (102) O'Regan, B. C.; López-Duarte, I.; Martínez-Díaz, M. V.; Forneli, A.; Albero, J.; Morandeira, A.; Palomares, E.; Torres, T.; Durrant, J. R. *J. Am. Chem. Soc.* **2008**, *130*, 2906.
- (103) Fox, M. A. *Acc. Chem. Res.* **2012**, *45*, 1875.
- (104) Abramavicius, D.; Palmieri, B.; Voronine, D. V.; František, Š.; Mukamel, S. *Chem. Rev.* **2009**, *109*, 2350.
- (105) Ren, X.-F.; Ren, A.-M.; Feng, J.-K.; Zhou, X. *Org. Electron.* **2010**, *11*, 979.
- (106) Drain, C. M.; Varotto, A.; Radivojevic, I. *Chem. Rev.* **2009**, *109*, 1630.
- (107) Harvey, P. D. Recent Advances in Free and Metalated Multi-Porphyrin Assemblies and Arrays. A Photophysical behaviour and Energy Transfer Perspective. In *The Porphyrin Handbook: Multi-porphyrins, Multiphthalocyanines, and Arrays*; Kadish, K. M., Smith, K. M., Guilard, R., Eds.; Academic press, Elsevier Science: San Diego, CA, 2003; Vol 18, p 63.
- (108) Maiti, N. C.; Mazumdar, S.; Periasamy, N. *J. Phys. Chem. B* **1998**, *102*, 1528.
- (109) Arai, Y.; Tsuzuki, K.; Segawa, H. *Phys. Chem. Phys. Chem.* **2011**, *14*, 1270.
- (110) Andrade, S. M.; Teixeira, R.; Costa, S. M. B.; Sobral, A. J. F. N. *Biophys. Chem.* **2008**, *133*, 1.
- (111) Li, X.; Zhang, L.; Mu, J. *Colloids Surf., A* **2007**, *311*, 187.
- (112) Luo, L.; Lo, C.-F.; Lin, C.-Y.; Chang, I. J.; Diau, E. W.-G. *J. Phys. Chem. B* **2005**, *110*, 410.
- (113) Hosomizu, K.; Oodoi, M.; Umeyama, T.; Matano, Y.; Yoshida, K.; Isoda, S.; Isosomppi, M.; Tkachenko, N. V.; Lemmetyinen, H.; Imahori, H. *J. Phys. Chem. B* **2008**, *112*, 16517.
- (114) Verma, S.; Ghosh, A.; Das, A.; Ghosh, H. N. *J. Phys. Chem. B* **2010**, *114*, 8327.
- (115) Marek, P. L.; Hahn, H.; Balaban, T. S. *Energy Environ. Sci.* **2011**, *4*, 2366.
- (116) Venkatraman, V.; Åstrand, P.-O.; Kåre Alsberg, B. *J. Comput. Chem.* **2014**, *35*, 214.
- (117) Ambrosio, F.; Martsinovich, N.; Troisi, A. *J. Phys. Chem. Lett.* **2012**, *3*, 1531.
- (118) Zhu, K.; Jang, S.-R.; Frank, A. J. *J. Phys. Chem. Lett.* **2011**, *2*, 1070.
- (119) Nazeeruddin, M. K.; Kay, A.; Rodicio, I.; Humphry-Baker, R.; Mueller, E.; Liska, P.; Vlachopoulos, N.; Grätzel, M. *J. Am. Chem. Soc.* **1993**, *115*, 6382.
- (120) Lan, J.-L.; Wei, T.-C.; Feng, S.-P.; Wan, C.-C.; Cao, G. *J. Phys. Chem. C* **2012**, *116*, 25727.
- (121) Ladomenou, K.; Kitsopoulos, T. N.; Sharma, G. D.; Coutsolelos, A. G. *RSC Adv.* **2014**, *4*, 21379.
- (122) Kay, A.; Grätzel, M. *J. Phys. Chem.* **1993**, *97*, 6272.
- (123) Nazeeruddin, M. K.; Humphry-Baker, R.; Officer, D. L.; Campbell, W. M.; Burrell, A. K.; Grätzel, M. *Langmuir* **2004**, *20*, 6514.
- (124) Wang, Q.; Campbell, W. M.; Bonfantani, E. E.; Jolley, K. W.; Officer, D. L.; Walsh, P. J.; Gordon, K.; Humphry-Baker, R.; Nazeeruddin, M. K.; Grätzel, M. *J. Phys. Chem. B* **2005**, *109*, 15397.
- (125) Campbell, W. M.; Jolley, K. W.; Wagner, P.; Wagner, K.; Walsh, P. J.; Gordon, K. C.; Schmidt-Mende, L.; Nazeeruddin, M. K.; Wang, Q.; Grätzel, M.; Officer, D. L. *J. Phys. Chem. C* **2007**, *111*, 11760.
- (126) Ishida, M.; Park, S. W.; Hwang, D.; Koo, Y. B.; Sessler, J. L.; Kim, D. Y.; Kim, D. *J. Phys. Chem. C* **2011**, *115*, 19343.
- (127) Park, J. K.; Lee, H. R.; Chen, J.; Shinokubo, H.; Osuka, A.; Kim, D. *J. Phys. Chem. C* **2008**, *112*, 16691.
- (128) Mai, C.-L.; Huang, W.-K.; Lu, H.-P.; Lee, C.-W.; Chiu, C.-L.; Liang, Y.-R.; Diau, E. W.-G.; Yeh, C.-Y. *Chem. Commun.* **2010**, *46*, 809.
- (129) Liu, Y.; Lin, H.; Li, J.; Dy, J. T.; Tamaki, K.; Nakazaki, J.; Nakayama, D.; Nishiyama, C.; Uchida, S.; Kubo, T.; Segawa, H. *Phys. Chem. Chem. Phys.* **2012**, *14*, 16703.
- (130) Wu, H.-P.; Ou, Z.-W.; Pan, T.-Y.; Lan, C.-M.; Huang, W.-K.; Lee, H.-W.; Reddy, N. M.; Chen, C.-T.; Chao, W.-S.; Yeh, C.-Y.; Diau, E. W.-G. *Energy Environ. Sci.* **2012**, *5*, 9843.
- (131) Zervaki, G. E.; Angaridis, P. A.; Koukaras, E. N.; Sharma, G. D.; Coutsolelos, A. G. *Inorg. Chem. Front.* **2014**, *1*, 256.
- (132) Luechai, A.; Pootrakulchote, N.; Kengthanomma, T.; Vanalabhpata, P.; Thamyongkit, P. *J. Organomet. Chem.* **2014**, *753*, 27.
- (133) Zhang, X.; Zhu, Y.; Wu, X.; He, H.; Wang, G.; Li, Q. *Res. Chem. Intermed.* **2014**, *1*.
- (134) Hamamura, T.; Dy, J. T.; Tamaki, K.; Nakazaki, J.; Uchida, S.; Kubo, T.; Segawa, H. *Phys. Chem. Phys. Chem.* **2014**, *16*, 4551.
- (135) Liu, Y.; Lin, H.; Dy, J. T.; Tamaki, K.; Nakazaki, J.; Nakayama, D.; Uchida, S.; Kubo, T.; Segawa, H. *Chem. Commun.* **2011**, *47*, 4010.
- (136) Zervaki, G. E.; Papastamatakis, E.; Angaridis, P. A.; Nikolaou, V.; Singh, M.; Kurchania, R.; Kitsopoulos, T. N.; Sharma, G. D.; Coutsolelos, A. G. *Eur. J. Inorg. Chem.* **2014**, *2014*, 1020.
- (137) Lewtak, J. P.; Gryko, D. T. *Chem. Commun.* **2012**, *48*, 10069.
- (138) Hayashi, S.; Tanaka, M.; Hayashi, H.; Eu, S.; Umeyama, T.; Matano, Y.; Araki, Y.; Imahori, H. *J. Phys. Chem. C* **2008**, *112*, 15576.
- (139) Ball, J. M.; Davis, N. K. S.; Wilkinson, J. D.; Kirkpatrick, J.; Teuscher, J.; Gunning, R.; Anderson, H. L.; Snaith, H. J. *RSC Adv.* **2012**, *2*, 6846.
- (140) Davis, N. K. S.; Thompson, A. L.; Anderson, H. L. *Org. Lett.* **2010**, *12*, 2124.
- (141) Davis, N. K. S.; Pawlicki, M. o.; Anderson, H. L. *Org. Lett.* **2008**, *10*, 3945.
- (142) Davis, N. K. S.; Thompson, A. L.; Anderson, H. L. *J. Am. Chem. Soc.* **2011**, *133*, 30.
- (143) Jiao, C.; Zu, N.; Huang, K.-W.; Wang, P.; Wu, J. *Org. Lett.* **2011**, *13*, 3652.
- (144) Eu, S.; Hayashi, S.; Umeyama, T.; Matano, Y.; Araki, Y.; Imahori, H. *J. Phys. Chem. C* **2008**, *112*, 4396.
- (145) Kira, A.; Matsubara, Y.; Iijima, H.; Umeyama, T.; Matano, Y.; Ito, S.; Niemi, M.; Tkachenko, N. V.; Lemmetyinen, H.; Imahori, H. *J. Phys. Chem. C* **2010**, *114*, 11293.
- (146) Hayashi, H.; Touchy, A. S.; Kinjo, Y.; Kurotobi, K.; Toude, Y.; Ito, S.; Saarenpää, H.; Tkachenko, N. V.; Lemmetyinen, H.; Imahori, H. *ChemSusChem* **2013**, *6*, 508.
- (147) Ouyang, Q.; Zhu, Y.-Z.; Zhang, C.-H.; Yan, K.-Q.; Li, Y.-C.; Zheng, J.-Y. *Org. Lett.* **2009**, *11*, 5266.

- (148) Li, L.-L.; Diau, E. W.-G. *Chem. Soc. Rev.* **2013**, *42*, 291.
- (149) Diau, E. W.-G.; Li, L.-L. Porphyrin-Sensitized Solar Cells. In *Handbook of Porphyrin Science*; Kadish, K. M., Smith, K. M., Guilard, R., Eds.; World Scientific Publishing Company: Singapore, 2013; Vol 28, p 279.
- (150) Yeh, C.-Y.; Lin, C.-Y.; Diau, E. W.-G. Push-Pull Porphyrins for Efficient Dye-Sensitized Solar Cells. In *Multiporphyrin Arrays Fundamentals and Applications*; Dongho, K., Ed. Pan Stanford Publishing: Boca Raton, FL, 2012; p 701.
- (151) Martinez-Diaz, M. V.; de la Torre, G.; Torres, T. *Chem. Commun.* **2010**, *46*, 7090.
- (152) Campbell, W. M.; Burrell, A. K.; Officer, D. L.; Jolley, K. W. *Coord. Chem. Rev.* **2004**, *248*, 1363.
- (153) Walter, M. G.; Rudine, A. B.; Wamser, C. C. *J. Porphyrins Phthalocyanines* **2010**, *14*, 759.
- (154) Panda, M. K.; Ladomenou, K.; Coutsolelos, A. G. *Coord. Chem. Rev.* **2012**, *256*, 2601.
- (155) Imahori, H. *Key Eng. Mater.* **2011**, *451*, 29.
- (156) Imahori, H.; Kurotobi, K.; Walter, G. M.; Rudine, B. A.; Wamser, C. C. 80 Porphyrin- and Phthalocyanine-Based Solar Cells. In *Handbook of Porphyrin Science*; Kadish, K. M., Smith, K. M., Guilard, R., Eds.; World Scientific Publishing Company: Singapore, 2012; Vol 18, p 57.
- (157) Li, X.; Wang, H.; Wu, H. Phthalocyanines and Their Analogs Applied in Dye-Sensitized Solar Cell. In *Functional Phthalocyanine Molecular Materials*; Jiang, J., Ed.; Springer-Verlag: Berlin, 2010; Vol 135, p 229.
- (158) Giribabu, L.; Kanaparthi, R. K. *Curr. Sci.* **2013**, *104*, 847.
- (159) Mathew, S.; Yella, A.; Gao, P.; Humphry-Baker, R.; Curchod, B. F. E.; Ashari-Astani, N.; Tavernelli, I.; Rothlisberger, U.; Nazeeruddin, M. K.; Grätzel, M. *Nat. Chem.* **2014**, *6*, 242.
- (160) Griffith, M. J.; Sunahara, K.; Wagner, P.; Wagner, K.; Wallace, G. G.; Officer, D. L.; Furube, A.; Katoh, R.; Mori, S.; Mozer, A. J. *Chem. Commun.* **2012**, *48*, 4145.
- (161) Brennan, B. J.; Llansola Portoles, M. J.; Liddell, P. A.; Moore, T. A.; Moore, A. L.; Gust, D. *Phys. Chem. Phys. Chem.* **2013**, *15*, 16605.
- (162) Di Carlo, G.; OrbelliBiroli, A.; Pizzotti, M.; Tessore, F.; Trifiletti, V.; Ruffo, R.; Abbotto, A.; Amat, A.; De Angelis, F.; Mussini, P. R. *Chem.—Eur. J.* **2013**, *19*, 10723.
- (163) Ishida, M.; Hwang, D.; Koo, Y. B.; Sung, J.; Kim, D. Y.; Sessler, J. L.; Kim, D. *Chem. Commun.* **2013**, *49*, 9164.
- (164) Zeng, Z.; Zhang, B.; Li, C.; Peng, X.; Liu, X.; Meng, S.; Feng, Y. *Dyes Pigm.* **2014**, *100*, 278.
- (165) Imahori, H.; Umeyama, T.; Ito, S. *Acc. Chem. Res.* **2009**, *42*, 1809.
- (166) Ma, R.; Guo, P.; Cui, H.; Zhang, X.; Nazeeruddin, M. K.; Grätzel, M. *J. Phys. Chem. A* **2009**, *113*, 10119.
- (167) Ma, R.; Guo, P.; Yang, L.; Guo, L.; Zhang, X.; Nazeeruddin, M. K.; Grätzel, M. *J. Phys. Chem. A* **2010**, *114*, 1973.
- (168) Gobeze, H. B.; Das, S. K.; D'Souza, F. *J. Phys. Chem. C* **2014**, *118*, 16660.
- (169) Liu, J.; Yang, X.; Sun, L. *Chem. Commun.* **2014**, *49*, 11785.
- (170) Brumbach, M. T.; Boal, A. K.; Wheeler, D. R. *Langmuir* **2009**, *25*, 10685.
- (171) Lindsey, J. S. *Acc. Chem. Res.* **2009**, *43*, 300.
- (172) Dos Santos, T.; Morandeira, A.; Koops, S.; Mozer, A. J.; Tsekouras, G.; Dong, Y.; Wagner, P.; Wallace, G.; Earles, J. C.; Gordon, K. C.; Officer, D.; Durrant, J. R. *J. Phys. Chem. C* **2010**, *114*, 3276.
- (173) Ju, M.-G.; Liang, W. *J. Phys. Chem. C* **2013**, *117*, 14899.
- (174) Karthikeyan, S.; Lee, J. Y. *J. Phys. Chem. A* **2013**, *117*, 10973.
- (175) Santhanamoorthi, N.; Lo, C.-M.; Jiang, J.-C. *J. Phys. Chem. Lett.* **2013**, *4*, 524.
- (176) Guo, M.; He, R.; Dai, Y.; Shen, W.; Li, M.; Zhu, C.; Lin, S. H. *J. Phys. Chem. C* **2012**, *116*, 9166.
- (177) Zhang, X.; Chen, Q.; Sun, H.; Pan, T.; Hu, G.; Ma, R.; Dou, J.; Li, D.; Pan, X. *Spectrochim. Acta, Part A* **2014**, *118*, 564.
- (178) Li, Y.-c.; Feng, Y.-q.; Wang, Y.-t.; Fan, C.-c.; Liu, X.-j.; Li, X.-g.; Zhang, B. *Int. J. Quantum Chem.* **2014**, *114*, 222.
- (179) Ramakrishna, G.; Verma, S.; Jose, D. A.; Kumar, D. K.; Das, A.; Palit, D. K.; Ghosh, H. N. *J. Phys. Chem. B* **2006**, *110*, 9012.
- (180) Ooyama, Y.; Yamada, T.; Fujita, T.; Harima, Y.; Ohshita, J. *J. Mater. Chem. A* **2014**, *2*, 8500.
- (181) Mao, J.; He, N.; Ning, Z.; Zhang, Q.; Guo, F.; Chen, L.; Wu, W.; Hua, J.; Tian, H. *Angew. Chem., Int. Ed.* **2012**, *51*, 9873.
- (182) Gou, F.; Jiang, X.; Li, B.; Jing, H.; Zhu, Z. *ACS Appl. Mater. Interfaces* **2013**, *5*, 12631.
- (183) Barozzino Consiglio, G.; Pedna, F.; Fornaciari, C.; Fabrizi de Biani, F.; Marotta, G.; Salvatori, P.; Basosi, R.; De Angelis, F.; Mordini, A.; Parisi, M. L.; Peruzzini, M.; Reginato, G.; Taddei, M.; Zani, L. *J. Organomet. Chem.* **2013**, *723*, 198.
- (184) Massin, J.; Ducasse, L.; Toupane, T.; Olivier, C. *J. Phys. Chem. C* **2014**, *118*, 10677.
- (185) Ooyama, Y.; Inoue, S.; Nagano, T.; Kushimoto, K.; Ohshita, J.; Imae, I.; Komaguchi, K.; Harima, Y. *Angew. Chem., Int. Ed.* **2011**, *50*, 7429.
- (186) Ooyama, Y.; Yamaguchi, N.; Imae, I.; Komaguchi, K.; Ohshita, J.; Harima, Y. *Chem. Commun.* **2013**, *49*, 2548.
- (187) Shibayama, N.; Ozawa, H.; Abe, M.; Ooyama, Y.; Arakawa, H. *Chem. Commun.* **2014**, *50*, 6398.
- (188) Cui, J.; Lu, J.; Xu, X.; Cao, K.; Wang, Z.; Alemu, G.; Yuang, H.; Shen, Y.; Xu, J.; Cheng, Y.; Wang, M. *J. Phys. Chem. C* **2014**, *118*, 16433.
- (189) Angaridis, P. A.; Lazarides, T.; Coutsolelos, A. C. *Polyhedron* **2014**, *82*, 19.
- (190) Daphnomili, D.; Landrou, G.; Prakash Singh, S.; Thomas, A.; Yesudas, K.; K, B.; Sharma, G. D.; Coutsolelos, A. G. *RSC Adv.* **2012**, *2*, 12899.
- (191) Daphnomili, D.; Sharma, G. D.; Biswas, S.; Justin Thomas, K. R.; Coutsolelos, A. G. *J. Photochem. Photobiol. A* **2013**, *253*, 88.
- (192) Ooyama, Y.; Hagiwara, Y.; Mizumo, T.; Harima, Y.; Ohshita, J. *New. J. Chem.* **2013**, *37*, 2479.
- (193) Lu, J.; Xu, X.; Li, Z.; Cao, K.; Cui, J.; Zhang, Y.; Shen, Y.; Li, Y.; Zhu, J.; Dai, S.; Chen, W.; Cheng, Y.; Wang, M. *Chem.—Asian J.* **2013**, *8*, 956.
- (194) Jin, B.; Wu, W.; Zhang, X.; Guo, F.; Zhang, Q.; Hua, J. *Chem. Lett.* **2013**, *42*, 1271.
- (195) Delcamp, J. H.; Yella, A.; Nazeeruddin, M. K.; Grätzel, M. *Chem. Commun.* **2012**, *48*, 2295.
- (196) Franchi, D.; Calamante, M.; Reginato, G.; Zani, L.; Peruzzini, M.; Taddei, M.; Fabrizi de Biani, F.; Basosi, R.; Sinicropi, A.; Colonna, D.; Di Carlo, A.; Mordini, A. *Tetrahedron* **2014**.
- (197) Mao, J.; Wang, D.; Liu, S.-H.; Hang, Y.; Xu, Y.; Zhang, Q.; Wu, W.; Chou, P.-T.; Hua, J. *Asian J. Org. Chem.* **2013**, *3*, 153.
- (198) Wang, L.; Yang, X.; Li, S.; Cheng, M.; Sun, L. *RSC Adv.* **2013**, *3*, 13677.
- (199) Cecconi, B.; Mordini, A.; Reginato, G.; Zani, L.; Taddei, M.; Fabrizi de Biani, F.; Angelis, F. D.; Marotta, G.; Salvatori, P.; Calamante, M. *Asian J. Org. Chem.* **2014**, *3*, 140.
- (200) He, H.; Gurung, A.; Si, L. *Chem. Commun.* **2012**, *48*, 5910.
- (201) Jin, X.; Yu, X.; Zhang, W.; Zhou, J.; Tang, G.; Zhong, C. *Polym. Compos.* **2013**, *34*, 1629.
- (202) Ooyama, Y.; Sato, T.; Harima, Y.; Ohshita, J. *J. Mater. Chem. A* **2014**, *2*, 3293.
- (203) Breivogel, A.; Wooh, S.; Dietrich, J.; Kim, T. Y.; Kang, Y. S.; Char, K.; Heinze, K. *Eur. J. Inorg. Chem.* **2014**, *2014*, 2720.
- (204) Verbitskiy, E. V.; Cheprakova, E. M.; Subbotina, J. O.; Schepochkin, A. V.; Slepukhin, P. A.; Rusinov, G. L.; Charushin, V. N.; Chupakhin, O. N.; Makarova, N. I.; Metelitsa, A. V.; Minkin, V. I. *Dyes Pigm.* **2014**, *100*, 201.
- (205) Ma, T.; Inoue, K.; Noma, H.; Yao, K.; Abe, E. *J. Photochem. Photobiol. A* **2002**, *152*, 207.
- (206) Kalyanasundaram, K.; Grätzel, M. *Coord. Chem. Rev.* **1998**, *77*, 347.
- (207) Jasieniak, J.; Johnston, M.; Waclawik, E. R. *J. Phys. Chem. B* **2004**, *108*, 12962.
- (208) Cherian, S.; Wamser, C. C. *J. Phys. Chem. B* **2000**, *104*, 3624.

- (209) Pechy, P.; Rotzinger, F. P.; Nazeeruddin, M. K.; Kohle, O.; Zakeeruddin, S. M.; Humphry-Baker, R.; Grätzel, M. *J. Chem. Soc., Chem. Commun.* **1995**, 65.
- (210) Lopez-Duarte, I.; Wang, M.; Humphry-Baker, R.; Ince, M.; Martinez-Diaz, M. V.; Nazeeruddin, M. K.; Torres, T.; Grätzel, M. *Angew. Chem., Int. Ed. Engl.* **2012**, 51, 1895.
- (211) Odobel, F.; Blart, E.; Lagrée, M.; Villieras, M.; Boujtita, H.; El Murr, N.; Caramori, S.; Bignozzi, C. A. *J. Mater. Chem.* **2003**, 13, 502.
- (212) Boschloo, G. K.; Goossens, A. *J. Phys. Chem.* **1996**, 100, 19489.
- (213) Rochford, J.; Chu, D.; Hagfeldt, A.; Galoppini, E. *J. Am. Chem. Soc.* **2007**, 129, 4655.
- (214) Rangan, S.; Coh, S.; Bartynski, R. A.; Chitre, K. P.; Galoppini, E.; Jaye, C.; Fischer, D. *J. Phys. Chem. C* **2012**, 116, 23921.
- (215) de Tacconi, N. R.; Chanmanee, W.; Rajeshwar, K.; Rochford, J.; Galoppini, E. *J. Phys. Chem. C* **2009**, 113, 2996.
- (216) Imahori, H.; Hayashi, S.; Hayashi, H.; Oguro, A.; Eu, S.; Umeyama, T.; Matano, Y. *J. Phys. Chem. C* **2009**, 113, 18406.
- (217) 5-(4-Carboxyphenyl)-10,15,20-tris(2,4,6-trimethylphenyl) porphyrinatozinc(II) sensitizer has been extensively reported and studied in DSSCs by the same authors and others, and have received diverse names "ZnP", "Zn-1", or "Zn-3": see ref 165 and refs 218–222 below.
- (218) Imahori, H.; Hayashi, S.; Umeyama, T.; Eu, S.; Oguro, A.; Kang, S.; Matano, Y.; Shishido, T.; Ngamsinlapasathian, S.; Yoshikawa, S. *Langmuir* **2006**, 22, 11405.
- (219) Watson, D. F.; Marton, A.; Stux, A. M.; Meyer, G. *J. J. Phys. Chem. B* **2003**, 107, 10971.
- (220) Watson, D. F.; Marton, A.; Stux, A. M.; Meyer, G. *J. J. Phys. Chem. B* **2004**, 108, 11680.
- (221) Hayashi, S.; Tanaka, M.; Hayashi, H.; Eu, S.; Umeyama, T.; Matano, Y.; Araki, Y.; Imahori, H. *J. Phys. Chem. C* **2008**, 112, 15576.
- (222) Tanaka, M.; Hayashi, S.; Eu, S.; Umeyama, T.; Matano, Y.; Imahori, H. *Chem. Commun.* **2007**, 2069.
- (223) Hart, A. S.; Kc, C. B.; Gobezie, H. B.; Sequeira, L. R.; D'Souza, F. *ACS Appl. Mater. Interfaces* **2013**, 5, 5314.
- (224) Bertoluzzi, L.; Boix, P. P.; Mora-Sero, I.; Bisquert, J. *J. Phys. Chem. C* **2014**, 118, 16574.
- (225) Bisquert, J. *J. Phys. Chem. B* **2002**, 106, 325.
- (226) Fabregat-Santiago, F.; Bisquert, J.; Palomares, E.; Otero, L.; Kuang, D.; Zakeeruddin, S. M.; Grätzel, M. *J. Phys. Chem. C* **2007**, 111, 6550.
- (227) Wang, Q.; Moser, J.-E.; Grätzel, M. *J. Phys. Chem. B* **2005**, 109, 14945.
- (228) Fabregat-Santiago, F.; Bisquert, J.; Garcia-Belmonte, G.; Boschloo, G.; Hagfeldt, A. *Sol. Energy Mater. Sol. Cells* **2005**, 87, 117.
- (229) Ye, S.; Kathiravan, A.; Hayashi, H.; Tong, Y.; Infahsaeng, Y.; Chabera, P.; Pascher, T.; Yartsev, A. P.; Isoda, S.; Imahori, H.; Sundström, V. *J. Phys. Chem. C* **2013**, 117, 6066.
- (230) Xue, X.; Zhang, W.; Zhang, N.; Ju, C.; Peng, X.; Yang, Y.; Liang, Y.; Feng, Y.; Zhang, B. *RSC Adv.* **2014**, 4, 8894.
- (231) Namuangruk, S.; Sirithip, K.; Rattanatwan, R.; Keawin, T.; Kungwan, N.; Sudyodsuk, T.; Promarak, V.; Surakhot, Y.; Jungsuttiwong, S. *Dalton Trans.* **2014**, 43, 9166.
- (232) Liu, Y.; Xiang, N.; Feng, X.; Shen, P.; Zhou, W.; Weng, C.; Zhao, B.; Tan, S. *Chem. Commun.* **2009**, 2499.
- (233) Xiang, N.; Zhou, W.; Jiang, S.; Deng, L.; Liu, Y.; Tan, Z.; Zhao, B.; Shen, P.; Tan, S. *Sol. Energy Mater. Sol. Cells* **2011**, 95, 1174.
- (234) Griffith, M. J.; Sunahara, K.; Furube, A.; Mozer, A. J.; Officer, D. L.; Wagner, P.; Wallace, G. G.; Mori, S. *J. Phys. Chem. C* **2013**, 117, 11885.
- (235) Wagner, K.; Griffith, M. J.; James, M.; Mozer, A. J.; Wagner, P.; Triani, G.; Officer, D. L.; Wallace, G. G. *J. Phys. Chem. C* **2011**, 115, 317.
- (236) Wang, Q.; Zhang, Z.; Zakeeruddin, S. M.; Grätzel, M. *J. Phys. Chem. C* **2008**, 112, 7084.
- (237) Lin, V. S.; DiMagno, S. G.; Therien, M. J. *Science* **1994**, 264, 1105.
- (238) Ragoussi, M.-E.; de la Torre, G.; Torres, T. *Eur. J. Org. Chem.* **2013**, 2013, 2832.
- (239) Stromberg, J. R.; Marton, A.; Kee, H. L.; Kirmaier, C.; Diers, J. R.; Muthiah, C.; Taniguchi, M.; Lindsey, J. S.; Bocian, D. F.; Meyer, G. J.; Holten, D. *J. Phys. Chem. C* **2007**, 111, 15464.
- (240) Rangan, S.; Katalinic, S.; Thorpe, R.; Bartynski, R. A.; Rochford, J.; Galoppini, E. *J. Phys. Chem. C* **2010**, 114, 1139.
- (241) Lee, C.-W.; Lu, H.-P.; Lan, C.-M.; Huang, Y.-L.; Liang, Y.-R.; Yen, W.-N.; Liu, Y.-C.; Lin, Y.-S.; Diau, E. W.-G.; Yeh, C.-Y. *Chem.–Eur. J.* **2009**, 15, 1403.
- (242) He, H.; Gurung, A.; Si, L.; Sykes, A. G. *Chem. Commun.* **2012**, 48, 7619.
- (243) Gou, F.; Jiang, X.; Fang, R.; Jing, H.; Zhu, Z. *ACS Appl. Mater. Interfaces* **2014**, 6, 6697.
- (244) Lin, C.-Y.; Lo, C.-F.; Luo, L.; Lu, H.-P.; Hung, C.-S.; Diau, E. W.-G. *J. Phys. Chem. C* **2009**, 113, 755.
- (245) Lo, C.-F.; Luo, L.; Diau, E. W.-G.; Chang, I. J.; Lin, C.-Y. *Chem. Commun.* **2006**, 1430.
- (246) Guo, M.; Li, M.; Dai, Y.; Shen, W.; Peng, J.; Zhu, C.; Lin, S. H.; He, R. *RSC Adv.* **2013**, 3, 17515.
- (247) Gundlach, L.; Ernstorfer, R.; Willig, F. *J. Phys. Chem. C* **2007**, 111, 13586.
- (248) Vail, S. A.; Krawczuk, P. J.; Guldii, D. M.; Palkar, A.; Echegoyen, L.; Tomé, J. P. C.; Fazio, M. A.; Schuster, D. I. *Chem.–Eur. J.* **2005**, 11, 3375.
- (249) Tachibana, Y.; Haque, S. A.; Mercer, I. P.; Durrant, J. R.; Klug, D. R. *J. Phys. Chem. B* **2000**, 104, 1198.
- (250) Clark, C. C.; Meyer, G. J.; Wei, Q.; Galoppini, E. *J. Phys. Chem. B* **2006**, 110, 11044.
- (251) Abrahamsson, M.; Johansson, P. G.; Ardo, S.; Kopecky, A.; Galoppini, E.; Meyer, G. *J. J. Phys. Chem. Lett.* **2010**, 1, 1725.
- (252) Lin, C.-Y.; Wang, Y.-C.; Hsu, S.-J.; Lo, C.-F.; Diau, E. W.-G. *J. Phys. Chem. C* **2010**, 114, 687.
- (253) Boyle, N. M.; Rochford, J.; Pryce, M. T. *Coord. Chem. Rev.* **2010**, 254, 77.
- (254) Zhou, W.; Zhao, B.; Shen, P.; Jiang, S.; Huang, H.; Deng, L.; Tan, S. *Dyes Pigm.* **2011**, 91, 404.
- (255) Eu, S.; Hayashi, S.; Umeyama, T.; Oguro, A.; Kawasaki, M.; Kadota, N.; Matano, Y.; Imahori, H. *J. Phys. Chem. C* **2007**, 111, 3528.
- (256) Rao, P. D.; Dhanalekshmi, S.; Littler, B. J.; Lindsey, J. S. *J. Org. Chem.* **2000**, 65, 7323.
- (257) Lee, C. Y.; She, C.; Jeong, N. C.; Hupp, J. T. *Chem. Commun.* **2010**, 46, 6090.
- (258) Panda, M. K.; Sharma, G. D.; Thomas, K. R. J.; Coutsolelos, A. G. *J. Mater. Chem.* **2012**, 22, 8092.
- (259) Werner, F.; Gnichwitz, J.-F.; Marczak, R.; Palomares, E.; Peukert, W.; Hirsch, A.; Guldii, D. M. *J. Phys. Chem. B* **2010**, 114, 14671.
- (260) Ambre, R.; Chen, K.-B.; Yao, C.-F.; Luo, L.; Diau, E. W.-G.; Hung, C.-H. *J. Phys. Chem. C* **2012**, 116, 11907.
- (261) Warnan, J.; Buchet, F.; Pellegrin, Y.; Blart, E.; Odobel, F. *Org. Lett.* **2011**, 13, 3944.
- (262) Khan, T. K.; Bröring, M.; Mathur, S.; Ravikanth, M. *Coord. Chem. Rev.* **2013**, 257, 2348.
- (263) Pasunooti, K. K.; Song, J.-L.; Chai, H.; Amaladass, P.; Deng, W.-Q.; Liu, X.-W. *J. Photochem. Photobiol., A* **2011**, 218, 219.
- (264) Liang, M.; Chen, J. *Chem. Soc. Rev.* **2013**, 42, 3453.
- (265) Jiang, X.; Karlsson, K. M.; Gabrielsson, E.; Johansson, E. M. J.; Quintana, M.; Karlsson, M.; Sun, L.; Boschloo, G.; Hagfeldt, A. *Adv. Funct. Mater.* **2011**, 21, 2944.
- (266) Liang, M.; Xu, W.; Cai, F.; Chen, P.; Peng, B.; Chen, J.; Li, Z. *J. Phys. Chem. C* **2007**, 111, 4465.
- (267) Seo, K. D.; Lee, M. J.; Song, H. M.; Kang, H. S.; Kim, H. K. *Dyes Pigm.* **2011**, 94, 143.
- (268) Lee, M. J.; Seo, K. D.; Song, H. M.; Kang, M. S.; Eom, Y. K.; Kang, H. S.; Kim, H. K. *Tetrahedron Lett.* **2011**, 52, 3879.
- (269) Kang, M. S.; Kang, S. H.; Kim, S. G.; Choi, I. T.; Ryu, J. H.; Ju, M. J.; Cho, D.; Lee, J. Y.; Kim, H. K. *Chem. Commun.* **2012**, 48, 9349.
- (270) Choi, I. T.; Ju, M. J.; Kang, S. H.; Kang, M. S.; You, B. S.; Hong, J. Y.; Eom, Y. K.; Song, S. H.; Kim, H. K. *J. Mater. Chem. A* **2013**, 1, 9114.

- (271) Kang, S. H.; Kang, M. S.; Choi, I. T.; Hong, J. Y.; Ju, M. J.; Kim, H. K. *ChemElectroChem* **2014**, *1*, 637.
- (272) Kang, S. H.; Choi, I. T.; Kang, M. S.; Eom, Y. K.; Ju, M. J.; Hong, J. Y.; Kang, H. S.; Kim, H. K. *J. Mater. Chem. A* **2013**, *1*, 3977.
- (273) Kang, M. S.; Choi, I. T.; Kim, Y. W.; You, B. S.; Kang, S. H.; Hong, J. Y.; Ju, M. J.; Kim, H. K. *J. Mater. Chem. A* **2013**, *1*, 9848.
- (274) Imahori, H.; Matsubara, Y.; Iijima, H.; Umeyama, T.; Matano, Y.; Ito, S.; Niemi, M.; Tkachenko, N. V.; Lemmetyinen, H. *J. Phys. Chem. C* **2010**, *114*, 10656.
- (275) Hsieh, C.-P.; Lu, H.-P.; Chiu, C.-L.; Lee, C.-W.; Chuang, S.-H.; Mai, C.-L.; Yen, W.-N.; Hsu, S.-J.; Diau, E. W.-G.; Yeh, C.-Y. *J. Mater. Chem.* **2010**, *20*, 1127.
- (276) Pellejà, L.; Kumar, C. V.; Clifford, J. N.; Palomares, E. *J. Phys. Chem. C* **2014**, *118*, 16504.
- (277) Chang, Y.-C.; Wang, C.-L.; Pan, T.-Y.; Hong, S.-H.; Lan, C.-M.; Kuo, H.-H.; Lo, C.-F.; Hsu, H.-Y.; Lin, C.-Y.; Diau, E. W.-G. *Chem. Commun.* **2011**, *47*, 8910.
- (278) Wang, C.-L.; Chang, Y.-C.; Lan, C.-M.; Lo, C.-F.; Diau, E. W.-G.; Lin, C.-Y. *Energy Environ. Sci.* **2011**, *4*, 1788.
- (279) Wu, C.-H.; Pan, T.-Y.; Hong, S.-H.; Wang, C.-L.; Kuo, H.-H.; Chu, Y.-Y.; Diau, E. W.-G.; Lin, C.-Y. *Chem. Commun.* **2012**, *48*, 4329.
- (280) Lo, C.-F.; Hsu, S.-J.; Wang, C.-L.; Cheng, Y.-H.; Lu, H.-P.; Diau, E. W.-G.; Lin, C.-Y. *J. Phys. Chem. C* **2010**, *114*, 12018.
- (281) Wang, C.-L.; Lan, C.-M.; Hong, S.-H.; Wang, Y.-F.; Pan, T.-Y.; Chang, C.-W.; Kuo, H.-H.; Kuo, M.-Y.; Diau, E. W.-G.; Lin, C.-Y. *Energy Environ. Sci.* **2012**, *5*, 6933.
- (282) Lu, H.-P.; Mai, C.-L.; Tsia, C.-Y.; Hsu, S.-J.; Hsieh, C.-P.; Chiu, C.-L.; Yeh, C.-Y.; Diau, E. W.-G. *Phys. Chem. Chem. Phys.* **2009**, *11*, 10270.
- (283) Bareja, E. M.; Gonzalez-Pedro, V.; Ropoll-Sanchis, T.; Wu, H.-P.; Li, L.-L.; Yeh, C.-Y.; Diau, E. W.-G.; Bisquert, J. *J. Phys. Chem. C* **2011**, *115*, 10898.
- (284) Wu, S.-L.; Lu, H.-P.; Yu, H.-T.; Chuang, S.-H.; Chiu, C.-L.; Lee, C.-W.; Diau, E. W.-G.; Yeh, C.-Y. *Energy Environ. Sci.* **2010**, *3*, 949.
- (285) Bessho, T.; Zakeeruddin, S. M.; Yeh, C.-Y.; Diau, E. W.-G.; Grätzel, M. *Angew. Chem.* **2010**, *122*, 6796; *Angew. Chem., Int. Ed.* **2010**, *49*, 6646.
- (286) Masi Reddy, N.; Pan, T.-Y.; Christu Rajan, Y.; Guo, B.-C.; Lan, C.-M.; Diau, E. W.-G.; Yeh, C.-Y. *Phys. Chem. Chem. Phys.* **2013**, *15*, 8409.
- (287) Hsu, H.-Y.; Chiang, H.-C.; Hu, J.-Y.; Awasthi, K.; Mai, C.-L.; Yeh, C.-Y.; Ohta, N.; Diau, E. W.-G. *J. Phys. Chem. C* **2013**, *117*, 24761.
- (288) di Nunzio, M. R.; Cohen, B.; Pandey, S.; Hayse, S.; Piani, G.; Douhal, A. *J. Phys. Chem. C* **2014**, *118*, 11365.
- (289) Ropoll-Sanchis, T.; Guo, B.-C.; Wu, H.-P.; Pan, T.-Y.; Lee, H.-W.; Raga, S. R.; Fabregat-Santiago, F.; Bisquert, J.; Yeh, C.-Y.; Diau, E. W.-G. *Chem. Commun.* **2012**, *48*, 4368.
- (290) Warnan, J.; Favereau, L.; Meslin, F.; Severac, M.; Blart, E.; Pellegrin, Y.; Jacquemin, D.; Odobel, F. *ChemSusChem* **2012**, *5*, 1568.
- (291) Lee, C. Y.; Hupp, J. T. *Langmuir* **2010**, *26*, 3760.
- (292) Luo, J.; Xu, M.; Li, R.; Huang, K.-W.; Jiang, C.; Qi, Q.; Zeng, W.; Zhang, J.; Chi, C.; Wang, P.; Wu, J. *J. Am. Chem. Soc.* **2014**, *136*, 265.
- (293) Jiao, C.; Huang, K.-W.; Guan, Z.; Xu, Q.-H.; Wu, J. *Org. Lett.* **2010**, *12*, 4046.
- (294) Li, C.; Liu, M.; Pschirer, N. G.; Baumgarten, M.; Müllen, K. *Chem. Rev.* **2010**, *110*, 6817.
- (295) Wang, C.-L.; Hu, J.-Y.; Wu, C.-H.; Kuo, H.-H.; Chang, Y.-C.; Lan, Z.-J.; Wu, H.-P.; Diau, E. W.-G.; Lin, C.-Y. *Energy Environ. Sci.* **2014**, *7*, 1392.
- (296) Wu, C.-H.; Chen, M.-C.; Su, P.-C.; Kuo, H.-H.; Wang, C.-L.; Lu, C.-Y.; Tsai, C.-H.; Wu, C.-C.; Lin, C.-Y. *J. Mater. Chem. A* **2014**, *2*, 991.
- (297) Mathew, S.; Iijima, H.; Toude, Y.; Umeyama, T.; Matano, Y.; Ito, S.; Tkachenko, N. V.; Lemmetyinen, H.; Imahori, H. *J. Phys. Chem. C* **2011**, *115*, 14415.
- (298) Zhiyong, Y.; Mielczarski, E.; Mielczarski, J. A.; Laub, D.; Kiwi-Minsker, L.; Renken, A.; Kiwi, J. *J. Mol. Catal. A: Chem.* **2006**, *260*, 227.
- (299) Chang, Y.-C.; Wu, H.-P.; Reddy, N. M.; Lee, H.-W.; Lu, H.-P.; Yeh, C.-Y.; Diau, E. W.-G. *Phys. Chem. Chem. Phys.* **2013**, *15*, 4651.
- (300) Lu, J.; Xu, X.; Cao, K.; Cui, J.; Zhang, Y.; Shen, Y.; Shi, X.; Liao, L.; Cheng, Y.; Wang, M. *J. Mater. Chem. A* **2013**, *1*, 10008.
- (301) Wang, Y.; Xu, L.; Wei, X.; Li, X.; Agren, H.; Wu, W.; Xie, Y. *New J. Chem.* **2014**, *38*, 3227.
- (302) Yella, A.; Mai, C.-L.; Zakeeruddin, S. M.; Chang, S.-N.; Hsieh, C.-H.; Yeh, C.-Y.; Grätzel, M. *Angew. Chem., Int. Ed.* **2014**, *53*, 2973.
- (303) Susumu, K.; Duncan, T. V.; Therien, M. *J. Am. Chem. Soc.* **2005**, *127*, 5186.
- (304) Seth, J.; Palaniappan, V.; Wagner, R. W.; Johnson, T. E.; Lindsey, J. S.; Bocian, D. F. *J. Am. Chem. Soc.* **1996**, *118*, 11194.
- (305) Wang, Q.; Ito, S.; Grätzel, M.; Fabregat-Santiago, F.; Mora-Sero, I.; Bisquert, J.; Bessho, T.; Imai, H. *J. Phys. Chem. B* **2006**, *110*, 25210.
- (306) Haid, S.; Marszalek, M.; Mishra, A.; Wielopolski, M.; Teuscher, J.; Moser, J.-E.; Humphry-Baker, R.; Zakeeruddin, S. M.; Grätzel, M.; Bäuerle, P. *Adv. Funct. Mater.* **2012**, *22*, 1291.
- (307) Kurotobi, K.; Toude, Y.; Kawamoto, K.; Fujimori, Y.; Ito, S.; Chabera, P.; Sundström, V.; Imahori, H. *Chem.—Eur. J.* **2013**, *19*, 17075.
- (308) Gu, X.; Sun, Q. *Phys. Chem. Chem. Phys.* **2013**, *15*, 15434.
- (309) Péchy, P.; Renouard, T.; Zakeeruddin, S. M.; Humphry-Baker, R.; Comte, P.; Liska, P.; Cevey, L.; Costa, E.; Shklover, V.; Spiccia, L.; Deacon, G. B.; Bignozzi, C. A.; Grätzel, M. *J. Am. Chem. Soc.* **2001**, *123*, 1613.
- (310) Nazeeruddin, M. K.; De Angelis, F.; Fantacci, S.; Selloni, A.; Viscardi, G.; Liska, P.; Ito, S.; Takeru, B.; Grätzel, M. *J. Am. Chem. Soc.* **2005**, *127*, 16835.
- (311) Gao, F.; Wang, Y.; Shi, D.; Zhang, J.; Wang, M.; Jing, X.; Humphry-Baker, R.; Wang, P.; Zakeeruddin, S. M.; Grätzel, M. *J. Am. Chem. Soc.* **2008**, *130*, 10720.
- (312) Chen, C.-Y.; Wang, M.; Li, J.-Y.; Pootrakulchote, N.; Alibabaei, L.; Ngoc-le, C.-h.; Decoppet, J.-D.; Tsai, J.-H.; Grätzel, C.; Wu, C.-G.; Zakeeruddin, S. M.; Grätzel, M. *ACS Nano* **2009**, *3*, 3103.
- (313) Yu, Q.; Wang, Y.; Yi, Z.; Zu, N.; Zhang, J.; Zhang, M.; Wang, P. *ACS Nano* **2010**, *4*, 6032.
- (314) Han, L.; Islam, A.; Chen, H.; Malapaka, C.; Chiranjeevi, B.; Zhang, S.; Yang, X.; Yanagida, M. *Energy Environ. Sci.* **2012**, *5*, 6057.
- (315) Wang, Y.; Chen, B.; Wu, W.; Li, X.; Zhu, W.; Tian, H.; Xie, Y. *Angew. Chem., Int. Ed.* **2014**, *53*, 10779.
- (316) Sun, X.; Wang, Y.; Li, X.; Agren, H.; Zhu, W.; Tian, H.; Xie, Y. *Chem. Commun.* **2014**, *50*, 15609.
- (317) Yi, C.; Giordano, F.; Cevey-Ha, N.-L.; Tsao, H. N.; Zakeeruddin, S. M.; Grätzel, M. *ChemSusChem* **2014**, *7*, 1107.
- (318) Di Carlo, G.; Caramori, S.; Trifiletti, V.; Giannuzzi, R.; De Marco, L.; Pizzotti, M.; Orbelli Biroli, A.; Tessore, F.; Argazzi, R.; Bignozzi, C. A. *ACS Appl. Mater. Interfaces* **2014**, *6*, 15841.
- (319) Presolski, S. I.; van der Weegen, R.; Wiesfeld, J. J.; Meijer, E. W. *Org. Lett.* **2014**, *16*, 1864.
- (320) Kwok, E. C.-H.; Chan, M.-Y.; Wong, K. M.-C.; Yam, V. W.-W. *Chem. Eur. J.* **2014**, *20*, 3142.
- (321) Sreenivasu, M.; Suzuki, A.; Adachi, M.; Kumar, C. V.; Srikanth, B.; Rajendar, S.; Rambabu, D.; Kumar, R. S.; Mallesham, P.; Rao, N. V. B.; Kumar, M. S.; Reddy, P. Y. *Chem.—Eur. J.* **2014**, *20*, 14074.
- (322) Li, W.; Si, L.; Liu, Z.; Zhao, Z.; He, H.; Zhu, K.; Moore, B.; Cheng, Y.-B. *J. Mat. Chem. A* **2014**, *2*, 13667.
- (323) Zhao, L.; Wagner, P.; Elliott, A. B. S.; Griffith, M. J.; Clarke, T. M.; Gordon, K. C.; Mori, S.; Mozer, A. J. *J. Mat. Chem. A* **2014**, *2*, 16963.
- (324) Zhang, M.-D.; Zhang, Z.-Y.; Bao, Z.-Q.; Ju, Z.-M.; Wang, X.-Y.; Zheng, H.-G.; Ma, J.; Zhou, X.-F. *J. Mat. Chem. A* **2014**, *2*, 14883.
- (325) Stangel, C.; Bagaki, A.; Angaridis, P. A.; Charalambidis, G.; Sharma, G. D.; Coutsolelos, A. G. *Inorg. Chem.* **2014**, *53*, 11871.
- (326) Si, L.; He, H. *J. Phys. Chem. A* **2014**, *118*, 3410.

- (327) Rao, V. G.; Dhital, B.; He, Y.; Lu, H. P. *J. Phys. Chem. C* **2014**, *118*, 20209.
- (328) Lu, J.; Zhang, B.; Yuan, H.; Xu, X.; Cao, K.; Cui, J.; Liu, S.; Shen, Y.; Cheng, Y.; Xu, J.; Wang, M. *J. Phys. Chem. C* **2014**, *118*, 14739.
- (329) Rangan, S.; Batarseh, A.; Chitre, K. P.; Kopecky, A.; Galoppini, E.; Bartynski, R. A. *J. Phys. Chem. C* **2014**, *118*, 12923.
- (330) Zhang, J.; Zhang, J.-Z.; Li, H.-B.; Wu, Y.; Geng, Y.; Su, Z.-M. *Phys. Chem. Chem. Phys.* **2014**, *16*, 24994.
- (331) Lu, J.; Zhang, B.; Liu, S.; Li, H.; Yuan, H.; Shen, Y.; Xu, J.; Cheng, Y.; Wang, M. *Phys. Chem. Chem. Phys.* **2014**, *16*, 24755.
- (332) Ornsø, K. B.; Pedersen, C. S.; García-Lastra, J. M.; Thygesen, K. S. *Phys. Chem. Chem. Phys.*, **16**, 16246.
- (333) Li, W.; Si, L.; Liu, Z.; Wu, H.; Zhao, Z.; Cheng, Y.-B.; He, H. *Org. Electron.* **2014**, *15*, 2448.
- (334) Zhang, C.-R.; Han, L.-H.; Zhe, J.-W.; Jin, N.-Z.; Shen, Y.-L.; Gong, J.-J.; Zhang, H.-M.; Chen, Y.-H.; Liu, Z.-J. *Comput. Theor. Chem.* **2014**, *1039*, 62.
- (335) Xia, H.-Q.; Chen, J.; Bai, F.-Q.; Zhang, H.-X. *J. Porphyrins Phthalocyanines* **2014**, *18*, 406.
- (336) Chae, S. H.; Yoo, K.; Lee, Y. S.; Cho, M. J.; Kim, J. H.; Ko, M. J.; Lee, S. J.; Choi, D. H. *J. Porphyrins Phthalocyanines* **2014**, *18*, 569.
- (337) Balantseva, E.; Miletto, I.; Coluccia, S.; Berlier, G. *Microporous Mesoporous Mat.* **2014**, *193*, 103.
- (338) Ambre, R. B.; Chang, G.-F.; Zanwar, M. R.; Yao, C.-F.; Diau, E. W.-G.; Hung, C.-H. *Chem. Asian J.* **2013**, *8*, 2144.
- (339) Ambre, R. B.; Chang, G.-F.; Hung, C.-H. *Chem. Commun.* **2014**, *50*, 725.
- (340) Fry, H. C.; Liu, Y.; Dimitrijevic, N. M.; Rajh, T. *Nat. Commun.* **2014**, *5*, 1.
- (341) Hamamura, T.; Nakazaki, J.; Uchida, S.; Kubo, T.; Segawa, H. *Chem. Lett.* **2014**, *43*, 655.
- (342) Hamamura, T.; Nakazaki, J.; Uchida, S.; Kubo, T.; Segawa, H. *Chem. Lett.* **2014**, *43*, 796.
- (343) Mane, S. B.; Hung, C.-H. *New. J. Chem.* **2014**, *38*, 3960.
- (344) Zhang, X.; Du, Y.; Chen, Q.; Sun, H.; Pan, T.; Hu, G.; Ma, R.; Sun, Y.; Li, D.; Dou, J.; Pan, X. *Spectrochim. Acta Part A* **2014**, *133*, 514.
- (345) Ip, C. M.; Eleuteri, A.; Troisi, A. *Phys. Chem. Chem. Phys.* **2014**, *16*, 19106.
- (346) Kapilashrami, M.; Zhang, Y.; Liu, Y.-S.; Hagfeldt, A.; Guo, J. *Chem. Rev.* **2014**, *114*, 9662.
- (347) Chen, L.; Dai, H.; Zhou, Y.; Hu, Y.; Yu, T.; Liu, J.; Zou, Z. *Chem. Commun.* **2014**, *50*, 14321.
- (348) Yang, S.; Zheng, Y. C.; Hou, Y.; Yang, X. H.; Yang, H. G. *Phys. Chem. Chem. Phys.* **2014**, *16*, 23038.
- (349) Jeanbourquin, X. A.; Li, X.; Law, C.; Barnes, P. R. F.; Humphry-Baker, R.; Lund, P.; Asghar, M. I.; O'Regan, B. C. *J. Am. Chem. Soc.* **2014**, *136*, 7286.
- (350) Mincuzzi, G.; Vesce, L.; Schulz-Ruhtenberg, M.; Gehlen, E.; Reale, A.; Di Carlo, A.; Brown, T. M. *Adv. Energy Mater.* **2014**, *4*, 1400421.
- (351) Cui, X. R.; Wang, Y. F.; Li, Z.; Zhou, L.; Gao, F.; Zeng, J. H. *ACS Appl. Mater. Interfaces* **2014**, *6*, 16593.
- (352) Park, B.-w.; Pazoki, M.; Aitola, K.; Jeong, S.; Johansson, E. M. J.; Hagfeldt, A.; Boschloo, G. *ACS Appl. Mater. Interfaces* **2014**, *6*, 2074.
- (353) Sampaio, R. N.; O'Donnell, R. M.; Barr, T. J.; Meyer, G. J. *J. Phys. Chem. Lett.* **2014**, *5*, 3265.
- (354) Davies, M. L.; Watson, T. M.; Holliman, P. J.; Connell, A.; Worsley, D. A. *Chem. Commun.* **2014**, *50*, 12512.
- (355) Matta, S. K.; Kakiage, K.; Makuta, S.; Veamatahau, A.; Aoyama, Y.; Yano, T.; Hanaya, M.; Tachibana, Y. *J. Phys. Chem. C* **2014**, DOI: 10.1021/jp5088338.
- (356) Pazoki, M.; Taghavinia, N.; Hagfeldt, A.; Boschloo, G. *J. Phys. Chem. C* **2014**, *118*, 16472.
- (357) Kusumawati, Y.; Hosni, M.; Martoprawiro, M. A.; Cassaignon, S.; Pauporté, T. *J. Phys. Chem. C* **2014**, *118*, 23459.
- (358) Fattori, A.; Cangiotti, M.; Fiorani, L.; Lucchi, S.; Ottaviani, M. *F. Langmuir* **2014**, *30*, 13570.
- (359) Hosseini, Z.; Diau, E. W.-G.; Mehrany, K.; Taghavinia, N. *ChemPhysChem* **2014**, *15*, 3791.
- (360) Narra, S.; Nishimura, Y.; Witek, H. A.; Shigeto, S. *ChemPhysChem* **2014**, *15*, 2945.
- (361) Kuzmych, O.; Johansson, E. M. J.; Nonomura, K.; Nyberg, T.; Skompska, M.; Hagfeldt, A. *Mater. Sci. Eng., B* **2014**, *187*, 67.
- (362) Tian, H.; Soto, A.; Xu, B. O.; Sun, L.; Hagfeldt, A.; Fabregat-Santiago, F.; Mora-Sero, I.; Kang, Y. S.; Bisquert, J.; Barea, E. M. *Nano* **2014**, *09*, 1440005.
- (363) Pazoki, M.; Lohse, P. W.; Taghavinia, N.; Hagfeldt, A.; Boschloo, G. *Phys. Chem. Chem. Phys.* **2014**, *16*, 8503.
- (364) Idigoras, J.; Tena-Zaera, R.; Anta, J. A. *Phys. Chem. Chem. Phys.* **2014**, *16*, 21513.
- (365) Pazoki, M.; Oscarsson, J.; Yang, L.; Park, B. W.; Johansson, E. M. J.; Rensmo, H.; Hagfeldt, A.; Boschloo, G. *RSC Adv.* **2014**, *4*, S0295.
- (366) Latini, A.; Aldibaja, F. K.; Cavallo, C.; Gozzi, D. *J. Power Sources* **2014**, *269*, 308.
- (367) Syrrokostas, G.; Leftheriotis, G.; Yianoulis, P. *Renewable Energy* **2014**, *72*, 164.

NOTE ADDED IN PROOF

Since the time in which this review was accepted and during the editing process of this manuscript, the progress of porphyrins in the DSSC field has kept growing fast. Relevant papers in this connection are cited now in references 315–345. These new references include meso-substituted porphyrin dyes^{315–339} and other related derivatives,^{340–345} as well as innovating TiO₂ nanomaterials,^{346–348} theoretical computational studies, processing and mechanistic aspects.^{349–367}